Combined statistical and dynamic modeling for real time forecasting of rain induced landslides in Matara district, Sri Lanka - a case study

Dissertation

der Mathematisch-Naturwissenschaftlichen Fakultät

der Eberhard Karls Universität Tübingen

zur Erlangung des Grades eines

Doktors der Naturwissenschaften

(Dr. rer. nat.)

vorgelegt von

M.Sc. Halvithana A. G. Jayathissa

aus Alawwa, Sri Lanka

Tübingen

2010

Tag der mündlichen Qualifikation:	01.12.2010
Dekan:	Prof. Dr. Wolfgang Rosenstiel
1. Berichterstatter:	Prof. Dr. Klaus-Dieter Balke
2. Berichterstatter:	Prof. Dr. Edwin Fecker
3. Berichterstatter:	Prof. Dr.-Ing. Dietrich Schröder

Abstract

Among the natural hazards, landslides are attracting more and more attention due to its increasing effect on economic and human losses. While hazard zonation mapping plays a vital role in identifying the vulnerable zones for future land-use planning activities, designing of early warning systems and adequate mitigation measures in landslide-prone areas, lack of real time early warnings significantly increases the damages world wide.

Landslides associated with intense rain during monsoon and inter-monsoon seasons are the most pressing natural disaster in the Central Highland of Sri Lanka. About 13,000 km^2 (20% area of the country) within ten administrative districts are considered to be prone to landslides and almost 42% of the total population of the country is living in these districts. According to the available records, major landslides occurred during past three decades until 2008 have caused a loss of more than 775 human lives making over 90,000 people homeless. Most significantly, Galle, Matara, and Hambantota districts which had not been considered earlier as landslide prone regions were severely affected by the catastrophic event occurred on 17^{th} May 2003 killing more than 150 people in a single day. 855 houses were completely destroyed and another 2858 were damaged rendering almost 20,000 people homeless. Every year huge economic and human losses are recorded and damages are on the rise throughout the island. This is because people live everywhere at their own risk and use even the marginal lands for housing, farming, infrastructure and development activities without an adequate attention to the problem as a result of higher demand of lands with rising population. Thus, as a measure to save lives and property it is incumbent upon to develop real time prediction models for such regions to manage future events successfully. Under the present study a contribution is made to evaluate the capabilities of available static and dynamic modeling approaches to cope with the real time forecasting of rain induced landslides within Matara district of Sri Lanka.

Theoretically, slope instability hazard zonation is defined as the mapping of areas with an equal probability of occurrence of landslides in a given area within a specific period of time. However, calculation of landslide probability is extremely difficult, since there is no simple relationship between magnitudes of landslide events and return periods and as well as due to lack of reliable historical records of landslide dates and triggering events. Thus, susceptibility assessment to identify the critical locations and establishment of triggering thresholds to predict the timing of the events can be considered as a realistic approach in landslide hazard zonation.

The models to predict the locations of future landslides are fairly well developed. They can be generally divided into two groups: direct or semi-direct susceptibility mapping in which the degree of susceptibility is determined by the mapping expert and, indirect susceptibility mapping in which either statistical or deterministic models are used to predict landslide-prone areas. Statistical methods involve both bivariate as well as multivariate techniques. Deterministic models use sound physical models such as stability models as used in geotechnical engineering, or hydrological models used to give an estimation of infiltration and pore water pressures. With the introduction of GIS, in particular indirect methods have gained enormous popularity because of its computational power and due to its capability to handle and analyze data with high degree of spatial variability.

Under the present study, indirect mapping methodology was followed and at the outset five susceptibility maps were prepared using 13 landslide causative factors and existing landslide data within an area of 263 km^2. Two of the commonly applied bivariate methods such as Information Value method and

Weights of Evidence (WOE) modeling and, multivariate Logistic Regression (LR) modeling were utilized for the analysis. Under WOE, three different approaches were followed in which two of them were using fully automated capabilities of ArcSDM (Spatial Data Modeler) with different number of landslide training sites and the remaining by calculation based on ArcGIS spatial analyst. From the final outputs, two of the five susceptibility maps show almost similar result according to the predicted amount of landslides while others differ greatly. Among comparison of them, both the similar maps prepared with equally weighted factor combinations are found to be the best fit susceptibility models for the study area. They are the maps delivered by the simplest bivariate methodologies of Information Value method and WOE modeling based on ArcGIS spatial analyst. Unlike the other three models that differ greatly to each other predicting less than 13% of the existing landslides, both the similar models predict almost 47% of the existing landslides within the very high susceptibility zone. Finally, the model delivered by the Information Value method was chosen and by assigning different percentage of factor weightings according to the expert judgment and testing the success with trial and error procedure, the model was further improved and the study area was reclassified into three susceptibility zones, high, medium and low. In the final expert weighted landside susceptibility map, the zone corresponding to high susceptibility class constitutes 14.78% of the total study area predicting 65.09% of the existing landslides. A 50.69% of the study area is designated to be low susceptible with corresponding 6.03% of the existing landslides. The remaining area is classified into medium susceptibility class.

Rainfall is commonly known as one of the principal landslide triggers. Thus the concept of hydrological triggering thresholds can be utilized for the prediction of timing of rain induced landslides. Hydrological triggering thresholds can be established in a statistical or in a deterministic way. In many regions however statistical thresholds can not be established due to lack of reliable records of landslide locations and associated rainfall intensities and hence deterministic models have to be used. In a deterministic way, factor of safety (F_s) values of individual slopes can be calculated for any given rainfall events. With the help of such maps prepared for various rainfall scenarios, hydrological triggering thresholds in which the factor of safety becomes critical for different areas can be established. If the expected future rainfall events can be predicted by the long term historical data or by the antecedent rainfall or known by real time meteorological data via telemetered network of recording rain gauges, the slopes which may become unstable during a particular event can be predicted.

In the present study, a hydrological slope stability model was used within the PCRaster environment and dynamic slope stability conditions according to a given rainfall event during a month of May 2003 were calculated. Necessary soil samples from 26 locations within the study area as well as rainfall data were collected and soil samples were tested in the NBRO laboratory. Deterministically calculated F_s map for a selected basin on 17th May 2003 was validated with the actual landslide event. Due to the simplistic assumptions used in the model equations and the uncertainties associated with the spatially variable input data, only 21% of the actual landslide area was accurately predicted by the model. However, even if the majority of the unstable pixels in the safety map do not overlap completely with the actual landslide areas, almost 62% of the unstable pixels are located within an area of 100 m buffer from the rupture zone of the existing landslides showing evidence of instabilities within the region of near proximity to those failures. Hence the model is accepted as a reasonable approach to identify the slope stability conditions according to the daily or antecedent rainfall for preliminary predictions. Subsequently, this information combined with the best fit susceptibility model collectively with expertise about the terrain conditions can be more appropriately used for better landuse planning activities, prediction of landslide events and more importantly for the development of real time early warning systems.

Acknowledgement

At the outset, I wish to express my sincere gratitude to Prof. Dr. Klaus-Dieter Balke, Prof. Dr. Edwin Fecker, and Prof. Dr.-Ing. Dietrich Schröder for being my supervisors, giving me necessary guidance, and supplying me with required facilities and materials for the success of my research work. I am strongly impressed by their valuable comments and advices provided to me where necessary while granting me sufficient time and independency throughout the study.

It is also highly appreciated and, my heartfelt thanks are due to Mr. Matthias Flegr who helped me for applying the DAAD scholarship as well as made very valuable comments throughout the whole study and provided necessary assistance and encouragements standing firmly in all the aspects of matters which I faced during my entire stay in Germany.

Special thanks are also due to the Institute of Geosciences, University of Tübingen, Department of Geomatics, Computer Science and Mathematics, University of Applied Sciences, Stuttgart and Institute of Soil Mechanics and Rock Mechanics, University of Karlsruhe for providing me necessary facilities required during my study and Prof. Dr.-Ing. Edelbert Vees, Dr. Hans Joachim Rosner and Mr. Thomas Mutschler for their friendly support. I would like to extent my sincere thanks also to the DAAD for the financial assistance which made this research possible.

My earnest thanks also go to the staff of the Landslide Studies and Services Division (LSSD) of the National Building Research Organization (NBRO) in Sri Lanka for their favorable support and good cooperation extended to me during the field data collection, sample testing and digitization work and permitting me to use all the data authorized to the NBRO.

Lastly, I would like to extend my sincere gratitude to my parents for their continuing support, which I could always rely upon and Chandrasiri Hewa who has been a helpful friend through out my stay in Germany.

Tübingen, December 2010

Gedruckt mit Unterstützung des Deutschen Akademischen Austauschdienstes

Contents

Figures

Page

Tables

Page

1 Introduction

1.1 General background

World's natural hazards are many folds such as earthquakes, volcanic eruptions, tsunamis, hurricanes or tropical cyclones, droughts, hot and cold weathers, lightening and thundering, wildfires, floods, and landslides. They can be considered as a sort of consequences of exogenic and endogenic processes of the earth and extra-terrestrial processes of the solar system. These events are in fact natural agents that maintain the stability of the dynamic Earth and transform vulnerable human conditions into disasters. In very general term, disasters can be expressed as,

$$\text{Disaster} = \text{Hazard} * \text{Vulnerability}$$

Disasters hurt, injure and kill people, cause emotional stress, trauma and economic hardship by destroying homes, infrastructures, industries and businesses and spelling financial ruins for many. Losses from natural disasters reduce the face of sustained economic development in many countries and often lead to a heavy drain on available resources, diverting them from pursuing development goals. According to the World Bank records, average damages caused by natural disasters for every decade in the world are estimated to 100 billion US dollars economically with a severe suffering of at least a million people. Therefore, it is obvious, the economic development and associated human settlements that ignores appropriate disaster management plans can increase a country's vulnerability to natural hazards and exacerbate the impact.

Natural hazards can happen anywhere, but for a combination of reasons, political as well as geographic, most large scale disasters occur in the region between the Tropic of Cancer and the Tropic of Capricorn which encompasses most of the poorer developing nations resulting great sufferings especially to the poorest strata of the population. According to the statistics, 60% of all major disasters recorded in the word occur in the Asia-Pacific region, which is exposed to almost every type of natural hazards and hence this region is considered as the most disaster prone area in the world (Report on disaster mitigation in Asia and the Pacific, 1991).

As per the disaster management aspect is concerned, pre-disaster risk reduction measures such as prevention of hazard occurring, mitigation measures to reduce the magnitude of disaster and preparedness measures to respond rapidly and effectively to disaster situations are in major concern to enhance the safety. However, except in few cases where preventive measures are applicable such as construction of dams or diversion channels to flood control, prevention of many natural hazards are unlikely. Hence, mitigation and preparedness measures can be considered as the most pragmatic pre-disaster reduction measures. Prior prediction of the events (hazard) and timely early warnings are widely practiced, accepted, and very important preparedness measures in disaster management. Thus, hazard prediction models especially with real time forecasting capabilities can play a pivot role in this context.

Among the natural hazards, landslides are attracting more and more attention due to its increasing effect on economic and human losses since they frequently occur in many parts of the world. Landslide is a general term covering a wide variety of mass movements and processes involving down slope transport of soil and rock material in mass under gravitational influence. Although this is a part of the Earth's denudation process and thus considered as a natural phenomenon, slopes which stood safe for centuries

are now frequented by landslides (Figure 1.1) and hence socioeconomic losses due to its impact are growing. This is mainly due to the expand of human activities into more vulnerable hill slopes under the pressure of rising population and associated demands for lands and infrastructure facilities, without an adequate attention to the problem.

Figure 1.1: Landslide disasters in Southern California (Schuster, 1995) and El Salvador (2001).

Despite the fact that, difficulty to accurately quantify the global distribution of landslide hazards and damages, some of the most devastating events of the twentieth century can be summarized as follows. In Kedri, east Java, Indonesia, 5160 deaths were recorded destroying 104 villages due to lahars (debris flow from volcanoes) in 1919. On 16th December 1920, loess dry-flows in Gansu Province, China, which were triggered by a magnitude 8.6 earthquake, caused death of 100,000 to 200,000 people (Close and McCormick, 1922). According to Derbyshire et al. (2000), thousands of landslides occurred throughout a region of 50,000 km^2 in Gansu Province and surroundings, including more than 650 landslides that were greater than 0.5 km wide killing an estimated 180,000 people, damming many streams and rivers, and significantly changing the geomorphology of the region. In 1933, an earthquake magnitude to 7.5 Richter scale caused more than 9300 people to death out of which 6800 were directly from landslides and the remaining were drowned when a landslide dam failed in Sichuan province, China. About 18,000 lives were lost in Tajikistan in 1949 as boulders buried Khait and other villages and farms to a depth up to 150 m by landslides occurred due to an earthquake magnitude to 7.5 Richter scale.

In Kanogawa River valley, Shizuoka, Japan, landslides and debris flows caused by typhoon storms in September 1958 killed 1094 people and destroyed nearly 20,000 houses. A flood wave generated by the failure of slopes of a reservoir behind the Vaiont dam in the Italian Alps due to heavy and prolonged rain in 1963 overtopped the dam and washed away villages at the down slope with the loss of 2000-3000 people. Widespread Debris slides, avalanches, and flows induced by heavy and intense rain in Rio de Janeiro, Brazil in January 1966 caused about 1000 casualties. Again in January 1967, a similar incident killed 1200 people in south west of Rio de Janeiro.

The Mt. Huascaran landslide (debris avalanche-debris flow) in the Peruvian Andes, 1970, destroyed the city of Yungay killing 18,000 people: it was triggered by an earthquake of 7.7 magnitudes (Plafker and Ericksen, 1978). In 1985, lahars killed about 22,000 people at Armero, Colombia.

Nearly one meter of rain in less than a 3 day period in December 1999 in North coast of Venezuela near Caracas created widespread shallow landslides and debris flows and floods along a 40 km coastal strip causing deaths to nearly 30,000 people and destroying 8000 residences and 700 apartments (Sidle and Ochiai, 2006). Rapid deep-seated rain induced landslide/debris flow that buried the village of Guinsahugon in the Philippines on 17th February 2006 took lives of 1800 people.

These statistics demonstrate that the landslides triggered by earthquakes and lahars typically cause the largest loss of lives due to their unexpected and widespread nature even if intense rainfalls and typhoons are also much responsible for many major events. Majority of the landslides which claimed high amount of death tolls were mainly in developing nations. For these mass movements that occurred without any obvious precursor, the lack of advanced warning systems significantly increased the death toll. Additionally, it can be noted that deep seated, slow moving earth-flows or slumps do not cause extensive loss of lives. While such deep-seated landslides may generate huge costs, the rate of movement generally affords sufficient time for people to safely evacuate the area of impact.

The nation most severely affected by landslides is Japan, which suffers estimated total landslide losses of four billion US dollars annually. Despite the different property values in the United States, Italy, and India, total annual economic losses due to landslides have been estimated to range from one to two billion US dollars for each country (Based on Schuster, 1996; Sidle and Ochiai, 2006). However, given the lower property values in the developing nations like India and China, the landslide costs in these mountainous countries are very high. Countries like New Zealand, Canada, and Nepal generally incur landslide damage

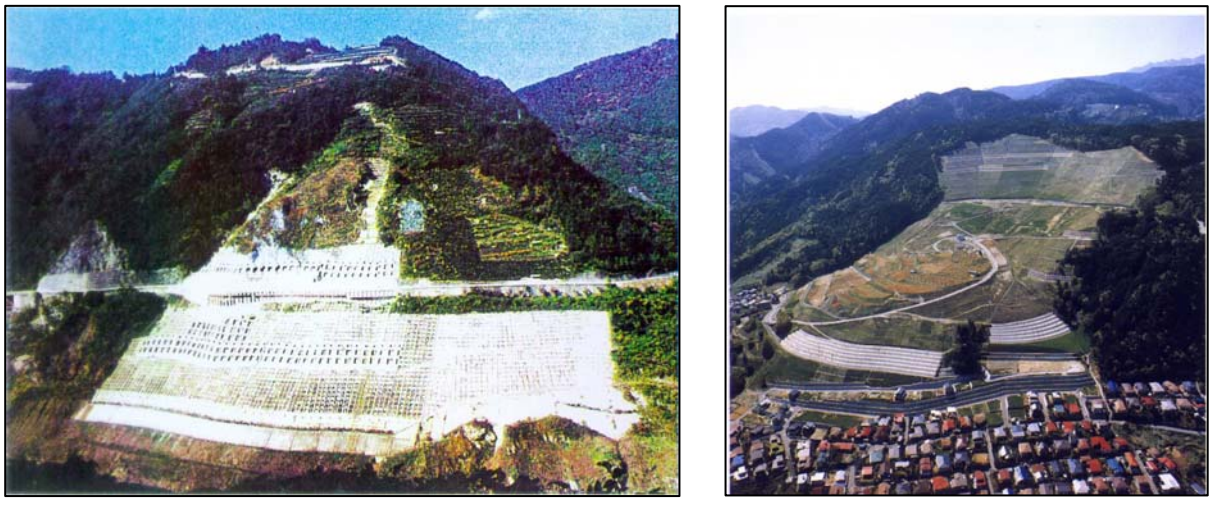

Figure 1.2: Landslide mitigation activities in Japan.

in rural areas; thus, costs are proportionally lower (Sidle and Ochiai, 2006). Many other countries have comparatively lesser, but major annual landslide losses according to their economy, severely affecting the sustainable development goals. However, practices around the world have shown that adequate hazard mitigation and preparedness is possible and such measures can be utilized to minimize the damages.

While some landslides can be controlled by mitigation activities (Figure 1.2), preparedness measures such as timely early warning are the only possibility for many events.

During last four decades, many researches have been conducted with a view to develop various kinds of landslide prediction models. Although the localized studies on individual landslide can provide in depth information, research on the basis of spatial distribution of landslide is an essential task since landsliding is a widespread phenomena in an area. The initial work started with making landslide inventory maps and later improved to qualitative mappings with subjective decision rules of the expert. Gradual development of the researches and the computer revolution made it possible to apply complex statistically supported quantitative techniques such as bivariate or multivariate and deterministic analyzes to make relationships between the causative factors and the spatial distribution of landslides. In this aspect, the joint analysis of all the terrain variables in relation to the spatial distribution of landslides has gained enormously by the introduction of Geographic Information systems (GIS), the ideal tool for the analysis of parameters with high degree of spatial variability (van Westen, 2000).

So far, many static and dynamic models based on different approaches have been locally tested, validated and improved in various parts of the world. However, a numerous number of problems remain still unsolved hindering accurate prediction of landslide hazards especially when real time forecasting is in concern. This is mainly due to the complexity of the landslide processes which involve critical combinations of extremely heterogeneous causative factors and uncertainty associated with the prediction of triggering events. The causative factors can be many kinds; some are known, qualitatively or quantitatively measurable and can be statistically analyzed. Some may be still unknown. Therefore, more and more studies with the introduction of various factor combinations into modern analytical methodologies are still necessary to come out with more appropriate models.

In the context of Sri Lanka case, landslide susceptibility maps are prepared on the basis of model developed in 1995 by a method of collective wisdom of experts considering the occurrence of landslides in a particular area (Badulla and Nuwara Eliya districts) using six major factor combinations. The method has been applied since then to many other parts of the country without in depth consideration to the local situations. While this aspect might lead to deliver problematic result or erroneous interpretation of landslide susceptibility in other areas, those maps that have no any temporal implications or information about the intensity of triggering events has very limited role in managing the events successfully. However, due to lack of resources, expertise knowledge and research interest and competition, inadequate attempts have been taken so far for the improvement of the model and the development of real time forecasting methodologies in the country.

The aim of this research is therefore first to prepare landslide susceptibility maps for the study area by direct analysis of available field data using different quantitative analytical methodologies within the GIS environment. After selecting the best fit susceptibility model among comparison of them, statistical information about the critical combinations of the causative factors will be discussed. Subsequently, the concept of dynamic modeling for slope stability will be used to calculate the hydrological triggering thresholds for various slopes in the area. Combination of both the static and dynamic models collectively with professional expertise about the terrain conditions can finally be used for real time forecasting of landslides within the study area based on rainfall inputs.

The study can be used as an initiation step to attract the interest of research oriented landslide hazard zonation in the country if successfully implemented which remains as a challenging task for future work and validation process.

1.2 Literature review

Late 1960s, a number of maps were prepared in the United States showing slope stability conditions (Blanc and Cleveland, 1968), incidence of landslides expressed by relative amount of landslide deposits (Radbruch-Hall, 1970; Radbruch-Hall and Crowther, 1973), landslide deposits (Brabb and Pampeyan, 1972) and qualitative landslide susceptibility (Dobrovoiny, 1971; Scott, 1972; Davis, 1974a, j; Pomeroy, 1974, etc.). The qualitative susceptibility assessment was firstly based on field reconnaissance of geology based recognition of instability factors around the observed landslides in order to make susceptibility zonations (see section 3.1 for the definitions of susceptibility and hazard zonation) in the area with the landslide inventory being a basic step. The method drew on the subjective expertise of each author.

Similar qualitative landslide incidence maps have been made in different countries using the terms zones exposed to landslide risks or slope instability (ZERMOS program by French Laboratoire de Ponts et Chausse´s, Paris: Antoine, 1977; Humbert, 1977; Landry, 1979; Meneroud and Calvino, 1976; Meneroud 1978, etc.; Mahr and Malgot, 1978 in Slovakia; Kienholtz, 1978 in Switzerland, Rodrıguez Ortiz et al., 1978; Hinojosa and Leon, 1978 in Spain, etc.). An example of the main qualitative susceptibility maps published by the USGS (Radbruch, 1970; Scott, 1972; Davies, 1974; Pomeroy, 1974, etc.) is a map showing landslide areas susceptible to landsliding in the Morrison Quadrangle, Jefferson County, Colorado, Scott (1972) which distinguished four zones.

Semi-quantitative susceptibility hazard or slope instability maps based on analysis of slope angles, lithology and relative amounts of landslip material have been published (Blanc and Cleveland, 1968; Bowman, 1972; Radbruch and Crowther, 1973; Dobrovolny and Schmoll, 1974; Nilsen and Brabb, 1977; Nilsen and Wrigth, 1979). The landslide map of California was made by Radbruch and Crowther (1973) into 1: 1,000,000 scales. Here, the rating were related to slope angle below 5^0 and rainfall of less than 10 inch (25.4 cm) with very little evidence of landsliding as unit 1 and at the opposite extreme, to areas heavily covered by large amount of landslides as unit 6. Nilsen and Wrigth (1979) in a 1:125,000 scale landslide map of the San Francisco Bay region distinguished slope angle units of $< 5^0$, $5–15^0$ and $> 15^0$, and lithological groups of no landslide deposits, susceptible bedrock, susceptible superficial deposits and landslide deposits. Combining these two criteria of slope angle and lithological groups they classified the region into six zones: (1) stable, (2) generally stable, (3) moderately stable, (4) moderately unstable and (5) unstable. The areas subject to liquefaction was defined as Zone 1A. These maps, at different scales, were oriented toward the classification of land units based on the evidence of landsliding. However, as there was no attempt at temporal forecasting, from the point of view of Varnes (1978) they would be considered closer to landslide inventories than to landslide hazard maps.

Stevenson (1977), proposed hazard and risk maps which was based on numerically rated or weighted slope and geological factors with geotechnical data. Other significant contributions were linear risk maps of roads (Meneroud, 1978) and geotechnical stability maps which rate soil and rock mechanics parameters such as cohesion, friction angle or rock massif discontinuities (Vecchia, 1978). They generally

proposed landslide risk[1] zonations or a terrain index showing the stability of hillsides. The term "risk" used here could be considered similar to landslide susceptibility. According to Varnes (1984), as the term "terrain index" is also intended to show a quantitative rating of stability, it is closer to the concept of susceptibility than hazard or risk.

Landslide susceptibility was quantitatively first approached by Brabb et al. (1972). They introduced a semi-quantitative method consisting of a bivariate analysis of landslide area percentages in slope angle intervals, expressed by relative susceptibility numbers, from which a susceptibility zonation was obtained. This pioneering paper offered a formal definition of landslide susceptibility as an indication of how prone to landsliding a land unit may be. It also offered a method to classify terrain units with a relative susceptibility number based on geological units, slope angle and percentage of landslides in the unit, which was a very difficult task to apply at that time.

Another approach to mapping landslides involves landslide density or isopleth maps. Campbell (1973) presented a nominally objective method for a statistical assessment of regional landslide distribution based on Schmidt and Mac Cannel (1955). The technique was based on a landslide inventory at a 1:24,000 scale (Campbell, 1973) by estimating the surface covered by landslide deposits using a number of contiguous circles displayed on a grid, calculating the percentage of the surface area covered by each circle and contouring equal percentage intervals.

With the computer revolution, Lessing et al. (1976) in West Virginia (USA), Newman et al. (1978) in the San Francisco Bay region and Carrara et al. (1977, 1978) in the Ferro basin (Calabria, Italy), introduced computer techniques to analyze landsliding factors in order to obtain what they called slide-prone areas, landslide susceptibility or landslide hazard zonations, all of which lacked any temporal forecasting. The widespread availability of computing power allowed statistically supported landsliding zonations to be obtained, e.g. landslide susceptibility using discriminate factors (Simons et al., 1978) and landslide hazard using bivariate (Neulands, 1976) or multivariate analysis (Carrara, 1983).

One of the really significant contributions to landslide research comes from the pioneering work of Carrara and Merenda (1976), Carrara (1983) and Carrara et al. (1977, 1978). Varnes (1984) described the contributions of Carrara et al. (1978), on the landslides in the basin of the Calabria–Lucania border, Italy, as ''one of the more advanced and accessible state-of-the-art analyses of land attributes for production of landslide hazard maps, utilizing computer processing''. The objectives were to statistically define slope instability by multivariate analysis and, using a computer, to create a slope instability hazard map. Their work initially used large square grid cells (200 * 200 m) as the basis for analysis. Whereas, later studies evolved towards the use of morphometric units, but the method itself has not undergone major changes.

Another example of multivariate analysis of landsliding using a GIS was presented by Bernknopf et al. (1988) who applied multiple regression analysis to a data set using presence or absence of landslides as the dependent variable and the factors used in the slope stability model (soil depth, soil strength, slope angle) as independent variables. Here, the resulting regression function allows the computation of landslide probability for each pixel. Also Baeza (1994) largely contributed to multivariate analysis and

[1] Risk is defined as the probability of meeting danger or suffering harm or loss. In relation to disaster, risk has been more specifically described as the probability that a disaster will occur, using relative terms such as high risk, average or medium risk and low risk to indicate the degree of probability.

mapping of the incidence of shallow landslides in the Pyrenees (Spain) using a statistical computer package.

The matrix-assessment approach (DeGraff and Romesburg, 1980) is an objective and quantitative method for establishing an index of instability over an area and evaluating landslide susceptibility. It is based on measured attributes of the bedrock, slope and aspect from aerial photo interpretation and field work and a landslide inventory. The total areas covered by landslides were placed in each appropriate cell and the amount of landslide terrain with the same particular combinations of bedrock, slope or aspect units was identified. A management unit matrix was constructed from all bedrock, slope and aspect combinations for landslide locations, giving rise to different management units within the matrix. Based on this method a quantitative landslide susceptibility zonation was obtained by grouping all the susceptibility values into classes. A non-hierarchical clustering method (Anderberg, 1973) using a W-function, by minimizing the sum of squared deviations about the three equally distributed groups, was adopted to obtain susceptibility classes for the final landslide susceptibility classification (DeGraff and Romesburg, 1980). Method has a little room left for personal judgment and was designed for large areas of wild lands. The use of the GIS matrix method has been made possible by the development of microcomputers and software over the last decades.

Landslide hazard assessment based on simple relationships with rainfall characteristics have been applied at both the global (Caine, 1980) and regional (Cannon and Ellen, 1985; Canuti et al., 1985; Larsen and Simon, 1993) scales. When coupled with real time data, such analyses can provide the basis for early warning systems for shallow landslides (Keefer et al., 1987; Iiritano et al., 1998). For earthquake-triggered landslides, simple relations between earthquake magnitude and distance to the epicenter have proved to be useful general indicators for landslide hazard assessment (Keefer, 1984). However, the major problem with earthquake analysis is uncertainties associated with future earthquake locations, magnitude and timing.

In Sri Lanka, a landslide susceptibility assessment model had been developed making attempts to arrive at decisions based on collective wisdom (LHMP user manual, SRL 1989/001). The study was based on the field data collected from 1200 landslides in Nuwara-Eliya and Badulla districts during a five years (1989 to 1995) research project conducted by Landslide Studies and Services Division (LSSD) of the National Building Research Organization (NBRO). Six major causative factors with sub factors were considered and data was collected into 1: 10,000 scales. Although the out puts of the statistical analysis of the terrain factors were considered, relative weightings for major factors and scores for sub factors and factor classes had been designed on the basis of collective wisdom of the experts, as it was not possible to obtain a unanimous agreement on a highly subjective matters relying only on statistical data. The model has been used since 1995 for the prediction of landslide susceptibility of existing slopes in all the parts of the country.

Deterministic slope stability models have been used since the beginning of 20th century to calculate the stability of individual slopes (Nash, 1987). Only recently, several researchers have started to use the same models for the calculation of slope stability maps for large areas such as catchments (Ward et al., 1981, Ward et al., 1982; Okimura and Kawatani, 1987; Brass et al. 1989; Benda and Zhang, 1990; Murphy and Vita-Finzi 1991; Van Asch et al., 1992, 1993; Van Westen et al., 1993; Terlien et al., 1995; Terlien, 1996). Most examples deal with infinite slope models, since they are simple to use for each pixel separately. Hammond et al. (1999) presented methods in which the variability of the factor of safety is

calculated from selected input variables utilizing Monte Carlo techniques. This implies a large number of repeated calculations, which are readily supported by the use of GIS. Hydrological models are frequently used to give an estimation of the maximum pore water pressures to be expected on the potential slip surfaces. The use of deterministic hydrological models in combination with stability models has been successfully applied by Terlien et al. (1995) and Terlien (1996).

With the development of powerful computers and the application of GIS, all kind of methods and techniques have gained enormously easing very laborious work involved in data processing and analyses. Following sections provide some of the most important literature of GIS based landslide analysis.

Fall and Azzam (1998) used GIS to prepare a map indicating natural risk in the coastal area of Dakar, Senegal. GIS analysis was made in ArcInfo and ArcView (ESRI) to obtain a natural risk map based on three groups of instability factors: hydrogeology, coastal erosion and geotechnical parameters showing six zones of coastal slope dynamics. Also another risk assessment approaches were proposed by Kawakami and Saito (1984), Lee et al. (2001). The presence or absence of instability processes and hazard was proposed as a tool for better land-use planning of a coastal area affected by rapid urban development. Wachal and Hudak (2000) used GIS techniques to assess landsliding in a 1,500-2000 km^2 area in Travis Country (USA), based on four factors: slope angle, geology, vegetation and distance to faults. Four classes of relative susceptibility were derived weighting these factors according to their contribution to instability processes. Moreiras (2004) proposed landslide incidence or susceptibility (Moreiras, 2005) zonation for a 1,600 km^2 area west of Mendoza city, Argentina, based on air photo interpretation, digital analysis of satellite Spot and Landsat images and field control. The degree of relative susceptibility were assigned from GIS analysis taking into account both lithology and slope angle and a landslide inventory.

A very interesting new GIS methodology was proposed by Parise and Jibson (2000) to obtain a landslide seismic susceptibility rating. An inventory of landslides that occurred during the Northridge earthquake (1994, M: 6.7, California, USA) in the Santa Susana quadrangle was made. Distances to the epicenter fault zone and data about the dynamic intensity were expressed as Arias intensities (Arias, 1970). These were considered as a basis for a landslide susceptibility index (LSI is expressed as the ratio in percentage of the area covered by landslides in each geological unit to the total area of the outcrops of that unit) and landslide frequency index (number of landslide per km^2). A zonation of four relative susceptibility classes was obtained with a resolution of 10 * 10 m at a scale of 1:24,000: very high (>2.5% landslide area or >30 LS/ km^2), high (1.0–2.5% landslide area or 10–30 LS/km^2), moderate (0.5–1.0% landslide area or 3–10 LS/km^2) and low (<0.5% landslide area and <3 LS/km^2).

GIS based rock fall hazard assessment and analysis was accomplished by many authors, for instance Ayala-Carcedo et al. (2003) analyzed a rock fall front in the Sierra de la Cabrera (Madrid, Spain) by a heuristic approach using ArcInfo (ESRI).

One of the first papers in the United States on a wholly GIS assessment of landslide susceptibility, hazard and risk (Mejıa-Navarro et al., 1994) used weighted factors in algorithms, relating debris flow susceptibility and determinant factors. The research was a pilot project done in ArcInfo (ESRI) and GRASS GIS to test the usefulness of GIS in an integrated planning decision support model evaluating different geological hazards. The base maps were at scales of between 1:4,000 and 1:25,000. Debris flow hazard susceptibility, at a scale 1:24,000, was derived from an algorithm which modeled the influence of several factors.

Another example of a weighting factor procedure was used by Temesgen et al. (2001) in a study of the Wondogenet area in the eastern margin of the Ethiopian rift in a raster GIS. Estimates were made of the frequencies of landslide occurrence considering lithology, drainage network, geology, slope angle, slope aspect and vegetation cover. Priority weightings were assigned on the basis of observed landslide densities for each class and the resultant maps were overlain to produce susceptibility maps. The final integration was made using pixel attributes, algebraic calculations and arithmetic means. The landslide hazard map was derived from the integration of all the susceptibility maps.

Van Westen et al. (2003) evaluated the importance of expert geomorphological knowledge in the production of landslide susceptibility maps using GIS supported indirect bivariate statistical analysis. A raster GIS software (ILWIS) and a cartographic package (ACE) were used to obtain an excellent 1:10,000 scale map. The test area was a mountain zone of 20.8 km^2 in the Alpago basin, Italy. The data set was obtained at a 1:5,000 scale with a pixel resolution of 3 * 3 m. Detailed geomorphological mapping was undertaken and data on lithology, structural geology, superficial materials, slope classes, land use and distances from streams, roads and houses were collected. Direct and indirect landslide susceptibility mapping was undertaken. Direct mapping was performed after digitizing the geomorphological units assessed on the basis of susceptibility attributes determined directly from field observations. Indirect landslide susceptibility mapping was obtained from a statistical analysis of the result of overlaying the factor and inventory maps. The density of landslides in the area occupied by each factor, compared with the density of landslides in the entire area, was considered to be an expression of the importance of each factor in the instability process. Then, using the weights of evidence method (Bonham-Carter, 1994), indirect landslide susceptibility mapping was performed using the GIS. For this purpose, six different combinations of factors were tested against the results of the direct susceptibility mapping. The use of detailed geomorphological information in a bivariate analysis raised the overall accuracy of the final susceptibility map considerably. The authors concluded that the ‘‘actual generation of the susceptibility maps are best done by knowledge-driven methods, such as multiclass index overlaying or fuzzy logic methods’’.

Ayalew et al. (2004) developed a GIS based model which took account of both landslide frequencies and expert knowledge of the factors that influence slope instability in Tsugawa area of the Agano River, Japan, following layering and the assignment of six weighted factors using the linear combination method. IDRISI was used by Ayalew and Yamagishi (2005) to design a landslide susceptibility map of a 105 km^2 area in the Kakuda-Yahiko Mountains of Japan by the logical regression method combined with bivariate statistical analyses. Also an interesting contribution to rank landslides weighted factors in a GIS application to an area in the Apennines (Italy) is presented by Donati and Turrini (2002).

Following the pioneering papers by Carrara and Merenda (1976), Carrara et al. (1977, 1978), Carrara (1983), it became clear that multivariate analysis and GIS were particularly suitable for landslide mapping, although external statistical packages were usually required for part of the data analysis (Chung, 1995; Baeza and Corominas, 1996; Luzi and Pergalani, 1996a, b; Chung and Fabri, 1999; Baeza and Corominas, 2001; Lee and Min, 2001; Marzorati, 2002; Park and Chi, 2003; Ercanoglu et al., 2004; Süzen and Doyuran, 2004b; Xie et al., 2004; Carrara and Guzzetti, 1995; Carrara et al., 1991a, b, 1992, 1995, 2003; Guzzetti et al., 1999, 2000, 2004, etc.). Some approaches adopted a probabilistic treatment of data for slope instability, such as the Monte Carlo method (Zhou et al., 2003). These methods have also been combined with uncertainty approaches. Many published papers used statistical techniques including

weighting factors, expert assessment techniques, fuzzy logic or neural networks in slope stability maps based on probabilistic reliability index methods.

Hong Kong has been one of the most important sources of contributions to landslide forecasting maps and techniques. Good examples of GIS (ArcView, ESRI) applications to landslide susceptibility mapping are those authored by Dai et al. (2000), and Dai and Lee (2001, 2002a and b) for Lantau Island, which is frequently threatened by landslide events. Their methodology is based on ArcView (ESRI) and SPSS (statistical package) multivariate logistic regression of presence–absence of dependent variables relating landslides and various contributory factors. The scale used was 1:20,000 with a resolution of 20 * 20 m with an inventory of 800 landslides.

Yongin area in South korea was mapped by Lee and Min (2001) using bivariate and multivariate analysis and ArcInfo (ESRI) GIS. They used 14 different factors with the pixel resolution of 10 * 10 m. Internal validation was undertaken by checking the correlation between landslides and susceptibility classes in both statistical methods demonstrating good results and proving that the bivariate analysis is much easier to perform. Santacana et al. (2003) studied part of La Pobla de Lillet village (Pyrenees, Spain) by statistical multivariate and discriminant analysis using ArcInfo (ESRI). Seven different factors were integrated and spatial validation was undertaken.

Süzen and Doyuran (2004a) studied an area of 200 km^2 in the Asarsuyu basin (Turkey) at a scale 1:25,000, using GIS and two methods of statistical analysis: bivariate and multivariate multiple regressions. The first method was quicker but less accurate while the second, more complex, method provided a better correspondence between the factor analysis and landslides. Thirteen factors were considered and analyzed for their relationship with an inventory of 49 landslides of different types, mostly earth flow and shallow translational slides. The zonation was validated by comparing the zonation with previous landslide activity.

Ercanoglu et al. (2004a) made a landslide susceptibility map of 64 km^2 of the Yenice region of Turkey using GIS to overlay factors weighted by statistical multivariate and factorial analysis techniques. Spatial validation was undertaken by relating 57 recorded landslides to the susceptibility zones. Lee (2004) made a landslide susceptibility map of the Janghung area (South Korea) using bivariate and multivariate statistical methods and a pixel size of 10 *10 m. Most of the landslides in the 41 km^2 study area were superficial movements. The bivariate method analyzed the probability relationship (landslide frequency) in each of 13 classes of contributory factors. Multivariate logistic regression, although a complex and time consuming process, resulted in a better correspondence of recorded landslides with defined susceptibility levels. Also Dias and Zuquette (2004) presented an interesting probabilistic landslide susceptibility mapping in Ouro Preto, Brazil and Ohlmacher and Davis (2003) a logistic regression method to landslide hazard mapping in Kansas, USA.

More powerful computing has become available allowing new GIS matrix methods (Irigaray, 1990, 1995- cited by Chacon et al., 2006) to deal with increasing numbers of attributes. For instance, in the Betic Cordillera (Southern Spain), a region of about 15,000 km^2 has been covered by landslide susceptibility maps by many authors (cited by Chacon et al., 2006, pp. 359) using the GIS matrix method. Maps at scales from 1:2,000 to 1:50,000 have been prepared using Spans GIS (Tydac-Intera), ArcInfo and ArcGIS (ESRI), depending on the research objectives. Few other authors such as Cross (1998, 2002) used the GIS

packages PANACE, DERIVATIVE and MIRAGE and Clerici et al. (2002) used GRASS GIS for similar kind of landslide analysis.

All the methods discussed above analyze landsliding factors in order to obtain slide-prone areas or landslide susceptibility maps. However, the main issue in landslide hazard research is to identify the future occurrence of landslides in a given area in a given time. According to Varnes (1984), *slope instability hazard zonation* is defined as the mapping of areas with an equal probability of occurrence of landslides in a given area within a specific period of time. Hence, while susceptibility maps provide zonations of areas with similar instability or similar conditions that may generate landslides, a true landslide hazard map should offer a zonation of areas with similar probabilities of landslides in a given period of time, based on quantitative analysis of data (Chacon, 2006).

Einstein (1988) suggested the temporal projection of susceptibility mapping based on higher probabilities of new landslides occurring within higher susceptibility zones. Recent validation of a susceptibility map (Irigaray et al., 1999, 2006) confirmed this view, when 125 new landslides occurred after heavy rainfalls in 1997 in the Iznajar river dam area (Granada, Spain) where a susceptibility map had been completed in 1994 using an inventory of 833 older landslides. Some 61.9% of the 1997 landslides plotted in the very high susceptibility zone and 23.1% in the high susceptibility zone. Similar practical validations were successfully obtained by many other authors too for instance like in southwestern Sierra Nevada (Spain) and in Torre Vedras (Portugal).

Terlien et al. (1995) and Terlien (1996, 1997) modeled temporal and spatial variations in rainfall-triggered landslides, based on remarkably detailed research using field instrumentation and a large number of geotechnical tests. The main steps were identification of the triggering mechanism of landslides, selection of appropriate hydrological models, selection of slope stability models for input data on established triggering mechanisms, determination of the spatial distribution of input data, determination of pore water fluctuations and maximum pore water pressure on potential slip surfaces and the preparation of the landslide hazard map including the distribution of failure probabilities for different triggering mechanisms. The maps were tested by checking locations of recent landslides and observed landslide frequencies. Terlien (1996) discussed in detail the relative importance and the difficulties of obtaining the input parameters. He indicated great difficulty in assessing spatial distribution of factors important for landslide mapping, such as pore water pressure, the relations between soil moisture and pressure head and the relation between unsaturated hydraulic conductivity and soil moisture. For groundwater- triggered landslides, it is also difficult to assess important parameters such as soil cohesion, soil angle of friction, leakage into bedrock and effective porosity.

The results of hazard assessments of landslides undertaken for both shallow and deep landslides triggered by rainfall or groundwater in Manizales, Colombia (Terlien, 1996, 1997) were observed to be very conservative. The model for the considered period of time identified potential landsliding areas 5–10 times larger than the actual areas affected by observed landslides. This apparent failure of the temporal spatial assessment was believed to be resulted from inaccurate assessment of the landslide frequency and the poor quality of input data.

Spatial prediction, performed using SINMAP (Stability Index Mapping) after Pack et al. (1998), was based on limit equilibrium failure analysis using an infinite slope stability model and a steady-state hydrological model (TOPMODEL) as described by Beven and Kirkby (1979) and Connell et al. (2001).

The stability index (SI) was defined as probability of slope stability [SI = Probability (F_s>1)] over the distribution of uncertain parameters (cohesion c, friction angle ϕ, effective rainfall Q, and soil transmissivity T). The stability index was employed to define six hazard classes from high stability (SI>1.5) to low stability (SI=0). Several different landslide stability maps were produced from SINMAP for different precipitation conditions showing increasing instability area as percentages. The model was used by authors to predict rainfall triggered landslides and the resulting maps were considered to be helpful for citizens, land use planners and engineers, to reduce losses by means of prevention, mitigation and avoidance of such events.

SHALSTAB is another physically based model for shallow landslide analysis combines digital terrain data with near surface through-flow and the infinite slope model (Montgomery and Dietrich, 1994; Dietrich and Montgomery, 1998; Montgomery et al., 1998). The model has been held well in many areas such as in northern California, Washington, and Oregon (Montgomery and Dietrich, 1994; Dietrich, 2001). Whereas, further applications have revealed that model frequently over predicts landslides and performs best in steep catchments underlain by shallow bedrock and worst in less steep catchments underlain by thick glacial deposits (Montgomery et al., 1998; Borga et al., 2002b; Fernandes et al., 2004).

Based on non-distributed landslide model by Sidle (1992), a distributed, physically based slope stability model (dSLAM) was developed to analyze shallow rapid landslides at the catchments scale within a GIS framework (Wu, 1993; Wu and Sidle, 1995, 1997; Sidle and Wu, 1999). This model assesses the spatial and temporal effects of timber harvesting on slope stability. The distributed model incorporates (1) infinite slope analysis; (2) continuous temporal changes in root cohesion and vegetation surcharge; and (3) stochastic influence of actual rainfall patterns on pore water pressure. Recent improvements to the model (now IDSSM) include the ability to simulate multiple harvesting cycles, more efficient handling of rainfall inputs, and an updated distributed shallow groundwater model (DSGMFW) (Dhakal and Sidle, 2003 2004a, b; Sidle and Dhakal, 2003).

TRIGRS is one of the few distributed models to incorporate the effects of rainfall infiltration on dynamic pore pressure response in soils (Baum et al., 2002). This model extends Iverson's (2002) infiltration-based landslide model to the catchments scale by adding a solution for an impermeable basal boundary at a finite depth and including a simple runoff routing scheme. Major assumptions include nearly saturated soil conditions, well-documented flow field, and relatively isotropic and homogeneous soil hydrological properties.

Iida (2004) developed a hydro-geo-morphological model for shallow landslide prediction that considers both the stochastic character of rainfall intensity and duration, and the deterministic aspects controlling slope stability, where the short term probability of landsliding is defined as the probability that the saturated soil depth exceeds a critical value. The model was applied to an area east of Hamada, Japan, where extensive landsliding occurred during a heavy rainstorm in 1988.

One of the few distributed approaches to deep-seated landslide modeling was developed by Miller (1995). The model incorporates topographic, geologic, and soils data from 1:24,000 scale maps with Bishop's modified method of slices stability analysis (Bishop, 1995) within a GIS framework. The model was applied to the Montague Creek basin in northwest Washington; soils were assumed to be completely saturated. Considerable discrepancies existed between predicted areas of instability and actual failure (Miller, 1995), partly due to the constant saturation assumption.

Using the method of isopleth maps (Campbell 1973), Coe et al. (2000) prepared a map of the city of Seattle (Washington, USA) based on a landslide database. Records spanned the period from 1897 to March 1998, with information on dates from November 1909. This 88.4 year record was converted into a density map, using a moving count circle on a grid of 25 * 25 m, by means of software developed by the authors. The map was made using ArcInfo (ESRI) GIS. The historic mean recurrence interval for each landslide density value was calculated by dividing the period covered by the database record (88.4 years) by the landslide count of the numerator in the density value (Crovelli, 2000). The next step was the calculation of the exceedance probability of landslides considering a time range of 1–100 years and an area of 625 m^2 per cell in a landslide density grid using a Poisson probability model. This is a model for the occurrence of random point events in ordinary time which is, naturally, continuous (Crovelli, 2000). The model considers landslides as point events occurring in an independent way, with the probability of occurrence proportional to the time interval and with probability distributions remaining equal for all time intervals. Although these are unrealistic assumptions for natural landslides, the model was considered a best first-approximation as a more accurate model might be extremely complex and mathematically intractable (Crovelli, 2000). The model was expressed by $PN(t) \geq 1 = 1 - e^{-t/\mu}$ where μ is the future mean recurrence interval estimated by the historic mean recurrence interval, and t is a period of time in the future for the exceedance probability calculated for 1, 5, 10, 25, 50 and 100 years periods. Continuing research has been undertaken to integrate the map with landslide susceptibility models and maps of Seattle (USGS). If susceptibility values could be calibrated with exceedance probabilities determined from historic data in well-documented areas, then these values could be estimated directly from susceptibility values (Coe et al., 2000).

An excellent basic paper, founded on theoretical considerations and a practical case study, was that of Borga et al. (2002) who presented a ‘‘distributed, physically based slope stability model for shallow landsliding’’ which ‘‘uses a ‘quasi-dynamic’ wetness index to predict the spatial distribution of soil saturation in response to a rainfall of specified duration, and allows to account for both topographic and climatic control on slope failure’’. The paper included a comprehensive review of the origin and current state of physically based slope models. The test area was 5 km^2 areas in the Rio Cordon catchments (Eastern Italian Alps). A quasi-dynamic wetness index, defined by a simple algebraic expression of the coupled subsurface flow and slope stability model, was proposed for a better understanding of the relationships between topography and rainfall variability. Its influence on shallow landsliding offered significant improvements over steady-state models. From this model, it proved possible to derive the probability of failure initiation as a function of topography and climate. The authors concluded that the success of their methodology depended on the quality of the database. They also mentioned the need for consistent procedures for measurement and recording of landslide activity. Another example of wetness index application is presented by Gritzner et al. (2001).

Carrasco et al. (2003) made a susceptibility map of a sector of the Jerte valley (Central System, Spain) affected by torrential flooding. They used statistical methods with a Bayesian approach and two indices: a landslide susceptibility index (LSI) and a surface percentage index (SPI). Five different factors were used to analyze an inventory of 830 landslides produced during recent heavy rainfall at a scale of 1:25,000 and the pixel size of 25 * 25 m. A hazard map was also derived from relationships between landslide susceptibility areas and a rainfall probabilistic temporal assessment of the basin.

Corominas et al. (2003) undertook a GIS integrated landslide susceptibility analysis and hazard assessment at a scale of 1:5,000 in the Principality of Andorra in the inner Pyrenees Mountains. A

landslide inventory of rock fall, slides and flows, lithological map and landslide activity map were introduced into a GIS and supplemented with a statistical analysis of temporal data on landslide events and rainfall series. Susceptibility was assessed from analysis of lithology and slope thresholds for each landslide type, coupled with numerical models of the run-out zone related to the magnitude of the landslides. The hazard analysis was based on the susceptibility zoning and additional data on landslide magnitude and frequency, related to the database of temporal data on landslide and rainfall events. A map showing high, medium, low and very low landslide hazard zones was produced and is a basic document in the building codes of Andorra. Also an interesting assessment of landslide activity using dendrogeomorphological techniques is proposed by Corominas et al. (2004).

Lan et al. (2004) mapped landslide hazard in the Xiaojiang watershed (Yunnan Province of Southwest China). Spatial analysis and prediction of relationships between rainfall during heavy storms and landslides was undertaken using ArcInfo (ESRI). A certainty factor (CF) model which is a probability function originally developed by Shortlife and Buchanan (1975) and modified by Heckerman (1986), introduced in GIS landslide research by various authors (Chung and Fabbri, 1993, 1998; Binaghi et al., 1998) was used. The factors analyzed were lithological groups, structure, distance to major faults and geomorphology (slope angle, slope aspect and elevation). The analysis of the different factor layers and the relationships of these to the landslide inventory provided a hazard classification by CF value.

Frattini et al. (2004) also used physically based models to simulate transient hydrological and geotechnical processes on the slopes of Sarno (Southern Italy) affected by a May 1998 earthquake. They used an infinite slope stability analysis coupled with two simple hydrological models: a quasi-dynamic model to compute the contribution of lateral inflow to slope instability by simulating the time-dependent evolution of the water table; and a diffusion model used to consider the influence of water pore pressure developed from vertical infiltration during heavy rainstorms. The latter model succeeded in predicting correctly the triggering time of more than 70% of the landslides in an unstable area representing only 7.3% of the total catchments. The quasi-dynamic model was able to predict correctly slope instability in zero-order basins where the failures developed into large debris flows. The results confirmed the author's view of the influence of both vertical and lateral water fluxes in the triggering of landslides during the Sarno earthquake.

Xie et al. (2004b) developed an excellent GIS application for landslide time-hazard assessment based on coupled infiltration and slope stability models that took account of increasing rainfall-induced pore water pressure using ArcGIS (ESRI). The case study area was about 3.4 km^2 around Harabun, in the northern part of the Sasebo district, Kyushu (south-western Japan) where a representative landslide occurred in July 1997. Slope stability calculations were based on limit equilibrium plane failure, taking account also of time-space changes in geotechnical conditions with depth of the wetting front over time. The evolution of slope safety factor with time and the triggered landslide areas were shown in different maps.

Artificial neural network (ANN), fuzzy logic and grey systems, probabilistic analysis of the slope safety factor by the reliability index and fractal analysis are the other methods applied by many authors in landslide studies. GIS packages such as ArcInfo, ArcView, GRASS, IDIRISI and statistical software R, SPSS, SAS and Matlab has been gained wide recognition in all such analysis.

1.3 Summary

Deterministic slope stability models have been used since the beginning of 20th century to calculate the stability of individual slopes (Nahh, 1987). However, due to the difficulties of applying site specific analysis to widespread landslide occurrences and necessity to identify potentially unstable sites prior to development activities and predict the future events for disaster management activities over large areas, concepts of landslide susceptibility and hazard zonation assessments were begun. While susceptibility maps provide zonations of areas with similar instability conditions based on terrain parameters, a true landslide hazard map should offer spatial as well as temporal assessments, using series of data on rainfall or earthquake depending on the likely triggering mechanism.

The initial work started in late 1960s with mapping of landslide deposits. Afterwards the methods were developed to qualitative and semi-quantitative susceptibility mapping firstly based on analysis of few simple terrain factors such as slope angle, lithology and landslides. While qualitative susceptibility assessments drew on the subjective decisions of the expert, the quantitative assessments were improved mainly by applying bivariate and multivariate statistical techniques allowing room for the analysis of virtually any numbers of landslide causative factors utilizing computer processing. With the introduction of powerful computers and GIS and other software like statistical and slope stability analysis, a variety of complicated analysis became easily attainable and feasible. Use of deterministic models for the calculation of slope stability maps for large areas such as catchments based on geotechnical data have started recently. Most work deal with infinite slope models, since they are simple to use for each pixel separately. Application of probabilistic approaches where uncertainty of the terrain parameters can be incorporated contributed greatly to the advancement of such models. However, all these approaches have spatial meaning only and lack any temporal assessments.

In addition to site factors, the concept of uncertainty or probability has been incorporated into landslide models, particularly related to triggering mechanisms. While these approaches are very useful to predict the probability of landsliding on natural hill slopes in space and time, such analysis can seldom be executed for many regions due to lack of simple relationship between the magnitudes of landslide events and return periods, and reliable historic records of landslide dates and triggering events. Also, landslide hazard assessments based on simple relationships with rainfall or earthquake characteristics have been applied at both the global and regional scale. When coupled with real time data, they can provide the basis for early warning systems for shallow landslides.

Despite the developments so far achieved, for the significant improvement of actual landslide hazard assessments, three major issues need to be still overcome: (1) methods that can be applied in broader geographic areas or in areas that experience multiple failure types need to be developed; (2) a clear focus need to be placed on the underlying processes that relates to slope failures; and (3) temporal as well as spatial attributes of landslide susceptibility need to be incorporated in the analysis. The first problem can partly be addressed by developing separate criteria, as well as mapping and factor-weighting rules for different failure types. The second issue is difficult to implement especially in data-sparse regions, but as remotely sensed data become more available and more accurate, it may be possible to incorporate such factors into hazard assessments. In this aspect, it is important to focus on specific factors that are intrinsic to landslide initiation in the region of concern. Thirdly, addressing temporal aspects has typically fallen into the realm of physically based models.

As a theoretical advance from empirical landslide models based solely on rainfall characteristics, numerous infiltration based models have been developed for individual sites in both two and three dimensions (e.g., Anderson et al., 1988, Sammori and Tsuboyama, 1990; Haneberg, 1991). Such models offer the advantages of physics based approach to asses the dynamic changes of positive and negative pressure heads in the soil mass during the infiltration process and thus are valuable to predict the timing of slope failures relative to rainfall inputs at individual sites with simple slope configurations. These models estimate the stability of slopes in terms of factor of safety (F_s). Recent advances in incorporating sophisticated GIS and DEM technology into distributed, physically based modeling has facilitated the prediction of landslides at the catchments scale (Montgomery and Dietrich, 1994; Wu and Sidle, 1995; Dhakal and Sidle, 2003; Lida, 2004).

Distributed physically based models are potentially the most advanced and powerful tools in landslide hazard analysis, particularly when they incorporate DEM data based on Lidar (Dietrich et al., 2001), actual rainfall inputs (Baum et al., 2002; Dhakal and Sidle, 2004a), and long term landuse scenarios (e. g., Dhakal and Sidle, 2003). However, widespread application of these models has been limited because they require distributed input data and expertise with GIS and computer modeling. While some data can be augmented by remote sensing and extracted from DEMs, to be effective these geotechnical based models require accurate distributed data on soil depth and other critical soil properties; such data are typically not readily available. Additionally, many of the models combine digital terrain data with near surface through flow and infinite slope model to analyze shallow rapid landslides at catchments scale. For simplicity, most of them assume that the slip surface of the landslide is running parallel to the topographic slope, well documented flow fields and slope parallel subsurface flow occurs, isotropic and homogeneous soil hydrological conditions and properties exist, and ignores the differences of soil behavior in the saturated and unsaturated zones, effect of vegetation root strength or continuous temporal changes in root cohesion and vegetation surcharge, storm characteristics such as mean and maximum hourly intensity and the temporal distribution of short term intensity and stochastic influence of actual rainfall patterns on pore water pressures. Furthermore, influence of other important terrain factors such as lithology, structural attitudes, land use and landform etc., are also ignored in these models. Thus, relying solely on physically based models lead to considerable discrepancies in the prediction of spatially scaled behavior of landslides and sometimes grossly misrepresents the field situations.

Hence, there is an essential need to improve available models and to develop new methodologies and techniques to assess complex hillslope processes and adopt suitable strategy to include various factors and types of slope failures in to analysis. However, rather than relying on a single method to address both the spatial and temporal aspects, combined approach of static and dynamic modeling can be used as one of the most pragmatic way to answer several issues associated with landslide hazard assessments. When such approaches are practiced with respect to local expertise and technology too, more appropriate and reliable result can be expected.

2 Landslide and slope stability

(Definition, classification and theoretical background of landslide and slope stability analyses)

2.1 General background and definition of landslides

Gravitational and seepage forces tend to cause instabilities in natural slopes, in slopes formed by excavation and in the slopes of embankments. Landslide or in broader sense mass movement is a phenomenon of denudation process, where soil or rock material is displaced along the slope mainly by gravitational forces. They occur when the shear strength of the slope material becomes smaller than the shear stress acting on it, resulting in shear failure along a slip surface.

The term landslide comprises almost all varieties of mass movements on slopes including rock falls, topples and debris flows that involve little or no true sliding (Varnes, 1984). According to Cruden (1991), the term landslide is used to denote the movement of a mass of rock, debris or earth down a slope. Therefore, the phenomena described as landslides are not limited either to the land or to sliding. The word is now used with more extensive meaning.

Varnes (1978) provided an idealized diagram showing the features of landslide which he called complex earth slide-earth flow which has been reproduced here as Figure 2.1.

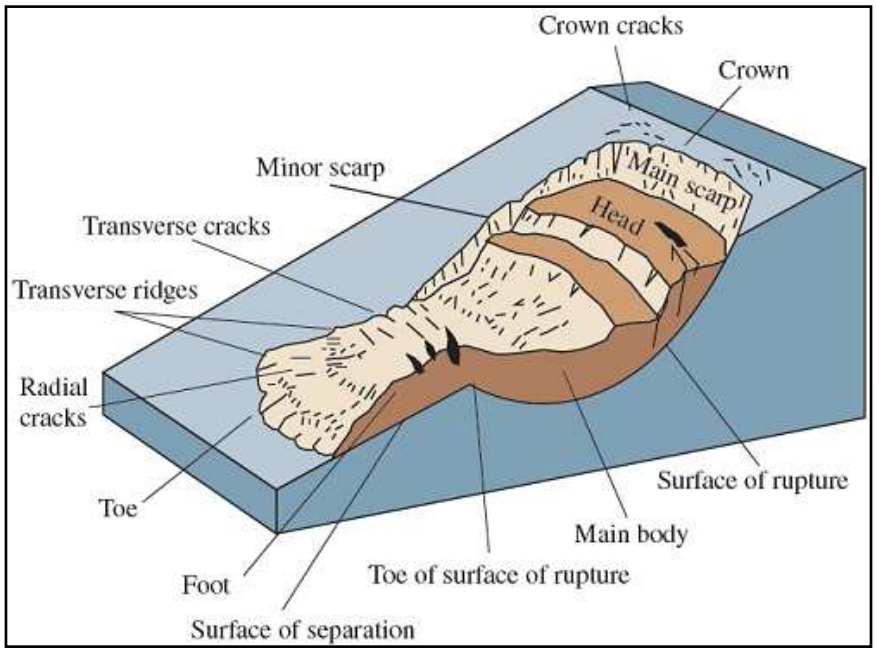

Figure 2.1: Block diagram of idealized complex earth slide-earth flow (Varnes, 1978).

Landslide in which the sliding surface is located within the soil mantle or weathered bed rock, typically to a depth from few decimeters to some meters are called shallow landslides. They usually include debris slides, debris flows, and failures of road cut-slopes.

Shallow landslides can often happen in areas that have slopes with high permeable soils on top of low permeable bottom soils. The low permeable, bottom soils trap the water in the shallower, high permeable soils creating high water pressure in the top soils. As the top soils are filled with water and become heavy, slopes can turn out to be very unstable and slide over the low permeable bottom soils. For instance if

there is a slope with silt and sand as its top soil and bedrock as its bottom soil, during an intense rainstorm, the bedrock will keep the rain trapped in the top soils of silt and sand. As the topsoil becomes saturated and heavy, it can start to slide over the bedrock and become a shallow landslide. Studies on shallow landslides prove that if permeability decreases with depth, a perched water table may develop in soils at intense precipitation. When pore water pressures are sufficient to reduce effective normal stress to a critical level, failure occurs.

Landslides in which the sliding surface is mostly deeply located below the maximum rooting depth of trees, typically to depths greater than ten meters are called deep seated landslides. Deep-seated landslides usually involve deep regolith, weathered rock, and/or bedrock and include large slope failure associated with translational, rotational, or complex movement.

2.2 Landslide activity

Broad aspects of landslide activity should be investigated and described during initial reconnaissance of landslide investigations. The terms relating to landslide age and state of activity defined by Varnes (1978) and some of his terms defining sequence or repetition of movement have been describe here.

Active landslides are those that are currently moving; they include first time movements and reactivations. A landslide that is again active after being inactive may be called *reactivated*. Slides that are reactivated generally move on pre-existing shear surfaces whose strength parameters approach residual (Skempton, 1970) or ultimate (Krahn and Morgenstern, 1979) values. Landslides that have moved within the last annual cycle of seasons but that are not moving at present were described by Varnes (1978) as *suspended.*

Inactive landslides are those that last moved more than one annual cycle of seasons ago. This state can be subdivided. If the causes of movement remain apparent, the landslide is *dormant*. However, if the river that has been eroding the toe of the moving slope changes course, the landslide is *abandoned* (Hutchinson, 1973; Hutchinson and Gostelow, 1976). If the toe of the slope has been protected against erosion by any remedial measures and have stopped the movement, the landslide can be described as *stabilized*.

Landslides often remain visible in the landscape for thousands of years after they have moved and stabilized. Such landslides were called *ancient* or *fossil* by Zaruba and Mencl (1982). When these landslides have been covered by other deposits, they are referred to as *buried* landslides. Landslides that have clearly developed under different geomorphic or climatic conditions, perhaps thousands of years ago can be called *relict*.

Varnes (1978) defined a number of terms that can be used to describe the activity distribution in a landslide. If the surface of rupture is extending in the direction of movement, the landslide is *advancing*, whereas if it is opposite, the landslide is said to be *retrogressive*. If the surface of rupture is extending at one or both lateral margins, the landslide is *widening.*

The style of landslide activity, or the way in which different movements contribute to the landslide can be also defined by terms originally established by Varnes (1978). Varnes defined *complex* landslides as those with at least two types of movements. However, it is now suggested that the term complex be limited to cases in which the various movements occur in sequence. The term *composite*, formerly a

synonym for complex, is now proposed to describe landslides in which different types of movement occur in different areas of the displaced mass, sometimes simultaneously. A *multiple* landslide shows repeated movements of the same type, often following enlargement of the surface of rupture. The newly displaced masses are in contact with previously displaced masses and often share a surface of rupture with them. A *successive* movement is identical in type to a multiple movement but in contrast to does not share displaced material or a surface of rupture with it. *Single* landslides consist of a single movement of displaced material, often as an unbroken block.

Other important aspect to be considered is the rate of movement scale of landslides. According to the Morgenstern's (1985) modified scale of landslide velocity, an important limit appears to lie between very rapid and extremely rapid movement, which approximates the speed of a person running (5 m/s) and between slow and very slow classes (1.6 m/year), below which some structures on the landslide are undamaged.

Water (or ice) is frequently involved in mass wasting by reducing the strength of slope materials and by contributing to plastic and fluid behavior of soil. Varnes (1978) suggested the following modifications to the terms first proposed by Radbruch-Hall (1978) to describe the water content of landslide materials by simple observations of the displaced material such as *dry*, *moist*, *wet* and *very wet*. The terms used here are more qualitative rather than quantitative.

According to Shroder (1971) and Varnes (1978), the material contained in a landslide may be described as either *rock*, a hard or firm mass that was intact in its natural place before the initiation of movement, or *soil*, an aggregate of solid particles, generally of minerals and rocks, that either was transported or was formed by the weathering of rock in place. Gases or liquids filling the pores of the soil form part of the soil. Soil is divided into *earth* and *debris.* Earth describes material in which 80 percent or more of the particles are smaller than 2 mm, the upper limit of sand size particles recognized by most geologists (Bates and Jackson, 1978). Debris contains a significant proportion of coarse material; 20 to 80 percent of the particles are larger than 2 mm. Although the division of material here is crude, it allows material to be named by a swift and even remote visual inspection. The terms used should describe the displaced material in the landslide before it was displaced. For instance, the term *rock fall* implies that the displacing mass was a rock mass at the initiation of the landslide even thought it may be debris after the landslide.

2.3 Classification of landslides

Slope movements have been classified in many ways, with each method having some particular usefulness or applicability related to the recognition, avoidance, control, or correction of the hazards (Sidle and Ochiai, 2006). The earliest widely used classification is that of Sharpe (1938) and the most workers since then owe some debt to him for his pioneering effort. More recent classifications are those of Varnes (1958, 1975, and 1978), Hutchinson (1988), Nemcok et al. (1972), and Sassa (1989). As such, these classification systems have been developed from either geo-morphological or geotechnical perspectives, they provide detailed descriptions of the mode of failure, materials, velocity, failure mechanism, and kinematics (motion of the mass) of landslides.

The widely used classification scheme developed by Varnes (1978) distinguishes five types of mass movements such as falls, topples, slides, spreads, and flows plus combinations of these principal types as

complex (Table 2.1), along with the type of material (bedrock, coarse soils and predominately fine soils). A single landslide may pass through several phases as it progresses down slope; such slope movements, particularly those of debris or earth, are considered complex, but one type usually predominates in different parts of the moving mass or at different times during the period of displacement. In this classification, Varnes (1978) avoids the specific use of the term creep which was used by Sharpe (1938); later modifications (Cruden and Varnes, 1996) note that creep process can be included in various landslide categories by using either very slow or extremely slow descriptors for rate of movements.

Table 2.1: An abbreviated and modified version of the landslide classification scheme developed by Varnes (1978).

Type of movement		**Type of material**		
		Bedrock	**Engineering soils**	
			Coarse	***Fine***
Falls		Rock fall	Debris fall	Earth fall
Topple		Rock topple	Debris topple	Earth topple
Slides	**Rotational**	Rock slump	Debris slump	Earth slump
	Translational	Rock block slide; rock slide	Debris block slide; debris slide	Earth block slide; earth slide
Lateral spreads		Rock spread	Debris spread	Earth spread
Flows		Rock flow (deep creep)	Debris flow (soil creep)	Earth flow (soil creep)
Complex slope movements (i.e., combination of two or more principal types of movements)				

(Source: Sidle and Ochiai, 2006, Landslides-Processes, Prediction, and Landuse)

The Table 2.2 shows a schematic landslide classification adopting the classification of Varnes 1978 and taking into account the modifications made by Cruden and Varnes, in 1996. Some integration has been made by using the definitions of Hutchinson (1988) and Hungr et al. (2001).

Table 2.2: Landslide classification scheme based on Varnes (1978), Cruden and Varnes (1996), Hutchinson (1988) and Hungr et. al. (2001) (Source: WIKIPEDIA).

Type of movement			**Type of material**		
			Bedrock	**Engineering soils**	
				Predominantly fine	***Predominantly coarse***
Falls			Rock fall	Earth fall	Debris fall
Topples			Rock topple	Earth topple	Debris topple
Slides	**Rotational**		Rock slump	Earth slump	Debris slump
	Translational	**Few units**	Rock block slide	Earth block slide	Debris block slide
		Many units	Rock slide	Earth slide	Debris slide
Lateral spreads			Rock spread	Earth spread	Debris spread
Flows			Rock flow	Earth flow	Debris flow
			Rock avalanche		Debris avalanche
			(Deep creep)	(Soil creep)	
Complex			Combination in time and/or space of two or more principal types of movement		

2.3.1 Fall

Falls are masses of soil or rock that dislodge from steep slopes and free-fall, bounce, or roll down slope (Figure 2.2). A fall starts with the detachment of soil or rock from a steep slope along a surface on which little or no shear displacement takes place. The material then descends mainly through the air by falling, bouncing, or rolling (Varnes, 1996).

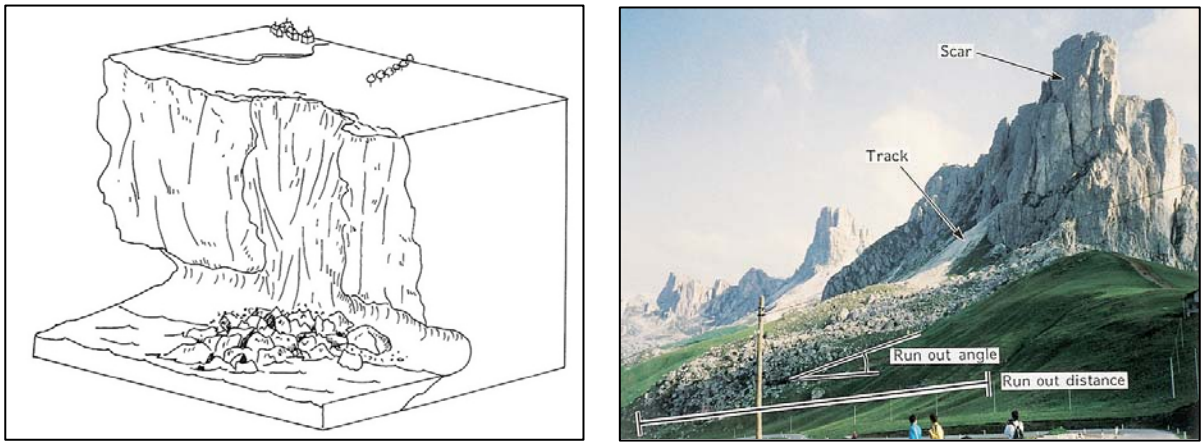

Figure 2.2: Types of landslides: diagrams showing rock fall.

Movement is very rapid to extremely rapid. Except when the displaced mass has been undercut, falling will be preceded by small sliding or toppling movements that separate the displacing material from the undisturbed mass.

Observations show that the forward motion of masses of soil or rock is often sufficient for free fall if the slopes below the masses exceed 76 degrees. The falling mass usually strikes a slope inclined at less than this angle (Ritchie, 1963), which cause bouncing. Rebound from the impact will depend on material properties. On long slopes with angle at or below 45 degrees (1:1), particles will have movement paths dominated by rolling.

2.3.2 Topple

A topple is the forward rotation out of the slope of a mass of soil or rock about a point or axis below the center of gravity of the displaced mass (Figure 2.3). Toppling is sometimes driven by gravity exerted by material upslope of the displaced mass and sometimes by water or ice in cracks in the mass (Varnes, 1996). Topples may lead to falls or slides of the displaced mass, depending on the geometry of the moving mass, the geometry of the surface of separation, and the orientation and extent of the kinematically active discontinuities. Topples range from extremely slow to extremely rapid, sometimes accelerating throughout the movement (David et al., 1996).

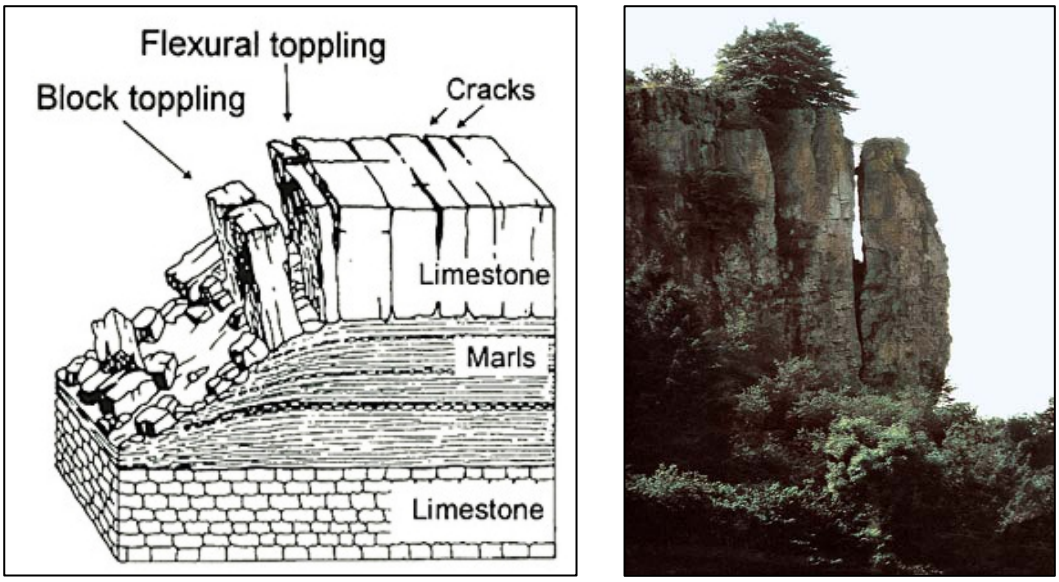

Figure 2.3: Types of landslides: diagrams showing toppling failure.

2.3.3 Slide

A slide is a down slope movement of a soil or rock mass occurring dominantly on the surfaces of rupture or on relatively thin zones of intense shear strain (Varnes, 1996) i.e. slides displace masses of material along one or more discrete planes. Movement does not initially occur simultaneously over the whole of what eventually becomes the surface of rupture; the volume of displacing material enlarges from an area of local failure. Often the first signs of ground movement are cracks in the original ground surface along which the main scarp of the slide will form. The displaced mass may slide beyond the toe of the surface

of rupture covering the original ground surface of the slope, which then becomes a surface of separation (David et al., 1996).

Slides are mainly rotational and translational. Varnes (1978) emphasized the distinction between rotational (Figure 2.4a) and translational (Figure 2.4b) slides as significant for stability analyses and control methods. In rotational sliding the slide plane is curved and the mass rotates backwards around an axis parallel to the slope; in translational sliding the failure surface is more or less planar and the mass moves parallel to the ground surface. Translational slides frequently grade into flows or spread. Rate of movements of slides either rotational or translational can be range from extremely slow to extremely rapid (>5 m/s).

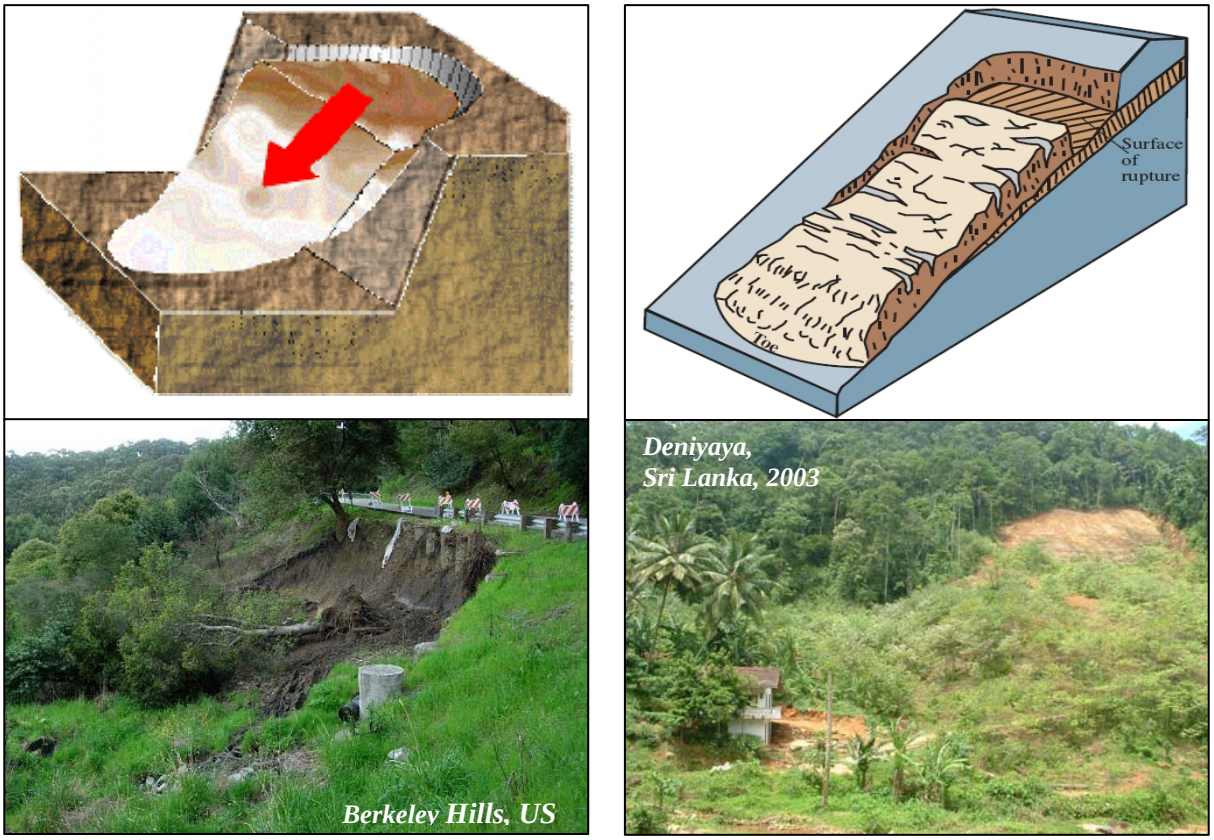

a. Rotational slide *b. Translational slide*

Figure 2.4: Types of landslides: diagrams showing rotational and translational slides.

Rotational slides move along a surface of rupture that is curved and concave (Varnes, 1996). If the surface of rupture is circular or cycloidal in profile, kinematics dictates that the displaced mass may move along the surface with little internal deformation. The head of the displaced material may move almost vertically downward, whereas the upper surface of the displaced material tilts backward towards the scarp. If the slide extends for a considerable distance along the slope perpendicular to the direction of motion, the surface of rupture may be roughly cylindrical. The axis of the cylindrical surface is parallel to the axis about which the slide rotates. Rotational slides in soils generally exhibit a ratio of depth of the surface of rupture to the length of the surface of rupture (D_r /L_r), between 0.15 and 0.33 (Skempton and Hutchinson, 1969). Most frequently rotational circular slides are associated with homogeneous, isotropic soil conditions and non circular slips with non- homogeneous conditions. However, natural materials are

seldom uniform and hence slope movements in these materials commonly follow inhomogeneities and discontinuities.

The scarp below the crown of a rotational slide may be almost vertical and unsupported. Further movements may cause retrogression of the slide into the crown. Occasionally, the lateral margins of the surface of rupture may be sufficiently high and steep to cause the flanks to move down and into the depletion zone of the slide. Water finding its way into the head of a rotational slide may contribute to a sag pond in the backward-tilted, displaced mass. This disruption of drainage may keep the displaced material wet and perpetuate the slope movement until a slope of sufficiently low gradient is formed (David et al., 1996).

Rotational failures may be (i) a *base failure*: the slip surface passes below the toe of the slope and intersects the ground away from the toe, (ii) a *toe failure*: the slip surface intersects the toe, or (iii) a *slope failure*: the slip surface intersects the slope line above the toe.

In *translational* slides the mass displaces along a planer or undulating surface of rupture, sliding out over the original ground surface (Varnes, 1996). Translational sides generally are relatively shallower than rotational slides. Therefore, ratios of D_r /L_r for translational slides in soils are typically less than 0.1 (Skempton and Hutchinson, 1969). The depths to the failure plane are usually in the range 1 to 4 m and the length of the slide is commonly great compared with the depth (Selby, 1993). The surfaces of rupture of translational slides are often broadly channeled-shaped in cross section (Hutchinson, 1988). While the rotation of the rotational slide tends to restore the displaced mass to equilibrium, translation may continue unchecked if the surface of separation is sufficiently inclined.

Translational slides are by far the most common form of landslide occurring in soils. They are always shallow features and have essentially straight slide planes where the form of the failure surface is influenced by the presence of an adjacent stratum of significantly different strength, most of the failure surfaces being likely to pass through the stratum of lower shear strength. The form of the slip surface often follows or would also be influenced by the presence of discontinuities such as faults, joints, fissures, pre-existing slips, foliation or bedding surfaces and contact between rock and soils or different density or permeability. They tend to occur where the adjacent stratum is at a relatively shallow depth below the surface of the slope: the failure surface tend to be plane and roughly parallel to the slope (Craig, 1999). As translational sliding continues, the displaced mass may break up, particularly if its velocity or water content increases. The disrupted mass may then flow, becoming a debris flow rather than a slide.

Unlike the failures which may occur as a result of deep percolation of water, and hence at a considerable time after a rainfall, translational slides nearly always occur during heavy rain. Rain storms with sufficient intensity or duration are required to raise the water-table to near the soil surface or fill pre-existing tension cracks. In low intensity rainfalls the removal of water from the soil by through flow can keep pace with infiltration, and in short duration falls, the field capacity of the soil may not be exceeded. Only when the capacity of the soil to drain is exceeded for long enough for water pressures to rise substantially can the soil lose sufficient strength to fail (Selby, 1993).

Translational slides on single discontinuities in rock masses are called *block* slides (Panet, 1969) or *planar* slides (Hoek and Bray, 1981) (Figure 2.5*a*). If the surface of rupture is formed by two

discontinuities that cause the contained rock mass to displace down the line of intersection of the discontinuities, called *wedge* slide or *wedge* failure (Figure 2.5*b*).

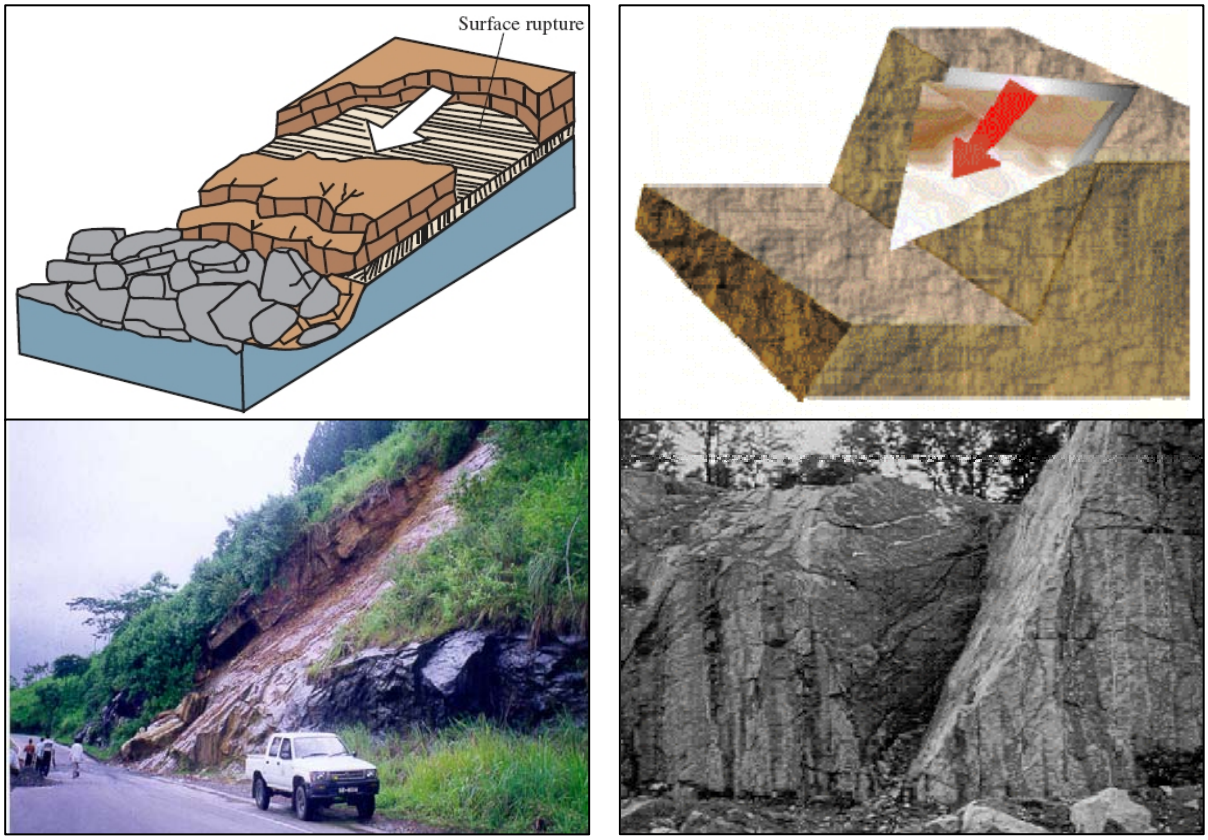

a. Block slide (Planer slide) *b. Wedge slide (failure)*

Figure 2.5: Types of landslides: diagrams showing block and wedge slides.

Compound slides are intermediate between rotational and translational slides and their D_r/L_r ratios reflect this position (Skempton and Hutchinson, 1969). As in the case of translational slides, compound slides tend to occur where there are similar situations in soil profile, but where the adjacent stratum is at greater depth, consisting of curved and plane sections in failure surface.

2.3.4 Lateral spread

Lateral spread is a term referring to landslides that commonly form on gentle slopes and that have rapid fluid-like flow movement, like water (Figure 2.6). The term spread was introduced to geotechnical engineering by Terzaghi and Peck (1948) to describe sudden movements on water bearing seams of sand or silt overlain by homogeneous clay or loaded by fills. According to Varnes, (1996), spread is defined as an extension of a cohesive soil or rock mass combined with a general subsidence of the fractured mass of cohesive material into softer underlying material. In spread, the dominant mode of movement is lateral extension accommodated by shear or tensile fractures (Varnes, 1978). Rate of movement can range from extremely slow to extremely rapid (>5 m/s). Lateral spreads, commonly induced by liquefaction of material in an earthquake.

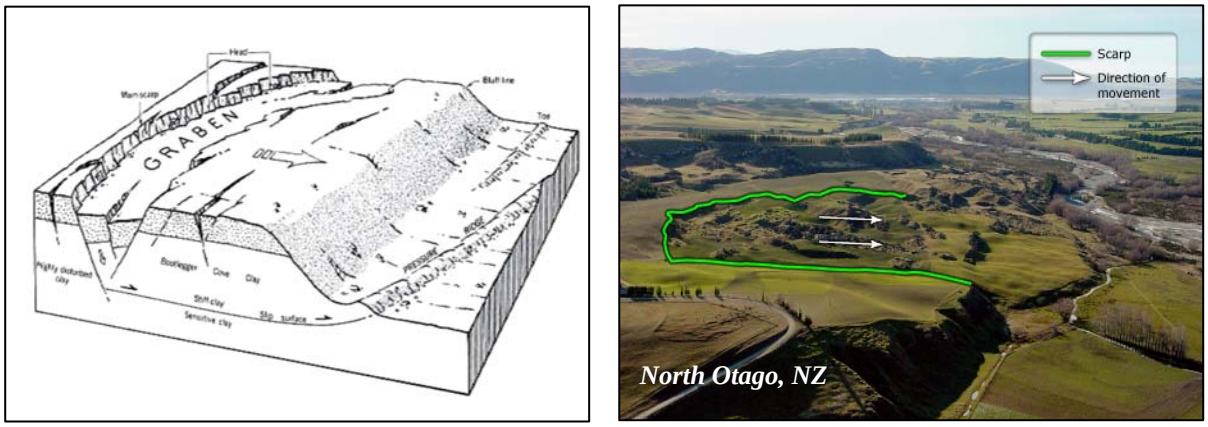

Figure 2.6: Types of landslides: diagrams showing lateral spread (Hansen, 1996).

2.3.5 Flow

A flow is a spatially continuous movement in which surfaces of shear are short–lived, closely spaced, and usually not preserved (Figure 2.7). Flows mobilize as a deforming, viscous mass without a discrete failure plane and occur when coarse debris, fine grained soil, or clay are liquefied. The distribution of velocities in the displacing mass resembles that in a viscous liquid. The lower boundary of the displaced mass may be a surface along which appreciable differential movement has taken place or a thick zone of distributed shear (Cruden and Varnes, 1996). Thus there is a gradation from slides to flows depending on water content, mobility, and evolution of the movement. Debris slides may become extremely rapid debris flows or debris avalanches as the displaced material loses cohesion, gains water, or encounters steeper slopes. The terms rock flows, debris flows, earth flows and mud flows are used according to the material types.

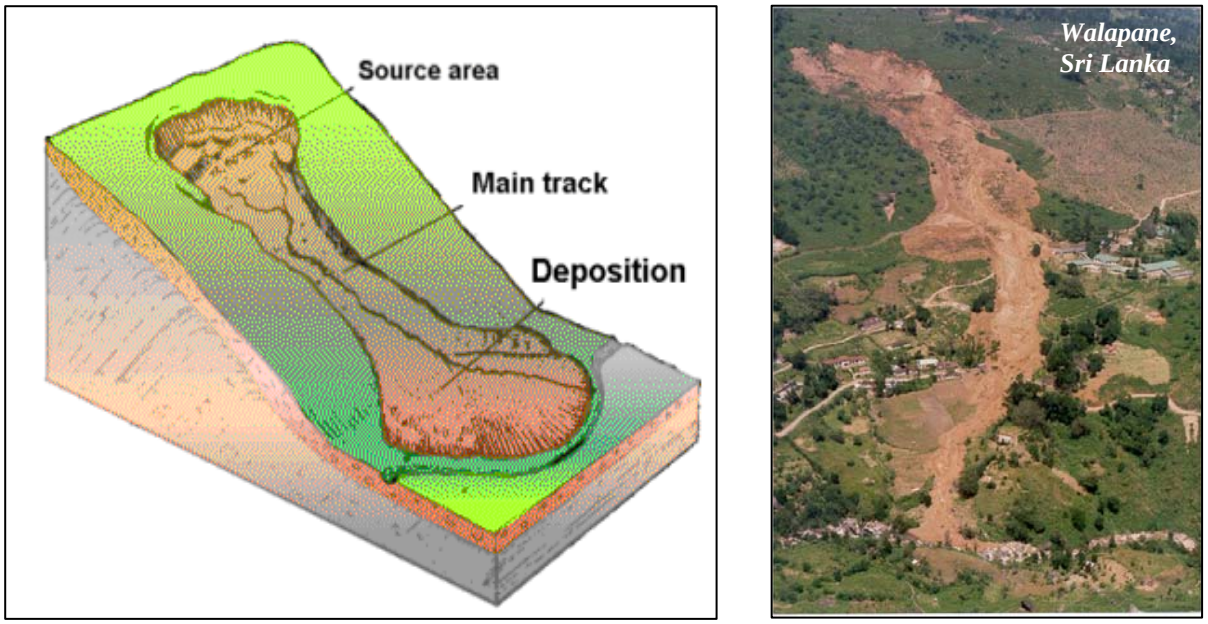

Figure 2.7: Types of landslides: diagrams showing flow.

2.3.6 Complex movements

Complex movement is a combination of two or more principal types of movements. Varnes defined *complex landslides* as those with at least two types of movements. However, it is now suggested that the term *complex* be limited to cases in which the various movements occur in sequence. The term *composite*, formerly a synonym for *complex*, is now proposed to describe landslides in which different types of movement occur in different areas of the displaced mass, sometimes simultaneously.

2.4 Theoretical background and slope stability analyses

Slope stability analysis and designing of appropriate stabilization methods play a major role in geotechnical engineering especially when construction is done on hill slopes. The field of slope stability encompasses the analysis of static and dynamic stability of slopes of earth and rock-fill dams, slopes of other types of embankments, excavated slopes, and natural slopes in soil and soft rock.

Among the modes of slope failures discussed above, slope stability analyses are focused only to slides where movements will always take place along a well defined failure surface remaining the moving material in contact with underlying solid mass. The *translational* and *rotational* are the usually assumed failure surfaces which can be theoretically analyzed. Thus, under this section, the theoretical backgrounds of the movements classified as slides (section 2.3.3) are discussed.

The knowledge of shear strength of a soil and its ability to resist the shear stress is an important part in the solution of many geotechnical problems concerning the slope stability analysis, earth pressure calculations, and ground failure computations and hence it is briefly discussed first.

2.4.1 Shear strength of soil

Slope stability analyses require a quantitative determination of soil shear strength. The shear strength of a soil is the resistance of a soil to failure in shear. The maximum value of the resisting shear at the time of failure is generally taken as the shear strength. This is a fundamental property that governs the stability of natural and constructed hillslopes; however, it is not a unique value but is strongly influenced by loading, unloading, and especially, water content.

If at a point on any plane within a soil mass the shear stress becomes equal to the shear strength of the soil, failure will occur. Thus, in such analysis the soil parameters that describe the behavior of a soil mass during a shear process is of major importance. These parameters can be determined in shear tests when the acting shear forces are increased until failure occurs (Figure 2.8).

The total resistance to shear or strength at failure (τ_f) of a soil was originally recognized and expressed by the French engineer Coulomb in 1776, as a linear function of normal stress (σ_n) on the failure plane. The shear strength of a soil consists of two components, cohesion intercept (c) and internal friction angle (ϕ):

$$\tau_f = c + \sigma_n \tan\phi \qquad (1)$$

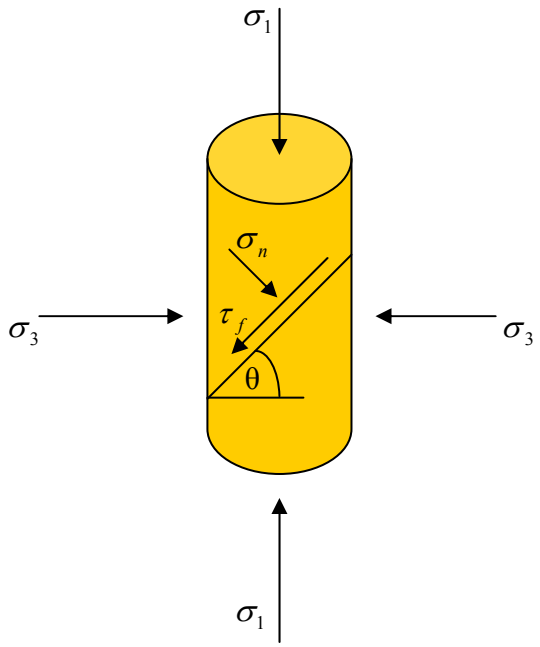

Figure 2.8: Stress conditions at failure (σ_1 and σ_3 are the major and minor principal stresses respectively).

The shear strength behavior of dry non-cohesive soil is determined by the granular skeleton or the so-called grain-to-grain contact. In cohesive soils external stress causes at first a pore water pressure as they are usually saturated with water. If the pore water can drain away, the pore pressure (u) decreases with increasing consolidation time and finally the stress is transferred to the grains. At this stage the stress (pressure) is called effective stress (σ'). Effective stress acting on a soil is calculated from two parameters, total stress (σ_{total}) and pore water pressure (u). At the beginning, pore water takes all the stresses but, at any time in the process the following condition is fulfilled:

$$\sigma_{total} = \sigma' + u \qquad (2)$$

Effective stresses are thus modified by pore water pressure and conditions of loading or testing and are not fundamental properties of the material.

The relationship for effective stress is first proposed by Karl von Terzaghi in 1936. For him, the term 'effective' meant the calculated stress that was effective in moving soil, or causing displacements. It represents the average stress carried by the soil skeleton. In accordance with Terzaghi's fundamental concept that shear stress in a soil can be resisted only by the skeleton of solid particles, shear strength is expressed as a function of effective normal stress (σ'_n):

$$\tau_f = c' + \sigma'_n \tan\phi' \qquad (3)$$

where c' and ϕ' are the shear strength parameters in terms of effective stress and σ'_n is the effective normal stress.

The most realistic position of the critical slip surface can be computed when effective strength parameters are used and when the most realistic pore water pressures are defined. Therefore, in order to find the

position of the critical slip surface, it is necessary to accurately define the soil properties in terms of effective strength parameters.

2.4.2 Methods of slope stability analysis

Experience has shown that the slopes of 1.5 to 1 (horizontal to vertical) are commonly stable. Therefore, such slopes are generally considered the standard for constructions. In many cases, however, the shear strength of the soil is low and hence the gravitational and seepage forces tend to cause instability in natural slopes, as well as slopes formed by excavation and in the slopes of embankments. The result can be a slope failure having a tendency of downward and outward movement of mass on a slip surface or a failure circle under the influence of gravity. In such cases smaller slope inclination has to be chosen. However, steeper slope inclinations are possible and can be found by slope stability analysis when the soil parameters are known. There are many calculation methods for analyzing the slope stability, but the basic idea is always that the active gravity forces or moments are compared with the resistant forces or moments. If the resistant forces prevail over the active forces, the slope is likely to be stable: otherwise a slide may occur. Usually, the stability of a slope is quantitatively expressed in terms of a factor of safety, F_s, where:

$$F_s = \frac{\text{Sum of resisting forces}}{\text{Sum of driving forces}} = \frac{\tau_f}{\tau} \qquad (4)$$

where τ is the shear stress acting down the shear plane due to the weight of the sliding mass.

The sum of resisting forces or effective shear strength at any point acting against the failure in the soil is given by the Coulomb equation (eq. 3). The driving force acting down the slope that may cause slope failure is provided by $Wsin\beta$, where W is the weight of the sliding mass and β is the slope angle.

When the forces promoting stability are exactly equal to the forces promoting instability $F_s = 1$, called critically stable; when $F_s < 1$ the slope is in a condition for failure; when $F_s > 1$ the slope is likely to be stable. However, the F_s is not an absolute indicator of slope failure, only an increasing the probability of stability as the value of F_s becomes larger because of the model assumptions and possible errors in the parameters. Most natural hill slopes upon which landsliding can occur have F_s values between about 1 and 1.3 (Selby, 1993), but such estimates depend upon an accurate knowledge of all the forces involved. For practical purposes design decisions always adopt very conservative estimates of stability. For more accurate analysis, the influence of ground water (seepage) with various types of failure surfaces (plane failure, circular, circular cylindrical failure) should be known. In most cases, slope stability can be considered as a two dimensional problem assuming conditions of plane strain.

To quantify the stability of slopes with the available data, *deterministic* and/or *probabilistic* approaches can be used. The deterministic approach adopts the *factor of safety* (F_s) as the index of stability, while the probabilistic method adopts the *probability of failure* (P_f) as the index of stability.

In deterministic analyses we define a *factor of safety* based on an appropriate potential failure mechanism. It is a number which in traditional calculation methods is arrived at without a consideration of various uncertainties associated with input data. Hence, accuracy of the determined factor of safety depends

directly on the accuracy of the input data. Commonly used analytical methods are *limit equilibrium, limit analysis* and *finite element*.

However, most of the input data such as physical properties of the soil (c', ϕ', γ_{soil}), pore water pressures (u) and even the slope and failure plane geometry are subjected to uncertainties. They can not be precisely known and therefore considered as random variables having a distribution of values for each of the parameter. Hence, calculated factor of safety itself becomes a random variable having its own distribution. A probabilistic approach is based on this concept that various out comes of a situation is possible recognising the uncertainties associated with input data. Thus, in order to pursue the probabilistic approach, statistical description of the data is necessary. Under this approach, first the stability of the slope is analysed using a conventional limit equilibrium method. Thereafter probability techniques are used giving consideration to the reliability (accuracy) of various input parameters and the *probability of failure* is estimated. The probability of failure is the probability that the factor of safety is less than or equal to unity. Its value reflects the magnitudes of significant parameters as well as their respective uncertainties. For instance, in probabilistic analysis, a Monte Carlo simulation is a procedure which allows each of the variables to be changed simultaneously according to some well defined rules.

In practice, limit equilibrium methods are widely used in the analysis of slope stability in spite of the limitations inherent in the method. The method is based purely on the principles of static with a single, constant factor of safety and says nothing about displacement. It is considered that failure is on the point of occurring along an assumed or a known failure surface. The shear strength required to maintain a condition of limiting equilibrium is compared with the available shear strength of the soil, giving the average (lumped) factor of safety along the failure surface (Craig, 1999). Inherent in limit equilibrium stability analyses is the requirement to analyze many trial slip surfaces and find the slip surface that gives the lowest factor of safety. In the analysis of natural slopes where the potential slip surface does not have sharp corners and there are no high stress concentrations, the conventional limit equilibrium method is more than adequate in spite of its limitations (Krahn, 2004).

2.4.3 Stability analyses of shallow translational slides

For simplicity, an infinite slope is assumed to evaluate the initiation mechanisms of slope failures. Translational slides are usually analyzed by this method which is a two dimensional analysis of a slice on the sides of which the forces are taken as being equal and opposite in direction and magnitude.

It is assumed that the slip surface is planer and parallel to the slope and the mobile slice is uniform in thickness resting on a slope of constant angle and infinite extent. This dispenses with the need to consider side and end effects, and is justified as translational slides are long in relation to their depth and width and are often uniform in cross section. This mode of analysis was employed by Skempton and De Lory (1957).

The forces acting at a point on a shear plane of a potential shallow slide are illustrated in Figure 2.9 and 2.10. The gravitational stress acts vertically, the normal stress is normal to the shear plane and is partly opposed by the up thrust or buoyancy effect of pore water pressure (u); the shear stress acts down the shear plane and is resisted by the shear strength of the soil.

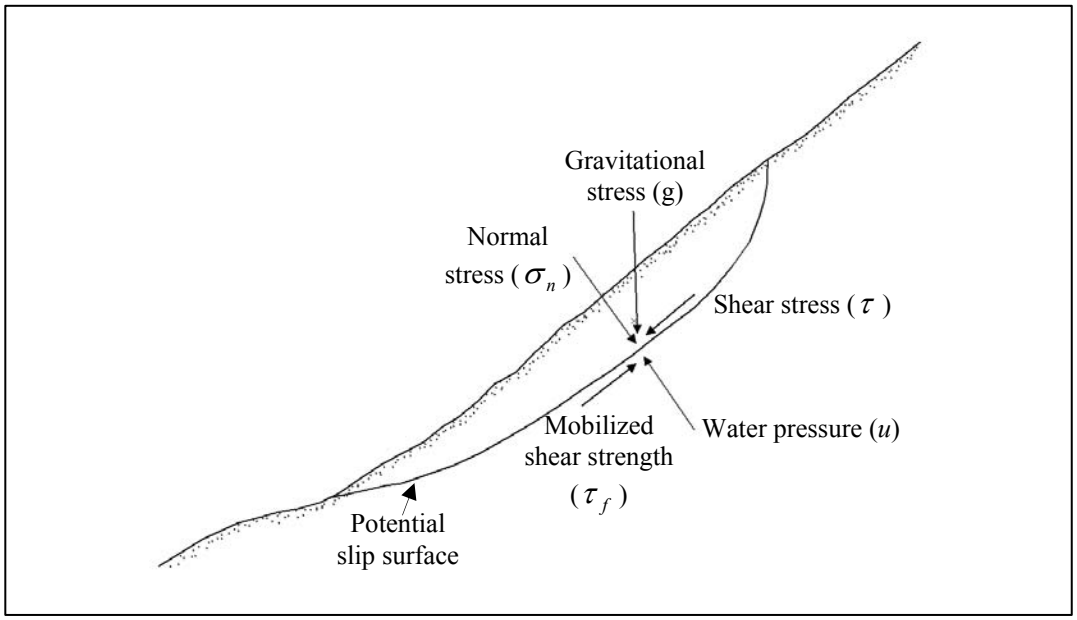

Figure 2.9: Forces acting at a point on a potential failure plane (prepared on the basis of Selby, 1993).

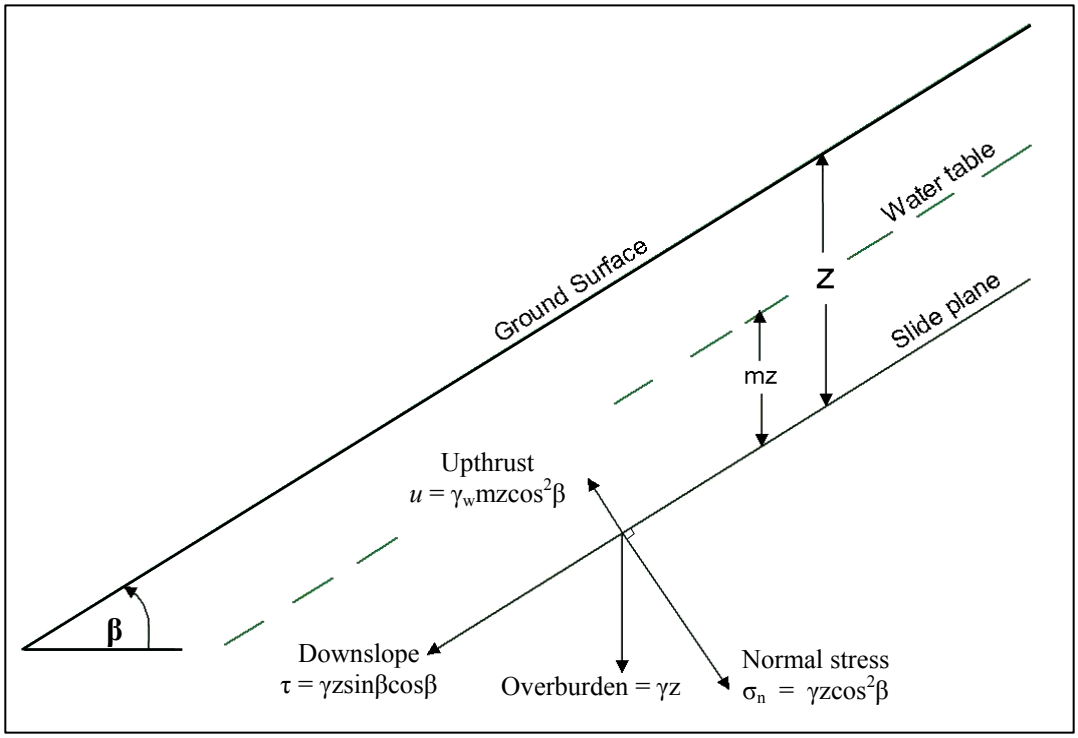

Figure 2.10: Stresses acting on a slope which is identified in an infinite slope analysis of translational landslide (γ_w = unit weight of water, γ = unit weight of the soil at natural moisture content; prepared on the basis of Selby, 1993).

The factor of safety is given by:

$$F_s = \frac{\left[c' + \left(\gamma z \cos^2 \beta - u\right)\tan\phi'\right]}{\gamma z \sin\beta \cos\beta} \qquad (5)$$

It is convenient to express the vertical height of the water table above the slip plane as a fraction of the soil thickness (z) above the sliding plane and this is denoted by m. Pore-water pressure on the slide plane, assuming seepage parallel to the slope, is then given by:

$$u = \gamma_w m z \cos^2 \beta \qquad (6)$$

thus

$$F_s = \frac{\left[c' + (\gamma - m\gamma_w) z \cos^2 \beta \tan \phi'\right]}{\gamma z \sin \beta \cos \beta} \qquad (7)$$

Where there is not a continuous water table with flow parallel to the soil surface an alternative form of analysis must be used.

Under most conditions the free soil water level can not rise above the soil surface and the pore pressure (u) is given by:

$$u = \gamma_w h \qquad (8)$$

where h is the piezometric height or the height to which water will rise in a stand pipe, inserted in the soil to the depth of the failure plane. Where seepage is not uniform, and directed out of the slope, it is convenient to use the ratio r_u between pore pressure and the weight of a vertical column of soil:

$$r_u = u / \gamma z, \text{ thus } u = r_u \gamma z \qquad (9)$$

The equation for determining the factor of safety then becomes (Haefli, 1948):

$$F_s = \frac{\left[c' + (\gamma z \cos^2 \beta - r_u \gamma z) \tan \phi'\right]}{\gamma z \sin \beta \cos \beta} \qquad (10)$$

Substituting $\gamma_w h / \gamma z$ for r_u this becomes:

$$F_s = \frac{\frac{c'}{\gamma z} + (\cos^2 \beta - \frac{\gamma_w h}{\gamma z}) \tan \phi'}{\sin \beta \cos \beta} \qquad (11)$$

Under most conditions the highest pore pressures will exit when ground water level is at the surface. As γ is usually about $2\gamma_w$ the corresponding value of r_u is approximately 0.5.

2.4.4 Stability analyses of rotational landslides

Deep rotational landslides are confined to clays and clay-rich soil, and do not occur in sands, because the strength of a soil due to cohesion only is not controlled by overburden pressure. Values of frictional strength for both clay and sand increase in proportion to the normal stress acting on a potential failure plane within a soil, thus for a frictional soil, strength increases with depth. In frictional materials the rate of strength increase with depth exceeds the rate at which shear stress increase and deep failures can not occur. For clays shear stresses may increase more than strength for each increment in depth, hence deep seated failures are possible, especially for clays in which $\phi_u = 0$ (Selby, 1993).

Rotational failures may be treated as a series of vertical slices (Figure 2.11) for each of which a modified infinite slope analysis is carried out and the values for each slice are then summed. Many different solution techniques for the method of slices have been developed. Basically all are very similar. The differences between the methods are what equations of static are included and satisfied, which inter-slice forces are included and what is the assumed relationship between the inter-slice shear and normal forces.

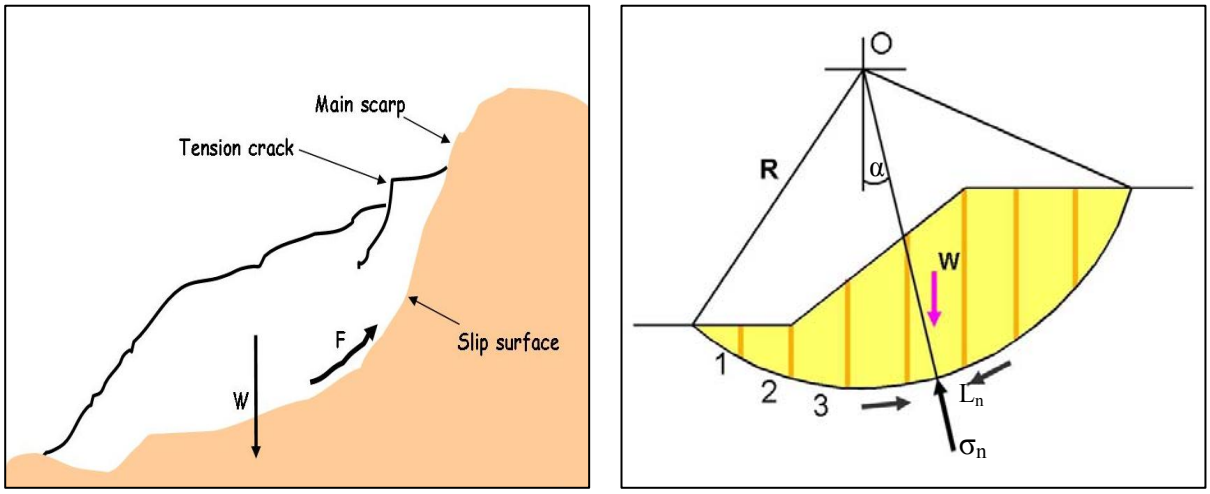

Figure 2.11: Geometry of a rotational slide and a trial slip circle. In the trial slip circle slipping mass is divided into slices and numbered as 1, 2, 3, etc., W – vertical load due to the slice, L_n – base length of a slice, R - radius of the slip circle, O – center of the slip circle, F – resisting forces.

The method of analysis by slices was first proposed by Fellenius (1936) and named after him. Alternatively it is called the Ordinary or Swedish Method of Slices. The method ignores all inter-slice forces and satisfied only moment equilibrium. Adopting these simplified assumptions made it possible to compute a factor of safety easily using hand calculations which was important at that time.

But, the value of F_s derived by this way is often 10 to 15 percent below the value derived by more rigorous methods and may be even more in error in certain cases (Whitman and Beiley, 1967). Most of the errors occur in the treatment of pore water pressure; some errors occur because of the method's assumption that all side forces on each slice act in a direction parallel to the failure plane and that normal forces are assumed to act at right angles to the failure plane. The Fellenius Method treats each slice as though it were nearly rectangular, but with increasing curvature of the failure plane this becomes an untenable assumption.

For a slice with a curved base and an upper surface which is not parallel to the failure plane, corrections have to be made. As a result an alternative method was proposed by Bishop (1955) and this was simplified by Janbu et al. (1956). The Simplified Bishop Method of Slices assumes that forces acting on each slice are in a horizontal and vertical direction. This assumption is not entirely valid but the method has been shown to provide values of F_s which are in the range of values derived by more rigorous methods and are seldom more than 2 percent in error.

The formula for the Simplified Bishop Method is:

$$F_s = \frac{\sum_{i=1}^{i=n}\left[c'b + (W - ub)\tan\phi'\right] * \left[1 / \left\{\cos\alpha\left(1 + \frac{\tan\alpha\tan\phi'}{F_s}\right)\right\}\right]}{\sum_{i=1}^{i=n}\left[W\sin\alpha\right]} \qquad (12)$$

where "*b*" is the horizontal width of the slice. In the equation, F_s appears on both sides making the equation nonlinear and hence requiring iterative procedure to calculate it.

The advent of electronic computers in the 1960s made it possible to more readily handle the iterative procedures inherent in the limit equilibrium method. This led to solve mathematically more rigorous formulations which include all inter-slice forces and satisfy all equations of statics. Two such methods are those that developed by Morgenstern and Price (1965) and by Spencer (1967).

A general limit equilibrium method (GLE) formulation was developed by Fredlund et al. in the 1970s (Fredlund and Krahn, 1977; Fredlund et al., 1981). This method encompasses key elements of most of the methods and provides a framework for discussing, describing and understanding all other methods. The GLE formulation is based on two factor of safety equations and allows for a range of inter-slice shear-normal force assumptions. One equation gives the factor of safety with respect to moment equilibrium *(F_m)* while the other equation gives the factor of safety with respect to horizontal force equilibrium *(F_f)*. The idea of using two factor of safety equations follows from the work of Spencer (1967) and the inter-slice shear forces here are handled with an equation proposed by Morgenstern and Price (1965).

In general, the main differences between all above methods are in the way they assess or handle the inter-slice forces; there is little to choose between them in their accuracy and hence the established methods give closely corresponding values of F_s (Fredlund and Krahn, 1977).

Modern limit equilibrium software for instance SLOPE/W, are making it possible to handle ever increasing complexity in the analysis. It is now possible to deal with complex stratigraphy, highly irregular pore water pressure conditions, a variety of linear and non linear shear strength models, virtually any kind of slip surface shape, concentrated loads, and structural reinforcement. Therefore, it is now easy to use one of the mathematically more rigorous methods than to use the simpler methods that only satisfy some of the statics equations.

2.5 Limitations and alternative forms of analysis to natural hill slopes

Despite the fact that the methods and approaches discussed above can handle now more complex situations, the application of semi-quantitative stability analyses to natural hillslopes has difficulties and limitations which tend to reside in two general areas: (1) difficulties in characterising and assessing the variability of factors that influence slope stability, and (2) inappropriateness of the inherent limit equilibrium methods for certain types of slope failures or strain conditions.

The uncertainties in analysis can arise for many reasons, but particularly by the followings: (1) the physical properties of the soil may vary from point to point along the failure plane; (2) the shape of the failure plane may not be known with certainty and it may vary from a simple planar or circular form; (3) pore-water pressures may vary in unknown or unpredicted ways; (4) the forces acting between slices may be significantly large; and (5) the assumption that stresses at the lateral margins of the slide can be ignored may be invalid (Selby, 1993).

All of the soil, topographic, geotechnical, and hydrological properties that affect stability analyses exhibit some level of anisotropy and heterogeneity in field sites. Additionally some parameters may vary over time or related to wetting conditions. The greatest uncertainties are usually associated with soil water, especially with its local variability of pressure and seepage. It varies with environmental conditions and consequentially with time. Such natural variability can lead to errors in stability calculations and therefore; the stability can only be evaluated for a certain point in time (Krahn, 2004).

Most studies or summaries of the spatial variability of soil shear strength parameters indicate that cohesion (c) is more variable than friction angle (ϕ). Given that factor of safety is more sensitive to cohesion than friction angle for typical ranges encountered in the field (Gray and Megahan, 1981; Sidle, 1984b), and given the generally higher natural variability in cohesion measured in most studies, it is apparent that variations in cohesion may strongly affect slope stability calculations.

Variability of soil properties that influence water movement and the dynamics of pore water pressure can strongly affect the stability of materials with friction strength. Numerous investigations have reported that most soil hydrologic properties such as hydraulic conductivity (K), infiltration capacity, and water flux are log-normally distributed and such variability is enhanced by the effect of macro pores and interconnected preferential flow pathways. Measurements of pore water pressure in unstable hillslopes indicate a high degree of spatial variability that may be affected by local site conditions such as preferential flow paths, anisotropic K values, bed rock unconformities, soil heterogeneities, and topography. Given the strong influence of pore water pressure on slope stability calculations, the temporal and spatial variability needs to be considered.

Also many field investigations have shown that soil depth can vary up to an order of magnitude over several meters of slope distance. As the calculations of factor of safety are very sensitive to soil depth (e.g., Gray and Megahan, 1981), these variations need to be considered. Variations in soil bulk density (or unit weight) are generally not as high as other parameters and, given the relative insensitivity of factor of safety to typical ranges of unit weight, realistic average values can often be applied.

One possibility to overcome the problems associated with input data is to use probability-based approach where such uncertainties can be incorporated; however, such modeling approaches cannot hope to capture

the spatial locations of actual landslides. Therefore, where uncertainties in stability analyses exist, better estimates of slope stability may be obtained from mapping the *susceptibility* of slopes to landsliding than from an approach based upon a study of the forces involved in instability. Landslide susceptibility maps seek to identify potential failure areas by mapping old landslide features and factors likely to cause failure in the future. The most probable sites for new landslides in susceptibility mapping are areas where sliding has occurred already, or areas which are similar to those where landslides have occurred.

Also, in the case of widespread landslides occurrences where typically happen rather frequently and have relatively small individual volumes, generally preclude high cost geotechnical analysis and, particularly, structural control measures. Further more, many of the highest risk landslide regions are in developing countries where both technical expertise and financial resources are limited. Thus, there is a need to develop and implement alternative landslide assessment methods for areas where certain critical data may be lacking, high cost technology is unavailable (Sidle and Ochiai, 2006), extent of landslide distribution is large and prediction of spatial distribution of future landslide occurrences is vital.

3 Slope instability hazard zonation and GIS

3.1 Overview and definitions

A great deal of research concerning slope instability hazard has been done over last four decades. Initially the investigations were oriented mainly towards solving problems at particular sites. Therefore, most researches emphasized site specific investigation techniques and the development of deterministic and probabilistic models. However, the heterogeneity of the natural environment and the large variability in geotechnical properties at the regional scale are in sharp contrast to the homogeneity required by deterministic models. This contrast, coupled with the costly and time consuming site investigation techniques makes such engineering approaches inappropriate for application over large areas. Furthermore, development projects in large areas must often be assessed during an early phase of planning and decision making process. In addition, many parts of hill slope where people have already settled without the knowledge of associated risk need to be spatially investigated. Hence, such planning and decision making activities in large areas need alternative methods of landslide assessments that provide appropriate guidelines for future development and disaster management plans. Conventional as well as pragmatic response to the above context is the estimate of spatially distributed slope stability by mapping the *susceptibility* or *hazard zonation* of slopes to landsliding. Under this concept, several analysis techniques that provide slope stability assessment based on a careful study of natural conditions of an area and analysis of all the possible parameters involved in slope instability processes have been developed.

Landslide susceptibility is a measure of how prone land units are to landsliding or in other expression the slope stability condition of a particular region. The susceptibility usually expresses only the likelihood that a phenomenon will occur in an area on the basis of the local terrain conditions without any temporal implications. Therefore susceptibility map shows zones with similar terrain conditions for landslide processes. According to Varnes (1984) *landslide hazard zonation* (LHZ) is defined as the mapping of areas with an equal probability of occurrence of landslides in a given area within a specific period of time. This includes assessment of terrain parameters for the likelihood of occurring such phenomenon (susceptibility) and the determination of the probability that a triggering event such as major rain fall or earthquake occurs. However, probability of occurrence of landslide is extremely difficult to determine especially for large areas, due to lack of simple relation between the magnitudes of landslide events and return periods, and reliable historic records of landslide dates and triggering events. Hence, hazard analysis is seldom executed in accordance with the definition given above (Soeters et al., 1996). Therefore in most hazard maps the legend classes generally do not give more information than the susceptibility of certain areas to landsliding or relative indications of the degree of hazard, such as high, medium and low. In most cases, the term hazard and susceptibility is frequently used synonymously or interchangeably.

Either it is susceptibility or hazard zonation, the procedure primarily required to: (1) identify the causative factors that are related to landslides, (2) estimate the relative contribution (degree of influence) of factors causing slope failures, (3) establish relationships between the factors and landslides occurrence and, (4) predict the future landslide events based on such relationships. That means one must look at the conditions under which landslides have occurred in the past, and use the critical combinations of factors for predicting the possible occurrence of landslides where comparable terrain conditions prevail, but

which are still landslide free. An area is then declared to be susceptible when the terrain conditions at a site are comparable to the areas where landslides occurred.

The occurrence of slope failures depends generally on complex interactions among large number of partially interrelated factors. Hence, analysis of landslide susceptibility (or hazard) requires evaluation of relationships between a variety of spatially dependent terrain conditions and spatial representation of landslides. A geographic information system (GIS) allows for the storage and manipulation of information concerning the different terrain factors as distinct data layers and thus provides an excellent tool for slope instability hazard zonation (Soeters et al., 1996). A geographic information system is defined as a "powerful set of tools for collecting, storing, retrieving at will, transforming, and displaying spatial data from the real world for a particular set of purposes" (Burrough, 1986). Generally a GIS consists of the components of data input and verification, data storage and data-base manipulation, data transformation and analysis, and data output and presentation. An ideal GIS for landslide hazard zonation combines conventional GIS procedures with image-processing capabilities and a relational data base. The system should be able to perform spatial analysis on multiple-input maps and connected attribute data tables. Necessary GIS functions include map overlay, reclassification, interpolation and a variety of other spatial functions incorporating logical, arithmetic, conditional, and neighborhood operations. In many cases landslide modeling requires the iterative application of similar analyses using different parameters. Therefore, the GIS should allow for the use of batch files and macros to assist in performing these iterations (Soeters et al., 1996).

As compared with conventional techniques, by means of GIS, a much larger variety of analysis techniques became attainable. Because of its speed of calculations, complex techniques requiring a large number of map overlays and table calculations became feasible. It also provides the possibility to improve models by evaluating results and adjusting the input variables. Here, user can achieve the optimum results by a process of trial and error, running the models several times which was difficult to achieve even once in the conventional manner. Therefore, more accurate results can be expected. In the course of a landslide hazard assessment project, the input maps derived from field observations can be progressively updated when new data are collected. Prepared data can be used by many users in an effective manner although the data entry (digitizing) is time consuming work.

3.2 Landslide causative factors and triggering events

In the process of evaluation of landslide hazard, knowledge of triggering events and causative factors is an imperative step. The difference between these two concepts is subtle but important. Generally, the phenomenon of landslide is directly associated with one or more triggering events. However, all the slopes which experience a certain triggering event at a time do not befall to be unstable. That implies, there are other factors which control the stability of slopes and, only the slopes which satisfy the critical combination of such factors will fall into sliding. Thus, causes combine to make a slope vulnerable to failure, and the trigger finally initiates the movement.

The causative factors that make the slope vulnerable to failure are the reasons that a landslide occurred in a particular location and are usually related to instabilities in slopes. They include geological, morphological, physical factors and factors associated with human activities. Some of the commonly known causative factors used in landslide analysis are lithology and the structural attitude of the bed rock,

weathering condition, soil properties and their thickness, slope gradient, land form, hydrological condition and drainage and land use and management.

There are some occasional cases that the trigger can not be determined due to results of some unknown processes or in fact a slow but steady decrease in material strength associated with the weathering of the rock that can not be detectable externally. However, mostly a trigger is an external stimulus such as intense rainfall, earthquake shaking, volcanic eruption, rapid snow melt, rapid change of water level, storm waves or rapid erosion that induce an immediate or near-immediate response in the slope materials by altering the stress condition within it.

Some authors describe landslide causes as "internal" and "external" referring to modifications in the conditions of the stability of the bodies. While the internal causes induce modifications in the material itself which decrease its resistance to shear stress, the external causes generally induce an increase of shear stress of the slope material, so that block or bodies are no longer stable resulting in shear failure along a slip surface.

Furthermore, the factors that form the basic characteristics of slopes that are prone to failure and need time to change are called primary causes, and include mainly geomorphic and geologic factors, and soil properties of the hill slope material (Sidle and Ochiai, 2006). They can be considered as static in nature for short time periods (static factors). Various kind of external factors that undergo changes within a short period of time such as fluctuation of ground water levels, ground motions or vibrations, etc., which affect the shear stress of the slope material, are the immediate causes of landslides. They are due to the result of triggering events and hence undergo changes within a short period of time (dynamic factors).

3.3 Analyses approaches and use of GIS

Various analyses approaches such as *heuristic* in which the degree of hazard (susceptibility) is determined by the mapping expert, *statistical* such as *bivariate* and *multivariate* techniques and, *deterministic* models have been proposed in literature.

Heuristic (knowledge driven) approach is an experience-based approach where direct or semi direct mapping methodology is followed. The hazard (susceptibility) levels are determined directly in the field by a landslide expert or by qualitative weightings of different causative factors using an expert knowledge about the existing landslides and their terrain conditions. The methods rely heavily on the professional experience, skills and commitments of the expert. Systematically collected data in GIS analysis can support the expert opinion and can be used to establish weight values for variables. However, final decision rules are mainly subjective and hence reasons for such rules can not be presented and output offers less reproducibility. Moreover, GIS can be used here as a drawing tool allowing rapid recording and editing of the data.

Statistical (data driven) and *deterministic* (theoretical models) approaches are quantitative methods where indirect mapping methodologies are followed. A model is determined basically by input data. Hence, in contrast to heuristic approach, the methods here depend on quality and accuracy of input data. Decision rules are mainly objective and reasons for such rules can be presented. Also, out put provides better reproducibility (can be progressively updated).

In the *statistical* approach numerical relationships among the observed landslide distribution and their controlling terrain factors are made. All possible terrain parameters can be entered into GIS and crossed for their analysis with a landslide distribution map. Both *bivariate* as well as *multivariate* techniques can be employed to examine each factor separately or several factors together, respectively, in combination with the presence or absence of landslides (Soeters and van Westen, 1996). Most approaches assume that landslides are more likely to occur under conditions similar to those of previous failures (Brabb, 1984; Varnes, 1984). It also assumes that causative factors for the mapped landslides remain constant over time (static).

In the *bivariate* analysis, each factor is evaluated separately (Figure 3.1). The method utilizes the normalized landslide densities derived using the landslide occurrence in each factor class for calculating weight values. Information value method (Yin and Yan, 1988; Kobashi and Suzuki, 1988) and weights of evidence modeling (Spiegelhalter, 1986; Bonham-Carter et al., 1990) are two common bivariate methods applied in LHZ mapping. Chung and Fabbri (1993) described several other methods, including Bayesian combination rules, Certainty factors, Dempster-Shafer belief function, and Fuzzy logic interpretation. Each method has its specific rules for data integration for producing total hazard map.

The *multivariate* analyses consider the interrelationships amongst factors in terms of selection and weighting (Figure 3.2). Since many input maps in LHZ are categorical variables, they must be first converted to numerical values. This can be done within the GIS environment by converting them into presence or absence (binary 0s and 1s) values or percentage cover within the predefined sample units, or ranking the parameter classes according to landslide density. A matrix that is created including landslides and all variables can be then analyzed using an external statistical package. Commonly used multivariate statistical methods in landslide hazard assessment are multiple regression, discriminant analysis and logistic regression. Multivariate methodology is typically data driven and therefore highly objective.

In general, the bivariate techniques are mostly preferred over multivariate ones as they enable to combine the professional experience of the expert into the process by selecting parameters subjectively. Also it provides the possibility of handling the analysis within the GIS environment itself unlike in multivariate techniques where usually external statistical packages are still needed.

Despite the problems related to collection of sufficient and reliable input data, *deterministic* approaches are increasingly used in landslide hazard analysis of large areas, especially with the aid of GIS (Figure 3.3). They use sound physical models such as slope stability models and hydrological models to express the hazard in the form of safety factors. In hydrological modeling and in slope stability calculations GIS can play an important role because of its computational power, and the elaboration of digital elevation models (DEMs) and derived maps such as slope maps, aspect maps and slope length maps (Wadge, 1988).

The main problem with deterministic models is their high degree of simplification. A deterministic method that is usually applied for translational slides is the infinite slope model (Ward et al., 1982) since they are simple to use for each pixel separately within the raster GIS environment. Hammond et al. (1992) presented methods in which the variability of the factor of safety is calculated from selected input variables utilizing Monte Carlo techniques. This implies a large number of repeated calculations, which are readily supported by use of a GIS (Soeters and van Westen, 1996).

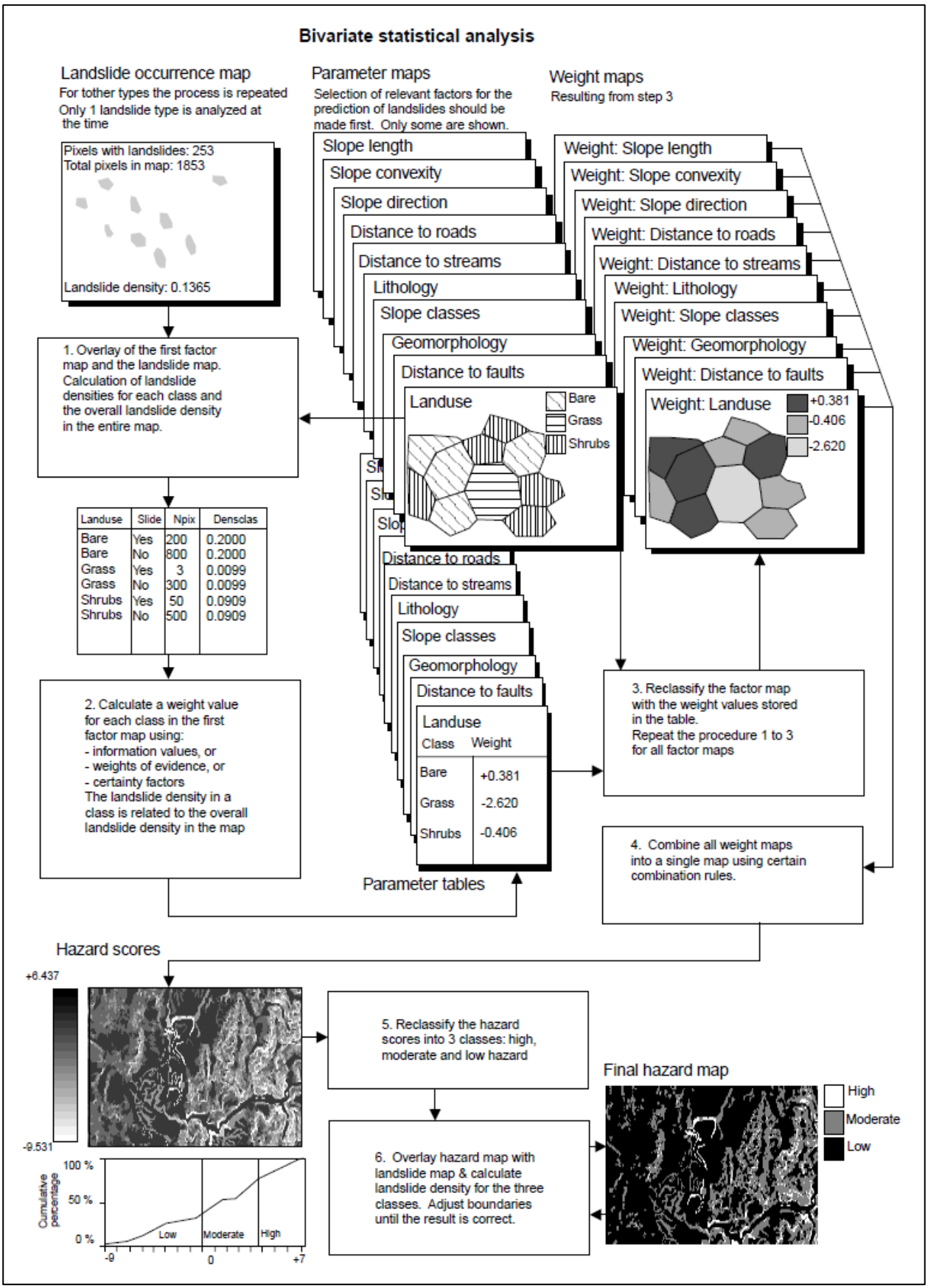

Figure 3.1 Procedure for GIS based bivariate landslide hazard analysis (Van Westen et al., 1997).

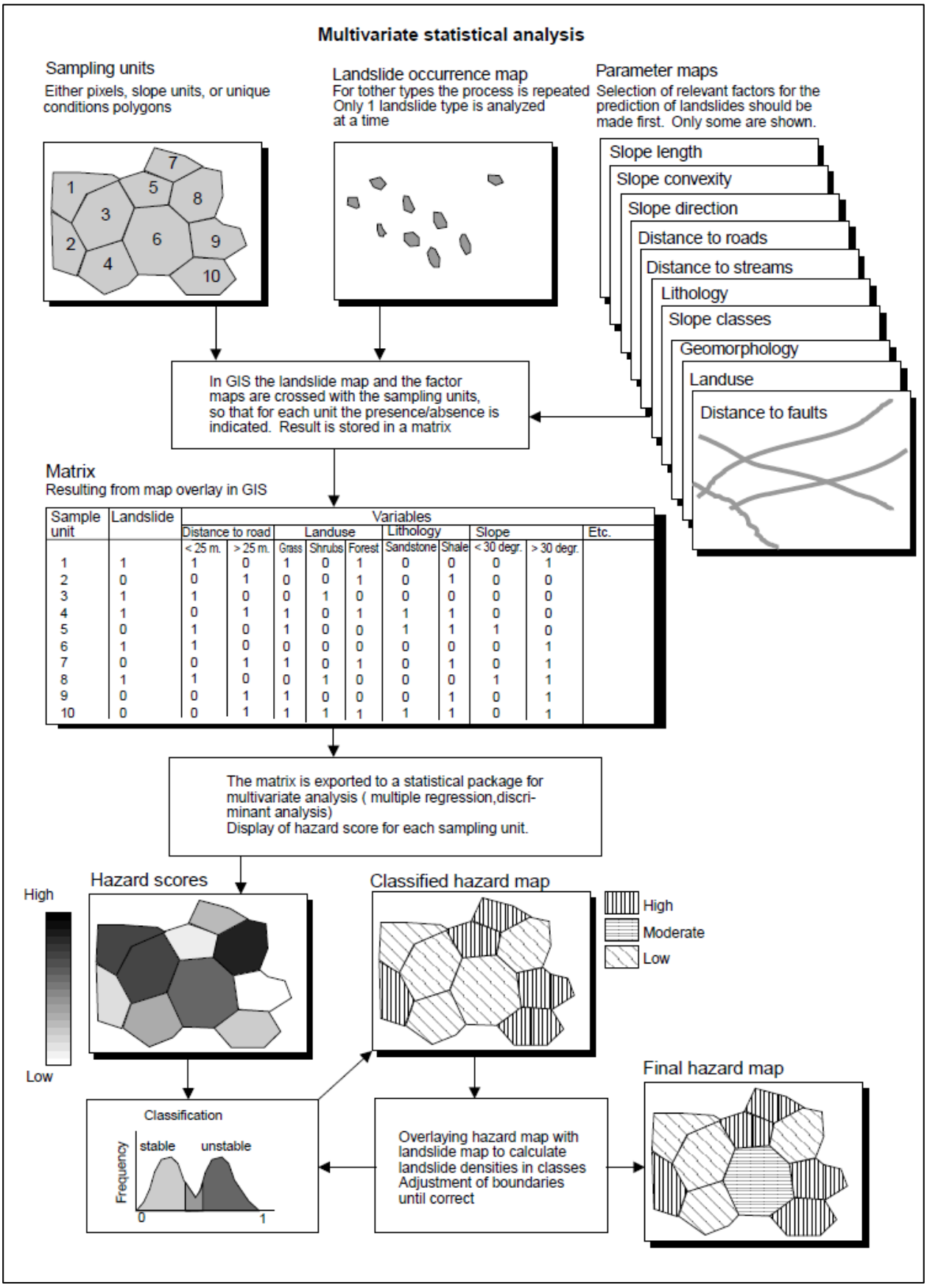

Sample unit	Landslide	Variables									
		Distance to road		Landuse			Lithology		Slope		Etc.
		< 25 m.	> 25 m.	Grass	Shrubs	Forest	Sandstone	Shale	< 30 degr.	> 30 degr.	
1	1	1	0	1	0	1	0	0	0	1	
2	0	0	1	0	0	1	0	1	0	0	
3	1	1	0	0	1	0	0	0	0	0	
4	1	0	1	1	0	1	1	1	0	0	
5	0	1	0	1	0	0	1	1	1	0	
6	1	1	0	0	0	0	0	0	0	1	
7	0	0	1	1	0	1	0	1	0	1	
8	1	1	0	0	1	0	0	0	1	1	
9	0	0	1	1	0	0	0	1	0	1	
10	0	0	1	1	1	1	1	1	0	1	

Figure 3.2 Procedure for GIS based multivariate landslide hazard analysis (Van Westen et al., 1997).

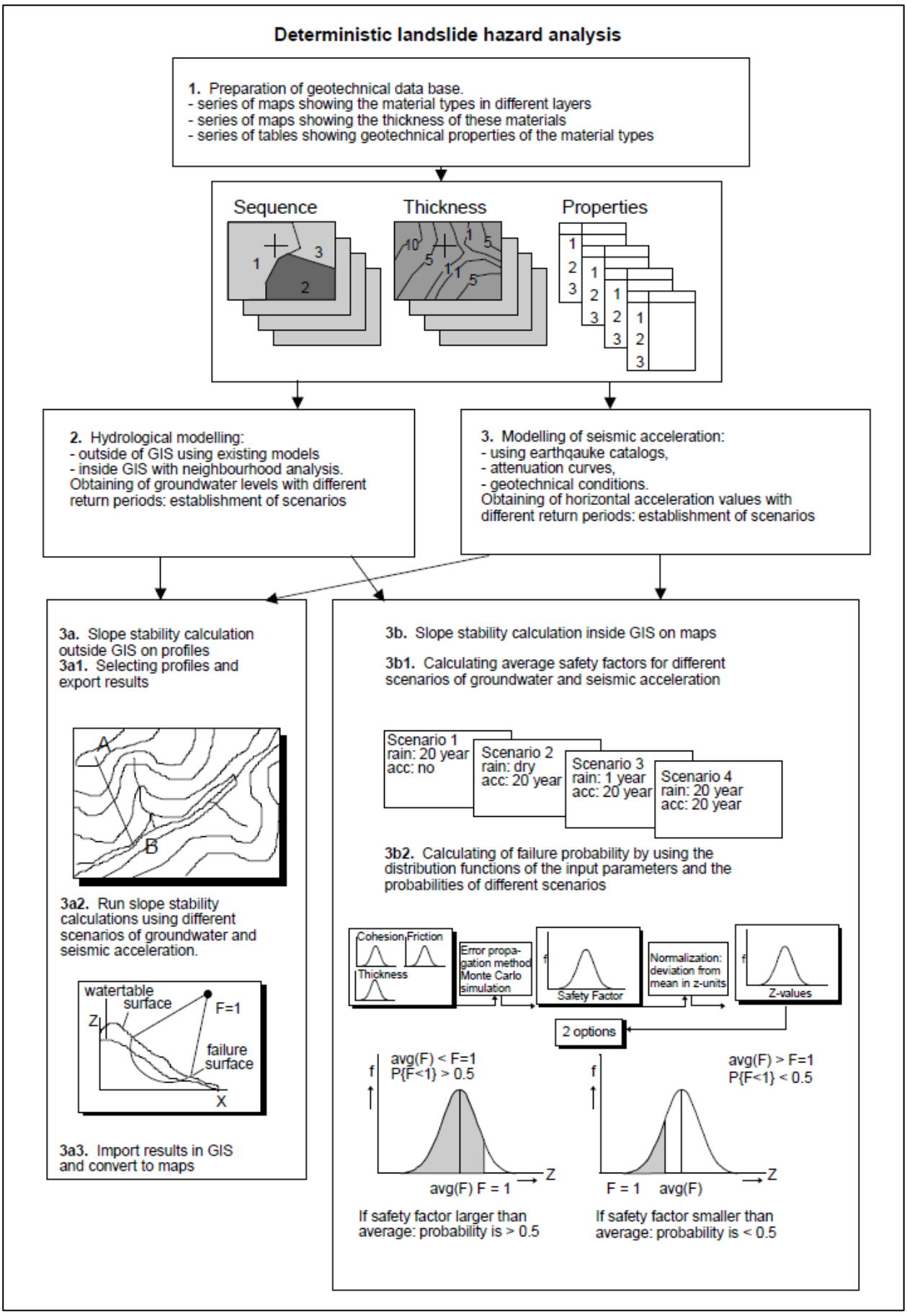

Figure 3.3 Procedure for GIS based deterministic slope stability analysis (Van Westen et al., 1997).

3.4 Types of landslide hazard mappings

According to Sidle and Ochiai (2006) landslide hazard models can be roughly divided into four categories:

(1) terrain hazard mapping
(2) simple rainfall-landslide and earthquake-landslide relationships
(3) multi factor, empirical landslide hazard assessments
(4) distributed, physically based models

Some of these methods are more amenable to assessing relative landslide hazard at regional scales, others can be used as predictive tools for more specific sites, and yet others can be used to develop real time warning systems.

3.4.1 Terrain hazard mapping

Terrain hazard mapping represent a somewhat general and qualitative level of landslide hazard assessment; topographic, geomorphic, and geologic information are utilized, as well as data on pre-existing landslides to generate maps with broad categories of landslide hazards. The identification of landslide hazard locations and downstream impact zones is somewhat subjective. Typically, such hazard mapping is developed or implemented by management agencies or regional governing bodies to evaluate the effect of various land-uses on the occurrence of landslides. Thus, the main focus may not be to predict landslide occurrence, but rather to reduce the risk of landslides hazard related to a particular land-use. For instance, such mapping procedures have been developed in Western Oregon (Oregon Department of Forestry, 2003) and British Columbia (British Columbia Ministry of Forests, 1995) to evaluate plans for timber harvest and road construction in areas susceptible to shallow, rapid landslides.

Recent advances in remote sensing techniques and the development and application of digital elevation models (DEMs) can improve terrain hazard mapping, especially when processed within geographic information systems (GIS). In particular, satellite imagery and light detection and ranging (Lidar or air borne laser scanning) are useful for assessing landslide locations as well as developing detailed DEMs and hillshade maps. High resolution DEMs produced from airborne laser altimetry can be used to assess surface characteristics of active and dormant landslides as well as delineating detailed topographic information useful in predicting areas of future landslides.

3.4.2 Simple rainfall-landslide and earthquake-landslide relationships

Landslide hazard assessment based on simple relationships with rainfall characteristics has been applied at both global and regional scales. When coupled with real time rainfall data, such analyses can provide the basis for early warning systems for shallow landslides. Thus these analyses are quite different than terrain hazard assessments, which are more focused on developing general stability hazard maps. A several rainfall-landslide relationships have been developed around the world assessing shallow landslide/debris flow occurrences on the basis of mean rainfall intensity and storm duration. However, it is strongly advisable to use such, much generalized form of equations to local situations only after a proper validation process.

Based on data from 40 major earthquakes in various settings around the world that ranged in local magnitude from 5.2 to 9.5, Keefer (1984) found that landslide distribution and type were strongly correlated with earthquake magnitude (M) and distance to the epicenter. To assess the lowest magnitude needed to trigger different types of landslides, intensity data of several hundred earthquakes in the USA was examined. The maximum area likely to experience some degree of landsliding during earthquakes ranged from zero at $M \approx 4.0$, to about 250 km^2 at M = 5.4, to a maximum of 500,000 km^2 at M = 9.2 (Keefer, 1984). Using the global data of Keefer (1984) plus seven additional earthquakes, Keefer and Wilson (1989) calculated the following regression relationship:

$$\log_{10} A' = M - 3.46(\pm 0.47) \qquad (3.1)$$

Where A' is the potential area affected by landslides (km^2) and M is the earthquake magnitude in the range of 5.5 to 9.2. Few other similar relationships have also been developed for earthquake triggered landslides, for instance in New Zealand and Greece.

While these general relationships between earthquake characteristics and landslide occurrence are useful for designating the susceptibility of seismically active regions to different types of landslide and for assessing the likely damages, the major problem of predicting the location, timing and magnitude of the earthquake still remains uncertain.

3.4.3 Multi factor, empirical landslide hazard assessments

Empirical landslide hazard assessment shares some common attributes with terrain hazard mapping but generally differ with respect to the number of factors considered, their relationship to past landsliding, and how the factors are evaluated in the context of the assessment. In empirical landslide analysis, the factors contributing to landslide initiation are typically established based on characteristics of existing landslides. The end product is focused on producing maps, or at least useable decision rules, that relate landslide hazards to measurable environmental attributes. Both bivariate and multivariate statistical techniques are commonly employed to establish such relationships among factors and landslides. Trigger mechanisms such as rainfall and seismic patterns, are usually not included because such hazard assessments focus only on conditions predisposing hillslope to failure.

Some hazard assessments have been developed using factor weightings based on past experience or professional judgments. Such qualitative hazard mapping based on professional judgment can be very effective if high quality distributed data and adequate expertise are available (e.g., Newman et al., 1978; Nilsen et al., 1979a). Here, the derived factor weighting estimates may vary considerably and lack objectivity and in other cases, individual factors are simply equally weighted or methodologies are inadequately specified.

In some recent cases, artificial neural networks (ANNs) methods have been also applied to overlay and weight causative factors (Lee et al., 2002a, 2003 and 2004). The method is applied mainly to shallow landslides, debris flows and shallow soil collapses. A combination of GIS techniques and the mathematical package MATLAB were employed in the above work to analyze the factors.

The concept of uncertainty or probability has been incorporated into landslide models (e.g., Ward et al., 1981; Sidle, 1992; Popescu et al., 1998), particularly related to triggering mechanisms, but also to site

factors. Dai and Lee (2003) introduced probabilistic analysis in a GIS based multi-factor landslide hazard model. Such models that use static causative factors and rainfalls of varying return periods can be used to predict the probability of landsliding on natural slopes in space and time.

3.4.4 Distributed, physically based models

As a theoretical advance from empirical landslide models based solely on rainfall characteristics, numerous infiltration-based landslide models have been developed for individual sites in both two and three dimensions (e.g., Anderson et al., 1988, Sammori and Tsuboyama, 1990; Haneberg, 1991). Such models offer the advantage of physics-based approach to assessing the dynamic changes in positive and negative (suction) pressure heads in the soil mass during the infiltration process and thus are valuable to predict the timing of slope failure relative to rainfall inputs at individual sites with simple slope configurations.

Physically based landslide models assess stability in terms of factor of safety (F_s). If single parameter input values are used to calculate F_s, method is most suitable for smaller areas. For large areas, variations in terrain and soil parameters must be included. Hence, distributed, physically based landslide models need to have two unique major requirements: (1) Spatially and, in some cases temporally distributed model parameters are necessary; and (2) the model out put must be spatially and temporally explicit because of the necessity to know the locations and timing of landslides (Sidle and Ochiai, 2006). Recent advances in incorporating sophisticated GIS and DEM technology into distributed, physically based modeling has facilitated the prediction of landslides at the catchments scale (Montgomery and Dietrich, 1994; Wu and Sidle, 1995; Dhakal and Sidle, 2003; Lida, 2004). The SHALSTAB, dSLAM and IDSSM, TRIGRS and SINMAP are some of the commonly known physically based models.

The SHALSTAB is a physically based model for shallow landslide analysis that combines digital terrain data with near surface through-flow and the infinite slope model. For simplicity, the model generally assumes that soils are cohesionless, slope parallel subsurface flow occurs, unit weights of soils in the saturated and unsaturated zones are equal, and ignores the effects of vegetation root strength (Dietrich et al., 2001). The model uses a coupled hydrology-slope stability equation to predict the slope instability on the basis of ratio of effective precipitation to transmissivity. However, due to the steady–state nature of rainfall inputs, SHALSTAB has not been tested for conditions where actual landslides were triggered during specific rain events; rather, effective rainfall was used. The dSLAM, a distributed, physically based slope stability model developed based on non-distributed landslide model by Sidle (1992) is used to analyze shallow rapid landslides at the catchments scale within a GIS framework (Wu, 1993; Wu and Sidle, 1995, 1997; Sidle and Wu, 1999). This model assesses the spatial and temporal effects of timber harvesting on slope stability. The distributed model incorporates (1) infinite slope analysis; (2) continuous temporal changes in root cohesion and vegetation surcharge; and (3) stochastic influence of actual rainfall patterns on pore water pressure. Recent improvements to the model (now IDSSM) include the ability to simulate multiple harvesting cycles, more efficient handling of rainfall inputs, and an updated distributed shallow groundwater model (DSGMFW) (Dhakal and Sidle, 2003 2004a, b; Sidle and Dhakal, 2003). In addition to the ability of dSLAM and IDSSM to utilize actual rainfall hyetographs as inputs, and thus predict temporal changes in F_s during storms, these models can explicitly analyze complicated scenarios of timber harvesting, making them useful tools for forest planning in potentially unstable terrain. The TRIGRS is one of the few distributed models to incorporate the effects of rainfall infiltration on dynamic pore pressure response in soils (Baum et al., 2002). This model extends Iverson's (2002) infiltration-

based landslide model to the catchments scale by adding a solution for an impermeable basal boundary at a finite depth and including a simple runoff routing scheme. Major assumptions include nearly saturated soil conditions, well-documented flow field, and relatively isotropic and homogeneous soil hydrological properties. The steady seepage component, and thus the accuracy of landslide predictions, strongly depends on the initial depth assigned to the water table and the steady infiltration rate (Baum et al., 2002). The SINMAP (Stability Index Mapping) after Pack et al. (1998) is another distributed shallow landslide model which is similar to SHALSTAB but employs different algorithms for calculating contributing area and specifying flow paths within a rectangular grid (Pack, 1997; Tarboton, 1997). The model is based on limit equilibrium failure analysis using an infinite slope stability model and a steady-state hydrological model (TOPMODEL) as described by Beven and Kirkby (1979) and Connell et al. (2001). The stability index (SI) is defined as probability of slope stability [SI = Probability (F_s>1)] over the distribution of uncertain parameters (cohesion c, friction angle ϕ, effective rainfall Q, and soil transmissivity T). The value of SI is employed to define six hazard classes from high stability (SI>1.5) to low stability (SI=0). Several different landslide stability maps are produced from SINMAP for different precipitation conditions showing increasing instability area as percentages. SINMAP has been used in a long-term model of the interaction of forest vegetation, forest fire, harvesting, and sediment yields in the Idaho Batholith (Istanbulluoglu et al., 2004).

3.5 Summary

In general, all above analysis approaches and models have characteristic advantages and disadvantages. Hence applying the appropriate method or integrating several methods for the optimal preparation of LHZ maps are important. For instance, even though the expert can qualitatively assess the overall conditions and extract the critical parameter combinations as does in heuristic approach, objective procedures such as statistical and deterministic are often desired to quantitatively support the slope instability assessment and vice versa.

With the introduction of GIS, in particular indirect methods have gained enormous popularity. The unique capability of GIS to handle the complex data sets for an effective analysis and calculations, improve the models by evaluating their results and adjusting the input variables by trial and error method and, update the database conveniently and rapidly, offer an efficient environment for hazard zonation studies. Beyond that, the ability to integrate qualitative and quantitative data through spatial relationships, use overlay functions where multiple maps can be combined and, develop digital elevation models (DEM) which subsequently can be used for preparation of slope, aspect and hillshade maps and hydrological modeling are worth mentioning.

Use of GIS allows for accurate and unbiased development of weighting factors typically used in such analysis. However it must be noticed that such weighting factors are only as good as the data bases from which they are derived. Also, it appears that with increasing sophistication of GIS, remote sensing, and statistical/analytical tools, there is a tendency to focus more on new methods rather than trying to understand causal linkages for specific types of landslides (e.g., Varnum et al., 1991; Guillande et al., 1995; Lee et al., 2002, 2004a). An advantage of these analytical methods (unbiased factor selection and weighting), can also be a disadvantage, in that geo-science and geotechnical expertise may be ignored in such assessments (Rollerson et al., 1997). Therefore, sometimes the simplest analytical methodology may produce the best landslide hazard assessment when thorough field mapping, good background information, and professional expertise are well combined.

4 Natural disasters and landslides in Sri Lanka

4.1 General background

Sri Lanka is an island, located within the tropics in the Asia–Pacific region between northern latitude of 5^0 55' and 9^0 51' and eastern longitude of 79^0 41' and 81^0 53', just south-east of the southern tip of the Indian sub continent (Figure 4.1), having an area of 65,610 km^2 with total population close to 20 million. The country has nine political provinces that divided into twenty-five administration districts (Figure 4.5) consisting of 246 sub-divisions. According to the statistics, Asia-Pacific region is considered as the most disaster prone region in the word (Report on disaster mitigation in Asia and the Pacific, 1991).

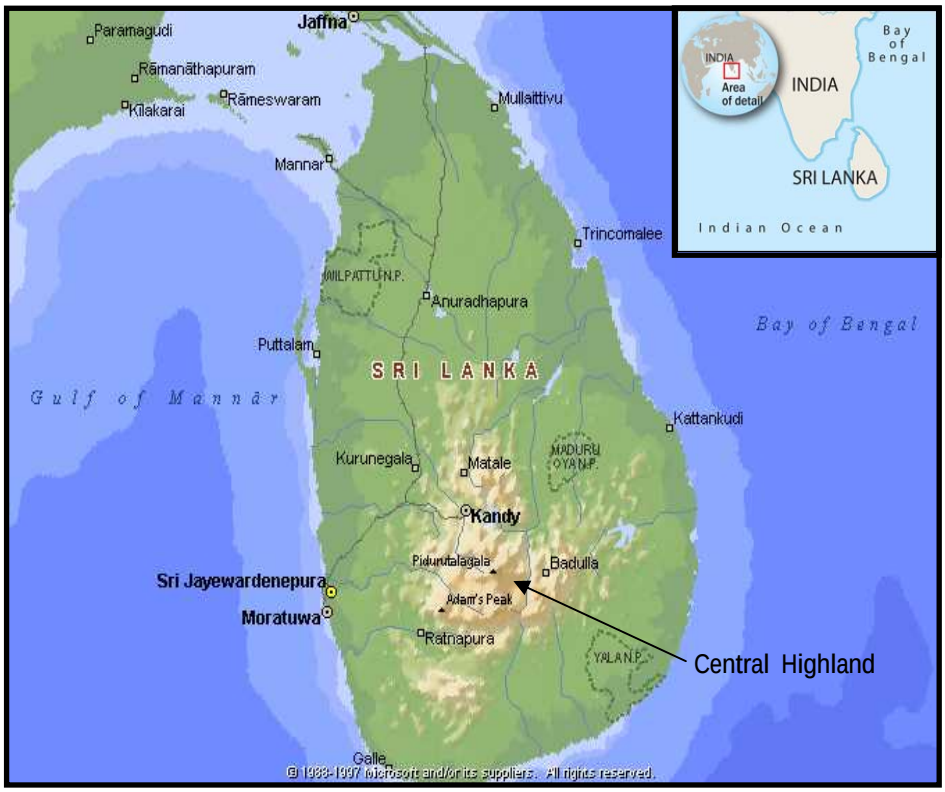

Figure 4.1: Map of Sri Lanka showing its location and the Central Highland.

Since most of the frequent disasters occurring in Sri Lanka are mainly linked with hydro-meteorological phenomenon and landslides are a geological hazard associated with topography, under following sub sections, general background of geology, topography and meteorological characteristics of the country are briefly discussed.

4.1.1 Geology

Geologically, nine-tenths of the country is underlain by highly crystalline metamorphic rocks of Precambrian age, some of them dating back to more than 2 billion years. They are considered to be formed by the transformation of ancient sediments under intense heat and pressure during mountain-building processes. On the basis of metamorphic rank and age, these rocks are classified into three distinct crustal units, namely the Highland complex (HC), the Wanni complex (WC) and the Vijayan complex (VC) (Kroner et al., 1991) (Figure 4.2a).

The Highland complex (ages 2.0-3.4 Ga) metamorphosed to granulite grade is the centrally located, NE-SW trending belt comprising mainly charnockitic gneisses and granulites, metasediments, basic granulites, gneisses and migmatites. The metasediments include quartzites, marbles, pelitic gneisses and garnet-sillimanite-schist (Khondalites). The HC is bounded on the east by younger (ages 1.1-1.8 Ga), amphibolite grade VC, composed mainly of granitic gneisses, basic gneisses and migmatites. The WC (ages 1.1-1.8 Ga) similar to those of the VC, lies west of the HC. It consists mainly of granitic gneisses, charnockitic gneisses and migmatites and the metamorphic grade ranges from amphibolite to granulite (Mathavan et al., 1998). The rest of the island mainly the north and north western portion contains relatively limited strata of sedimentation. Besides from recent deposits along river valleys, only two small fragments of Jurassic sediment (140-190 Ma) occur in Puttalam District, while a more extensive belt of Miocene limestone is found along the northwest coast, overlain in many areas by Pleistocene (1 Ma) deposits.

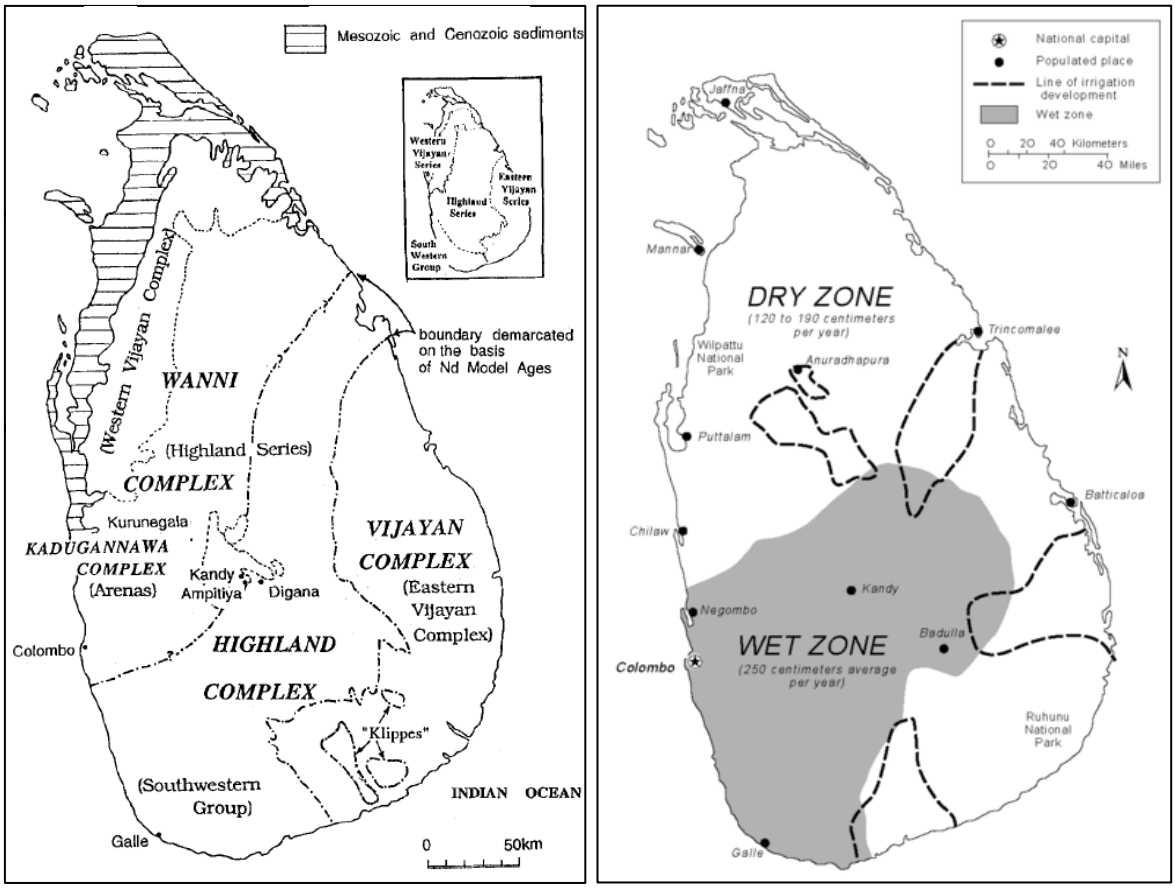

a. Major crustal units *b. Climatic zones*

Figure 4.2: Maps of Sri Lanka showing major geological divisions (Mathavan, 1999) and climatic zones.

4.1.2 Topography

Extensive tectonic activities such as, deformation, faulting, folding and erosion over time have produced a wide range of topographic features. Three zones are distinguishable by elevation: the Central Highlands, the plains, and the coastal belt. The highlands, mostly above 300 meters, occupy the south central part of Sri Lanka with many complex topographic features such as numerous peaks, high plateaus, basins,

valleys and escarpments. The reminder that surrounds the highland is extensive lowland except for several small hills that rise abruptly within it (Figure 4.1).

The south-central part of Sri Lanka the rugged Central Highlands is the heart of the country. The core of this area is a high plateau, running north-south direction for approximately 65 kilometers. This area includes Sri Lanka's highest mountains. Pidurutalagala is the highest at 2,524 m. At the plateau's southern end, mountain ranges stretch 50 kilometers to the west toward Adam's Peak at 2,243 meters and 50 kilometers to the east toward Namunakula at 2,036 m from mean sea level. Flanking the high central ridges are two lower plateaus. On the west is the Hatton Plateau, a deeply dissected series of ridges sloping downward toward the north. On the east, the Uva Basin consists of rolling hills covered with grasses, traversed by some deep valleys and gorges. To the north, separated from the main body of mountains and plateaus by broad valleys, lies the Knuckles Massif: steep escarpments, deep gorges, and peaks rising to more than 1,800 meters. South of Adam's Peak lies the parallel ridges of the Rakwana hills, with several peaks over 1,400 meters. The land descends from the Central Highlands to a series of escarpments and ledges at 400 to 500 meters above sea level before sloping down toward the coastal plains.

Most of the island's surface consists of plains between 30 and 200 meters above sea level. In the southwest, ridges and valleys rise gradually to merge with the Central Highlands, giving a dissected appearance to the plain. Extensive erosion in this area has worn down the ridges and deposited rich soil for agriculture downstream. In the southeast, a red, lateritic soil covers relatively level ground that is studded with bare, monolithic hills. The transition from the plain to the Central Highlands is abrupt in the southeast, and the mountains appear to rise up like a wall. In the east and the north, the plain is flat, dissected by long, narrow ridges of granite running from the Central Highlands. A coastal belt about thirty meters above sea level surrounds the island. Much of the coast consists of sandy beaches.

4.1.3 Meteorological characteristics

Due to its location within the tropics and in the Asiatic monsoon region, the climate of the island could be characterized as both tropical as well as monsoonal. Its position between 5 and 10 north latitude endows the country with year-round warm weather, moderated by ocean winds and considerable moisture. The variations in air temperature are small except in the mountainous area, whereas the rainfall variations are large. Therefore, the significant anomalies in climate are mainly decided by the temporal and spatial variations of rainfall, which have a strong influence on many frequent disasters, occur in the country.

The rainfall pattern in the island is influenced by the monsoon winds of the Indian Ocean and Bay of Bengal and is marked by four seasons. These seasons are distinguished by means of the timing of the two major monsoons, southwest and northeast monsoons and the transitional periods separating them, called inter-monsoon periods. The southwest monsoon is from May to September, when winds originate in the southwest, bringing moisture from the Indian Ocean. These winds encounter the slopes of the Central Highlands, unloading heavy rains on the mountain slopes and the southwestern sector of the island. The northeast monsoon is from December to February, when monsoon winds come from the northeast, bringing moisture from the Bay of Bengal. During these months, the northeastern slopes of the mountains receive heavy rains.

The inter-monsoon periods are from October to November and March to April. From October to November, periodic squalls occur and sometimes tropical cyclones bring overcast skies and rains to the southwest, northeast, and eastern parts of the island. The other inter-monsoonal period occurs with light, variable winds and evening thundershowers. The rainfall during the inter-monsoon periods is mainly due to convective thunderstorm activity.

The two major monsoons together account for about 2/3 of the year, clearly demonstrating the importance of the monsoons and the rainfall associated with them to the region. It is also characteristic to have long spells of dry days over most parts of the country except in the north and east during January and February, with ground frost appearing in the central hills.

The annual rainfall shows remarkable spatial variation, ranging from 1000 mm in the driest parts to more than 5000 mm in the wettest parts (Figure 4.2b). The southwest sector, along with the central highlands, stands out clearly as the wettest part of the island, with mean annual rainfall exceeding 2000 mm. Within the southwest sector, the maximum rainfall is in the lower to middle altitudes of the western slopes (300 – 1000 m), and above 1000 m the rainfall decreases again. The driest regions of the island are situated diametrically opposite to one another in two peripheral regions of Sri Lanka, the southeast and northwest; both regions receive annual average rainfall of between 1000 to 1250 mm.

The central highland forms an orographic barrier across the path of the monsoonal air masses affecting strongly the spatial patterns of winds, seasonal rainfall, temperature, relative humidity and other climatic elements, particularly during the monsoon seasons. An interesting feature of their role is that in general the windward and leeward sides of the highland flip to opposite sides with the rhythm of the monsoon change.

During the months of November to December, depressions forming in the Bay of Bengal (and Arabian sea) tend to intensify into cyclonic storms and move closer to Sri Lanka bringing much rain and wind; but chances of land fall along east coast are very low; only 17 out of some 1,300 storms since 1891. Devastation due to cyclones thus does not top the list of natural disasters except one of the most destructive event occurred in 1978 killing 834 people and destroying 6699 houses and damaging another 23273 (*DMC report, Sri Lanka*). However gust of strong winds during the southwest monsoon period cause damage to houses and other building structures in the southwest quarter of the island. Another phenomenon that increasingly threats the life and property is lightning; in the year, 1997, some 50 lives. Torrential rains too cause frequent floods displacing people and, also in the other extreme, prolonged dry spells sometimes affect agriculture adversely. Rain induced landslides in the hill country are on the increase as a natural calamity, during the recent years (*Courtesy: Meteorological department, Sri Lanka and Wikipedia*).

4.2 Natural disasters and their effect

The historical importance of enormous destructions by natural disasters to the country is not new. More often, the country has been affected by many events such as floods, landslides, cyclones, droughts, and lightening, except the less frequent but catastrophic events like earthquakes and tsunamis. The most well known oldest historic event is the princess Viharamaha Devi sacrificed to the sea to prevent inundation of the land by sea waves probably due to a tsunami event around 170 BC as recorded in the Mahavamsa and Rajawaliya – *monographs on the history of Sri Lanka*. According to the records in recent history, country

had experienced two earthquakes in 1615 AD and another in 1814 AD. It is also recorded a tsunami event in 1883 AD and another earthquake in 1938. Apart from those events, the country had experienced few other locally observed minor cases of earthquakes and tsunamis. Those historical evidences make obvious the country's vulnerability for such hazards too although it is situated away from the tectonically active regions and hence considered as stable.

During last 35 year period until 2008, about 40 major disaster events have been recorded in which more than 34,167 people were death and millions of people were affected. The total economic losses during last 20 year period until 2003 were calculated to US $ 5960 millions approximately. Among the very recent disasters, damages and destructions caused by the flash flood and landslides by heavy rain occurred on 16th and 17th May 2003 became one of the most significant event causing loss of 320 lives, destroying 10,222 houses and damaging another 28,593 dwellings. The total material losses island wide was estimated at over US $ 76.7 millions costing another US $ 10 million for relief efforts. The next well known cataclysmic event was the tsunami generated by an earthquake magnitude to 9.1 in Richter scale, off the west coast of northern Sumatra islands at 6:58:53 Sri Lankan time on December 26, 2004. More than 80% of the costal belt of Sri Lanka was severely affected by this event causing death to 30,959 people and affecting another 1,076,240 in different ways. Around 57,085 houses were completely destroyed damaging another 48,208 houses partly. Damages to infrastructures such as bridges, roads, railway lines, telecommunications, schools, harbors, and industries were immense. The total material losses island wide was estimated at over US $ 1.6 billions with unrecoverable social losses. Cost of the relief was approximately US $ 180 millions.

Despite the fact that, very less frequent events like tsunamis have caused severe damages to the country within very short span of time, the most frequent disasters in the country are mainly associated with seasonal rain fall pattern. Every year, floods, landslides, droughts, lightening and high winds occur in many parts of the country causing great damages to lives and economy and hence, they are considered as the most common disasters in Sri Lanka. Landslides are the most frequent and pressing problem in the Central Highland while floods cause major damages in the lowlands that surround it (Figure 4.1).

4.3 Landslide as a natural disaster

Many of the natural hill slopes in the country that stood safe for centuries when population was low and hence people mostly lived in river basins are now frequented by landslides and socioeconomic losses due to its impact are growing. This is mainly due to human intervention into previously virgin areas as a result of higher demand of land with rising population. Such demand has urged the communities to encroach hill slopes and even the marginal lands with potential landslide risk for living, industries, infrastructure facilities and agricultural purposes without an adequate attention to the problem. These are the slopes that are now frequented by landslides (Figure 4.3 and 4.4). When landslides on higher slopes occurred in the past, they were hardly noticed. Whereas, nowadays, landslides invariably kill people and destroy properties as the spread of people and infrastructures are so large that they live everywhere. Thus in Sri Lanka, landslides are attracting increasing attention especially within the central highland as the most frequent and major disaster (Figure 4.5).

The documented history of landslides in Sri Lanka is dated back to around 1869 with the recording of landslide damages along railway lines (Perera, 1925). Numerous cases occurred until 1903 reported 3 deaths; one engine driver, a firemen and a cleaner apart from many incidences where train services were

suspended for weeks and railway lines were diverted due to landslide damages. In 1964, landslides in Kalutara district killed 25 people and the toll at Nawalapitiya rose to 19. Again on 22nd October 1977, 26 people were killed at Gonadika estate in Kalutara district. 9 deaths in Rathnapura district and another 11 in Matale district were recorded in 1982. Again in 1984, 18 people were killed in different locations in Kalutara district. Here, an antecedent one day rainfall of 500 mm was observed at Matugama. In Kegalle, 10 deaths were reported in May 1985.

In 1986 alone, a rather unexpected spate of landslides caused as many as 51 human deaths and rendered almost 5000 homeless (eg., Figure 4.4a). Most of the incidences were recorded in Badulla and Nuwara-Eliya districts associated with one day rainfall ranging from 90 to some 299 mm depending on the location. Again in 1989, many more landslides occurred to take a toll of more than 225 human lives rendering about 1200 people homeless and destroying many properties. In June 1992 a major railway traffic was disrupted for weeks due to a landslide occurred in Watawala. This was again reactivated in June 1993 severely disrupting the railway traffic (Figure 4.4d). In 1993, 48 deaths were recorded out of which 31 were by a single incidence at Helauda in Rathnapura. The event was preceded by 300 mm of rainfall in the previous three days. Afterward, 22 deaths were evidenced in 1997. Although many more damages and deaths were recorded by later events, next most significant landslide event was in May 2003 which took more than 150 lives in different parts of the country within 2 days of antecedent rainfall (eg., Figure 4.3b where 67 people were death). By this single event, 855 houses were completely destroyed and another 2858 were damaged rendering almost 20,000 homeless. From 2004 to 2008, 99 deaths were recorded out of which 26 in 2006, 45 in 2007 and 16 in 2008. Total of 51,997 people were affected damaging almost 4000 houses and completely demolishing another 821 dwellings. During this period, highest damage was recorded in 2007 in which more than 31,000 rendered homeless (eg., Figure 4.3a). Overall, major landslides occurred during past three decades until 2008 have caused loss of more than 775 lives making about 90,000 people homeless. Total number of houses destroyed was recorded to 2000 approximately damaging another 7218 (*Sources: Landslide inventory-LSSD, NBRO and DMC database*).

Presently ten Administrative Districts, namely *Badulla, Nuwaraeliya, Rathnapura, Kegalle, Kandy, Matale, Kalutara, Galle, Matara and Hambantota* that encompass total area of 20,744 km^2 in which more than 13,000 km^2 (20% land area of the country) are considered to be prone to landslides (Figure 4.5). According to 2001 statistics, 42% of the total population of the country is living in these districts. Livelihood of the majority of people living in theses district are agriculture-oriented, so they tend to cultivate the available lands regardless of the steep terrain conditions that are prone to landslides. It is also obvious that the greater part of the communities live in the landslide prone areas are below the poverty line and hence neither they have access to stable and safe land nor economically strong to invest on landslide mitigations, which make them more and more vulnerable to the threat.

When the triggering mechanism of the slope failures are in concern, even though minor earthquake activities and other triggering events too could act to loosen the slope materials, none of the landslides have been so far recorded due to any triggers other than rain. Hence, intense rainfall associated with monsoon seasons are considered as the major triggering factor that induces landslides in Sri Lanka. Most disastrous landslides are sudden events with short onset time and rapid run out velocities during intense rainfalls. They occur mainly at the middle or at the top most portions of the slopes. Due to its unexpected nature, even the communities living along the run-out track and at the down stream impact zones get no time to escape. Therefore, safety of the humans who lives in such situations could be enhanced only by adopting adequate preparedness and mitigation measures such as hazard zonation mapping for the prior

identification of the vulnerable sites, timely early warning systems, evacuation plans and stabilization procedures.

(a) Landslide occurred in a potential hill slope acquired by communities

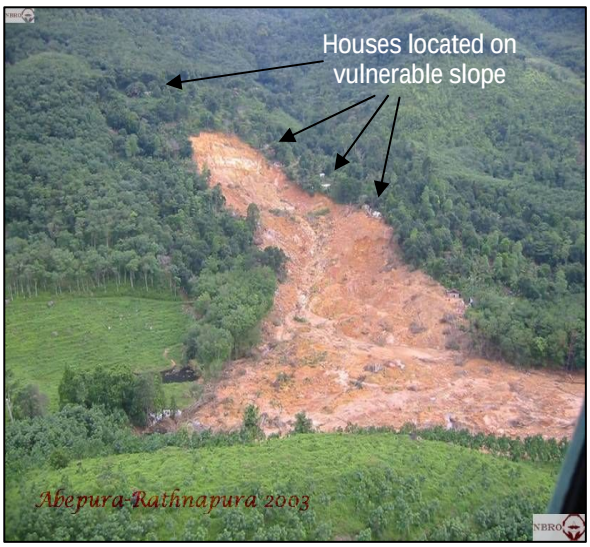

(b) Landslide and vulnerable communities

(c) Living on old landslides (Deniyaya)

Figure 4.3: Human intervention into vulnerable hill slopes and landslide disaster in Sri Lanka: (a) *Kiriwanaella, Walapane landslide in which 12 people were killed and 5 houses were buried - Jan. 2007; (b) Elapatha, Ambepura-Rathnapura landslide occurred on 17th May 2003 killing 67 people.*

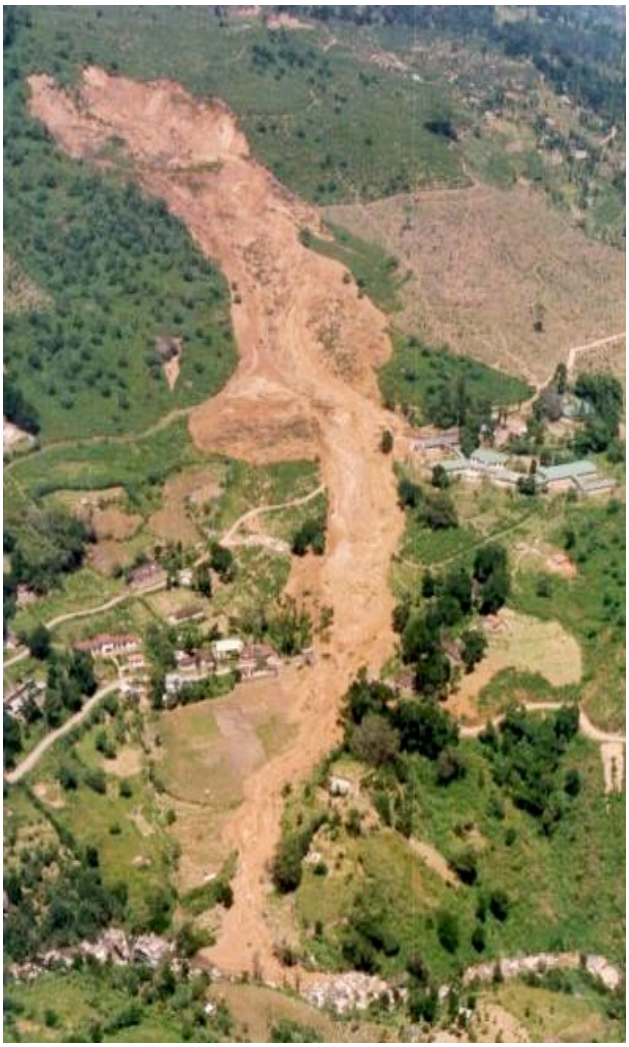

(a) Walapane, Mulhalkele landslide - 1986

(b) Beragal landslide - 2008

(c) Padiyapelella landslide - 2007

(d) Watawala landslide which damaged major railway line – 1992/1993

Figure 4.4: A few recent Sri Lankan landslides showing their damages and vulnerable communities.

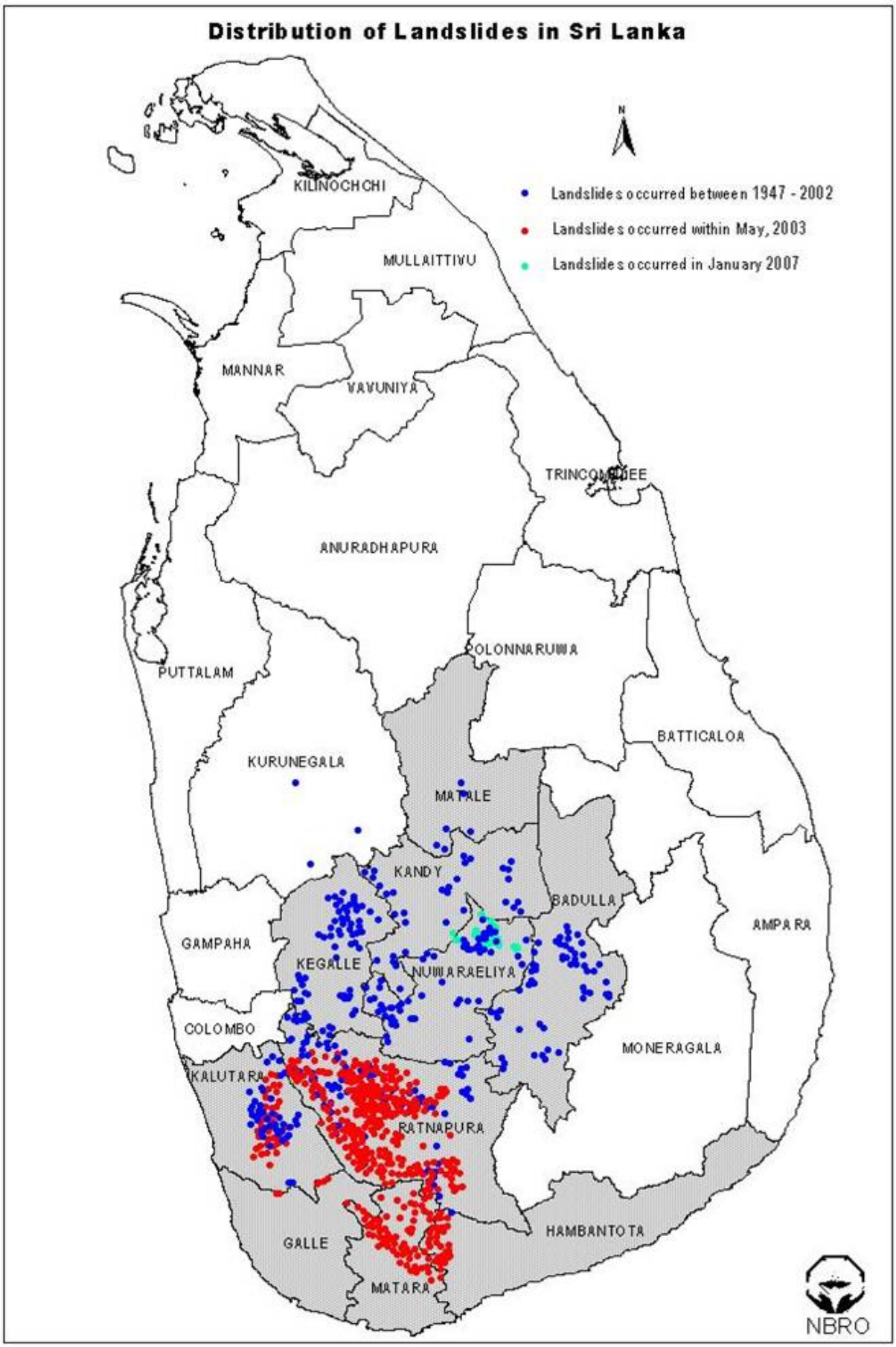

Figure 4.5: Distribution of landslides in Sri Lanka showing landslide prone districts and major events: red dots indicate landslides occurred in May 2003.

4.3.1 Landslide studies in Sri Lanka

Sri Lankan landslides have been studied and reported upon by Cooray (1958), Dahanayake (1983), Vitanage (1986) and Perera (1992) and the casual descriptions can be found in professional publications (National Building Research Organization, Geological Survey and Mines Bureau and Personal collections) and unpublished reports. However, their rigorous scientific documentation and research started only recently. The interest taken by the government to study landslide prone areas in detail and to carry out mitigation activities led to assign a separate institution (National Building Research Organization-NBRO) with the assistance from United Nations Center for Human Settlement (UNCHS) (*Landslide manual SRL 89/001*).

A model was developed by Landslide Studies and Services Division (LSSD) of the NBRO under a five year project called Landslide Hazard Mapping Project (LHMP), which was started in mid 1989 and lasted in mid 1995. For the study, relevant data of almost 1200 major landslides within two districts (Badulla and Nuwaraeliya) of the hill country were collected. Outcome of the data analysis and the experience gained by the landslide experts about the terrain conditions were used in the process of development of the model. Relative weightings for major factors and scores for sub factors and factor classes were given according to their degree of influence (Table 4.1). Final hazard (susceptibility) levels were defined on the basis of total scores. The NBRO user manual which is the final output of the project was published in 1995.

The model has been applied since then to predict the landslide susceptibility of existing slopes taking geology and their structure, soil types and their thickness, slopes, landform, land use and management as well hydrology and drainage into consideration. After collecting field data according to above factors into 1: 10,000 scale base maps, the model scores are assigned selecting the smallest possible uniform polygons within each factor map. Then they are summed and slopes are classified according to total scores. Under this program, field data of an area of nearly 4,600 km^2 of the central highland of Sri Lanka has been collected but for majority of the areas, final susceptibility maps are yet to be produced (*LSSD progress report*).

The total process starting from demarcating uniform areas in each factor map to the preparation of corresponding weight maps is done manually. Then, the mapping units are digitized as polygon features since GIS is used as a map overlaying and reclassifying tool in the next steps of the workflow. All the factor maps such as land use, soil type, slope category, etc., where the basic mapping units are made up of areas can be directly used as uniform polygons in GIS and weights can be easily assigned. This holds only partly for the geology map, where lithology as area features but structural attitudes as linear or point features are involved. Therefore, very laborious effort is needed for the manual preparation of geology weight maps, especially when complex terrain conditions and large amount of data are involved. This has been one of the major reasons for the set back of conclusion of landslide hazard zonation maps in many parts of the country.

Under the present study, an approach is introduced to automate the process of preparation of geology weight maps within the GIS environment (Jayathissa et al., 2009). In addition to that, hydrological modeling capabilities in GIS can be effectively utilized to replace the similar kind of manual procedure needed to prepare hydrology weight maps too. These methods that are extremely efficient and effective

compared to the manual procedures can be employed to improve the quality and accelerate the whole LHZ mapping project in Sri Lanka.

Table 4.1: Relative weightings for major factors, sub factors and factor classes based on the NBRO model (NBRO user manual, 1995).

Major factors & Max. weighting	Sub factors & Maximum weighting	Sub factor elements (factor classes) Linguistic rating (x) and Scores (z)	x	z
20		Marble	very low	0
		Weathered rock	low	1
	Lithology 8	All others	medium	3
		Charnockite, Granulite or bedrock not exposed	high	5
		Quartzite	very high	8
		Dip & scarp 71-90	very low	0
Bedrock Geology & Geological structures	Amount of dip & type of slope 4	Dip & scarp 56-70	low	1
		Dip 11-30, scarp 46-55 & all intermediate slopes	medium	2
		Dip 0-10, scarp 31-45	high	3
		Dip 31-55, scarp 0-30	very high	4
		Angle 26-120	very low	0
	Deviation angle (degrees) 6	Angle 11-25 or 121-155	low	2
		Angle 156-180	high	4
		Angle 0-10	very high	6
	Other Discontinuities 2	To be decided on case to case basis	very low	0
			very high	2
10		Bare bedrock	very low	0
Type of natural soil and their thickness	Soil cover (m) 10	Colluvium <1, Residual <2	low	2
		Colluvium 1-3, Residual 2-8	medium	8
		Colluvium 3-8, Residual >8	high	9
		Colluvium >8, Residual >8	very high	10
25		Slope category I (>40)	very high	25
Slope range & category	Slope range & category (degrees) 25	Slope category II (31-40)	high	16
		Slope category III (17-31)	medium	13
		Slope category IV (11-17)	low	7
		Slope category V (0-10)	very low	5
20		Relief >350	Very low	1
	Relief amplitude (m) 5	Relief 0-170	medium	2
		Relief 170-350	very high	5
	Hydrological map unit area (sq. km) 4	Area 0-0.07 or > 0.5	very low	1
		Area 0.07-0.2	medium	2
Hydrology & Drainage		Area 0.2-0.5	very high	4
	Hydrological map unit shape (form factor) 4	0.6-1.0	very low	1
		0.3-0.6	medium	2
		< 0.3	very high	4
	Drainage density (km/sq. km) with or without soil cover 5	With >5 or without >10	very low	1
		With 3-5 or without 6-10	medium	2
		With 0-3 or without <6	very high	5
	Proximity to water bodies 2	To be decided on case to case basis	very low	0
			medium	1
			very high	2
15		JT1, JC, JQ, JWb, W1, S1	very low	3
Land use & Management	Land use & Management 15	JT2,JR,JWp,HP,HK,HM,HW,W2,W3,W4, S2,S4	medium	8
		HA, G1, G2, S3, N1, N2, N3, N4	very high	15
10		F11,F12,F31-35,F43,F91-92, F94,A10-13, X1,X2	very low	1
Landform	Landform 10	F41,F42,F44-48,F53	medium	3
		F51,F52,F54-58,X13,X14	high	5
		F61,F62,F71-74,F81-83, F92,X11,X15	very high	10

4.4 Study area, background information and data collection

Area of current research interest is located within the Southern Province of Sri Lanka (Figure 4.7). The area encompasses approximately 263 km^2. Elevation in the study area ranges from 46 m to 1138 m from

mean sea level. The area receives heavy rains every year with southwest monsoon from May to September experiencing floods in Galle and Matara districts in Ginganga and Nilwala basins.

The Southern Province comprises of Galle, Matara and Hambantota districts (Figure 4.5) having an area of about 5500 km^2 with about 12% of the country's population. The province margins to the sea having about 260 km long coastal line. Even though floods, landslides, droughts and sea erosions are considered to be the most frequent natural hazards occur in the region, the tsunami occurred on 26th Dec. 2004 became a tragedy in the recent history destructing entire coastal line of the province.

The devastation caused by flash flood and landslides on 17th May 2003 associated with 3 consecutive days cumulative rainfall preceding the event was unprecedented and the people in the districts of Rathnapura, Matara, Hambantota, Galle and Kalutara were severely affected. The most significant fact is that Galle, Matara, and Hambantota districts which had not been considered earlier as landslide prone areas were highly affected by this catastrophic event killing 54 people in a single day by landslides (Figure 4.6). The recorded daily rainfall on 17th May 2003 within the study area ranged from 155 mm as the minimum to 730 mm as the maximum (Table 4.6).

Figure 4.6: A few cataclysmic landslides occurred within the study area on 17th May 2003.

After the event, NBRO established a regional office in the Southern Province of Sri Lanka in July 2004, with a view to consulting local authorities and people for future disaster management activities, collecting field data and researching landslides problems, and preparing landslide hazard zonation maps in the region. Under this project, priority areas were selected on the basis of density of landslides occurred in the past and the density of populations under the threat. The total extent which can be considered as vulnerable for the hazard is about 1200 km^2 out of which more than 50% are within Matara district (Figure 4.5). In some areas especially within Matara district, landslide density exceeds 15 landslides per square kilometer.

The field data relevant to the NBRO model for the selected high priority area of 263 km^2, mainly within the Matara district covering 1:10,000 scale base map sheets of 81/17, 81/18, 81/22, 81/23, 87/02, 87/03, 87/08 and 87/13 (Figure 4.7 and 4.8) were collected. An area of a map sheet is 40 km^2.

The data comprises:

- *Existing landslides – 513 in which 506 are rain induced shallow translational landslides,*
- *Bedrock Geology,*
- *Structural data (folds, faults and strike and dip data of rock foliation and major joints),*
- *Soil type and their thickness,*
- *Elevation data (contours),*
- *Landform,*
- *Land use and management,*
- *Hydrology and drainage.*

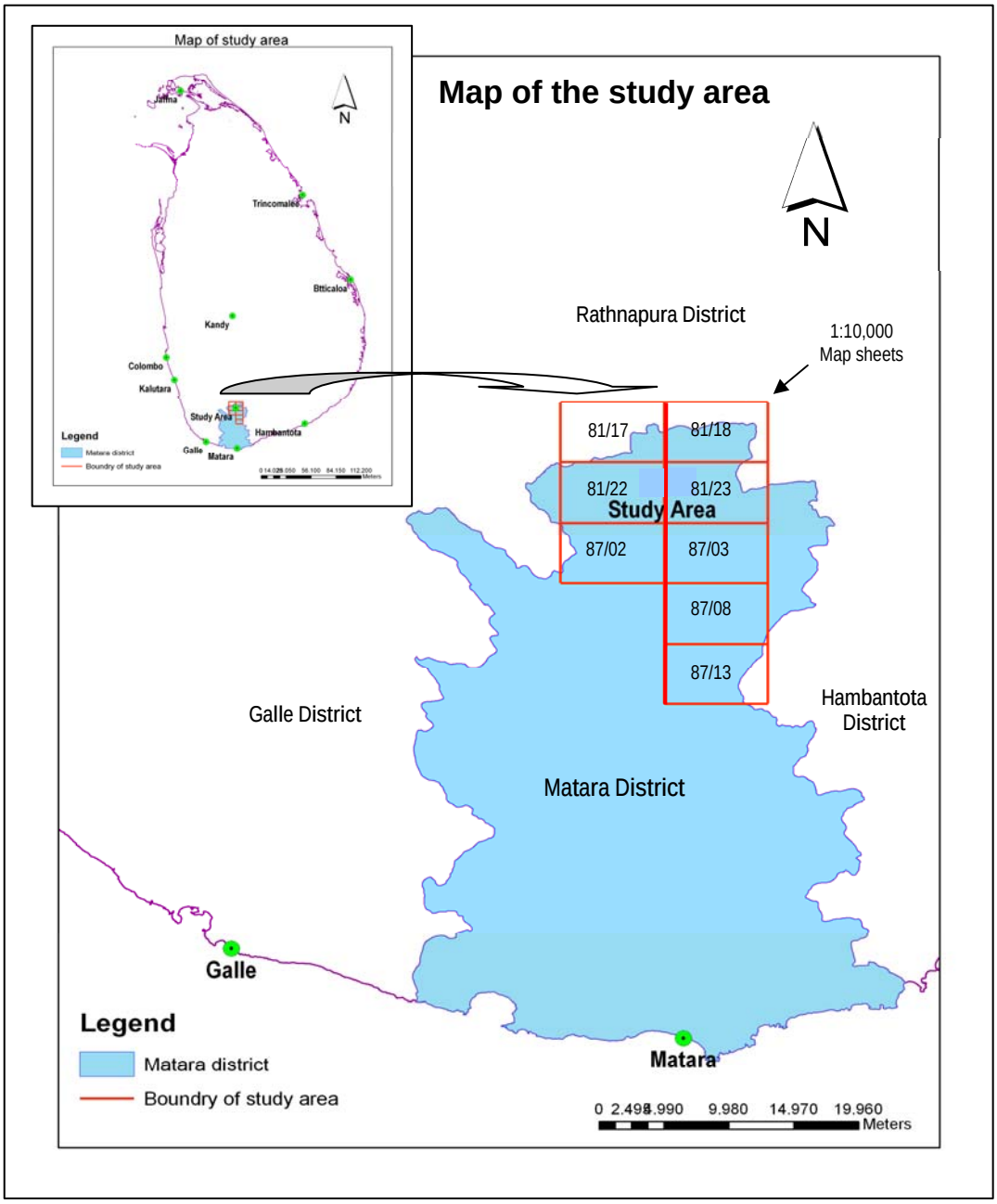

Figure 4.7: Map of the study area showing Matara district and 1:10,000 map sheets (*The study area encompasses the total area of map sheet numbers of 81/22, 81/23, 87/02, 87/03, 87/08, 87/13 and parts of the maps of 81/17 and 81/18).*

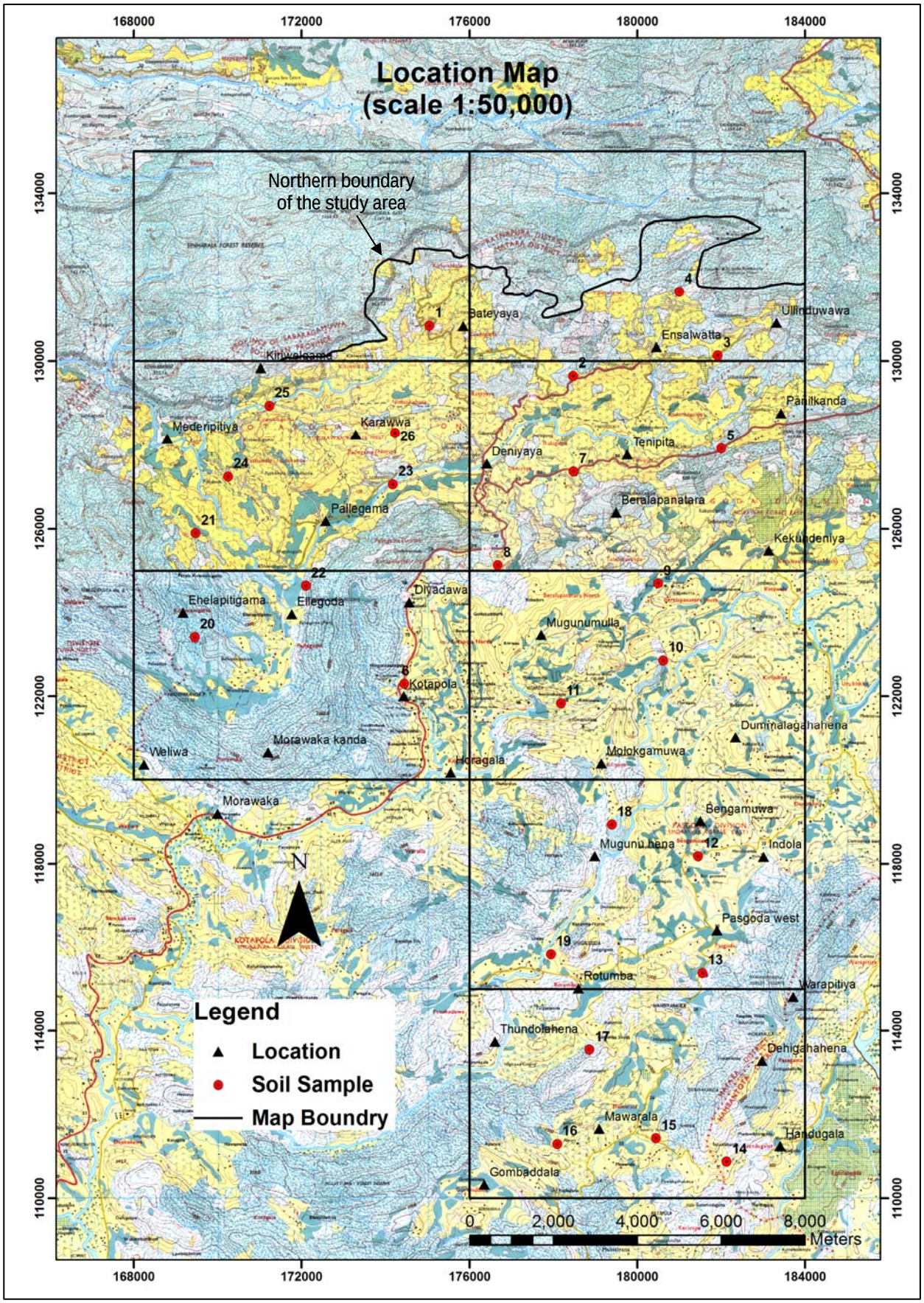

Figure 4.8: 1:50,000 map of the study area showing locations and soil sampling sites (Table 4.2 and 4.3).

Although the work continued further to other areas, data collection within the study area was ended in August 2005. The working group comprised by a team of multidisciplinary specialists with landslide expertise from the Landslide Studies and Services Division (LSSD) and the Human Settlement Division (HSD) of the NBRO. Digitization of the field data were completed in 2008 by the Computer and GIS section of the LSSD. Soil samples were collected from the chosen locations (Figure 4.8) within the study area in 2007 and tested in the geotechnical laboratory of the NBRO (Table 4.2 and 4.3). They include 26 undisturbed samples (UDS) and 28 disturbed samples.

Table 4.2: CU Triaxial test results (effective shear strength parameters) for the undisturbed soil samples.

UDS Sample number	Cohesion C´ (kPa)	Friction angle φ' (deg)	Soil classification
1	3.0	34.0	MS (Sandy Silt)
2	2.0	36.8	MS
3	16.0	24.5	MH (Inorganic silt, fine sandy or silty soil)
4	16.5	25.0	MH
5	15.0	29.0	MV
6	16.0	26.2	MH
7	20.0	27.0	ME (Clayey Silt)
8	20.0	20.0	MV
9	15.1	30.3	MH-MV
10	13.0	21.0	MH (Clayey Silt)
11	11.0	29.0	MH
12	9.0	35.0	SM (Silty Sand)
13	14.0	28.0	MH-MV
14	10.0	29.3	MV
15	17.5	26.0	MH
16	8.0	34.0	SM
17	8.0	33.0	MS
18	7.2	36.0	SM-MH (Sandy silt with high plastic clay fines)
19	10.0	34.0	SM
20	1.0	28.0	MH
21	2.0	36.0	SM-MH
22	7.3	36.0	SM-MH
23	6.0	32.0	SM-MH
24	5.2	36.0	SM-MH
25	8.0	34.0	MS-MH
26	8.0	33.0	MI-SM

Table 4.3: Summary of soil classification test results for the disturbed soil samples.

Sample No.	Depth (m)	Classification	Moisture Content w (%)	Specific Gravity G_s	Particle Size Distribution				Atterberg Limit		
					Gravel (%)	Sand (%)	Silt (%)	Clay (%)	Liquid Limit (%)	Plastic Limit (%)	Plasticity Index (%)
1	1.00 - 2.00	MS	03.6	2.63	10	42	27	21	68	22	46
2	1.00 - 2.00	MS	34.1	2.64	07	46	24	23	54	32	22
3	1.00 - 2.00	MH	36.8	2.59	07	35	25	33	65	38	27
4	1.00 - 2.00	MH	31.7	2.64	08	36	20	36	56	38	18
5	1.00 - 2.00	MV	38.6	2.62	03	17	46	34	82	50	32
6	1.00 - 2.00	MH	39.3	2.61	03	39	26	32	69	46	23
7	1.00 - 2.00	ME	44.8	2.89	03	13	44	40	96	53	43
8	1.00 - 2.00	MV	52.1	2.37	04	18	30	48	82	45	37
9	1.00 - 2.00	MH-MV	35.9	2.63	05	39	23	33	70	39	31
10	1.00 - 2.00	MH	33.6	2.67	05	26	30	39	58	44	14
11	1.00 - 2.00	MH	41.8	2.73	01	46	28	25	63	44	19
12	1.00 - 2.00	SM	29.2	2.77	09	48	25	18	48	38	10
13	1.00 - 2.00	MH-MV	55.9	3.45	02	29	45	24	70	58	12
14	1.00 - 2.00	MV	33.4	2.75	07	35	23	35	74	45	29
15	1.00 - 2.00	MH	30.3	2.71	03	38	16	43	63	42	21

16	1.00 - 2.00	SM	30.0	2.71	13	47	13	17	49	30	19
17	1.00 - 2.00	MS	42.5	2.69	11	41	20	28	64	44	20
18	1.00 - 2.00	SM-MH	37.1	2.69	12	44	17	27	57	38	19
19	1.00 - 2.00	SM	37.9	3.32	10	45	22	23	Non plastic		
20	1.00 - 2.00	MH	43.5	2.72	05	32	30	33	69	43	26
21	1.00 - 2.00	SM-MH	33.9	2.73	24	32	23	21	62	40	22
22	1.00 - 2.00	SM-MH	37.4	2.67	12	42	18	28	61	42	19
23	1.00 - 2.00	SM-MH	26.3	2.68	13	38	22	27	57	39	18
24	1.00 - 2.00	SM-MH	44.2	2.66	08	61	16	15	71	49	22
25	1.00 - 2.00	MS-MH	28.2	2.60	24	36	03	37	94	46	48
26	1.00 - 2.00	MI-SM	24.7	2.64	05	47	26	22	46	34	12
27	1.00 - 2.00	SM-MH	32.8	2.63	09	17	36	38	51	34	17
28	1.00 - 2.00	MV	49.5	2.68	04	33	20	43	75	47	28

In addition to that, available rainfall data from seven rainfall stations located within the study area have been collected from the Meteorological Department of Sri Lanka for a period of eleven years (from 1997 to 2005).

Table 4.4: Annual rainfall for seven rainfall stations within the study area (from 1997 to 2007).

Year	Dampahala	Alapala-deniya	Deniyaya Willie group	Deniyaya Aninkanda	Mawerella Estate	Natagala	Pallegama
1997	3035.7	--	--	3977.0	--	4081.7	3413.3
1998	2492.8	--	--	3011.6	--	2783.2	3440.5
1999	2788.4	--	4294.6	3707.6	3455.9	3946.9	4373.7
2000	2643.0	4407.0	3379.5	3033.2	3681.2	3582.3	3678.3
2001	2046.2	3091.1	2658.2	2839.1	2830.2	1964.1	2615.3
2002	2397.2	3463.6	3406.5	2705.4	3629.6	2224.4	3022.2
2003*	**2957.2**	**4525.6**	**4654.1**	**3278.1**	**4577.5**	**3456.4**	**3403.4**
2004	2515.9	3647.6	3203.0	2927.2	2926.1	3318.0	3312.7
2005	2344.5	3813.4	2739.2	2913.6	2866.0	2390.0	3562.7
2006	2679.8	3445.0	3846.7	3744.1	3026.5	3142.2	3468.2
2007	2185.5	--	2984.4	2934.9	2656.0	--	1486.6

*Year on which the landslide incident occurred.

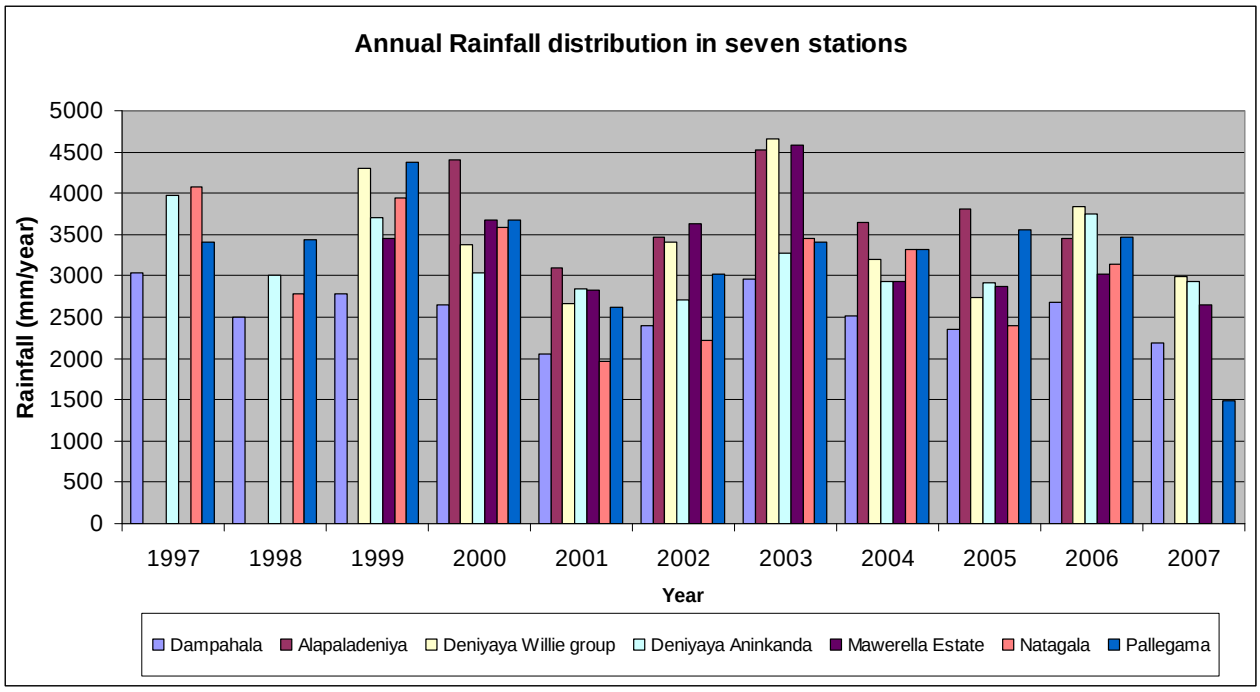

Figure 4.9: Annual rainfall distribution for the seven rainfall stations within the study area.

According to the Figure 4.9, in general, the highest rainfall distribution was recorded in the year 2003 where the incidence of landslide occurred while comparatively higher rainfalls were recorded in the years of 1997, 1999 and 2000.

Table 4.5: Monthly rainfall for the seven rainfall stations within the study area for the year 2003.

Month of 2003	Alapala-deniya	Dampahala	Deniyaya Willie Group	Deniyaya Aninkanda	Mawerella Estate	Natagala	Pallegama
Jan.	134.5	82.5	120.7	115.5	118.8	67.7	53.4
Feb.	213.9	114.3	174.0	27.0	148.6	50.8	110.4
March	536.0	573.2	558.1	610.5	652.8	439.9	383.2
April	300.5	260.1	388.4	417.0	805.3	529.8	357.3
May*	**656.6**	**516.8**	**1140.0**	**755.0**	**523.9**	**--**	**465.3**
June	344.5	132.7	268.1	156.5	141.0	--	242.5
July	317.1	195.5	371.3	251.5	250.6	252.4	323.4
Aug.	272.2	100.9	169.5	75.0	141.5	304.2	179.6
Sept.	350.5	143.2	302.6	148.5	382.0	220.8	318.1
Oct.	491.1	165.7	318.2	333.1	250.0	374.4	339.9
Nov.	716.5	535.3	503.5	388.5	837.0	859.6	408.1
Dec.	192.2	137	339.7	--	326.0	356.8	222.2

*Month on which the landslide incident occurred.

Table 4.6: Daily rainfall for the seven rainfall stations within the study area for May, 2003.

Day- May 2003	Alapala-deniya	Dampahala	Deniyaya Willie Group	Deniyaya Aninkanda	Mawerella Estate	Natagala	Pallegama
1	1.8	19.2	18.8	24.0	0.0	No data	10.3
2	0.0	0.0	16.3	8.5	0.0		6.8
3	0.0	0.0	2.9	0.0	5.0		0.0
4	12.4	2.4	3.4	3.0	0.0		10.6
5	54.4	130.1	82.9	87.0	131.0		19.4
6	37.0	8.9	18.4	60.0	0.0		96.4
7	1.7	0.0	0.0	0.0	0.0		0.0
8	6.0	0.0	0.0	0.0	0.0		0.0
9	14.7	4.1	7.5	0.0	3.0		6.4
10	0.0	0.0	4.3	3.0	0.0		3.4
11	6.2	0.0	3.7	7.0	59.3		8.3
12	45.2	20.5	30.6	49.0	62.0		0.0
13	22.2	7.9	13.2	9.0	0.0		0.0
14	0.0	0.0	22.0	29.0	0.0		0.0
15	**0.0**	**60.5**	**15.0**	**0.0**	**0.0**		**0.0**
16*	**97.3**	**105.1**	**163.0**	**147.5**	**0.0**		**0.0**
17*	**328**	**155.0**	**730.0**	**319.0**	**182.0**		**298.8**
18	**4.5**	**0.0**	**1.0**	**0.0**	**81.6**		**0.0**
19	0.0	0.0	1.8	0.0	0.0		0.0
20	0.0	0.0	0.0	0.0	0.0		0.0
21	0.0	0.0	0.0	0.0	0.0		0.0
22	0.0	0.0	0.0	0.0	0.0		0.0
23	0.0	0.0	0.0	0.0	0.0		0.0
24	0.0	0.0	0.0	0.0	0.0		0.0
25	15.0	3.1	2.2	6.0	0.0		0.0
26	10.2	0.0	3.0	3.0	0.0		0.0
27	0.0	0.0	0.0	0.0	0.0		0.0
28	0.0	0.0	0.0	0.0	0.0		3.8
29	0.0	0.0	0.0	0.0	0.0		0.0
30	0.0	0.0	0.0	0.0	0.0		1.1
31	0.0	0.0	0.0	0.0	0.0		0.0

*Days on which the landslide incident occurred.

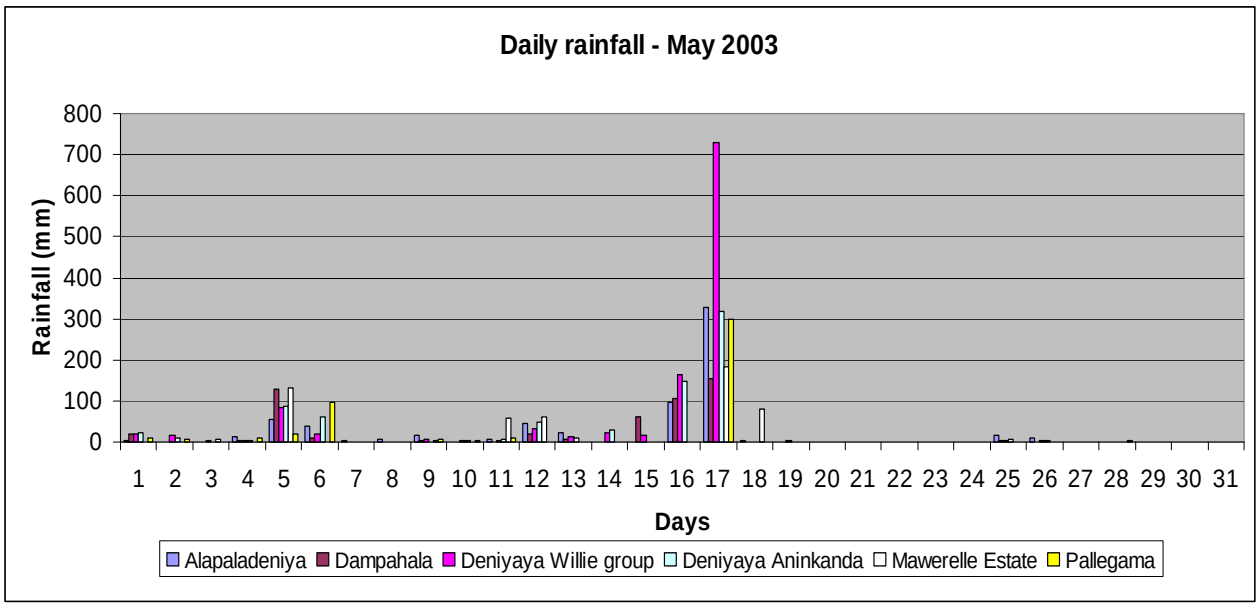

Figure 4.10: Daily rainfall distribution for the seven rainfall stations within the study area - May 2003.

4.5 Data preparation

Since the field data collection and the digitization were done as separate maps on the basis of the necessities of the NBRO, it was a prior task to organize them according to the present study requirements. The work included data checking, correction, editing and combining of the map sheets and introduction of new features and attributes where necessary. Some factors like structural attitudes were entirely re-digitized introducing necessary attributes. By editing the landslide distribution map that shows the entire landslide features such as zone of initiation, flow path and zone of accumulation, a surface of rupture map was created. This is important because the analyses should be focused only to the area of rupture to find the terrain conditions that facilitate the initiation of landslides. The map consists of 506 rain induced shallow landslides which vary in area from 14.6 m^2 to 122053.9 m^2 with a mean area of 4364.8 m^2. About 80% of the landslides are smaller than the mean area. Derived maps such as slope, aspect, stream network and watershed were prepared using the digital elevation model created from 1:10,000 scale contour data with 10 m contour intervals.

In the GIS based analysis approaches, relationships between the observed landslide distribution and their controlling factors are made on the basis of area calculations. Hence, all the factors such as land use, soil type, slope category, etc., where the basic mapping units are made up of areas can be directly used as uniform polygons or grids in GIS. This holds not for geological structures where structural attitudes are marked as linear or point measurements in factor maps. Due to this reason, structural factors are often neglected or dealt frivolously in GIS based landslide analysis even though they are considered as a major cause for slope instability. Under the present study, an effective approach was introduced to integrate the geometry of structural planes of rock in relation to the morphological slopes considering deviation angle, apparent dip, under/over dip - under/over scarp situations, and presence of weak zones such as lineaments, folds, faults and joints (Jayathissa et al., 2009a).

With the introduction of the combined structural parameters and the derived factors, total of 13 landslide causative factors were prepared for the analysis. They are static factors (section 3.2) and include:

- *Lithology (bedrock geology),*

- *landuse,*
- *landform,*
- *soil type,*
- *soil thickness (soil depth),*
- *slope angle (gradient),*
- *slope aspect,*
- *deviation angle,*
- *under/over dip - under/over scarp angle,*
- *watershed,*
- *distance to springs, streams* and *joints (up to 300 m distance from the feature was divided into 50 m range categories. Distance away from 300 m is considered as zone of no influence).*

Beside the preparation of above mentioned factor data for the use of susceptibility analysis, following tests were carried out to find out the necessary geotechnical soil parameters (Table 4.2 and 4.3):

- *CU Tri-axial test with effective strength parameters (c' φ'),*
- *water content (w),*
- *specific gravity (G_s),*
- *soil classification test with limits (particle size distribution and Atterberg limit tests).*

With the use of above test results and the standard geotechnical equations, additional parameters like,

- *void ratio (e),*
- *porosity (n),*
- *saturated unit weight (γ_{sat}),*
- *permeability (k),*
- *specific yield and*
- *specific retention*

which can be subsequently used to research the variation of factor of safety (F_s) conditions with rainfall intensities in dynamic modeling were calculated (Table 4.7).

Interpolation techniques were applied to create continuous surfaces for the point data such as structural attitudes and soil parameters. After experiments of many techniques such as Kriging, Radial Basic Functions, Global and Local Polynomial Interpolations, Spline, Natural Neighbor and Inverse Distance Weighting (IDW) for each type of data, the IDW[2] was preferred over other interpolation methods.

For the entire data preparation processe ESRI ArcInfo 9.2 was used. Despite the fact that vector format is very supportive in data editing and manipulation, both the vector and raster structures had to be employed according to the circumstances, but finally all the vector layers were converted to raster structure for the

[2] IDW is an exact deterministic interpolator. Therefore, pixel values in the interpolated surface do not go beyond the limits of input data, which is needed for dip directions (0°- 360°) and dip angle (0°- 90°) are concerned. The ability to control the power, number of points and barrier polylines are other important characteristics to have a representative prediction surface especially for data like angles and directions.

use of analysis. Considering the landslide with an area of 14.5 m^2 as the smallest feature to be identified, grid size of 3 m was used as a common raster resolution.

Table 4.7: Calculated soil parameters data using available test results.

Sample No.	Void Ratio (e)	Porosity n =e/(1+e)	Saturated unit weight (kN/m^3)	Permeability (m/s)	Specific Yield (S_y %)	Specific Retention (n-S_y)
1	9.47	8.65	24.42	--	7.0	1.65
2	89.92	47.35	18.28	--	7.5	39.85
3	95.31	48.80	17.80	E-5 to E-10	4.0	44.80
4	83.69	45.56	18.57	E-5 to E-10	3.5	42.06
5	101.13	50.28	17.71		3.6	46.68
6	102.65	50.65	17.60	E-5 to E-10	4.2	46.45
7	129.47	56.42	17.89	--	2.3	54.12
8	123.55	55.27	15.82	--	1.3	53.97
9	94.29	48.53	18.04	E-5 to E-10	4.2	44.33
10	89.71	47.29	18.45	E-5 to E-10	2.8	44.49
11	114.20	53.31	17.73	E-5 to E-10	7.0	46.31
12	80.80	44.69	19.41	E-5 to E-8	12.0	32.69
13	192.86	65.85	18.02	--	7.0	58.85
14	91.80	47.86	18.76	--	4.0	43.86
15	82.09	45.08	19.02	E-5 to E-10	--	--
16	81.30	44.84	19.06	E-5 to E-8	6.5	38.34
17	114.30	53.34	17.55	--	4.7	48.64
18	99.80	49.95	18.11	E-5 to E-8	6.0	43.95
19	125.83	55.72	19.89	1.05 E-5	8.0	47.72
20	118.32	54.20	17.54	E-5 to E-10	3.8	50.40
21	92.55	48.06	18.62	E-5 to E-8	10.0	38.06
22	99.88	49.97	18.01	E-5 to E-8	4.8	45.17
23	70.48	41.34	19.48	E-5 to E-8	5.0	36.34
24	117.55	54.03	17.30	--	16.0	38.03
25	73.19	42.26	18.87	--	--	--
26	65.18	39.46	19.55	--	9.0	30.46
27	86.32	46.33	18.39	E-5 to E-8	2.8	43.53
28	132.74	57.03	16.89		--	--

5 Objectives and methodologies of the study

5.1 Objective

Hazard predictions and early warnings against landslides are usually not meaningful unless given in relation to the exact location and timing of the anticipated event. In the context of Sri Lankan case, landslide predictions are mainly based on the susceptibility maps prepared using six major terrain factors according to the method described in the section 4.3.1. Although these conventional maps could be mostly useful for future development activities in regard to deciding on safe slopes during planning and construction stages, they lack any temporal implications or information about the intensity of triggering events and hence have no role in predicting the timing of the hazard.

Almost all the Sri Lankan landslides investigated to date are known to be rain induced. Hence, the timing of the hazard could be predicted on the basis of rainfall forecasts (Meteorological predictions) or if real time rainfall data is available. A few attempts have been made so far to find a connection between incidences of landslides and cumulative rainfall of a certain number of days, immediately preceding the landslide events. For instance, in addition to some individual events where the said connection was found, studies on 64 landslides in the hill country of Sri Lanka, conducted by the NBRO has also yielded the conclusion that if the cumulative rainfall on three consecutive days exceeds 200 mm and if the rains are found to continue, the probability of landslides occurrence should be considered high (Bhandari et al., 1991). However, this statistical threshold of rainfall is deployed only as a regional early warning indicator regardless of the location, terrain conditions and hazard potential and therefore the chances of raising false alarms were higher than the chances of reliable forecasts. Thus, it is a vital task to develop more appropriate regional scale models for the prediction of both the spatial and temporal aspects of the landslide events on the basis of rainfall intensities.

Additionally, the fact remains that rainfall alone or susceptibility mapping alone is not a good enough early warning indicator especially when real time forecasting is in concern. It is inappropriate to rely wholly on rainfall ignoring causative factors, or rely on susceptibility mapping, ignoring triggering events.

The objective of this research study is therefore first to prepare landslide susceptibility maps considering the local terrain conditions by means of indirect mapping methodologies and to combine the best fit model with a dynamic slope stability model. According to the calculated factor of safety values for different rainfall scenarios, hydrological triggering thresholds[3] for the various slopes can be set up. Thus, the final output expected will be a "Dynamic Hazard Map" which can give an insight idea of the variation of slope stability conditions within the different susceptibility zones according to the rainfall intensities. Ultimately it could be used to forecast spatial and temporal occurrences of slope instabilities and thereby to give real time early warnings of landslide hazards in the study area to minimize the losses caused.

The methodologies employed to achieve the above objectives are discussed in the next sections.

[3] Hydrological triggering can be defined as a decrease in shear strength due to an increase in pore water pressure on the potential failure surface which finally results in a slope failure. Pore water pressure increases may be directly related to rainfall infiltration and percolation (saturation from above) or may be the result of the build up of a perched water table or a ground water table (saturation from below) (Terlien, 1998).

5.2 Overview of the methodology

Many static and dynamic modeling approaches have been proposed in literature for landslide hazard zonation and prediction. Whereas, due to the limitations of scientific approaches to the complex natural processes, these models can only be thought as abstract descriptions or acceptable representations of reality. Hence each model has its own limitations and characteristic advantages and disadvantages. Therefore, selection of the best fit model for a particular area or a data set among comparison of many possible approaches can yield an output that may closely represent the natural processes to an acceptable level.

Given the above fact, under present study several static (cartographic) models were first prepared using different statistical approaches and then the best fit model was selected and finally the model was improved further by expert knowledge. Subsequently, a concept of dynamic modeling was adopted for the analysis of factor of safety conditions of various slopes with regards to the change of rainfall over time. The entire procedure includes two main steps:

(i) Preparation of landslide susceptibility models - static modeling,

(ii) Preparation of a combined hydrological slope stability model - dynamic modeling.

Whole analysis was built on raster structure with grid resolution of 3 m. For geo-processing, ESRI's ArcInfo 9.2 and 9.3 were used. The SPSS version 17 was utilized for the necessary statistical analysis that can not be performed within the GIS environment. PCRaster version 2, a freeware developed by the Utrich University, the Netherlands, was employed to perform the dynamic modeling part.

5.3 Preparation of landslide susceptibility models (static modeling)

The central idea of static modeling is the derivation of new cell attributes from the attributes already present, or from attributes of neighboring cells. It does not necessarily represent a process over time. An out put map is a variable that has fixed cell values representing one static state in the property of cells.

Landslide susceptibility models are static models used to rank the slope stability conditions of an area into ranges from stable to unstable. Susceptibility analyses use the local terrain conditions (static factors-section 3.2 and 4.5) for the evaluation of hazard and therefore the out put shows the areas with similar terrain conditions for landslide processes without any temporal implications.

In the present study, five susceptibility maps were prepared using both bivariate as well as multivariate analyses techniques. The methods in the study include:

(1) Information Value method (Landslide Index method)

(2) Weights of Evidence modeling (WOE)

(a) Using ArcGIS spatial analyst
(b) Using ArcSDM (Spatial Data Modeler) with 506 training sites
(c) Using ArcSDM with 22137 training sites

(3) Logistic Regression model (LR)

The methods one and two use bivariate techniques (section 3.3). Under WOE, three models were prepared using two different approaches. The third method is the most commonly applied multivariate technique in landslide studies (section 3.3).

5.3.1 Information Value method (landslide index method)

As the analysis technique is bivariate, the influence of factors is evaluated separately (interrelationships among the factors are not considered and use the assumption of conditional independence). This means that the different parameter maps are considered to be independent with respect to the probability of the occurrence of landslides. The weight value for a parameter class is defined as the natural logarithm of the landslide density in the class divided by the landslide density in the entire map.

$$W_i = \ln\left[\frac{DensClass}{DensMap}\right] = \ln\left[\frac{Npix(S_i)/Npix(N_i)}{\sum Npix(S_i)/Npix(N_i)}\right] \qquad (5.1)$$

W_i = weight for a certain parameter class
DensClass = landslide density within the parameter class
DensMap = landslide density within the entire map
$Npix(S_i)$ = number of landslide pixels in a certain parameter class
$Npix(N_i)$ = total number of pixels in a certain parameter class

The natural logarithm is used to give negative weights when the landslide density is lower than normal and positive weights when it is higher than normal. The equation yields a zero value for weights when the landslide distribution is regular (*DensClass = DensMap*).

After the calculation and assigning of individual weight for each class into parameter maps, they can be combined into a single weight map using a certain combination rule. The weights calculated for different factors generally may vary in dissimilar ranges. Hence, before combining them into a single map normalization of factor weights is necessary. Otherwise the influence of factors with higher weight values will be subjugated over the factors with lower weight values in the final map.

In the present study, percentage of influence of individual factor is considered equally (factors were weighted equally). The calculated weights were first assigned to the factor classes in the pixel basis and then they were normalized to the range of -1 to +1. The normalized factor weights were summated to get the total weight map.

5.3.2 Weights of Evidence modeling (WOE)

WOE is a data-driven bivariate technique, which is basically the Bayesian approach in a log-linear form (Spiegelhalter, 1986) and uses *prior* (unconditional) probability and *posterior* (conditional) probability. The method is applicable when sufficient data are available to estimate the relative importance of evidential themes via statistical means (Bonham-Carter, 1994). The method combines data from different

evidential themes to predict the occurrence of events. Each evidential theme is analyzed and an output consists of the odds of occurrence or logits. The logits are converted to natural logarithms and are used to calculate a positive and negative weight for each characteristic (Hansen, 2000). These individual theme weights can then be combined to predict an overall probability of the event.

The method was initially applied to non-spatial, quantitative, medical diagnoses to combine evidence from clinical diagnoses to predict diseases. In geosciences the method is applied extensively. For instance, this was used for mineral potential mapping (Bonham-Carter et al., 1988; Agterberg et al., 1989; Agterberg et al., 1990; Bonham-Carter et al., 1990) by implementing it in a Geographic Information System (GIS) framework.

For landslide susceptibility mapping, the WOE method calculates weight for each causative factor (evidential themes) of a landslide based on the presence or absence of landslides within the area. The spatial association between a set of evidential themes and a set of known landslide locations, which are expressed as the weights of evidence, is combined with the prior probability of occurrence of landslides to derive the posterior probability of occurrence of landslides, provided the evidential themes are conditionally independent with respect to the slides (Porwal et al., 2001).

The *prior probability* of an event is the probability of the event computed before the evidence (factor) is considered. It is simply the density of landslides in the entire area, i.e., the number of pixels with landslides divided by the total number of pixels in the map.

$$P_{prior} = P\{S\} = \frac{Npix(Slide)}{Npix(Total)} \tag{5.2}$$

Where,

$P_{prior} = P\{S\}$ = *unconditional probability of having a landslide S*

$Npix(Slide)$ = *number of pixels with landslide in the map*

$Npix(Total)$ = *total number of pixels in the entire map*

The prior probability can be modified by other sources of information or evidence. This revised probability of events, based on new evidence, is called posterior probability. In Bayesian statistics, posterior probability of a random event is the conditional probability that is assigned after the relevant evidence is taken into account. Considering the relationship a binary variable map (B_i) and a landslide map (S):

$$P\{S \mid B_i\} = \frac{P\{S \cap B_i\}}{P\{B_i\}} = \frac{Npix\{S \cap B_i\}}{Npix\{B_i\}} \tag{5.3}$$

$P\{S \mid B_i\}$ is the conditional probability of having a landslide in a unit B_i. This is the density of landslide within a certain unit, calculated as the number of landslide pixels within the unit, divided by the total number of pixels in the unit.

Via the conditional probability formulation, equation 5.3 can be written as,

$$P\{S \mid B_i\} = P\{S\} \cdot \frac{P\{B_i \mid \mathrm{S}\}}{\mathrm{P}\{B_i\}} \tag{5.4}$$

Posterior Probability *Prior Probability* *Factor*

This states that the conditional (posterior) probability of a landslide, given the presence of the factor B_i, equals the prior probability of the landslide $P\{S\}$, multiplied by the factor $P\{B_i \mid S\}/P\{B_i\}$. Similarly, the posterior probability of a landslide, given the absence of the factor B_i, can be determined as:

$$P\{S \mid \overline{B}_i\} = P\{S\} \cdot \frac{P\{\overline{B}_i \mid \mathrm{S}\}}{\mathrm{P}\{\overline{B}_i\}} \tag{5.5}$$

A similar model can be expressed in an odds form. In probability theory the *odds* in favor of an event is defined as follows:

$$Odds = \frac{\text{Probability that an event will occur}}{\text{Probability that it will not occur}} = \frac{P}{(1-P)} \tag{5.6}$$

where P is the probability of the event. Via the Odds formulation, the posterior odds of the landslide (S), given the presence or absence of any binary pattern (B_i or $\bar{B}_i$) is given by:

$$O\{S \mid B_i\} = O\{S\} \cdot \frac{P\{B_i \mid S\}}{P\{B_i \mid \overline{S}\}} \tag{5.7}$$

and

$$O\{S \mid \overline{B}_i\} = O\{S\} \cdot \frac{P\{\overline{B}_i \mid S\}}{P\{\overline{B}_i \mid \overline{S}\}} \tag{5.8}$$

where $O(S)$ is the prior odds of the slide, $[P(B_i \mid S) / P(B_i \mid \overline{S})]$ is called the factor or sufficiency ratio (LS) and $[P(\overline{B}_i \mid S) / P(\overline{B}_i \mid \overline{S})]$ is called the factor or necessity ratio (LN).

Bonham-Carter, 1994 defined positive and negative weights (w_i^+ and w_i^-) that combines the conditional probabilities as follows. Taking the natural logarithm and logit of the equations (5.7) and (5.8):

$$\ln O\{S \mid B_i\} = \ln O\{S\} + \ln\left(\frac{P\{B_i \mid S\}}{P\{B_i \mid \overline{S}\}}\right)$$

$$\operatorname{logit}\{S \mid B_i\} = \operatorname{logit}\{S\} + w^+ \tag{5.9}$$

where w^+ is the weights of evidence, presence of B_i, and

$$\ln O\{S \mid \overline{B}_i\} = \ln O\{S\} + \ln \frac{P\{\overline{B}_i \mid S\}}{P\{\overline{B}_i \mid \overline{S}\}}$$

$$\text{logit}\{S \mid \overline{B}_i\} = \text{logit}\{S\} + w^- \tag{5.10}$$

where w^- is the weights of evidence, absence of B_i. Hence:

$$w_i^+ = \log_e[P(B_i \mid S) / P(B_i \mid \bar{S})] \tag{5.11}$$

and

$$w_i^- = \log_e[P(\bar{B}_i \mid S) / P(\bar{B}_i \mid \bar{S})] \tag{5.12}$$

Where,

B_i = *presence of a potential landslide conditioning factor*

$\overline{B}_i$ = *absence of a potential landslide conditioning factor*

S = *presence of a landslide*

$\bar{S}$ = *absence of a landslide*

LS and *LN* are also referred to as likelihood ratios. If the pattern is positively correlated, *LS* is greater than 1 (w_i^+ is positive) and *LN* ranges from 0 to 1 (w_i^- is negative). If the pattern is negatively correlated, *LN* would be greater than 1 (w_i^- is positive) and *LS* ranges from 0 to 1 (w_i^+ is negative). If the pattern is uncorrelated with a landslide, then *LS* = *LN* = 1 ($w_i^+ = w_i^- = 0$) and the posterior probability would equal the prior probability, and the probability of a landslide would be unaffected by the presence or absence of the factor.

To quantify the spatial association between a map class and the occurrence of landslides, the contrast factor as mentioned in Bonham-Carter (1994) is defined:

$$C_w = \left(w^+\right) - \left(w^-\right) \tag{5.13}$$

The contrast factor is zero when the landslide pattern and map class pattern overlap only by the expected amount due to chance, positive when there is a positive association between the two patterns and negative when there is a negative association between the two patterns.

Almost all kind of natural processes are associated with few or many spatial variables. Hence, it is necessary to combine weights of all the factors, when more than one factor is involved. Based on Bayes' theorem, if factors are assumed conditionally independent, general expression for combining *i = 1, 2, 3……n* factors is given by the following equation:

$$\text{logit}\{S \mid B_1 \cap B_2 \cap B_3 \cap .....B_n\} = \text{logit}\{S\} + \sum_{i=1}^{n} w_i^+ \qquad (5.14)$$

If the i^{th} pattern is absent, w_i^+ will be replaced by w_i^-. If the data are absent or missing for any location, the weight values for the missing part are set to zero.

According to the equation 5.14, weights of the individual factor maps can be summated to obtain the total weight if the factors are conditionally independent. Expert selection or different types of statistical tests can be employed to test the dependency of the factors with respect to the landslides. Pairwise comparison, principal component analysis and logistic regression are some of the tests commonly used in landslide studies. Among them, pairwise comparison is the most employed method for testing conditional independence in the modeling approach using WOE (Regmi et al., 2009). In the present study, such statistical tests for checking the conditional independency were not performed and with the expert knowledge, all the evidential themes were included for the calculation of total weights.

The WOE model is generally applied using binary evidential themes i.e. with factor maps which contain two classes, representing the presence or absence of the factor. Real world geospatial data are usually multi-class or continuous. Hence this requires the analysis of many individual maps for each factor class separately (e.g. each landuse class separately for landuse map). Also, conversion of such data into binary type will result in the loss or distortion of information. Thus the extended weights of evidence model using multiclass predictor variable is preferred to binary weights of evidence model (Porwal et al., 2001). In the present study, WOE has been utilized with multi-class evidential themes using:

(i) ArcGIS Spatial Analyst and

(ii) Arc-SDM (Bonham-Carter et al., 1999).

(i) Using ArcGis Spatial Analyst

The method can be implemented by cross tabulating the landslide map with the factor (binary variable) maps. For each factor the following combinations are possible, of which the frequency, expressed as number of pixels.

Table 5.1: Cross- tabulation of landslide and binary variable maps (four possible combinations of a landslide conditioning factor and a landslide inventory map: N_{pix} = *number of pixels)*.

		Potential landslide conditioning factor (B_i)	
		Present	Absent
Landslides (*S*)	Present	N_{pix1}	N_{pix2}
	Absent	N_{pix3}	N_{pix4}

In order to compute these four combinations in the case of multiclass map, following columns are needed to be calculated in the joint-frequency table (cross table):

nmap = *total number of pixels in the map (= total count)*
nslide = *number of landslide pixels in the map (= total sum)*
nclass = *number of pixels in the class (= count)*
nslclass = *number of landslide pixels in the class (= sum)*

Hence,

N_{pix1} = *nslclass (= sum)*
N_{pix2} = *nslide-nslclass (= total sum-sum)*
N_{pix3} = *nclass-nslclass (= count-sum)*
N_{pix4} = *nmap-nslide-nclass+nslclass (= total count-total sum-count+sum)*

Based on equation 5.11 and 5.12 and Table 5.1, the weights of evidence can be written in number of pixels as follows:

$$w_i^+ = \log_e[(N_{pix1}/(N_{pix1} + N_{pix2}))/(N_{pix3}/(N_{pix3} + N_{pix4}))] \quad (5.16)$$

$$w_i^- = \log_e[(N_{pix2}/(N_{pix1} + N_{pix2}))/(N_{pix4}/(N_{pix3} + N_{pix4}))] \quad (5.17)$$

When the factor maps are multiclass maps, containing several classes, the presence of one factor class implies the absence of the other factor classes of the same map. Therefore, to obtain the total weight of a class ($w_{i-Total}$), the positive weight of the class should be added to the negative weights of the other classes in the same map. This can be done by applying following equation:

$$w_{i-Total} = \left(w_i^+\right) + \left(w_{Total}^-\right) - \left(w_i^-\right) \quad (5.18)$$

where $\left(w_{Total}^-\right)$ is the total of all negative weights in a multiclass map.

After the calculation of total weight for each factor class ($w_{i-Total}$) and assigning them into parameter maps, individual weight maps can be normalized to a range of -1 to +1 as in the case of Landslide Index method. Total weight map can be produced by summing up of all the normalized factor weights.

(ii) Using ArcSDM (Spatial Data Modeler)

In mapping the susceptibility of landslides using the WOE approach many researchers (e.g., Neuhauser and Terhorst, 2007; Dahal et al., 2008) commonly use point locations of landslides, as shown by either the center of the landslide polygon or the scarp or the locations of unit pixels that represent the area of the landslides. In this scenario, the probability of a landslide occurrence is the ratio of one landslide pixel from each existing landslide to the total number of the pixels in the entire area. This calculation ignores the sizes or magnitudes of the existing landslides. Furthermore, if the analysis does not have sufficient locations of landslides, the results obtained, based on the analysis of the parameters at the center of the landslides, might yield a biased result. These uncertainties can be reduced by entering the number of pixels covered by the landslide.

The approach is implemented in the ArcSDM (Spatial Data Modeller). In the present study ArcSDM 3.1 which is the compatible version of the ArcInfo 9.3 was used. Spatial Data Modeller is a free ArcGIS extension that provides a collection of tools for adding categorical maps with interval, ordinal, or ratio scale maps to produce a predictive map of where something of interest is likely to occur (Sawatzky et al., 2009). It provides the weights of evidence, logistic regression, fuzzy logic and neural network analysis capabilities. The extension works best when an evidential theme is reduced to just two classes (binary), although multiclass data can also be used (Raines et al., 2000).

WOE assumes there is one training site per unit cell. Training sites are points that represent areas consisting of the locations at which the point objects are known to be present. Huge number of training sites is generally a violation of basic assumption of WOE, which assumes the training site is a very small area and the total training sites are small. If the number of training sites gets very large, the Area Frequency and Site Reduction tools can fail in different ways. It is generally considered that more than 1000 training sites are excessive (Sawatzky et al., 2009). The prior probability has to be larger than 0.000001 or round off problem will occur. All evidential rasters must be integer rasters because in WOE uses a DBF table that is joined to the evidential layer (ArcSDM manual).

In the present study using ArcSDM 3.1, two models were tested with two different training site layers, one with center point of landslide polygons (total of 506 points) and other with the centers of the raster cells (10 * 10 m) representing the landslide locations (total of 22137 points).

5.3.3 Multivariate Logistic Regression (LR) model

The technique is multivariate and hence the influence of factors is evaluated simultaneously (section 3.3). Many researchers have used multiple regression, discriminate analysis and logistic regression for modeling landslide scenarios. Due to binary character of response and some predictor variables, and the dubious normality of some of the variables, a logistic regression procedure is preferred. The method considers several physical parameters (variables) that may affect the probability of an event and yields coefficients for each variable based on sample data. These coefficients which serve as weights in an algorithm can be used in GIS database to produce a map depicting the probability of landslide occurrence.

In statistics, logistic regression (logistic model or logit model) is used for predicting the probability (P) of occurrence of an event by fitting data to a logistic curve. It is a variation of ordinary regression which is applied when the dependent variable is a dichotomous variable and the independent variables (input) are continuous, categorical, or both. The algorithm of logistic regression applies maximum likelihood estimation after transforming the dependent into a logit variable (natural log of the odds of the dependent occurring or not). In this way LR estimates the probability of a certain event occurring. The form of the model is:

$$\text{logit}(P) = \log\left(\frac{P}{1-P}\right) = z \tag{5.19}$$

$$P = \frac{e^z}{e^z + 1} = \frac{1}{1 + e^{-z}} \tag{5.20}$$

where variable z is defined as:

$$z = \beta_0 + \beta_1 x_1 + \beta_2 x_2 + \beta_3 x_3 \cdots\cdots\cdots\cdots \beta_n x_n \qquad (5.21)$$

In the logistic function, (eq. 5.20), the input is z and the output is P. The variable z represents the exposure to some set of independent variables (x_i), while P represents the estimated probability of a particular outcome (landslide), given that set of explanatory variables.

In the model, each independent variable will have partial correlation to control the dependent variable. Hence, LR calculates each regressor (x_i) a coefficient (β_i) that measures its independent contribution to control the dependent variable. Finally, the variable z is a measure of the total contribution of all the independent variables used in the model and is known as the logit. The logistic function can take as an input (z) any value from negative infinity (-α) to positive infinity (+α); whereas the output (P) is confined to values between 0 and 1 on an S-shaped curve (Figure 5.1).

The β_0 is called the intercept and β_1, β_2, β_3,…….and β_n are the regression coefficients of the independent variables such as x_1, x_2, x_3,…….and x_n respectively. The intercept is the value of z when the value of all independent variables is zero (e.g., the value of z when there are no other contributing factors). Each of the regression coefficients describes the size of the contribution of particular factor. A positive regression coefficient means that that explanatory variable increases the probability of the outcome, while a negative regression coefficient means that variable decreases the probability of that outcome; a large regression coefficient means that the factor strongly influences the probability of that outcome; while a near-zero regression coefficient means that that factor has little influence on the probability of that outcome.

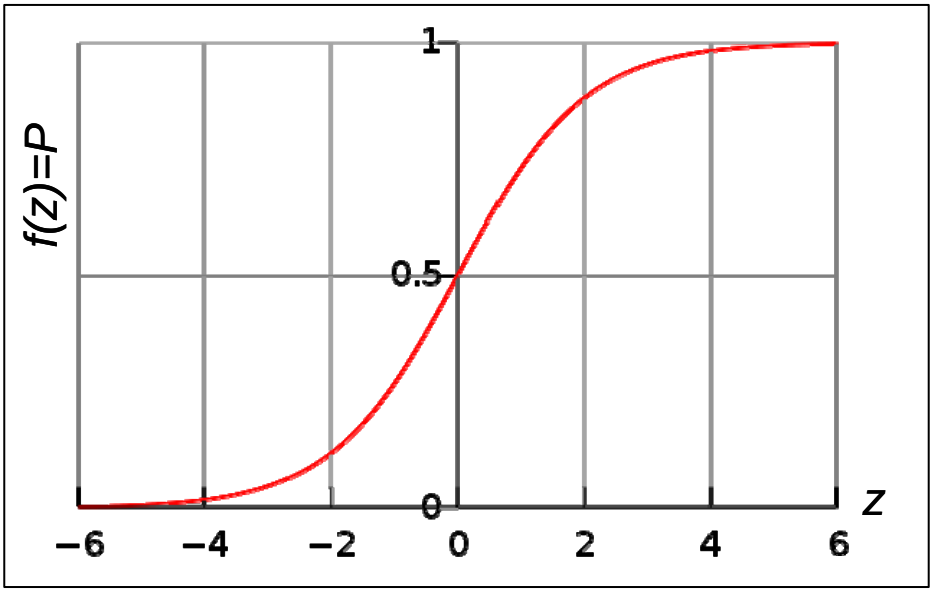

Figure 5.1: The logistic function, with z on the horizontal axis and $f(z)=P$ on the vertical axis.

Multivariate analysis can not be performed directly within the GIS environment. Therefore, using overall capabilities of GIS, first the necessary data matrix were created by determining the presence and absence of the dependent variable (landslide) and the independent variables (causative factors) within the predefined sample units of 100 * 100 m grids cells (section 3.3 and Figure 3.2). The regional GIS database was then exported to a statistical package (SPSS version 17) for the necessary analysis.

In the logistic regression, each factor class will be a separate variable for the model. Apart from the dependent variable landslide, all the 13 major factors considered in the study composed of 304 independent variables (factor classes). If the number of variables is small, LR produces good results. If there are many parameters, however, it would produce a long regression equation and may even create numerical problems. It may also work against some basic assumptions of LR such as the absence of strong correlation among independent variables (multicollinearity). It might also be difficult to understand statistical results and evaluate the role of each independent variable in the final model (Ayalew et al., 2005). Thus, number of variables was reduced to an acceptable level by using the method of Factor Analysis and Comparison of Means procedure.

For the selection of significant components, Factor Analysis method was applied if the Kaiser-Meyer-Olkin Measure of Sampling Adequacy is greater than 0.5 in the KMO and Bartlett's test. Here, Principal Component Analysis (PCA) was applied as an extraction method and all the components with Eigen values over 1 were selected. Rotation is used to improve the interpretability of the factors. One of the recommended orthogonal rotations of Varimax with Kaiser Normalization was employed to calculate the component transformation matrix. Since the rotation failed to converge in some of the factors where high number of factor classes (variables) is available, maximum iteration for convergence of 200 was utilized in the analysis.

Afterwards, number of components selected by the Factor Analysis was further reduced by the Comparison of Means procedure. Furthermore, the same procedure was directly applied for the reduction of variable to the factors where Kaiser-Meyer-Olkin Measure of Sampling Adequacy is lower than 0.5.

5.3.4 Susceptibility zonation, validation and selection of the best fit model

The susceptibility of an event (landslides) increases with increasing the total weight or probability values and zonations can be defined by reclassifying the maps into different ranges. Practically there is no straight forward statistical rule to categorize continuous data automatically and it is always unclear in landslide zonation mapping. In seeking a susceptibility map, the method adopted in literature by most of the researchers is to divide the histogram of the total weight or probability map into different categories based on expert opinions (Guzzetti et al., 1999; Lee and Min, 2001; Dai and Lee, 2002; Ohlmacher and Davis, 2003) or expert opinion basis along with the available classification methods.

In this study, total weight or probability maps were first reclassified into 5 major classes such as very low, low, medium, high, very high using Natural Breaks[4] (Jenks). They were then overlaid with the landslide distribution map and, landslide densities and total area covered by each class were calculated. Also, the performance of the susceptibility maps was tested by analyzing their success rate. The success rates illustrate how well the estimators (model) perform with respect to the event (landslides) used in constructing those estimators. Map crossing between predicted susceptibility maps and slope failures of the past events were carried out on the raster format.

[4] The Jenks Optimization method, also called The Jenks Natural Breaks classification method, is a data classification method designed to determine the best arrangement of values into different classes. This is done by seeking to minimize each class's average deviation from the class mean, while maximizing each class's deviation from the means of the other groups. In other words, the method seeks to reduce the variance within classes and maximize the variance between classes.

After the verification of susceptibility maps with the actual field conditions, a comparison was made among the maps prepared by different methods and attempted to choose the one that best suits the information and the scale of our investigation. The best fit model was further improved by the expert weightings and reclassified in to 3 different susceptibility zones such as high, medium and low. The class boundaries were adjusted until the resultant classes provided a satisfactory result with the use of existing landslide distribution map and expert judgment.

5.4 Preparation of a combined hydrological slope stability model (dynamic modeling)

Since the factors used in susceptibility analyses can be considered as time independent variables, those models represent a static conditions of slope stability and hence cannot be interpreted in real time processes. To overcome the problem, dynamic models which represent the rainfall dependent stability conditions of the slopes can be utilized.

Dynamic modeling is modeling of processes over time. Unlike in static modeling where an output map is a variable that has fixed cell values, here an output map is a variable that may have a different set of cell values for each time step. It means, several outputs are derived according to the defined time steps. This is done by computing new attributes as a function of attribute changes over time.

5.4.1 Dynamic modeling and PCRaster

For the dynamic modeling purposes, PCRaster version 2 package was used. PCRaster is a Geographical Information System (GIS) which consists of a set of computer tools for storing, manipulating, analyzing and retrieving geographic information. It is a raster-based system that uses a strict data type checking mechanism. PCRaster has relatively open database. The architecture of the system permits the integration of environmental modeling functions with classical GIS functions such as database maintenance, screen display and hard copy output. The modules for Cartographic and Dynamic Modeling are integrated with the GIS at a high level, which means that the GIS functions and modeling functions are incorporated in a single GIS and modeling language for performing both GIS and modeling operations (PCRaster Version 2 Manual).

Dynamic models are built with the language provided by PCRaster. Dynamic modeling language is an extension of the idea behind Map Algebra and Cartographic modeling. The language provides time operators for retrieving and storing dynamic data in iterative models. The iterative models are built in a structured *Dynamic Modeling script*. The script, which a program is written in the Dynamic Modeling language, consists of separate sections, each of which has a specific function in the dynamic model. The basic sections needed for building an iterative Dynamic Model are the *binding section, areamap section, timer section, initial section* and the *dynamic section*. The division in sections is an essential concept of the Dynamic Modeling language. It tells the computer how to execute a program and it helps the user to structure the components of a model (PCRaster Version 2 Manual).

In a dynamic model, for each time step a series of *pcrcalc* operations is consecutively performed using the resulting maps from the previous time step and/or external data that define the value of an attribute for that time step. This is done for all time steps of a model run. Thus a dynamic model can be seen as a

temporal sequence of static changes in the state of cells on map(s), each representing the change in the state of the modeled process over the time step.

5.4.2 Model description

Landslides are mostly triggered by a rise of pore water pressure in the slope, which decreases the resistance of soil material. Therefore, temporal occurrences of landslides are associated with the periods of high rain falls. In the present study, a combined hydrological slope stability model was employed to calculate the spatial and temporal changes of slope stability. To perform this task, additional geotechnical soil parameters as given in the Table 4.2 and Table 4.3 and mentioned in the section 4.5 is needed. The model description is based on Th. W. J. Van Asch and can be describes as follows:

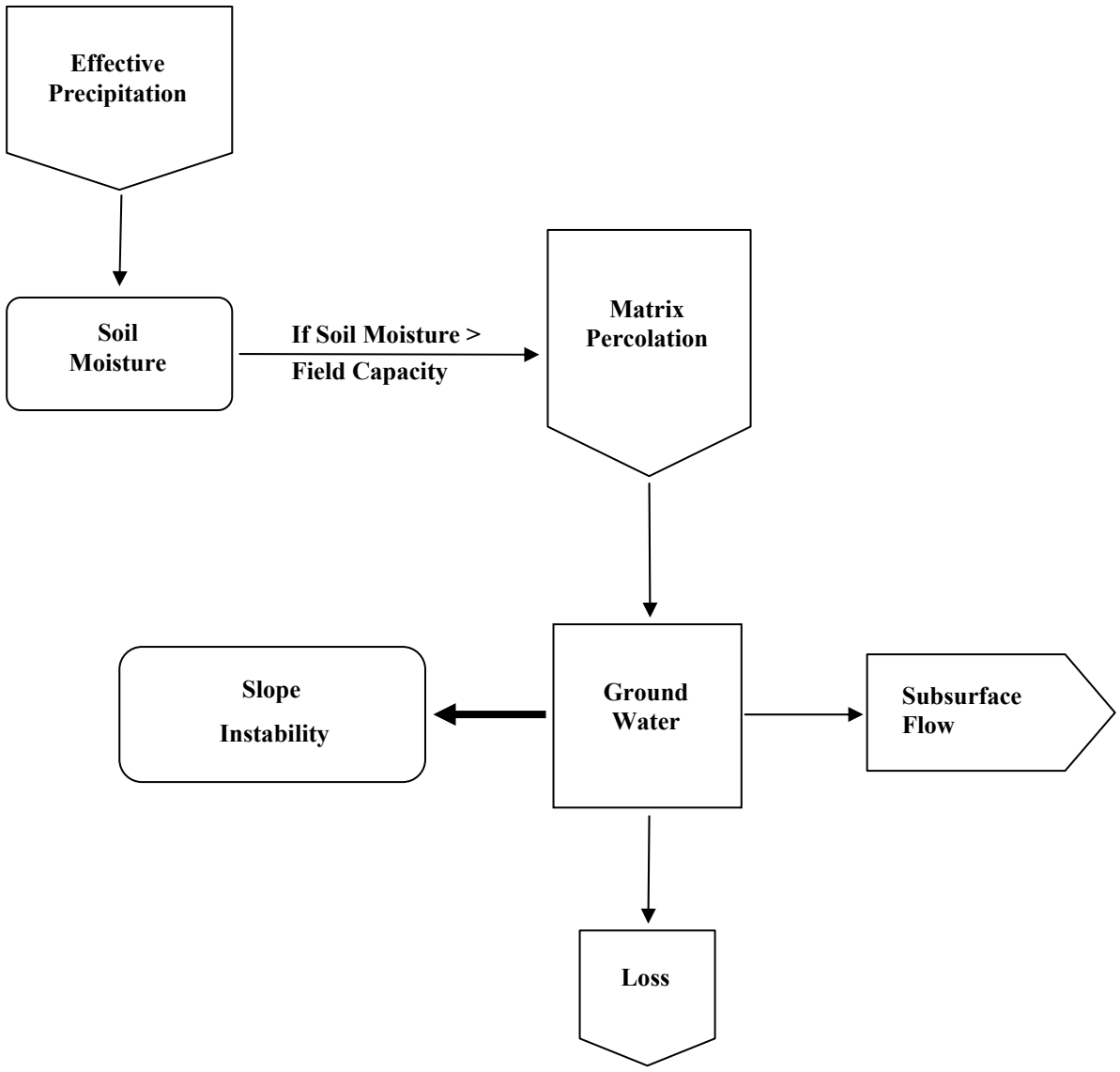

Figure 5.2: Flow chart of a combined hydrological slope stability model.

The model requires as an input effective precipitation. That means rain is supplied to the soil which is the gross precipitation minus the loss of water through interception and evapotranspiration. The rain input will percolate downwards in the unsaturated soil matrix to the ground water. Percolation of matrix water is only possible when the soil moisture content is above field capacity. The model assumes that the

unsaturated percolation of soil moisture to the ground water is taken place by gravity according to the following equation:

$$P_r = K_s \{(\theta - \theta_r)/(\theta_s - \theta_r)\}^a \qquad (5.22)$$

where,

P_r = *percolating flux (cm^3/day)*
K_s = *saturated hydraulic conductivity (cm/day)*
θ = *actual volumetric soil moisture content (cm^3/cm^3)*
θ_r = *residual volumetric moisture content (cm^3/cm^3)*
θ_s = *saturated volumetric moisture content (cm^3/cm^3)*
a = *constant (between 3 and 8)*

A perched ground water table will be developed at the lower boundary of the soil layer, which is assumed to be nearly impermeable. This boundary is assumed to be the transition from soil to unweathered rock. This ground water flow can be calculated by:

$$Q = K_s z_w B \sin\beta \qquad (5.23)$$

where,

Q = *ground water flow in cm^3 per time step*
K_s = *saturated hydraulic conductivity*
z_w = *height of the ground water table (cm)*
B = *width of flow (=width of pixel) (cm)*
$\sin\beta$ =*sinus of the topographical slope (-)*

A certain amount of ground water is assumed to be percolated into the unweathered rock. Ground water flow is routed in a down slope direction according to the DEM.

The stability of the slope is calculated in terms of factor of safety (F_s). For simplicity, an infinite slope model which is used for the analysis of translational slides is assumed to evaluate the initiation mechanisms of slope failures (section 2.4.3, Figure 2.9 and 2.10). It is assumed that the slip surface is planer and parallel to the topographic slope and the mobile slice is uniform in thickness resting on a slope of constant angle and infinite extent. In that case the stability can be calculated for each pixel. The factor of safety is given by:

$$F_s = \frac{\left[c' + \left(\gamma z \cos^2\beta - u\right)\tan\phi'\right]}{\gamma z \sin\beta \cos\beta} \qquad (5.24)$$

where,

F_s = *factor of safety*
c' = *soil cohesion (kN/m^2)*
γ = *unit weight of the soil (kN/m^3)*
z = *depth of the soil (slip surface) (m)*

u = *pore water pressure (kN/m^2)*

β = *angle of the topographical slope*

The pore water pressure is related to the height of the ground water above the slip surface in the slope as follows:

$$u = \gamma_w z_w \cos^2 \beta \qquad (5.25)$$

where,

γ_w = *unit weight of water (kN/m^3)*

z_w = *height of the water table above the slip surface (m)*

The height of the water table is related to the input of rain and the subsurface drainage of groundwater along the slope and it can be calculated with the hydrological model.

6 Results and discussion

6.1 General information

General information obtained from the digital maps within the GIS environment and used in the analysis is shown in the Table 6.1.

Table 6.1: General information.

	Vector Area (m^2)	Raster Area (m^2)
Total study area	263457229 (263.46 km^2)	263436651 (263.43 km^2)
Total landslide area	3423748 (3.42 km^2)	3423510 (3.42 km^2)
Percentage (%) of total landslide area	1.30%	1.30%
Total area of landslide rupture surface	2208579 (2.21 km^2)	2207475 (2.21 km^2)
% of landslide rupture surface area	0.84%	0.84%
Area of the smallest landslide (rupture)	14.62	18.00
Area of the largest landslide (rupture)	122053.90	122103.00
Mean area of landslide (rupture)	4364.80	4365.10
Total number of landslides in the study area	= 513	
Number of shallow landslides used in the analysis	= 506	
Number of landslides (rupture) smaller than the mean area	= 403	
Number of landslide causative factors used in the analysis	= 13 (see section 4.5)	
Total number of variables (factor classes)	= 257 (304 in the MLR* model)	
Pixel resolution	= 3 m	
Total number of pixels in the study area	= 29270739	
Total number of pixels where landslide (rupture) occurred	= 245275	
Landslide (rupture) density within the entire map (DensMap)	= 0.0084	

* Multivariate Logistic Regression

The landslide inventory map consists of 513 slides out of which 506 can be considered as shallow translational landslides. Since the analyses require only the initiation part of the landslides, a surface of rupture map was prepared for the selected shallow translational landslides. Area of surface of rupture varies from 14.62 m^2 to 122053.9 m^2 with a mean area of 4364.8 m^2. About 80% (403) of the landslides considered in the analyses are smaller than the mean area.

The vector area is the actual area mapped. The grid resolution of 3 m was selected as a common raster resolution considering the landslide with an area of 14.62 m^2 as the smallest feature to be identified and to minimize the difference between vector area (actual area) and raster area.

6.2 Analysis of distribution of parameter (factor) classes and landslides

Using the parameter data and landslide distribution map, extent of each factor class, total number of landslides and the area of landslide within each factor class were determined. Since the number of landslides or a total area of landslide within a parameter class is not a good indicator to measure the

influence of various factors for slope instabilities, density of landslide within each parameter class was estimated and utilized.

Distribution of the factor classes, landslide area and the landslide density within each of the factor classes are summarized into tables and graphs as follows. Data tables as well as the figures for the nominal data are arranged according to the descending order of landslide density.

Table 6.2: Distribution of lithology classes, area of landslide and landslide density within each class.

Type of Lihology	Area of the factor class (km^2)	Area of landslide (km^2)	LS* density within the factor class	Factor scores **
Ch	129.7495	1.3594	0.0105	0.2234
GtBtChGn	76.8362	0.5304	0.0069	-0.1938
Kh	38.5030	0.2582	0.0067	-0.2229
HbBtGn	9.2595	0.0464	0.0050	-0.5143
QtFpGn	0.7993	0.0026	0.0033	-0.9287
MetaGabbro	8.2892	0.0104	0.0013	-1.8960
Total area	**263.4367**	**2.2075**	--	--

* Landslide, ** Calculated factor scores (weights) for Information Value method (section 6.3.1)

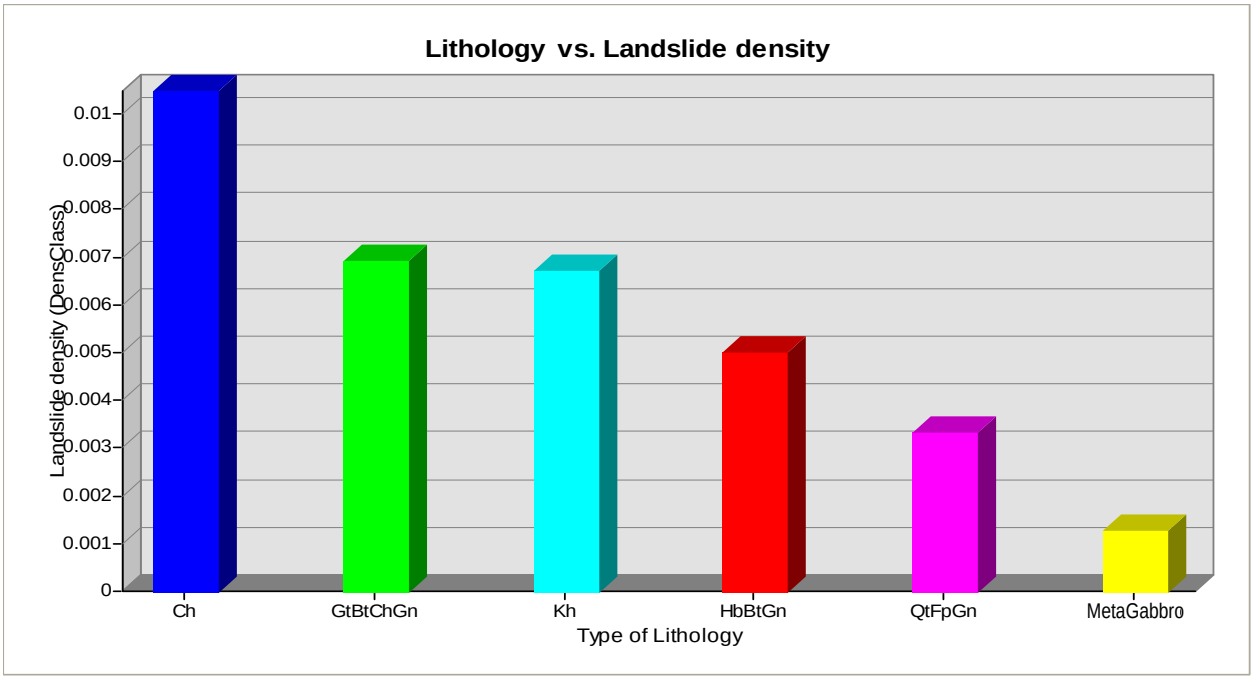

Figure 6.1: Landslide density (landslide area per unit area) according to the lithology classes.

According to the Table 6.2, majority of the study area (about 49%) is covered by rock type Charnockite (Ch). It records the highest landslide area (61.6%) and also the highest landslide density (Figure 6.1). Hence, if the influence of other factors were negligible, areas with the underlying rock type Charnockite can be considered as the highest vulnerable sites for landsliding which is also a highly accepted fact by many previous studies in Sri Lanka. This can be mostly due to the presence of higher joint density associated with Charnockite rock which provide weak zones and facilitate the infiltration of rain water aiding weathering and rising hydrostatic pressure within the subsurface. Other rock types such as Garnet-Biotite-Charnockitic Gneiss (GtBtChGn), Khondalite (Kh) and Hornblend-Biotite Gneiss (HbBtGn) show gradual decrease of the area of the factor class, landslide area and also the landslide density. In contrary,

Quartzo Feldspathic Gneiss, (QtFpGn) the least occurring rock type which covers less than 1% of the study area shows more than double the landslide density to rock type Meta Gabbros.

Table 6.3: Distribution of landuse classes, area of landslide and landslide density within each class.

Landuse map code	Area of the factor class (km^2)	Area of landslide (km^2)	LS density within the factor class	Factor scores
W2	7.3765	0.255825	0.03468	1.4204
JWb	0.5682	0.017550	0.03089	1.3045
JT1	25.8645	0.526041	0.02034	0.8867
W3	4.2973	0.043902	0.01022	0.1982
S2	0.3357	0.002907	0.00866	0.0329
HK	114.0487	0.911745	0.00799	-0.0471
JT2	28.2757	0.204534	0.00723	-0.1471
G1	2.4483	0.015786	0.00645	-0.2621
JR1	3.3538	0.021420	0.00639	-0.2716
S3	0.4696	0.002529	0.00539	-0.4420
S1	0.2838	0.001440	0.00507	-0.5016
S4	0.5747	0.002268	0.00395	-0.7530
HT	6.7486	0.025677	0.00380	-0.7895
W1	47.0018	0.140310	0.00299	-1.0321
JWp	1.0125	0.001926	0.00190	-1.4827
HP	18.1957	0.033615	0.00185	-1.5120
JR2	0.0451	0.000009	0.00020	-3.7380
G2	0.1019	0.000009	0.00009	-4.5522
HA	0.1794	0.000009	0.00005	-5.1181
JC	0.3084	0.000009	0.00003	-5.6599
G3	0.3418	0.000009	0.00003	-5.7628
HR	0.4676	0.000009	0.00002	-6.0762
HC	0.5506	0.000009	0.00002	-6.2396
W4	0.5863	0.000009	0.00002	-6.3024
Total area	**263.4367**	**2.207547**	--	--

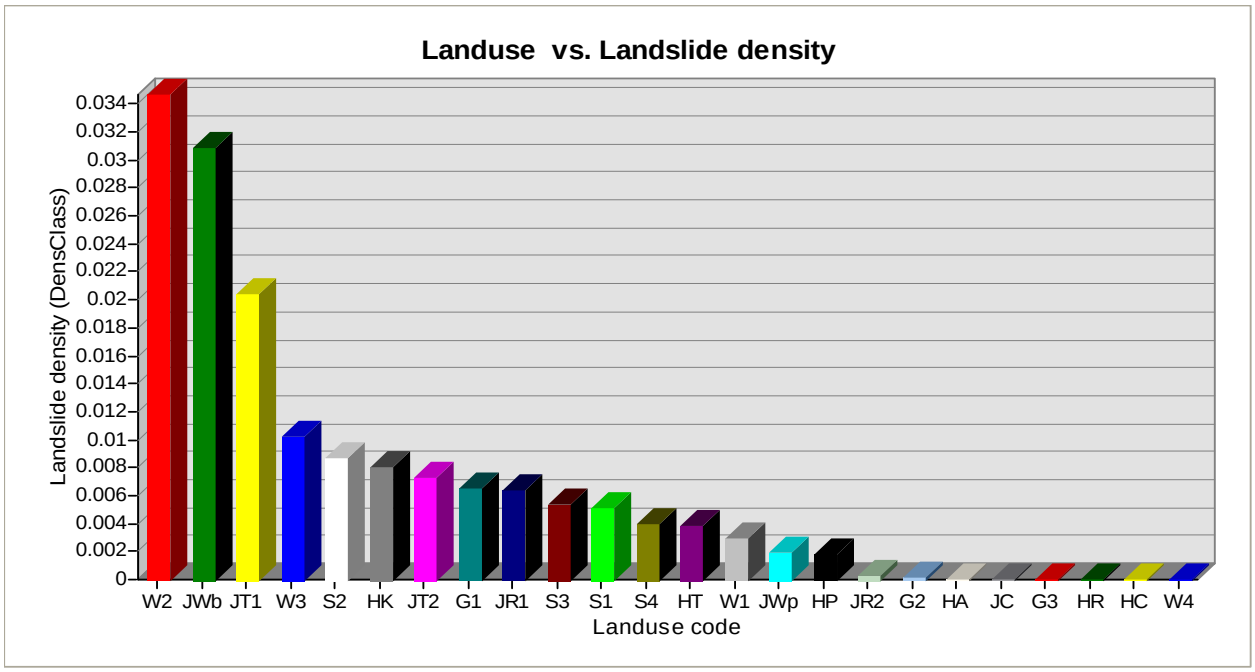

Figure 6.2: Landslide density according to the landuse classes (see Annex-II for landuse map code types).

As can be seen from the Figure 6.2, two major breaks of landslide densities can be recognized. The landuse codes W2, JWb and JT1 which covers the total land area of 33.81 km^2 (12.8%) record the highest landslide densities. The JT1 records the second highest landslide area of 0.5260 km^2 (23.83%). These 3 landuse codes represent degraded natural forests (50-70% cover), forest plantations (broadleaf varieties) and well managed tea estates (70-90% cover) accordingly. Although it is generally expected, these 3 landuse classes to be less vulnerable for sliding, result here are in contrary and this could be mainly due to the presence of other highly favorable conditions for slope instabilities such as steep slope angle, favorable geological structures, landform, etc., within these areas.

After a sudden drop of LS density at landuse code of W3 (secondary forest/scrubland), it gradually decreases up to the landuse code HP (terraced paddy). The total land area covered by these landuse classes together is 227.05 km^2 (86.2%). The group consists of the landuse code HK (agro forestry/homestead) which has the highest land area coverage of 114.05 km^2 (43.3%) recording the highest landslide area of 0.9117 km^2 (41.3%). W1 (dense natural forests) that comes under the same group has the second largest land area coverage of 47 km^2. Only a small percentage (about 2.5%) of the total area is covered by the landuse types belonging to the last category (codes JR2 to W4).

According to the Figure 6.3, four landform classes coded as X43, D31, E41, X33 shows the highest landslide densities. They are named as dissected and gullied surfaces with non converging incised drainage ways, straight hill slopes with relief amplitude 50 to 200 m, straight mountain slopes with relief amplitude greater than 200 m and fossil landslide scars. Total extent covered by these landform classes is 8.426 km^2 (3.2%). The next four classes that gives subsequently higher landslide density comes under one category, E (hilly and mountainous systems with elevation ranging from 200 m to 1200 m approximately). As shown by the Figure 6.3, many of the landform classes belonging to the category E records slightly higher landslide densities showing gradual decrease from class E44 to E33. A vast majority of the study area is covered by landform classes belonging to the category E which is equal to 239.16 km^2 (90.78%). The highest landslide area of 0.5552 km^2 (25% of the landslides) was recorded by the landform type E46.

As shown in the Table 6.5, residual soil (RS) is the most widespread soil type covering 232.95 km^2 (88.43%). Although the majority of the landslides or the highest landslide area of 1.4122 km^2 (63.97%) is given by this soil, RS records the least landslide density among all (Figure 6.4) soil types. Hence, unlike in lithology where majority of the study area is covered by highly vulnerable rock type Charnockite, here a vast majority of the land area is composed with the least vulnerable soil type residual.

While colluvium soil has the highest landslide density colluvium/residual soil comes to the second highest place. The result shows beyond doubt that the strength of material plays a major role in slope instabilities showing the lowest landslide density in residual soils which has the highest shear strength and giving the highest landslide density in colluvium soils due to its low resistance in shear. Colluvium soils are the loose soils which is transported and deposited.

High porosity and permeability in loose materials such as colluvium or colluvium/residual soil facilitate rain water infiltration which can subsequently cause for the increase of piezometric pressure within the material making slopes to be unstable rapidly. If the residual soil is overlain by colluvium soils (colluvium/residual) in a shallow depth, the boundary between two soil types can act as a weak zone such

as a permeability barrier, interface of change of density, compaction level or strength causing shallow landslides along the boundary.

Table 6.4: Distribution of landform classes, area of landslide and landslide density within each class.

Landform map unit	Area of the factor class (km^2)	Area of landslide (km^2)	LS density within the factor class	Factor scores
X43	0.2517	0.01283	0.050994	1.8059
D31	0.2618	0.01201	0.045851	1.6996
E41	7.5530	0.22508	0.029800	1.2687
X33	0.3596	0.00824	0.022899	1.0053
E44	14.5786	0.23534	0.016143	0.6557
E43	4.1503	0.06497	0.015654	0.6250
E46	39.2065	0.55524	0.014162	0.5248
E31	4.7195	0.06060	0.012840	0.4267
E35	30.5526	0.30416	0.009955	0.1723
E45	11.7563	0.11470	0.009756	0.1521
D36	0.6248	0.00512	0.008197	-0.0221
E48	9.5757	0.07776	0.008121	-0.0314
E33	9.5353	0.06034	0.006328	-0.2809
D12	4.5527	0.02813	0.006180	-0.3045
E42	17.2387	0.10077	0.005846	-0.3601
E13	1.6431	0.00929	0.005653	-0.3936
X44	0.4534	0.00251	0.005538	-0.4142
E38	11.7110	0.05785	0.004940	-0.5284
E32	39.8271	0.15666	0.003934	-0.7562
F11	2.5490	0.00998	0.003916	-0.7608
E14	0.7028	0.00241	0.003432	-0.8927
E47	2.2974	0.00683	0.002973	-1.0361
E36	11.6409	0.03429	0.002946	-1.0455
D35	2.2808	0.00554	0.002431	-1.2376
E12	0.3684	0.00086	0.002345	-1.2734
E37	18.5572	0.04296	0.002315	-1.2865
D11	3.8412	0.00681	0.001774	-1.5528
X42	0.3163	0.00053	0.001679	-1.6078
E25	0.3399	0.00047	0.001377	-1.8059
X21	0.0756	0.00009	0.001191	-1.9513
D32	6.8344	0.00509	0.000745	-2.4197
X11	0.0164	0.00001	0.000548	-2.7274
E26	0.0305	0.00001	0.000295	-3.3478
D33	0.0426	0.00001	0.000211	-3.6797
X13	0.0476	0.00001	0.000189	-3.7924
E22	0.0485	0.00001	0.000185	-3.8111
E24	0.0903	0.00001	0.000100	-4.4314
X41	0.1254	0.00001	0.000072	-4.7597
E21	0.1450	0.00001	0.000062	-4.9056
E23	0.1754	0.00001	0.000051	-5.0954
D34	0.6734	0.00001	0.000013	-6.4408
D37	0.9676	0.00001	0.000009	-6.8034
E34	1.1242	0.00001	0.000008	-6.9534
E49	1.5944	0.00001	0.000006	-7.3028
Total area	**263.4367**	**2.20759**		

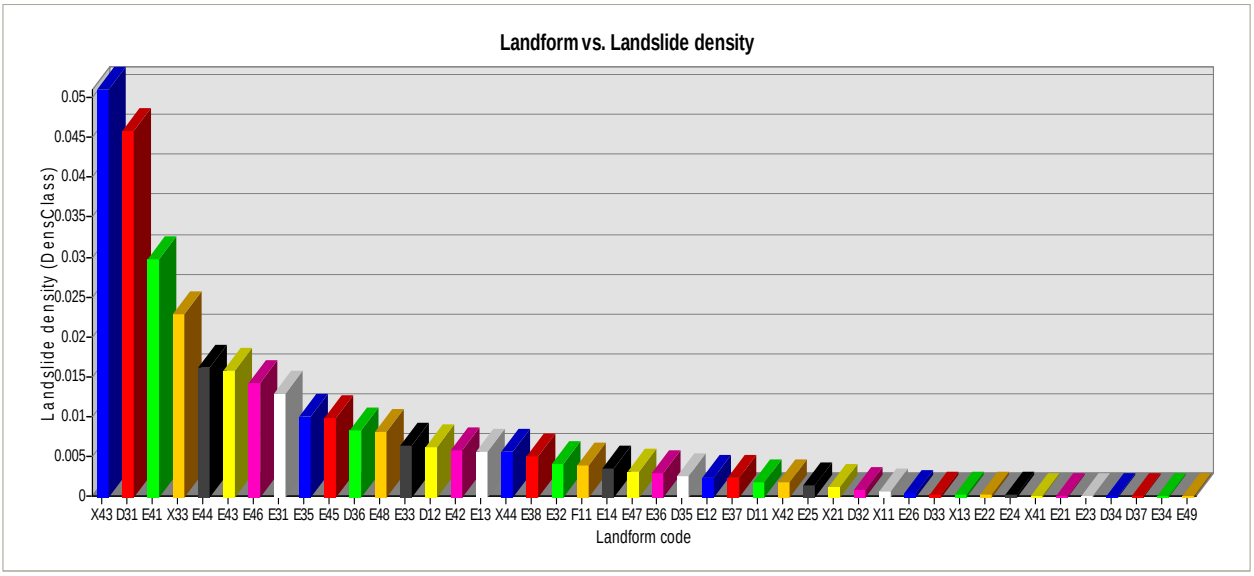

Figure 6.3: Landslide density according to the landform classes (see Annex-II for landform map code).

Table 6.5: Distribution of soil types, area of landslide and landslide density within each class.

Soil type	Area of the factor class (km^2)	Area of landslide (km^2)	LS density within the factor class	Factor scores
Colluvium (Coll)	21.1307	0.7055	0.0334	1.3824
Colluvium/Residual	5.2859	0.0510	0.0097	0.1418
Rock exposure (RE)	4.0672	0.0387	0.0095	0.1266
Residual (RS)	232.9529	1.4122	0.0061	-0.3237
Total area	**263.4367**	**2.2075**	--	--

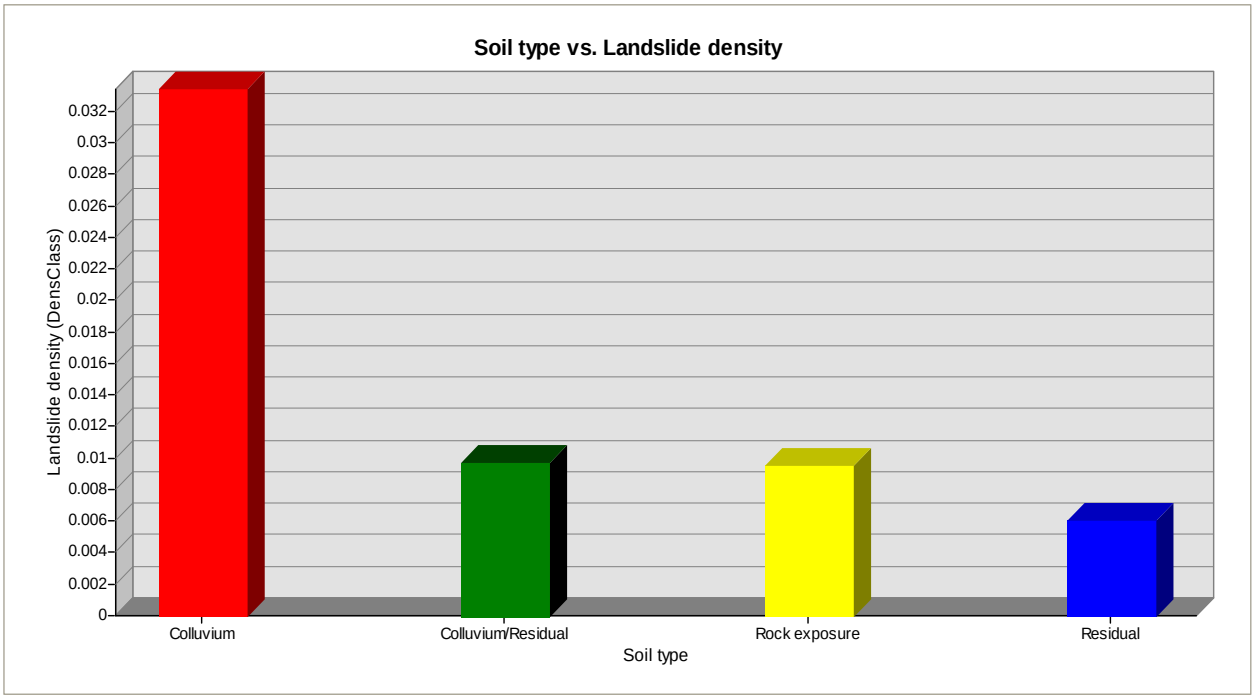

Figure 6.4: Landslide density according to the soil type classes.

Table 6.6: Distribution of soil thickness, area of landslide and landslide density within each class.

Soil thickness with type (m)	Area of the factor class (km^2)	Area of landslide (km^2)	LS density within the factor class	Factor scores
Coll>2+RS>3	0.0611	0.01740	0.28489	3.5263
Coll=4-5	0.7540	0.11861	0.15731	2.9324
Coll=1-2	0.2153	0.02062	0.09577	2.4361
Coll>3	3.9452	0.21092	0.05346	1.8532
RS=3	0.4314	0.01921	0.04452	1.6701
Coll=3-4	3.7924	0.14103	0.03719	1.4902
Coll>4	3.3646	0.09837	0.02924	1.2496
RS=2-4	0.0405	0.00102	0.02510	1.0971
Coll>2	4.8159	0.09003	0.01869	0.8024
Coll=2-3	1.2179	0.01812	0.01488	0.5739
RS=5-6	0.0428	0.00059	0.01388	0.5045
Coll=1+ RS>2	1.5926	0.02050	0.01287	0.4294
Coll=1-2+RS=1-2	0.0642	0.00078	0.01221	0.3761
Coll>2+RS>2	0.6949	0.00752	0.01083	0.2563
RE-Rock exposure	4.0672	0.03868	0.00951	0.1266
RS>3	66.0539	0.61920	0.00937	0.1122
RS>4	10.1646	0.09136	0.00899	0.0701
RS>5	1.7686	0.01275	0.00721	-0.1502
Coll=2	1.1792	0.00780	0.00662	-0.2361
RS=2-3	36.6017	0.23621	0.00645	-0.2611
RS=3-4	21.0435	0.10497	0.00499	-0.5187
RS=4-5	1.2424	0.00526	0.00423	-0.6835
RS>2	65.4768	0.25435	0.00388	-0.7688
RS<1	1.7656	0.00516	0.00292	-1.0539
Coll=1-2+RS>2	1.9228	0.00455	0.00236	-1.2656
RS=1-2	26.4204	0.06116	0.00232	-1.2864
RS<2	0.2014	0.00038	0.00188	-1.4964
Coll>2+RS=2	0.1564	0.00029	0.00184	-1.5151
RS=2	0.4625	0.00063	0.00136	-1.8168
RS=1	0.0214	0.00001	0.00042	-2.9933
RS>7	0.0258	0.00001	0.00035	-3.1787
RS=4	0.0393	0.00001	0.00023	-3.6010
RS<4	0.0423	0.00001	0.00021	-3.6729
Coll=1+RS=1	0.0449	0.00001	0.00020	-3.7324
Coll=1	0.1099	0.00002	0.00016	-3.9346
Coll=1+RS=1-2	0.0631	0.00001	0.00014	-4.0737
Coll=2+RS>1	0.0678	0.00001	0.00013	-4.1451
RS>6	0.0737	0.00001	0.00012	-4.2286
RS=1-3	0.2476	0.00001	0.00004	-5.4406
Coll=4	0.3793	0.00001	0.00002	-5.8668
Coll=1+RS>3	0.6182	0.00001	0.00001	-6.3554
RS>1	0.7866	0.00001	0.00001	-6.5962
Coll=3	1.3571	0.00001	0.00001	-7.1417
Total area	**263.4367**	**2.20759**	--	--

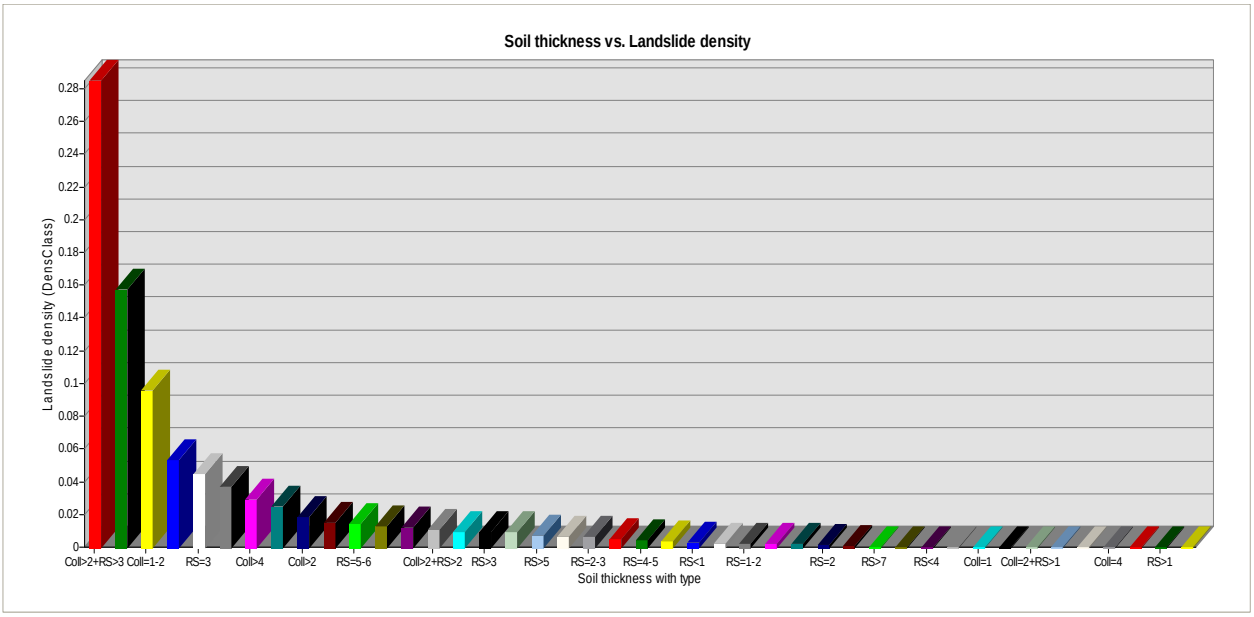

Figure 6.5: Landslide density according to the classes of soil thickness with type.

In the case of overburden landslides, the depth to solid rock is an important factor. Whereas, due to the high number and the complexity of the soil thickness classes arranged according to the type of soils, any logical pattern of landslide density can not be observed here. For instance, weak soil classes such as Coll=3 and Coll=4 gives lower landslide density than to the RS=3 even though the residual soil is considered as comparatively more stable than colluvium soils (Table 6.6 and Figure 6.5). The same situation is further confirmed by the Factor Analysis and Comparison of Means procedure applied in the data selection process in the multivariate logistic regression model too. This procedure shows that there seems to be no relevance of all the variables (factor classes) of this factor for explaining the occurrence of landslides (Table 6.23). Therefore, a kind of acceptable classification scheme of soil thickness classes according to soil types is necessary and need to be implemented for the step of field data collection.

Among all landslide causes, slope angle is considered as one of the most influencing factor for slope instabilities. This is mainly due to the increase of driving forces due to weight of the slope material with the rise of slope angle. As depicted by the Figure 6.6, landslide density increases gradually with the increase of slope angle until to the category of $45\text{-}48^0$. Then, the density increases more rapidly until it reaches to the maximum at the category of $63\text{-}66^0$ except the anomalies occur at the categories of $54\text{-}57^0$ and $57\text{-}60^0$. The results obtained here clearly demonstrate the theoretical understanding of influence of the slope angle towards the occurrence of landslides.

The highest landslide densities are recorded by three categories, slope angle ranging from 60 to 69^0 covering a total land area of 0.0593 km^2 (0.022%) with total landslide area of 0.0041 km^2 (0.185%). This demonstrates the vast majority of the study area does not belong to the slopes with the highest landslide densities.

The first part of the graph consists of all the slope angles ranging from 0 to 48^0 that covers a total land area of 260.71 km^2 (99.54%) with a total landslide area of 2.17 km^2 (98.36%). Considering the small jump occurred at the category of $6\text{-}9^0$, slopes from 0 to 6^0 can be regarded as gentle slopes where landslides are unlikely. The total land area covered by these slope ranges ($0\text{-}6^0$) are 48.6581 km^2 (18.47%) with a landslide area of 0.0425 km^2 (1.93%). Even though the highest landslide densities are not

Table 6.7: Distribution of slope angle, area of landslide and landslide density within each class.

Slope angle category (deg.)	Area of the factor class (km^2)	Area of landslide (km^2)	LS density within the factor class	Factor scores
0-3	21.4584	0.00576	0.00027	-3.44097
3-6	27.1997	0.03675	0.00135	-1.82494
6-9	25.8458	0.10055	0.00389	-0.76730
9-12	26.8527	0.16414	0.00611	-0.31543
12-15	27.1283	0.20501	0.00756	-0.10331
15-18	25.8370	0.22395	0.00867	0.03381
18-21	23.4798	0.23295	0.00992	0.16888
21-24	20.3729	0.22775	0.01118	0.28827
24-27	16.9474	0.20925	0.01235	0.38763
27-30	13.6006	0.19050	0.01401	0.51376
30-33	10.5509	0.16372	0.01552	0.61615
33-36	8.2345	0.13403	0.01628	0.66392
36-39	6.0445	0.10436	0.01726	0.72286
39-42	4.3464	0.08159	0.01877	0.80661
42-45	2.8063	0.05789	0.02063	0.90086
45-48	1.5053	0.03318	0.02204	0.96723
48-51	0.6831	0.01859	0.02722	1.17820
51-54	0.2955	0.00916	0.03101	1.30846
54-57	0.1286	0.00278	0.02163	0.94841
57-60	0.0583	0.00147	0.02515	1.09908
60-63	0.0323	0.00185	0.05746	1.92533
63-66	0.0184	0.00159	0.08638	2.33301
66-69	0.0086	0.00065	0.07500	2.19170
69-73	0.0014	0.00001	0.00633	-0.28063
Total area	**263.4367**	**2.20748**	--	--
Mean	**10.9765**	**0.09198**	**0.02150**	**0.43007**

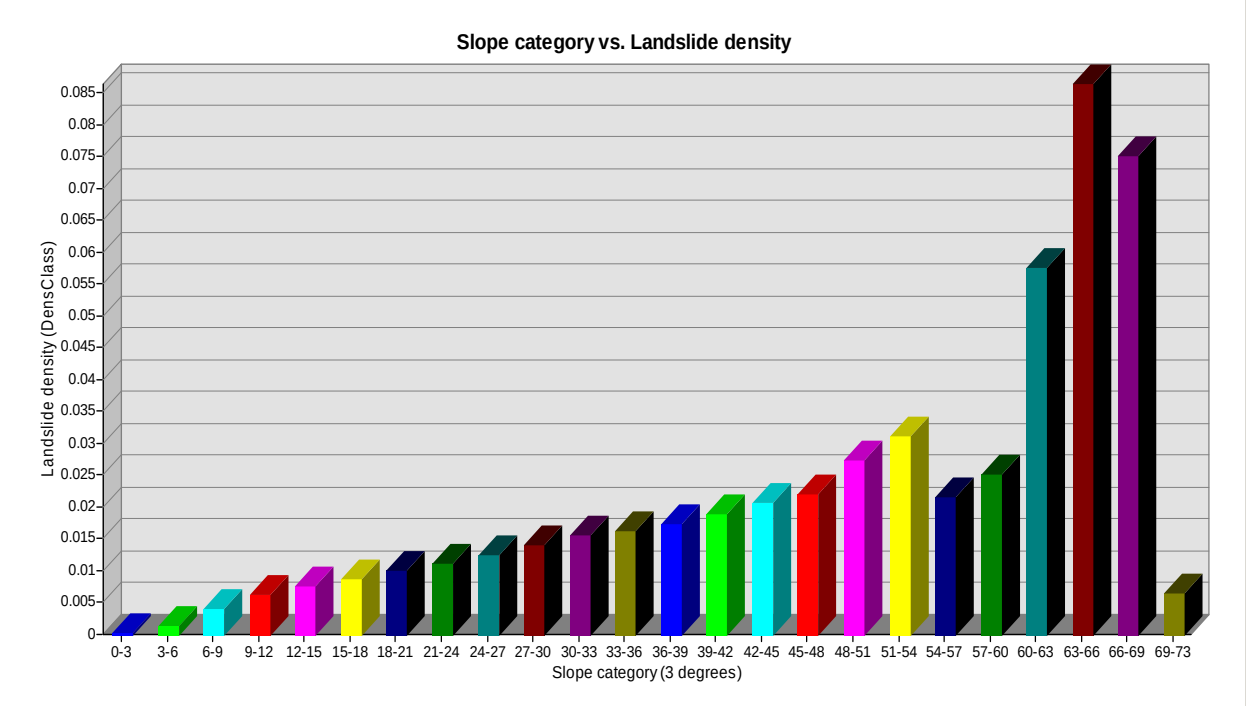

Figure 6.6: Landslide density according to the slope category (3 degrees category).

recorded in the range of 6-48^0, due to the total extent of the land (212.05 km^2) and the distribution of landslides, it can be considered as the most important part of the study area. And also, this is the area where much of the human activities are taking place with the risk of landslides.

Table 6.8: Distribution of aspect category, area of landslide and landslide density within each class.

Aspect category (degree)	Area of the factor class (km^2)	Area of landslide (km^2)	LS density within the factor class	Factor scores
0 (North)-10	6.1710	0.0410	0.0067	-0.23111
10-20	5.6238	0.0348	0.0062	-0.30309
20-30	5.5935	0.0332	0.0059	-0.34373
30-40	5.2758	0.0314	0.0060	-0.34150
40-50	5.6138	0.0350	0.0062	-0.29642
50-60	5.3295	0.0317	0.0059	-0.34365
60-70	5.7557	0.0368	0.0064	-0.27071
70-80	5.7896	0.0484	0.0084	-0.00157
80-90	6.2957	0.0672	0.0107	0.24166
90-100	6.7342	0.0768	0.0114	0.30876
100-110	6.9101	0.0718	0.0104	0.21489
110-120	7.5243	0.0872	0.0116	0.32377
120-130	7.7475	0.1113	0.0144	0.53926
130-140	8.9358	0.1277	0.0143	0.53355
140-150	8.8574	0.1052	0.0119	0.34840
150-160	9.6752	0.0888	0.0092	0.09127
160-170	9.5197	0.0856	0.0090	0.07010
170-180	9.6226	0.0746	0.0078	-0.07775
180-190	9.3044	0.0636	0.0068	-0.20362
190-200	8.6091	0.0572	0.0066	-0.23277
200-210	8.4185	0.0585	0.0070	-0.18674
210-220	7.7843	0.0568	0.0073	-0.13838
220-230	7.8396	0.0555	0.0071	-0.16789
230-240	7.0383	0.0501	0.0071	-0.16343
240-250	7.2450	0.0546	0.0075	-0.10552
250-260	7.0560	0.0440	0.0062	-0.29586
260-270	7.3403	0.0453	0.0062	-0.30672
270-280	7.3518	0.0395	0.0054	-0.44396
280-290	7.0823	0.0401	0.0057	-0.39304
290-300	7.3694	0.0382	0.0052	-0.47945
300-310	7.1367	0.0446	0.0062	-0.29321
310-320	7.8400	0.0555	0.0071	-0.16908
320-330	7.4892	0.0720	0.0096	0.13767
330-340	7.6628	0.0897	0.0117	0.33463
340-350	7.1808	0.0943	0.0131	0.44968
350-360	6.7131	0.0595	0.0089	0.05535
Total area	**263.4367**	**2.2075**	--	--
Mean	**7.3177**	**0.0613**	**0.0082**	**-0.05940**

Aspect is the direction that a slope faces. It is defined as the compass bearing in the downhill direction of the steepest slope. Figure 6.7 demonstrates two major directions of aspect with higher landslide densities in the study area. They can be considered as from 80-150^0 (E to SE) and 320-360^0 (NW to N). The total land area of the slopes facing towards those directions are 82.051 km^2 (31.15%) with total landslide area of 0.963 km^2 (43.62%). The highest landslide density is recorded by the category of 120-130^0.

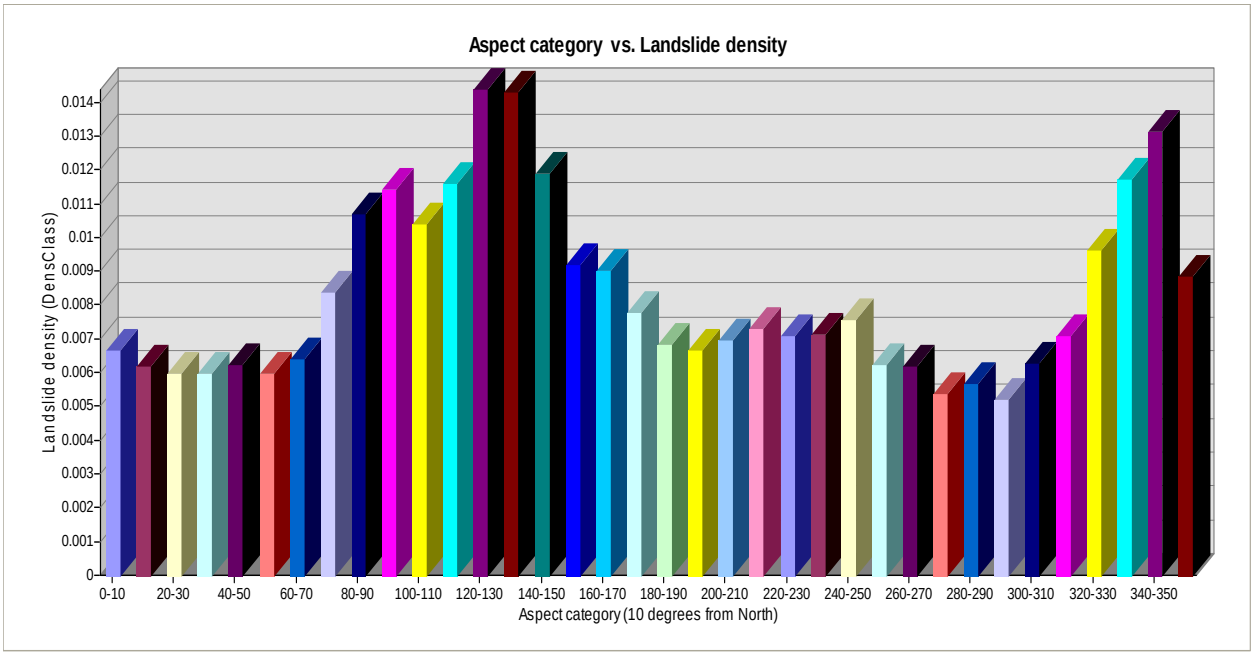

Figure 6.7: Landslide density according to the aspect category (10 degrees category from North).

The category which records the highest landslide area is 130-140^0 which is the class with the second highest landslide density. The most occurring slopes within the study area are the slopes with the aspect of 150 to 160^0 covering total land area of 9.675 km^2 (3.67%) with landslide area of 0.089 km^2 (4.03%).

The area of study is mainly exposed to the southwest monsoon rain which is from May to September. Although it is considered as the slopes facing to the direction of major rain falls are more vulnerable to failures, in the present study, highest landslide densities are given by the slopes facing almost orthogonal to the direction of major monsoon rains. As same as in the factor landuse, this could also be mainly due to the superimposing of other highly favorable slope instability factors within the areas.

All the rock types in the study area possess two major important structural properties, foliation and jointing. They are planer structures mostly presence underneath the soil overburden and play an important role in slope instabilities. The strike or dip direction of a rock structure is a measure of its orientation in space. The concept of deviation angle[5] is a method of relating the slope direction (aspect) to the attitude of the bed rock foliation.

As shown in the left part of the Figure 6.8, mainly, the landslide density decreases gradually with the increase of deviation angle from zero to 90^0 giving the highest density at the category of 10-20^0 with closely high values at the categories of 0-10^0 and 20-30^0. This demonstrates a good relationship between slope instabilities and deviation angles showing higher landslide densities on dip slopes (deviation angles around zero degrees) with a gradual decrease towards the intermediate slopes (deviation angle around 90^0). After it reaches to the minimum at the category of 80-90^0, if the slight anomalies are neglected, the density again increases from the intermediate slopes to the scarp slopes (deviation angle around 180^0).

[5] Deviation angle is defined as the horizontal angle between the azimuth of the slope direction, and the azimuth of the dip direction. The resulting deviation angle varies in magnitude between zero and 180 degrees and can be used to group the slopes into different categories of dip slopes, intermediate (oblique) slopes, and scarp (reverse) slopes.

Table 6.9: Distribution of deviation angle, area of landslide and landslide density within each class.

Deviation angle category (degree)	Area of the factor class (km^2)	Area of landslide (km^2)	LS density within the factor class	Factor scores
00-10	15.9297	0.1665	0.0104	0.2208
10-20	15.7237	0.1733	0.0110	0.2743
20-30	15.1632	0.1542	0.0102	0.1935
30-40	14.5509	0.1326	0.0091	0.0837
40-50	14.0917	0.1117	0.0079	-0.0559
50-60	13.6754	0.0928	0.0068	-0.2111
60-70	13.3862	0.0871	0.0065	-0.2526
70-80	13.2176	0.0814	0.0062	-0.3078
80-90	13.0599	0.0750	0.0057	-0.3781
90-100	13.1817	0.0860	0.0065	-0.2498
100-110	13.5291	0.1056	0.0078	-0.0710
110-120	13.8261	0.1198	0.0087	0.0336
120-130	14.2132	0.1303	0.0092	0.0898
130-140	14.8037	0.1265	0.0085	0.0195
140-150	15.5920	0.1274	0.0082	-0.0256
150-160	16.2599	0.1371	0.0084	0.0059
160-170	16.5901	0.1456	0.0088	0.0462
170-180	16.6425	0.1547	0.0093	0.1039
Dip slopes	128.7980	1.0745	0.0083	--
Scarp slopes	134.6384	1.1329	0.0084	--
Total area	**263.4367**	**2.2075**	**--**	**--**
Mean	**14.6354**	**0.1226**	**0.0083**	**-0.0267**

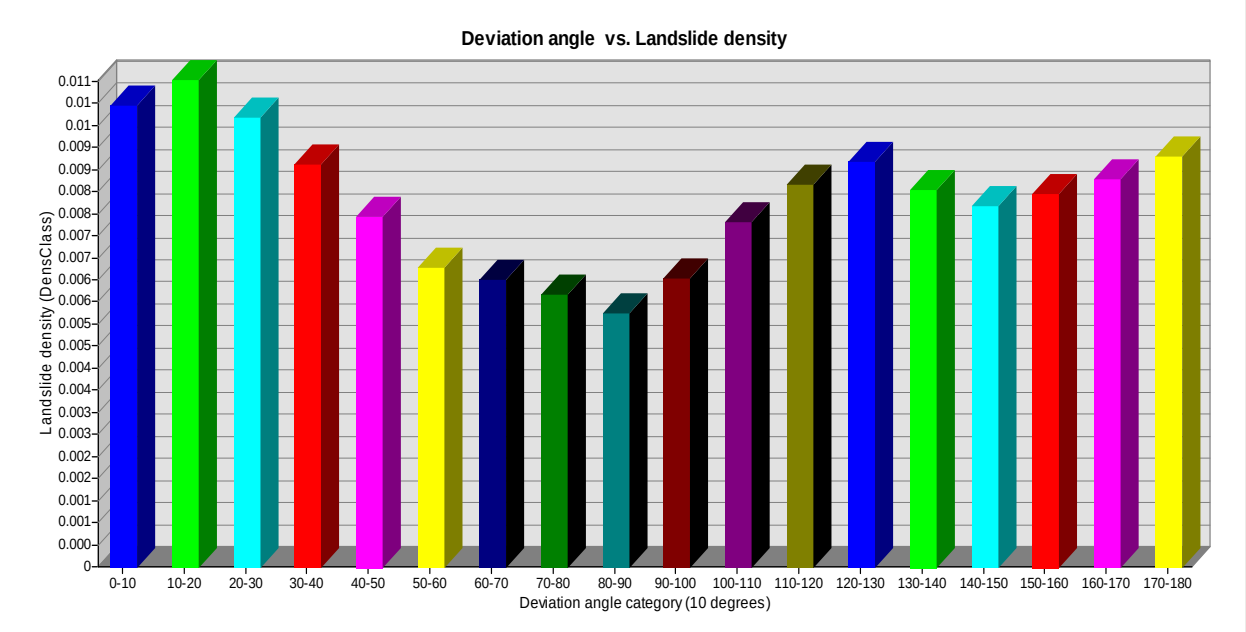

Figure 6.8: Landslide density according to the deviation angle (10 degrees category).

A dip slope is a slope where the dip direction of rock foliation or bedding plane is parallel or sub-parallel (i.e., small deviation angles) to the look direction (aspect) of the slope. Hence the situation provides favorable slip surfaces towards the direction of slope. Therefore, such slopes are considered to be more fragile and sensitive to sliding than oblique or reverse (scarp) slopes. Intermediate slopes are expected to

be the most stable. They are the areas with morphological slope and structural planes are orthogonal to each other. In the reverse slopes, dip direction of the rock foliation is opposite to the aspect of the morphological slope. Here, the joint systems act as planes of weakness and provide favorable conditions for different kinds of slope instabilities.

Except for the small anomalies, the results in the present study demonstrates a good correlation between field conditions and the above mentioned theoretical understanding of the influence of deviation angle in slope instabilities.

The total land area covered by the deviation angle range of $0\text{-}90^0$ is 128.7983 km^2 (48.89%) with total landslide area of 1.0745 km^2 (48.67%). Similarly the total land area covered by the deviation angle range of $90\text{-}180^0$ is 134.638 km^2 (51.11%) with total landslide area of 1.133 km^2 (51.32%). The statistics here demonstrate the total land area as well as the landslide area on the scarp slopes is slightly higher than that of dip slopes. However the landslide density on dip slopes (1.0745/128.7983 = 0.00834) is almost equal to the landslide density on scarp slopes (1.133/134.638 = 0.0084) showing equally vulnerable conditions on both type of slopes for landslides.

In addition to the influence of deviation angle, geometry (direction and angle) of the foliation or bedding planes of rock in relation to the morphological slopes is a critical factor in determining the slope stability. This situation can be assessed using the concept of under/over dip, under/over scarp angles.

The Figure 6.9 shows two distinct patterns of variations, one for dip slopes, i.e., from under dip angle 90^0 (UD80-90) to over dip angle 60^0 (OD50-60) and the second for scarp (reverse) slopes, i.e., from under scarp 90^0 (US80-90) to over scarp 60^0 (OS50-60).

Except for the sudden rise at the category of UD60-70, generally left part of the graph shows an increase of landslide density with the decrease of under dip angle (from the category of UD80-90 to UD00-10). Also the same situation of increase of density is continued from the over dip angle zero to 40^0 (from the category of OD00-10 to OD30-40). In this part, a change of gradient is occurred at UD20-30 and then density increases with a higher gradient up to the category of OD30-40. Afterwards, the density drops to the last over dip category of OD50-60.

In the case of scarp slopes too, apart from the anomalies at the categories of US70-80 and 60-70, a similar pattern of increase of landslide density can be seen with the decrease of under scarp angle (from the category of US80-90 to US00-10). Then, from the category of OS00-10 to OS30-40, it shows an increase of density with the increase of over scarp angle. An increase of the gradient is occurred here at US00-10 and from there, landslide density increases with a higher gradient up to the category of OS30-40. And then the density drops to the last over scarp slope category of OS50-60.

In general, increase of landslide density (gradient) within the scarp slopes (US and OS categories) is higher than that of the dip slopes (UD and OD categories). This demonstrates that the landslide density on scarp slopes is more sensitive to the change of angle than that of on dip slopes.

Table 6.10: Distribution of under/over dip - under/over scarp angle, area of landslide and landslide density within each class.

Under/over dip & scarp angle category (deg.)	Area of the factor class (km^2)	Area of landslide (km^2)	LS density within the factor class	Factor scores
UD80-90	0.0057	0.000009	0.00159	-1.6622
UD70-80	0.2106	0.000477	0.00227	-1.3081
UD60-70	0.7306	0.003096	0.00424	-0.6817
UD50-60	2.1850	0.006948	0.00318	-0.9689
UD40-50	5.6883	0.018801	0.00331	-0.9303
UD30-40	11.3484	0.041823	0.00369	-0.8214
UD20-30	18.5637	0.113877	0.00613	-0.3119
UD10-20	24.7409	0.194904	0.00788	-0.0617
UD00-10	26.2712	0.235755	0.00897	0.0685
OD00-10	21.0345	0.223947	0.01065	0.2395
OD10-20	11.5688	0.144945	0.01253	0.4022
OD20-30	4.7913	0.064584	0.01348	0.4754
OD30-40	1.4209	0.022329	0.01571	0.6288
OD40-50	0.2239	0.003033	0.01355	0.4804
OD50-60	0.0141	0.000018	0.00127	-1.8837
US80-90	0.0084	0.000009	0.00107	-2.0543
US70-80	0.2332	0.001818	0.00779	-0.0723
US60-70	0.7772	0.004086	0.00526	-0.4662
US50-60	2.1510	0.007299	0.00339	-0.9040
US40-50	5.8634	0.023625	0.00403	-0.7322
US30-40	11.1049	0.056295	0.00507	-0.5026
US20-30	18.2934	0.109566	0.00599	-0.3358
US10-20	24.6641	0.157149	0.00637	-0.2739
US00-10	27.3884	0.220833	0.00806	-0.0385
OS00-10	23.1155	0.250614	0.01084	0.2576
OS10-20	13.2544	0.182106	0.01374	0.4945
OS20-30	5.7188	0.087570	0.01531	0.6029
OS30-40	1.7711	0.027702	0.01564	0.6241
OS40-50	0.2790	0.004050	0.01452	0.5495
OS50-60	0.0145	0.000216	0.01487	0.5735
Total dip slope	128.7978	1.074546	0.00834	--
Total scarp slope	134.6374	1.132938	0.00842	--
Total under dip slope only	89.7442	0.615690	0.00686	--
Total over dip slope only	39.0536	0.458856	0.01175	--
Total under scarp slope only	90.4841	0.580680	0.00642	--
Total over scarp slope only	44.1534	0.552260	0.01251	--
Total area	**263.4352**	**2.207484**	**--**	**--**
Mean	**8.7812**	**0.073583**	**0.00801**	**-0.2871**
UD = Under Dip, **OD** = Over Dip, **US** = Under Scarp, **OS** = Over Scarp				

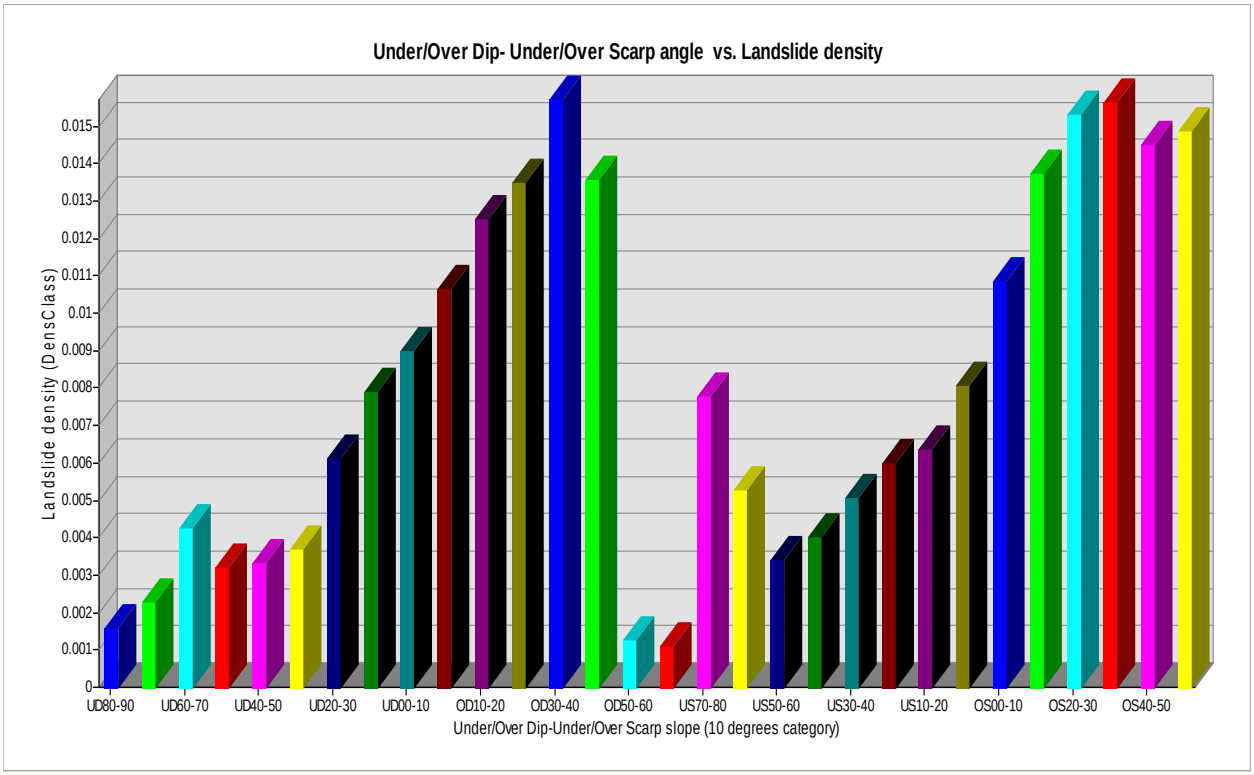

Figure 6.9: Landslide density according to the under/over dip-under/over scarp angle[6] (10^0 category).

Considering the categories of UD20-30 and US00-10 where the sudden increase of the gradient occur as the initiation points of the critical angles, angle ranges from the under dip of zero to 30^0 and the over dip of zero to 50^0 as well as the under scarp of zero to 10^0 and the over scarp of zero to 60^0 can be taken as the most influencing angels for slope instabilities. The total land area covered by these ranges is 180.157 km^2 (68.39%) with total landslide area of 1.776 km^2 (80.45%). This reveals the majority of the lands in the study area are underlain by the critical angle ranges of the factor.

The study area is composed of almost equal area of dip slopes and scarp slopes with almost equal distribution of landslides and hence having almost equal landslide densities in both types of slopes. While the under dip slopes cover more than double of the area of the over dip slopes, areas with over dip slopes show higher landslide densities than to the under dip slopes. More or less similar condition can be observed in the case of under scarp and over scarp slopes too. Hence, in comparison to the under dip and under scarp slopes, over dip and over scarp slopes illustrate higher vulnerable situations for slope instabilities.

Over dip and over scarp are the situations where morphological slope is always greater than to the dip of the structural plane making relatively unstable conditions than to the under dip and under scarp situations. Hence, except for the small anomalies that could be due to some errors associated with the data and the scale of the study, the analysis result presented here reveal the situation clearly.

[6] A dip slope is a slope where the dip direction of rock foliation or bedding plane is parallel or sub-parallel (i.e., small deviation angles) to the look direction of the slope. An opposite situation is called as a scarp (reverse) slope. A dip slope with a slope angle less than the dip angle is defined as *under dip*; here the foliation plan always runs into the ground, thus one can presume more stable conditions. On the contrary, a dip slope with a slope angle greater than the dip angle is defined as *over dip*; here the foliation plane can alight on the slope making relatively unstable situations. Similarly, *under scarp* and *over scarp* situations can be termed (Jayathissa et al., 2009a).

Table 6.11: Distribution of watershed, area of landslide and landslide density within each class.

Order of watershed	Area of the factor class (km^2)	Area of landslide (km^2)	LS density within the factor class	Factor scores
1st order	161.1316	1.5397	0.0096	0.1313
2nd order	51.4187	0.2846	0.0055	-0.4148
3rd order	23.0677	0.2323	0.0101	0.1839
4th order	13.1292	0.1019	0.0078	-0.0764
5th order	13.4934	0.0487	0.0036	-0.8429
6th order	1.1959	0.0003	0.0002	-3.6140
Total area	**263.4367**	**2.2075**	**--**	**--**
Mean	**43.9061**	**0.3679**	**0.0061**	**-0.7721**

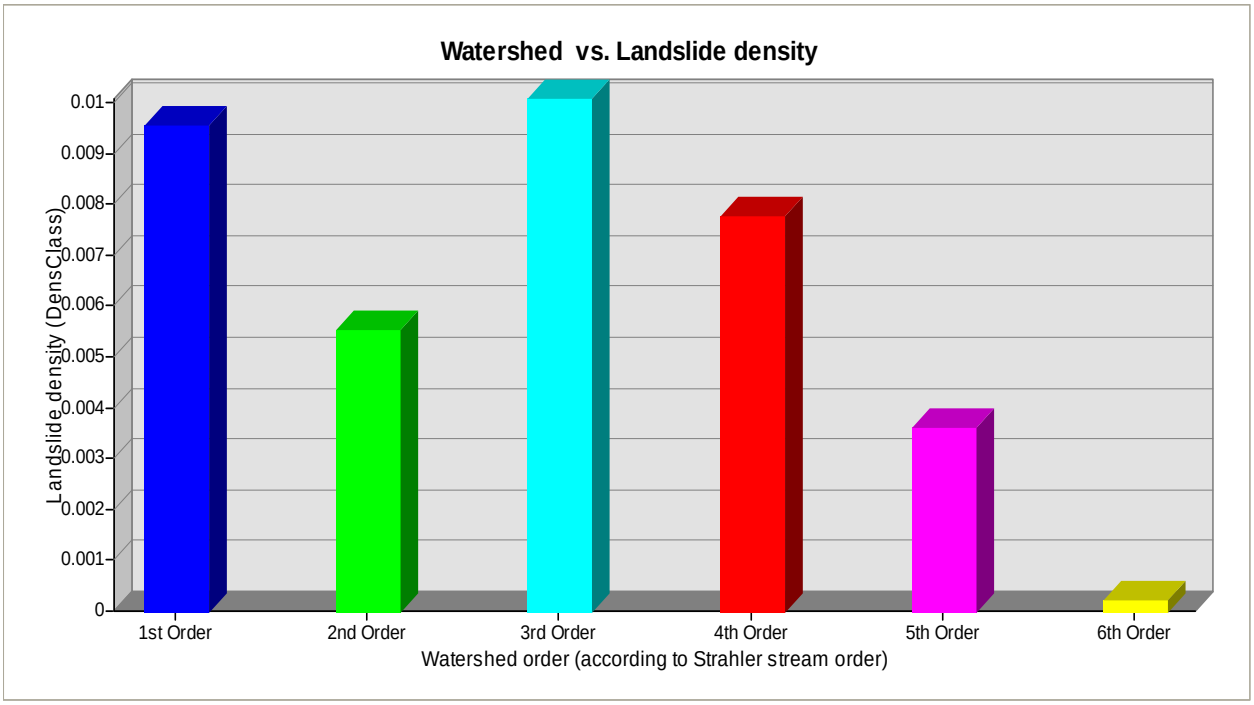

Figure 6.10: Landslide density according to the order of watershed.

In general, more landslides are expected to be occurred in the lower order watersheds with a decrease of densities towards the higher orders. This is because the lower order watersheds are associated with steep hilly terrains with V-shaped valleys and strong denudation activities. In the study, first order watersheds records the second highest landslide density while 3rd order being the highest, and from onward there is a gradual decrease up to the 6th order (Figure 6.10). Hence, from 3rd to 6th order, data in the study shows a good relationship. However, due to the anomaly occurred at the 2nd order where the density is lower than to both the 3rd and 4th orders and the highest density at the 3rd order, smooth relationship from the 1st order to the 6th order can not be seen. Similarly to the factors like landuse and aspect, this situation might be also due to the superimposing of other highly favorable instability factors within the areas.

According to the Table 6.11, about 161.13 km^2 (61.16%) of the study area is covered by the first order watersheds with a total landslide area of 1.5397 km^2 (69.75%). Although the 3rd order watershed records the highest density, total land area belongs to that category is only 23.07 km^2 (8.76%). Hence, lands covered by the 1st order watersheds can be considered as the most important part in relevance to the study.

Furthermore, in comparing to the field situations, ignoring the anomaly at the second order, watersheds from first order to third order can be taken as the most vulnerable areas for landslides.

Table 6.12: Euclidean distance from spring, area of landslide and landslide density within each class.

Euclidean distance from Spring (m)	Area of the factor class (km^2)	Area of landslide (km^2)	LS density within the factor class	Factor scores
00 - 50	0.6724	0.0588	0.0874	2.3447
50-100	1.2612	0.0450	0.0357	1.4482
100-150	1.6307	0.0191	0.0117	0.3334
150-200	1.9374	0.0128	0.0066	-0.2407
200-250	2.2212	0.0149	0.0067	-0.2204
250-300	2.5072	0.0110	0.0044	-0.6464
>300	253.2066	2.0460	0.0081	-0.0364
Total area	**263.4367**	**2.2075**	--	--
Mean	**37.6338**	**0.3154**	**0.0229**	**0.4261**

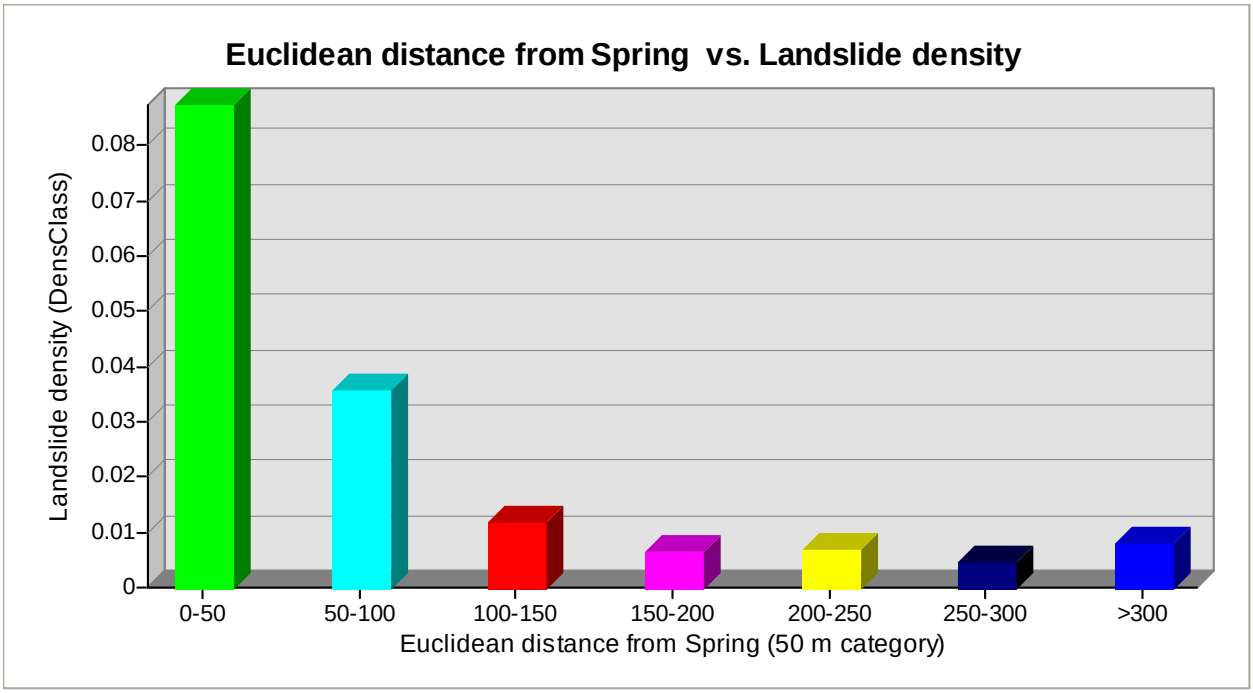

Figure 6.11: Landslide density according to the Euclidean distance from springs.

The Figure 6.11 clearly depicts a strong relationship between the distance from water springs and landslide density up to the limit of 300 m, although, there is a little increase beyond that distance. The region from 0 to 50 m can be considered as the most effective area having the highest landslide density. Whereas, in general, the distance up to 100 or 150 m show a considerable effect on the occurrence of landslides and then it diminishes rapidly.

Springs represent the regions of ground water convergence where high hydrostatic pressures can be expected within the subsurface and yield a considerable amount of subsurface erosion which can subsequently be strong reasons for slope instabilities. The results here clearly demonstrate this understanding of relation between springs and landslide occurrence in slopes.

Table 6.13: Euclidean distance from streams, area of landslide and landslide density within each class.

Euclidean distance from Stream (m)	Area of the factor class (km^2)	Area of landslide (km^2)	LS density within the factor class	Factor scores
00 - 50	80.1229	1.2588	0.0157	0.6286
50-100	67.5052	0.5405	0.0080	-0.0456
100-150	50.2703	0.2281	0.0045	-0.6134
150-200	32.4275	0.0927	0.0029	-1.0759
200-250	18.2705	0.0471	0.0026	-1.1794
250-300	8.8125	0.0239	0.0027	-1.1283
>300	6.0277	0.0165	0.0027	-1.1206
Total area	**263.4367**	**2.2075**	**--**	**--**
Mean	**37.6338**	**0.3154**	**0.0056**	**-0.6478**

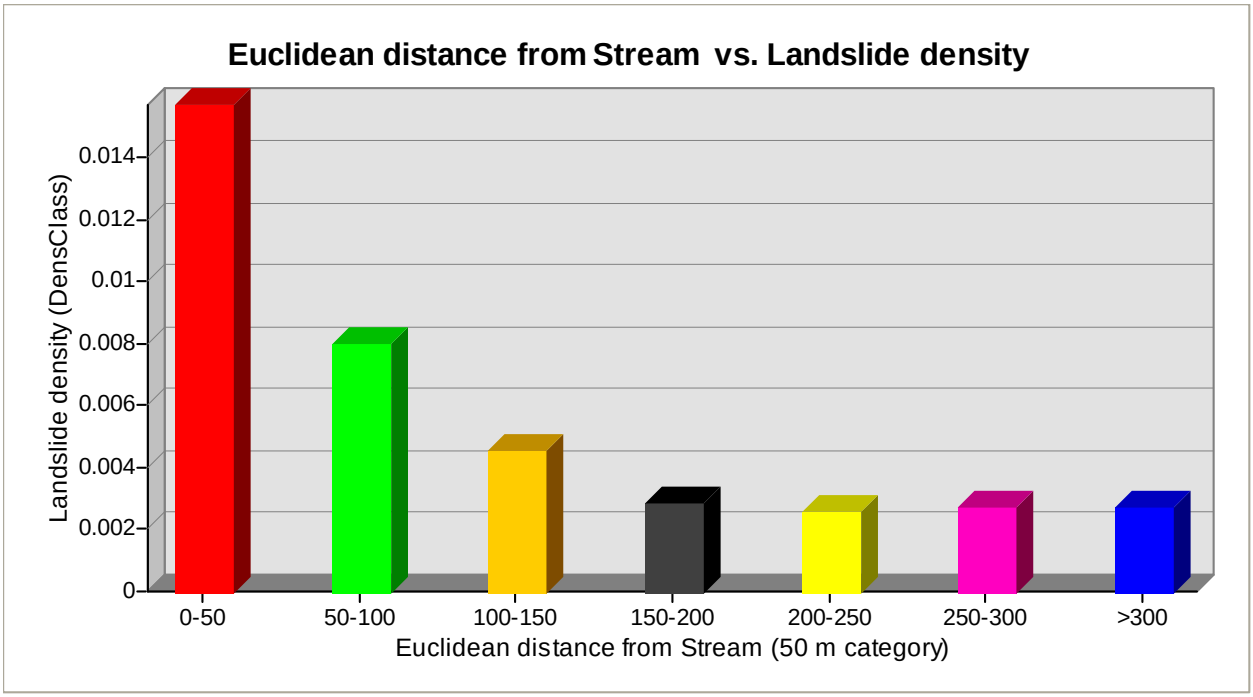

Figure 6.12: Landslide density according to the Euclidean distance from streams.

Similarly to the case of springs, landslide density decreases with the increase of distance from streams too showing a smooth curved relationship (Figure 6.12). While the area within the distance of 0-50 m shows the highest landslide density, up to 150 m can be considered as an important area for slope instabilities. After this limit the rate of decrease of density changes suddenly and follows almost parallel to the distance axis.

Streams are surface water bodies flowing along the valleys where ground water table alight on the slopes and runoff water is collected. Hence, near to the streams, slope materials are almost saturated with ground water with high hydrostatic pressures. At the same time, mostly valleys are the cutting edges of slopes (toe of the slopes) where high erosion activities are taken place due to runoff. The bank erosion reduces the toe support enhancing the instabilities in slopes. Therefore, high landslide density associated with close proximity to streams can be well understood.

Table 6.14: Euclidean distance from major joints, area of landslide and its density within each class.

Euclidean distance from joints (m)	Area of the factor class (km^2)	Area of landslide (km^2)	LS density within the factor class	Factor scores
00 - 50	2.1537	0.0583	0.0270	1.1719
50-100	6.2081	0.1144	0.0184	0.7880
100-150	9.4997	0.1732	0.0182	0.7775
150-200	12.0346	0.2004	0.0167	0.6868
200-250	13.6740	0.1655	0.0121	0.3679
250-300	14.7582	0.1359	0.0092	0.0940
>300	205.1084	1.3598	0.0066	-0.2342
Total area	**263.4367**	**2.2075**	--	--
Mean	**37.6338**	**0.3154**	**0.0155**	**0.5217**

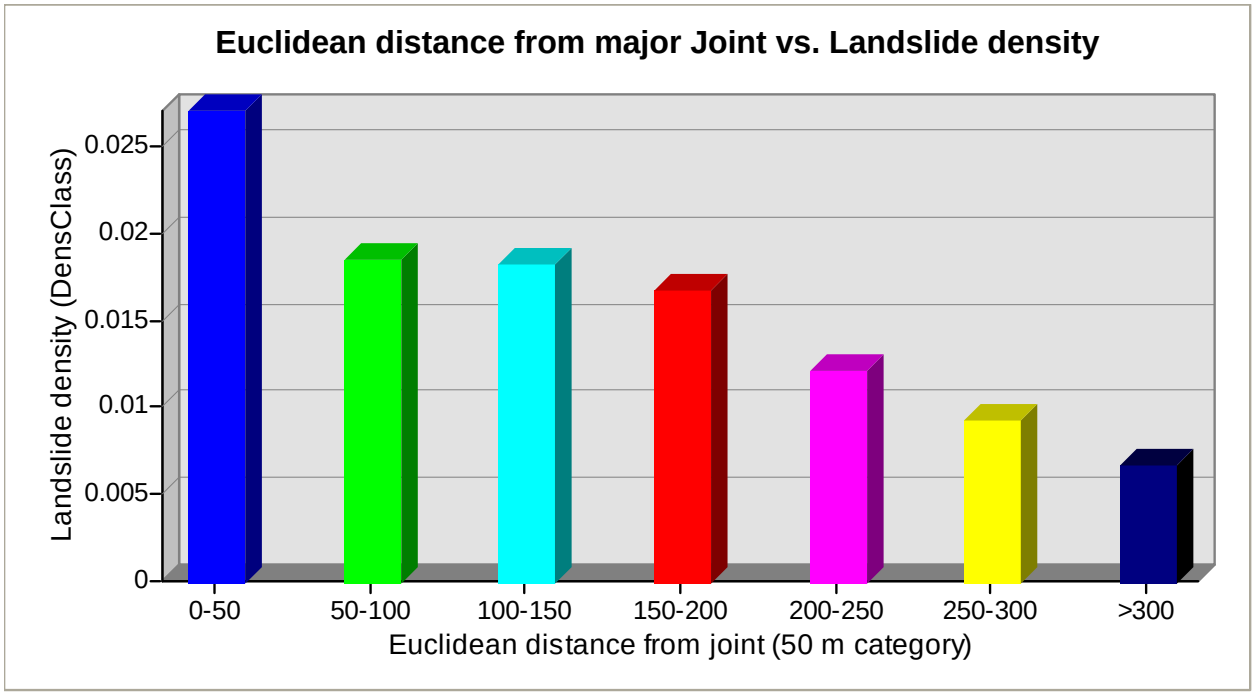

Figure 6.13: Landslide density according to the Euclidean distance from major joints.

As can be seen from the Figure 6.13, with the increase of distance from major joints, landslide density decreases while having the highest at 0-50 m distance with a sudden drop at the category of 50-100 m. Hence, a strong influence of joints for the occurrence of landslides can be expected within the range of zero to 50 m area while showing a considerably higher influence up to 200 m (up to the category of 150-200). After that, it shows a gradual decrease with the distance.

Joints refer to fractures in rock. They occur in parallel sets into one or more directions and are the second important structural property of rocks. This is a common property of all the rocks within the study area and presence of this property imparts a degree of permeability to non porous, crystalline rocks. They provide continuous or dissected structural planes beneath the slope material which can in many instances be acted as slip surfaces or weak zones. Also, joints facilitate ground water infiltration and movement which can subsequently be a reason for development of excess pore water pressures, internal erosion and deep weathering. Joints in some instances continue as planes of weakness into the weathered overburden

above. Hence, the form that landslides take in weathered overburden may, in fact, be partly controlled by jointing in the solid rock at depth. Therefore, it is evident that proximity to discontinuities such as topographic lineaments, faults or major joints increases the risk of slope instability. In the study, only the joint is considered and the explained situation is evident by the results.

6.3 Landslide susceptibility models

6.3.1 Information Value (Landslide Index) method

Following the method explained in the section 5.3.1, weight (factor scores) values for the each factor class was calculated using the equation 5.1. DensMap is a constant value and it is given in the Table 6.1. DensClass (landslide density within the factor class) and the calculated factor scores for each of the factor class are given in the Tables 6.2 to 6.14. Following graphs represent the variation of calculated scores (weights) for the factor classes in each of the parameter map (see Tables 6.2 to 6.14).

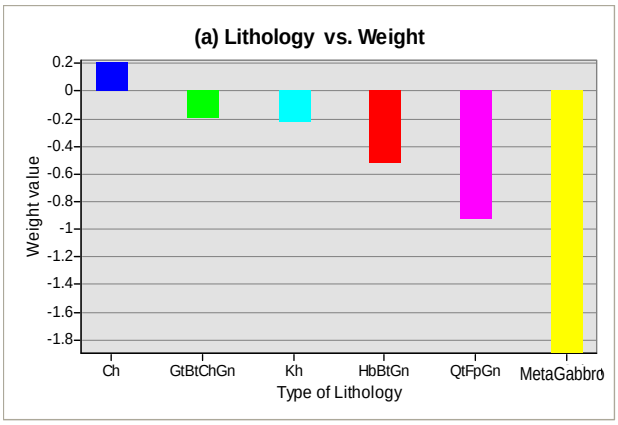

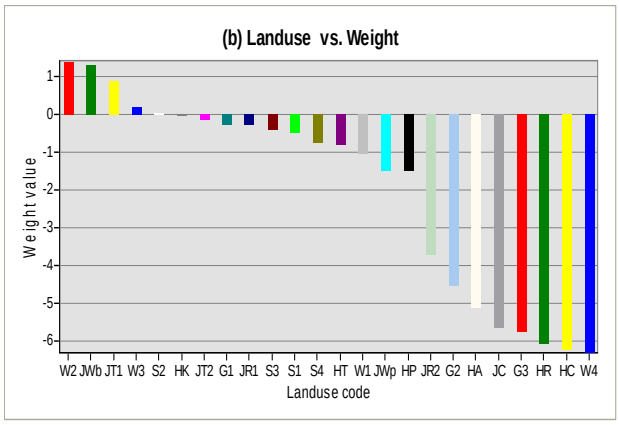

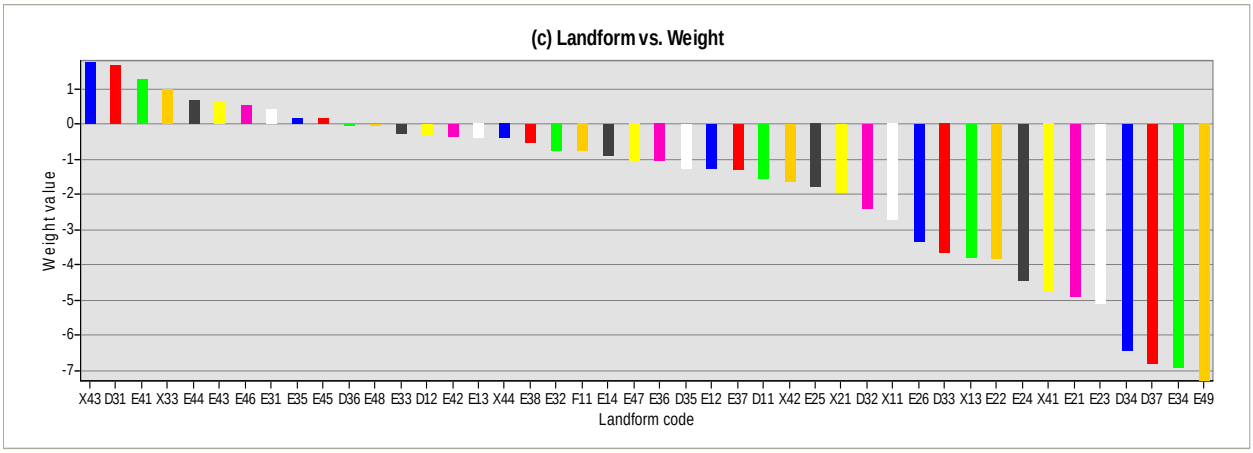

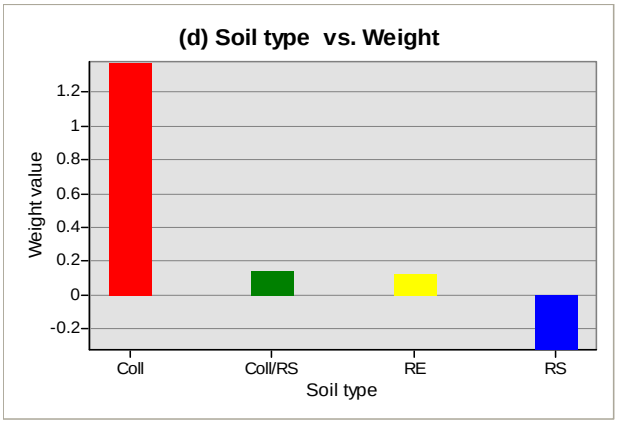

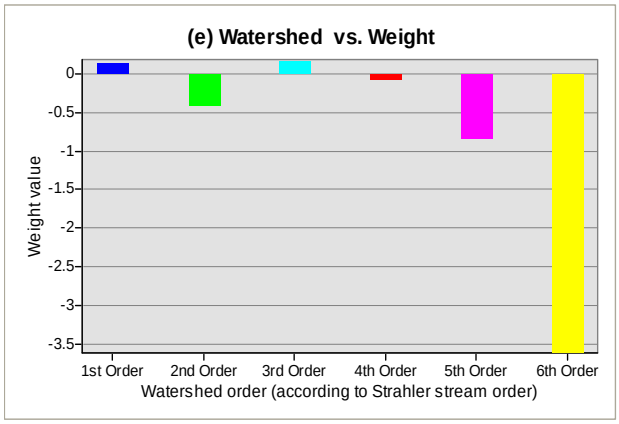

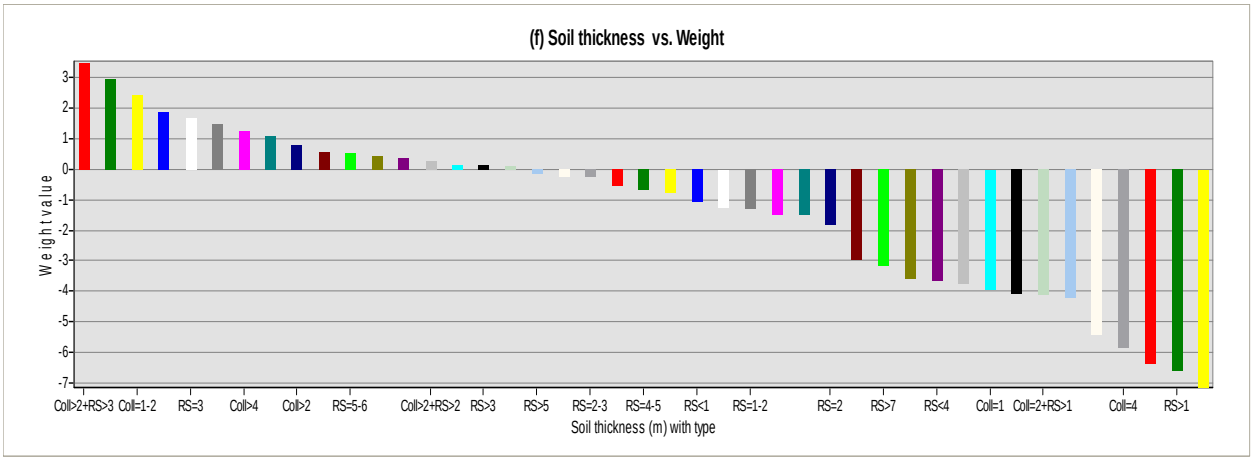
(f) Soil thickness vs. Weight
Weight value
3
2
1
0
-1
-2
-3
-4
-5
-6
-7
Coll>2+RS>3
Coll=1-2
RS=3
Coll>4
Coll>2
RS=5-6
Coll>2+RS>2
RS>3
RS>5
RS=2-3
RS=4-5
RS<1
RS=1-2
RS=2
RS>7
RS<4
Coll=1
Coll=2+RS>1
Coll=4
RS>1
Soil thickness (m) with type

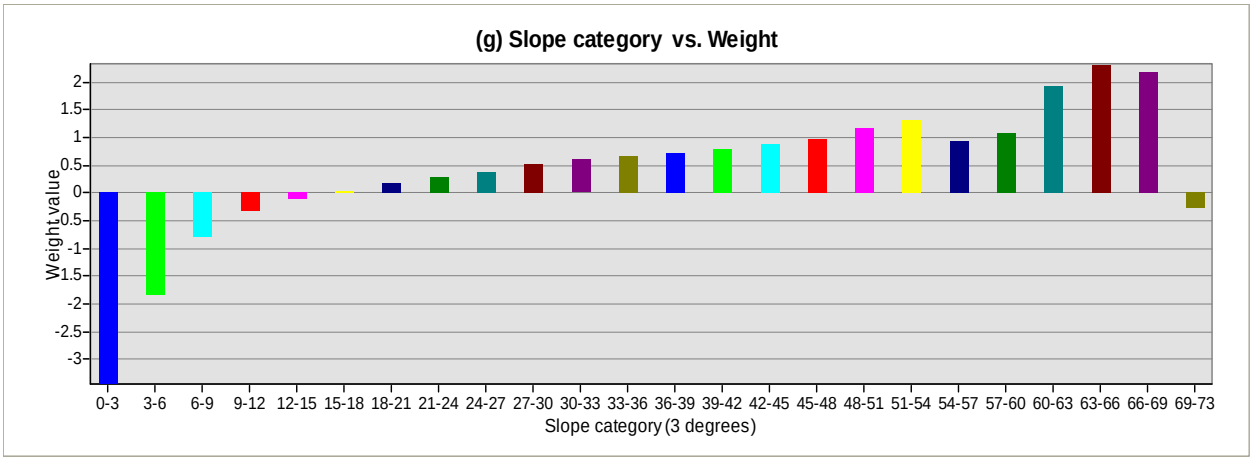
(g) Slope category vs. Weight
Weight value
2
1.5
1
0.5
0
-0.5
-1
-1.5
-2
-2.5
-3
0-3
3-6
6-9
9-12
12-15
15-18
18-21
21-24
24-27
27-30
30-33
33-36
36-39
39-42
42-45
45-48
48-51
51-54
54-57
57-60
60-63
63-66
66-69
69-73
Slope category (3 degrees)

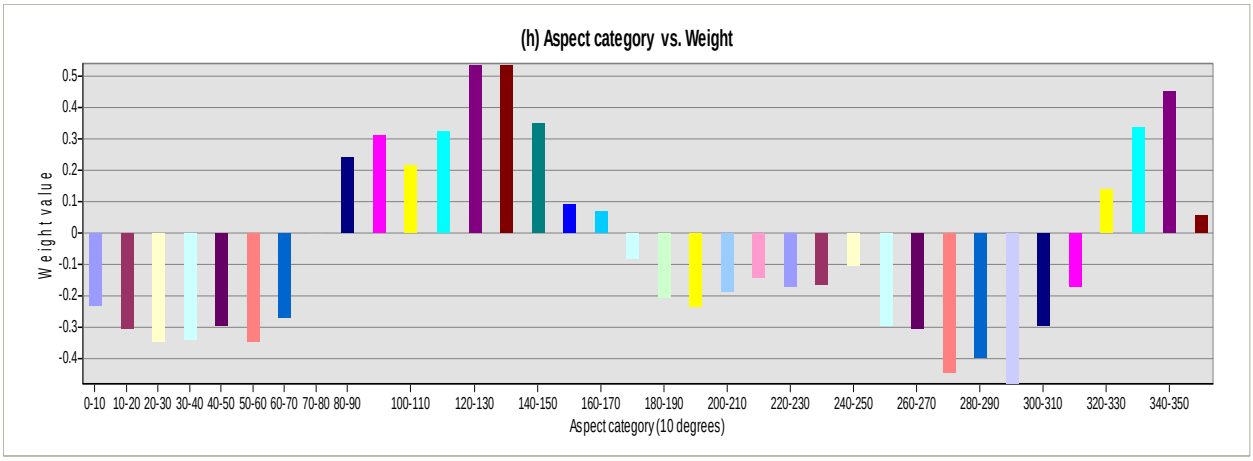
(h) Aspect category vs. Weight
Weight value
0.5
0.4
0.3
0.2
0.1
0
-0.1
-0.2
-0.3
-0.4
0-10
10-20
20-30
30-40
40-50
50-60
60-70
70-80
80-90
100-110
120-130
140-150
160-170
180-190
200-210
220-230
240-250
260-270
280-290
300-310
320-330
340-350
Aspect category (10 degrees)

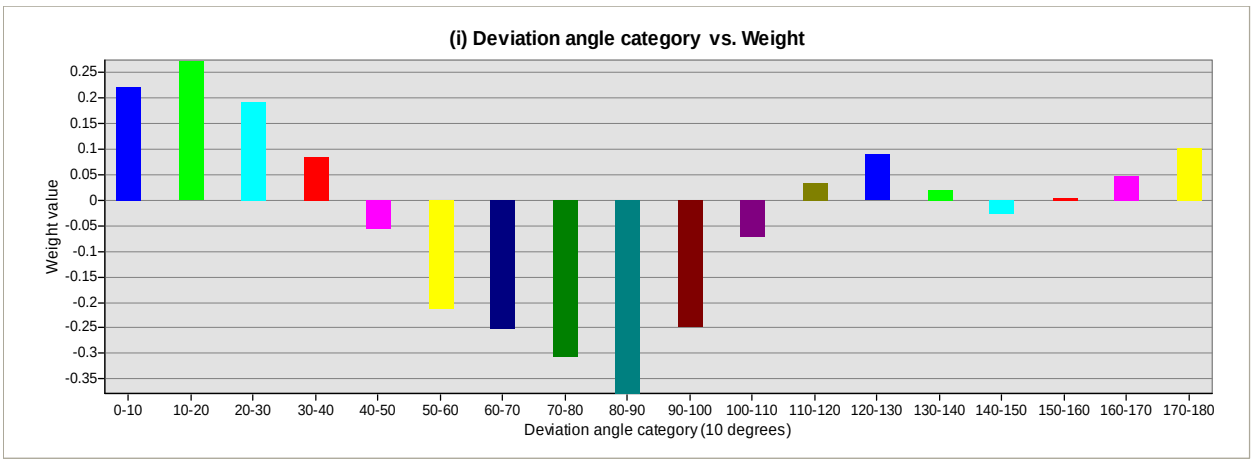
(i) Deviation angle category vs. Weight
Weight value
0.25
0.2
0.15
0.1
0.05
0
-0.05
-0.1
-0.15
-0.2
-0.25
-0.3
-0.35
0-10
10-20
20-30
30-40
40-50
50-60
60-70
70-80
80-90
90-100
100-110
110-120
120-130
130-140
140-150
150-160
160-170
170-180
Deviation angle category (10 degrees)

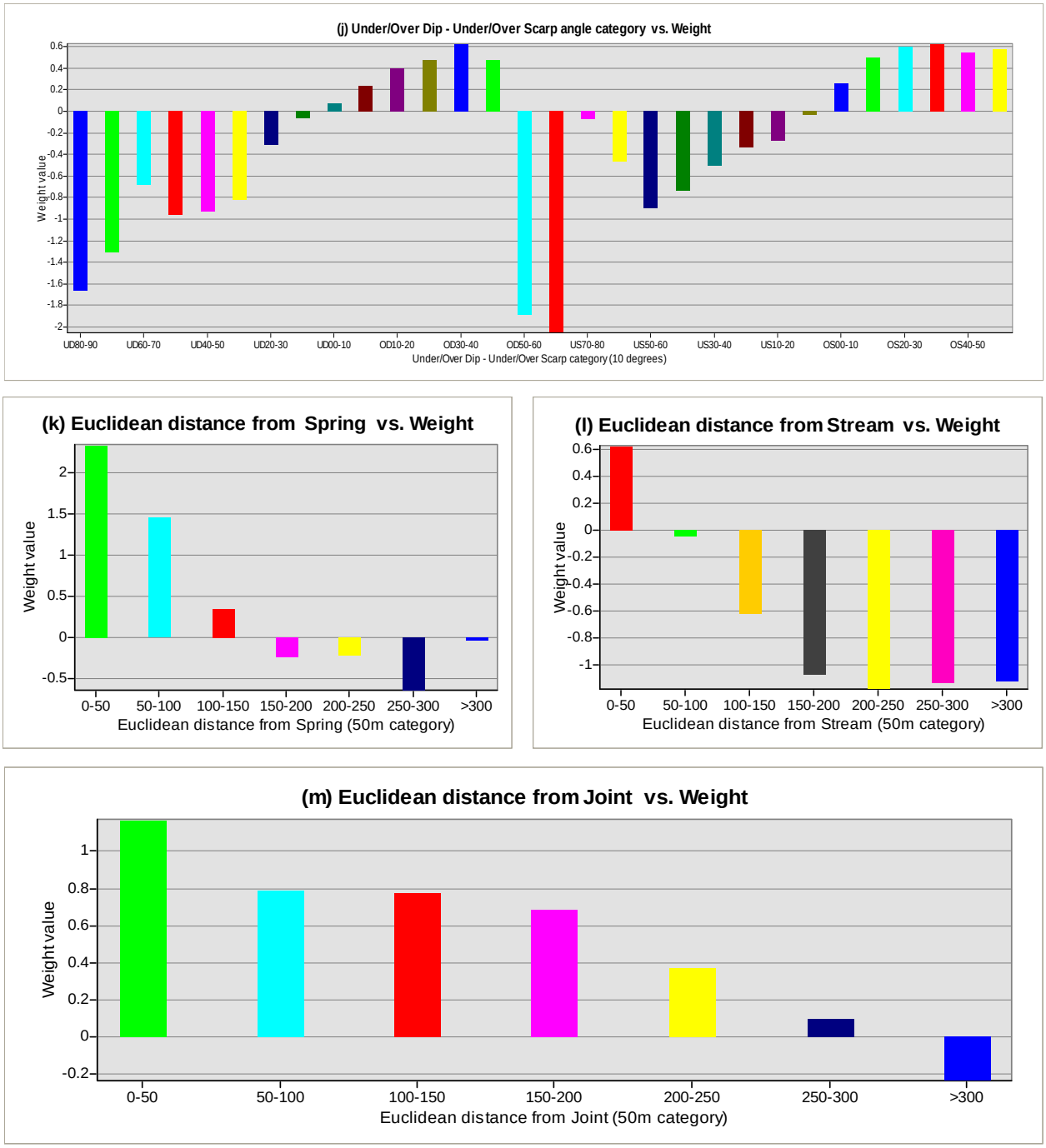

Figure 6.14: Calculated factor scores (weights) against the factor classes in each of the parameter map according to the Information Value method (related to data from Table 6.2 to 6.14).

The column charts *a* to *m* in the Figure 6.14 show the variation of calculated factor scores (weights) against the factor classes in an individual factor maps. A positive weight means that the factor class has higher landslide density than normal, while a negative weight means that that factor class shows lower landslide density than normal; size of the value represent the strength of contribution either into positive or negative directions.

In lithology (Table 6.2 and the Chart *a* in the Figure 6.14), only the rock type Charnockite shows positive weight while all the other rock types record negative scores. By the method of Comparison of Means procedure applied in the process of the variable selection in the multivariate logistic regression model, only the lithology type Charnockite was selected as a significant variable among all the lithology classes

(Table 6.23). Hence, the rock type Charnockite can be considered as the most contributing factor class for slope instabilities while rock type Meta Gabbro with extreme negative weights.

As can be seen from the Table 6.3 and the Chart *b* in the Figure 6.14, five of the landuse classes record positive weights. They are W2, JWb, JT1, W3, and S2 and covers total land area of 38.4423 km^2 (14.59%) with landslide area of 1.2791 km^2 (57.94%). However, the majority of the study area is covered by the landuse classes with negative weights; among them some categories like HR, HC, and W4 having weights far away from the normal.

While majority of the landform classes have negative weights, few with far away from the normal too, ten categories from X43 to E45 (Table 6.4) records positive scores (Chart *c* in the Figure 6.14) covering total land area of 113.3899 km^2 (43.04%) with landslide area of 1.5931 km^2 (72.17%). Hence, here too majority of the study area is composed of with the landform categories that have comparatively low influence for the occurrence of landslides.

Although three of the soil types give positive weights, the most significant is the colluvium soil (Table 6.5 and the Chart *d* in the Figure 6.14). Total area covered by this soil type is 21.1307 km^2. By Comparison of Means procedure applied for the selection of variables in the logistic regression model, only the colluvium soil is selected as a significant variable for the occurrence of landslides. Hence, the areas covered by the soil type colluvium can be considered as the most vulnerable sites for landslides. Residual soil, the most widespread soil type within the study area covering 232.95 km^2 (88.43%) has negative weights. Hence majority of the study area is composed of with the soil type which has comparatively low influence for the occurrence of landslides.

According to the Table 6.11 and the Chart *e* in the Figure 6.14, only the first and the third order watersheds record positive weights. When comparing the results with the field conditions, negative weights at the fourth, fifth and sixth order watersheds can be accepted, but some strange anomaly can be observed at the second order watershed.

The Table 6.6 and the Chart *f* in the Figure 6.14 demonstrate weight values for soil thickness classes. The score values vary from positive 3.53 to negative 7.14. Seventeen thickness classes, most of them associated with colluvium soils covering total land area of 19.5064 km^2 record positive weights. Although the colluvium soil has positive higher weights in the soil type classes (Chart *d* in the Figure 6.14), some of the thickness classes of colluvium soil like Coll =3, Coll=4, etc., record the highest negative weights in the soil thickness classes. Hence, it is not possible to explain here any relationship between soil thickness categories and landslides. By Factor Analysis and Comparison of Means procedure used for the variable selection in the logistic regression model too, there seems to be no relevance of all the variables of the parameter of soil thickness for explaining the occurrence of landslides (Table 6.23). This situation could be expected due to the complexity of the class categories, which is associated with different soil types and thicknesses.

As shown in the Table 6.7 and the Chart *g* in the Figure 6.14, slope angle ranges from 0 to 15^0 and 69 to 73^0 have negative weights. Within the range of 0 to 15^0, weight values increase gradually towards the zero with the minimum at 0-3^0 category. In general, this range can be considered as the most stable part of the slopes. Total land area covered by this range is 128.4849 km^2 (48.77%). Then, the weight values gradually increase towards the positive direction from 15^0 to 69^0 although there are some small anomalies.

Total land area covered by the slopes with positive weights is 134.9504 km^2 (51.23%). Slope angle is a major influencing factor in slope instability and driving forces are increasing with the increase of slope angle making slopes to be more vulnerable for sliding. The results in the study provide very comparable outcome with the theoretical understanding of the relationship between slope angle and landsliding.

The Table 6.8 and the Chart *h* in the Figure 6.14 illustrate two distinct directions of aspect with positive weights. They are from 80 to 170^0 and 320 to 360^0. Total land area covered by slopes facing to these directions is 101.2457 km^2 (38.43%).

Deviation angle vs. weight chart (Chart *i* in the Figure 6.14) demonstrates 3 separate regions of positive weights such as 0 to 40^0 (direction of dip slope), 110-140^0 (direction of intermediate to scarp slope) and 150 to 180^0 (direction of scarp slope). Among these 3 regions, the highest positive weights can be seen in the direction of dip slope. Dip slopes are always almost considered to be more vulnerable for sliding than scarp slopes due to very favorable planer structural conditions. Although it is difficult to give specific reasons to explain the situation in the range of 110-140^0 which could be due to superimposing of other highly favorable conditions such as steep slope angles, joint systems, the result presented in the study provide clear understanding about the relation between dip and scarp slopes and the occurrence of landslides. Total extent of lands underneath by the slopes with deviation angles having positive weights is equal to 153.7031 km^2 (58.35%).

As shown in the Table 6.10 and by the Chart *j* in the Figure 6.14, there are two distinct regions of under/over dip - under/over scarp with positive weights. They are within the range of under dip angle zero to over dip angle 50^0 and over scarp angle range from zero to 60^0. Total land area covered by these categories is 109.4640 km^2 (41.55%). The highest positive weights are recorded at the categories of OD30-40 and OS30-40. Over dip and over scarp slopes are considered to be more unstable due to the favorable geometric relations between structural attitudes and morphological slopes for sliding. When the situation is under dip, the structural plane always runs into the ground, thus one can presume more stable conditions. Whereas, small under dip angles, for instance like the category of 0 to 10^0, can still be considered as structural planes almost parallel to the morphological slope thus providing comparatively unstable conditions.

According to the Table 6.12 and the Chart *k* in the Figure 6.14, the distance up to 150 m from springs shows positive weights having the highest at the category of 0-50 m. Generally, it can be understood, both the first two categories, i.e., distance up to 100 m from the springs are the most vulnerable region for landslides.

The Table 6.13 and the Chart *l* in the Figure 6.14 demonstrate the way the distance from streams affect the occurrence of landslides. The chart shows up to 50 m distance from streams as the most important region with high positive weight value while having negative weights for all the categories beyond this distance.

As shown by the Table 6.14 and the Chart *m* in the Figure 6.14, influence of joints for slope instabilities extent to a distance more than that of springs and streams. All the categories up to the distance of 300 m shows positive weights while the highest value being at the category of 0-50 m. This simply means that the joint systems associated with the underneath rock layers play a vital role for the stability of slopes within it and also surroundings with greater influence.

Above calculated factor scores (weights) in the Tables 6.2 to 6.14 were first assigned to the corresponding factor maps and then they were normalized (standardized) to the range of -1 to +1. Here as a first step, the influence of each factor for the occurrence landslides was equally weighted. Hence, the final weight map was created by summing up of all the normalized factor weights of 13 factors considered in the analysis. The summation was done in the pixel basis and the total weight in the final map ranges from -6.01093 to +5.10187. The total weight map was then reclassified into five classes using Natural Breaks (Jenks) and crossed with the landslide map (Table 6.15). Figure 6.15*a* is the final out come with five susceptibility classes, very low, low, medium, high and very high according to their hazard potentials defined using Natural Breaks.

Table 6.15: Total weight (normalized) ranges, percentage of the total area and the existing landslide area.

Total weight range	Susceptibility class	Number of total pixels	Number of LS pixels	% of total pixels (% of total area)	% of LS pixels (% of LS area)
-6.0109 to -2.1909	Very low	3687011	916	12.5994	00.3735
-2.1909 to -1.1925	Low	8171130	10970	27.9228	04.4725
-1.1925 to -0.2375	Medium	8847296	40750	30.2334	16.6140
-0.2375 to 0.8912	High	6085255	78797	20.7948	32.1260
0.8912 to 5.1019	Very high	2472588	113842	08.4495	46.4140

As shown in the Table 6.15, percentage of landslide area increases with the increase of total weights. The weight range corresponding to very high susceptibility class encloses 46.41% of all the landslides within 8.45% of the total study area. Almost 80% of the landslides are predicted by both the very high and high susceptibility classes covering 29.24% of the total area. On the other hand, only a 0.37% of the landslides are enclosed by very low susceptibility class with another 4.47% by the low susceptibility class. These results demonstrate that the distribution of the total weights within the study area and the amount of landslides and total area represented by its value ranges are acceptable and good enough for a model to be compared with the actual field conditions.

6.3.2 Weights of Evidence modeling (WOE)

According to the method explained in the section 5.3.2, under WOE modeling, two techniques were employed for the estimation of factor scores (weights); one with the use of ArcGIS spatial analyst and the other with ArcSDM.

6.3.2.1 Using ArcGIS spatial analyst

The Table 6.16 (see Annex-I) shows the calculated total class weights ($W_{i\text{-}Total}$) and their respective contrast factors (C_w) for all the classes of the thirteen factors used in the analysis. The contrast factors and the total class weights were calculated according to the equations 5.13 and 5.18. The contrast factor represents the association between a factor class and landslides.

Apart from few cases, the weight values in the method follow a very similar pattern with the weight values of the Information Value method (compare the Tables 6.2 to 6.14 with the Table 6.16 in Annex-1). While the order of the scores remains almost unchanged, most of the values of WOE show slightly higher in positive weights and slightly lower in negative weights with comparison to the Information value method.

In the case of watershed, unlike in the Information Value method where 3rd order watershed has the highest scores (weight), in WOE model first order watershed records the highest value. Whereas the anomaly occurred at the 2nd order remains similar on both the models.

While the Information Value method records positive weights in the distance from spring up to 150 m, WOE records the positive weights until 250 m. However, the contrast factors for the categories greater than 150 m represent negative associations between the landslides and the distance from springs. In the cases of distance from streams and joints, almost similar pattern can be seen in both the models.

Calculated weights in the Tables 6.16 (Annex-I) were first assigned to the corresponding factor maps within the GIS environment and then they were normalized (standardized) to the range of -1 to +1. As the influence of each factor for the occurrence of landslide was equally weighted, final weight map was created by summing up of all the normalized factor weights. The summation was done in the pixel basis and the total weight in the final map ranges from -6.0842 to + 5.49013. The total weight map was reclassified into five classes using Natural Breaks (Jenks) and crossed with the landslide map (Table 6.17). Figure 6.15*b* shows the final out come with five major susceptibility classes, very low, low, medium, high and very high according to their hazard potentials defined using Natural Breaks.

Table 6.17: Total weight (normalized) ranges, percentage of the total area and the existing landslide area.

Total weight range	Susceptibility class	Number of total pixels	Number of LS pixels	% of total pixels (% of total area)	% of LS pixels (% of LS area)
-6.0842 to -2.3316	Very low	3700382	1018	12.6451	00.4150
-2.3316 to -1.2917	Low	8131609	9871	27.7878	04.0245
-1.2917 to -0.2518	Medium	8920633	40326	30.4841	16.4411
-0.2518 to 0.9689	High	6057224	78952	20.6991	32.1892
0.9689 to 5.4901	Very high	2453432	115108	08.3840	46.9302

The Table 6.17 demonstrates almost similar result as in the Table 6.15. Hence, the output here too can be considered as an acceptable representation to the actual field condition.

Even though the classification of both the maps provide similar result based on the total area and the amount of landslides falling into each susceptibility class, according to the spatial distribution of the classes, only 60% of analogous pixels in both the maps overlap showing 40% of spatial difference in the distribution.

6.3.2.2 Using ArcSDM (Spatial Data Modeler)

WOE method implemented in ArcSDM was utilized to explore the influence of causative factors for the occurrence of landslides with two different training site layers created by the landslide rupture surface map. One training site layer was created using an inside center of gravity (centroid) of the landslide rupture surface polygons. This layer consists of 506 training sites representing each point a respective landslide. Second training site layer consists 22137 points. This was created by rasterizing the landslide rupture surface layer into 10 m resolution grid and then converting each grid into a point. Table 6.18 provides the summary information about the data used in both the models.

Table 6.18: Summary information of the data used in ArcSDM models.

	Model-1	**Model-2**
Number of training sites	506	22137
Study area (km^2)	263.437	263.437
Unit cell area (km^2)	0.0001	0.0001
Confidence level of Studentized Contrast	0.01	0.05
Priori probability	0.0001925 (507*0.0001/263.437)	0.008403 (22137*0.0001/263.437)
Number of evidential themes (factors)	13 (see section 4.5)	13 (see section 4.5)

Using Calculate Weight tool, a series of weight tables were created for each evidential theme. A set of statistics, including the area, number of training points, w^+, w^-, contrast and their standard deviations, as well as the Studentized Contrast were calculated for each class in the specified class field and written to a DBF file. Out of 26 DBF files computed for the 13 major factors in both the models, for instance here only a simplified weight table of lithology is given as a Table 6.19.

Table 6.19: Calculated weights (w^+ and w^-), contrast factors and Studentized Contrasts for the Lithology classes with 506 landslide points (*Model-1*) and 22137 landslide points (*Model-2*).

Output weights table using 506 landslide training sites (points): *Model-1*						
Type of Lithology	Area (km^2)	No. of slide points	w^+	w^-	Contrast factor (C_w)	Studentized Contrast (C)
Ch	129.7495	294	0.1633	-0.1889	0.3523	3.9145
Kh	38.5030	53	-0.3352	0.0476	-0.3828	-2.6370
GtBtChGn	76.8362	124	-0.1761	0.0644	-0.2405	-2.3275
QtFpGn	0.7993	4	0.9560	-0.0049	0.9608	1.9136
MetaGabro	8.2892	7	-0.8238	0.0181	-0.8419	-2.2120
HbBtGn	9.2595	25	0.3386	-0.0148	0.3534	1.7226
Output weights table using 22137 landslide training sites (points): *Model-2*						
Type of Lithology	Area (km^2)	No. of slide points	w^+	w^-	Contrast factor (C_w)	Studentized Contrast (C)
Ch	129.7495	13641	0.2262	-0.2814	0.5076	36.5794
Kh	38.5030	2581	-0.2277	0.0343	-0.2620	-12.4691
GtBtChGn	76.8362	5311	-0.1968	0.0711	-0.2680	-16.9626
QtFpGn	0.7993	27	-0.9164	0.0018	-0.9182	-4.7601
MetaGabro	8.2892	103	-1.9186	0.0275	-1.9462	-19.6927
HbBtGn	9.2595	474	-0.4989	0.0143	-0.5132	-11.0242

Weights of Evidence assumes that the training site is a very small area and the total training sites are small. Hence, huge number of training sites is generally a violation of basic assumption of WOE. If the number of training sites gets very large, the Area Frequency and Site Reduction tools can fail in different ways. This is because the tool creates a complex table and it has to deal with too many training sites. A clue that can be used to understand the problem is the Studentized Contrast. A value of 7 or 8 might occur in a well formed model, but greater values should be suspected (Sawatzky et al., 2009).

In the study, while the Studentized Contrast values in the *Model-1* are closely comparable to the above limits, the *Model-2* records much higher values. The maximum Studentized Contrast value reported by the *Model-1* is 13.6826, whereas in the *Model-2*, some factor classes record its value up to 117.18.

After the calculation of all the 13 evidential theme weights for both the models separately, Calculate Response tool was employed to combine the evidence weighted by their associated generalization in the weights-of-evidence tables. This tool calculates the posterior probability response raster created from the sum of the weights, standard deviation (uncertainty) due to weights, variance (uncertainty) due to missing data, the total standard deviation (uncertainty) based on the evidence and how the evidence is generalized in the associated weights-of-evidence tables and confidence raster, i.e., raster showing the confidence that the reported posterior probability is not zero (ratio of the posterior probability to its standard deviation, an approximate student T-test). Then the Area Frequency Table tool can be used to create a DBF table with data for the Cumulative Area-Posterior Probability (CAPP) curve and various other efficiency curves (Success Rate Curve-SRC or Prediction Rate Curve-PRC). The CAPP curve is used to define the number and position of class breaks. The efficiency curves are used to evaluate or validate models. The next important test here is the Agterberg-Cheng CI Test. This tool reports three measures such as overall conditional independence, a conditional independence (CI) ratio and the Agterberg-Cheng test. These tests are necessary because Weights of Evidence, a Bayesian method, assumes conditional independence of the evidence with regards to the training sites.

The *Model-1* was successfully completed within about 30 minutes delivering raster layers of posterior probability (w_pprb), confidence (w_conf) and standard deviation due to the weight (w_std). However, the Area Frequency Table and the Agterberg-Cheng CI Test could not be performed. Calculation of the Area Frequency Table was failed after running 147 hours (more than 6 days) with error message of "invalid integer". Automatic restarting of the system aborted the process. The Agterberg-Cheng CI Test was failed with an exceptional value error.

Calculated posterior probability values in the w_pprb layer ranges from 0.00 to 0.959041 and it was reclassified into five classes using Natural Breaks (Jenks) and crossed with the landslide map (Table 6.20). Figure 6.15*c* is the final out put map with five major susceptibility classes, very low, low, medium, high and very high according to their hazard potentials defined using Natural Breaks.

According to the Table 6.20, percentage of the landslide area and also the total area drastically decreases with the increase of probability values. The probability range of 0.00-0.01124 that corresponds to the very low susceptibility class encloses 99.58% of the total land area predicting 95.68% of the existing landslides. Hence, only a negligible extent of the study area (less than 0.5%) is remained to represent the wide range of probabilities classified from low to very high susceptibility zones predicting merely a 5% of the existing landslides. Nearly a zero percent of the landslides are predicted by the highest probability

Table 6.20: Calculated probabilities of occurring landslides, percentage of the total area and the existing landslide area within each probability range (*Model-1*).

Probability range	Susceptibility class	Number of total pixels	Number of LS pixels	% of total pixels (% of total area)	% of LS pixels (% of LS area)
0.00000 to 0.01124	Very low	29148795	234686	99.5839	95.6828
0.01124 to 0.07118	Low	111619	9341	0.3813	3.8084
0.07118 to 0.21728	Medium	8666	1041	0.0296	0.4244
0.21728 to 0.50200	High	1167	198	0.0040	0.0807
0.50200 to 0.95904	Very high	335	9	0.0011	0.0037

range. Hence unlike in both of the above models where the distribution of the total weights and the amount of the landslides and the total area shown by its value ranges were comparable with actual field conditions, here an extremely biased output which is with great contrary to the field conditions was yielded. This can be mainly due to the insufficient number of landslide points entered in to the model (only 506 points in the training site layer). Hence the *Model-1* has a great disadvantage and seems to be impossible of classifying the probability values into representative susceptibility zones that can be fitted with the actual field data.

Similarly, posterior probability (w_pprb), confidence (w_conf) and standard deviation due to the weight (w_std) were calculated for the *Model-2*. Unlike in the *Model-1*, and in contrary to the number of training sites assumptions, here the Area Frequency tool was executed successfully within 134 hours (5.6 days). The out put table contains 629311 unique values and the Table 6.21 shows a small part of it. However,

Table 6.21: A small part of the Area Frequency Table calculated for the *Model-2*.

Raster Value (Posterior Probability)	**Area (km^2)**	**CAPP_Cum Area** (cumulative area posterior probability)	**Eff_CumArea** (cumulative area accumulated)	**Cum_Sites** (cumulative number of sites)	**I_CumSites** (inverse of Cumulative sites value)	**Eff_AUC** (efficiency area under the curve)
0.00000525	0.0900	6.36091	93.63909	203.09437	-103.09437	0.0000000694
0.00000525	1.0800	6.36095	93.63909	203.09437	-103.09437	0.0000008326
0.00000525	7.8300	6.36125	93.63905	203.09437	-103.09437	0.0000060365
0.00000525	0.1800	6.36126	93.63875	203.09437	-103.09437	0.0000001388
0.00000525	0.3600	6.36127	93.63874	203.09437	-103.09437	0.0000002775
0.00000525	0.3600	6.36128	93.63873	203.09437	-103.09437	0.0000002775
0.00000525	1.8900	6.36136	93.63872	203.09437	-103.09437	0.0000014571
0.00000525	0.2700	6.36137	93.63864	203.09437	-103.09437	0.0000002082
0.00000525	0.1800	6.36137	93.63863	203.09437	-103.09437	0.0000001388
0.00000525	11.1600	6.36180	93.63863	203.09437	-103.09437	0.0000086038
0.00000525	2.5200	6.36189	93.63820	203.09437	-103.09437	0.0000019428
0.00000525	2.7000	6.36200	93.63811	203.09437	-103.09437	0.0000020816
0.00000525	1.6200	6.36206	93.63800	203.09437	-103.09437	0.0000012489
0.00000525	0.8100	6.36209	93.63794	203.09437	-103.09437	0.0000006245
0.00000525	0.0900	6.36209	93.63791	203.09437	-103.09437	0.0000000694

the Cumulative Area-Posterior Probability (CAPP) curve and the other various efficiency curves such as SRC or PRC could not be successfully performed, especially due to lack of enough computer power. Although the sum of the EFF_AUC must be in between 0 to 1 (zero to 100%), the value delivered by the model is 1.595405, showing serious suspicion about the accuracy of the calculation. As same as in the *Model-1*, the Agterberg-Cheng CI Test was failed with an exceptional value error.

Calculated posterior probability values (w_pprb) in the *Model-2* ranges from 0.00 to 0.998174 and it was reclassified into five classes using Natural Breaks (Jenks) and crossed with the landslide map (Table 6.22). Figure 6.15*d* shows the final out come with five major susceptibility classes, very low, low, medium, high and very high according to their hazard potentials defined using Natural Breaks.

Table 6.22: Calculated probabilities of occurring landslides, percentage of the total area and the existing landslide area within each probability range (*Model-2*).

Probability range	Susceptibility class	Number of total pixels	Number of LS pixels	% of total pixels (% of total area)	% of LS pixels (% of LS area)
0.00 to 0.05069	Very low	27194320	134666	92.9067	54.9041
0.05069 to 0.19106	Low	1194114	37508	4.0796	15.2922
0.19106 to 0.39771	Medium	465467	21159	1.5902	8.6266
0.39771 to 0.65895	High	257521	20139	0.8798	8.2108
0.65895 to 0.99817	Very high	159160	31803	0.5438	12.9663

As can be seen from the Table 6.22, the percentage of landslide area gradually decreases with the increase of probability up to the high susceptibility class. However, percentage of total area follows a similar pattern as in the *Model-1*. The probability range of 0.00-0.05069 that corresponds to the very low susceptibility class encloses 92.91% of the total area with 54.90% of the existing landslides. Only a 7% of the total area is remained to represent the other four susceptibility classes. On the other hand, probability values corresponding to the very high susceptibility class encloses 12.97% of all the landslides with 0.54% of the study area. In addition to that, 21% of the landslides are predicted by both the very high and high susceptibility classes. The statistics demonstrate comparatively an improved situation in the *Model-2* than the *Model-1*. This can be solely due to the increase of number of landslide points in the training site layer although a huge number of training sites is a violation of a basic assumption of WOE and considered as more than 1000 training sites are excessive. However, the distribution of the amount of landslides and the total area represented by the higher probability values are still inadequate for a model to be compared with the actual field conditions.

6.3.3 Multivariate Logistic Regression (LR) model

As explained in the section 5.3.3, LR analysis technique was applied to prepare a landslide susceptibility map. While all the above methods consider each factor separately, LR model considers factors simultaneously and yields factor weights considering the interrelationship among the factors. The analysis was performed by dividing the study area into 100 * 100 m grid cells, and then determining the presence

and absence of landslides and each causative factor within those grid cells. The total number of grid cells within the study area is equal to 26,350 out of which only 1291 grid cells record landslides. It is generally recommended in LR model to use equal proportions of 1s (landslides) and 0s (no landslides) pixels. However, this is not usually the case in many works. In the present study, data from all over the area was used and hence this undoubtedly leads to an unequal pixel proportions.

Since there are 304 variables (factor classes) representing all the thirteen factors and it is too much for a good LR model, as a first step, similar variables were grouped together and reduced to a small number of components. Here, Factor Analysis procedure was applied first and then the number of components was further reduced by Comparison of Means procedure. The Table 6.23 shows the summary information of the number of variables in each factor, the variable reduction methods and the number of final component variables used in the LR model.

As a first step, 26 component variables selected by the above methods were input into the method of *Forward Stepwise* (*Wald*) for the pre-selection of component variables by their degree of influence. From that, 17 component variables that explained 18% of the variance of the landslides were selected. Considering the rate of increase of Pseudo R-Square measure (Nagelkerke R-Square), 11 component variables were again chosen by an expert assessment and input into the method *Enter* for the final analysis.

In assessing the overall quality of the model fit, several measures are available (Table 6.24). A key concept for understanding the tests used in LR is that of log likelihood. Usually, although the overall significance is tested using Model Chi-square, which is derived from the likelihood of observing the actual data under the assumption that the model that has been fitted is accurate, it is convenient to use -2 Log Likelihood (-2LL) value. Smaller values of the -2LL measure indicate better model fit.

The log likelihood value in the study is 8852.942. The Cox and Snell R^2 and Nagelkerke R^2 measure (pseudo R^2) operates which higher values indicating greater model fit. When a pseudo R^2 is greater than 0.2, it shows a relatively good fit (Clark and Hoskin, 1986). Both values obtained in the study are 0.054 and 0.166 respectively confirming that the statistical model weekly supports the validity of the system with the variables. However, since the pseudo R^2 value in the study is close to 0.2 and higher values in such kind of work can rarely be expected, model was accepted and the final coefficients for the 11 component variables were computed.

The coefficients calculated for the selected component variables by the final logistic regression model are given in the Table 6.25.

Table 6.23: Summary information about the variable reduction methods and the final components used in Logistic Regression (LR) model.

Major factor	No. of total factor classes	No. of components selected by Factor Analysis	No. of final components selected by method of CM or Bivariate Correlation	Remarks
Lithology	6	KMO=0.175, low KMO due to weak correlation. None of the variables were selected.	1 variable (Ch)	Number of variables are too less for Factor Analysis. Selection is solely done by the CM procedure.
Landuse	25	KMO=0.301 (weak correlation), none of the variables were selected.	3 variables (Jt1, W1 and Hp)	There is almost no correlation between the variables. Selection is done solely on the CM procedure.
Landform	44	KMO =0.257 (weak correlation), none of the variables were selected.	3 variables (E32, E37 and E46)	There is almost no correlation between the variables. Selection is done solely on the CM procedure.
Soil type	4	KMO=0.464 (weak correlation), none of the variables were selected.	1 variable (Colluvium)	No. of variables are too less for Factor Analysis. Selection is done solely on the CM procedure.
Soil thickness (m)	43	KMO=0.303 (weak correlation), none of the variables were selected.	none of the variables were selected	There seems to be no relevance of all the variables of this parameter for explaining the occurrence of landslides. Therefore indeed none is used for the final analysis.
Slope angle (1^0 category)	74	KMO=0.955 (strong correlation), 11 components were selected with 83.817% of total variance explained.	7 component variables	11 components were selected by Factor Analysis and then reduced further to 7 by CM procedure.
Aspect (10^0 category)	36	KMO=0.947 (strong correlation), 5 components were selected with 83.989% of total variance explained.	3 component variables	5 components were selected by Factor Analysis and then reduced further to 3 by CM procedure.
Deviation angle (10^0 category)	18	KMO=0.896 (strong correlation), 3 components were selected with 82.109% of total variance explained.	1 component variable	3 components were selected by Factor Analysis and then reduced further to 1 by CM procedure.
Under-over dip scarp angle (10^0 category)	30	KMO=0.783 (strong correlation), 8 components were selected with 73.846% of total variance explained.	3 component variables	8 components were selected by Factor Analysis and then reduced further to 3 by CM procedure.
Watershead	6	KMO=0.325 (weak correlation), none of the variables were selected.	none of the variables were selected.	There seems to be no relevance of all the variables of this parameter for explaining the occurrence of landslides. Therefore indeed none is used for the final analysis.
Spring distance (50 m category)	6	KMO=0.670 (medium correlation), 2 components were selected with 80.903% of total variance explained.	1 component variable	2 components were selected by Factor Analysis and then reduced further to 1 by CM procedure.

Stream distance (50 m category)	6	KMO=0.777, 2 components were selected with 80.418% of total variance explained. Although the KMO value shows good correlation, selection is not logical and can not be accepted.	1 variable (Stream distance 0-50m)	All the variables can be considered by CM procedure. However, finally only the variable stream distance 0-50 m category was selected by the method of bivariate correlation (using Pearson's correlation coefficient).
Joint distance (50 m category)	6	KMO=0.661, (medium correlation), 2 components were selected with 78.820% of total variance explained.	2 component variables	2 components were selected by Factor Analysis and the both were selected by CM procedure too.
Total	304		26	
FA=Factor Analysis, CM=Comparison of Means, KMO=Kaiser-Meyer-Olkin Measure of Sampling Adequacy, No.=number				

Table 6.24: Overall model summary representing the goodness of fit for the final LR model.

-2 Log likelihood	Cox and Snell R-Square	Nagelkerke R-Square
8852.942	0.054	0.166

Table 6.25: Estimated regression coefficients for the final model.

Final component variables	β **coefficient**
Joint Distance-from 0 to 150 m	0.233
Spring Distance-from 0 to 150 m	0.176
Stream Distance-from 0 to 50 m	1.405
Landform code E46	0.465
Landuse code JT1	0.603
Landuse code W1	-0.843
Slope angle $17–32^0$	0.606
Slope angle $33\text{-}44^0$	0.376
Slope angle 45-50	0.313
Slope angle 5-10	-0.231
Slope angle 0-4	-0.368
Constant	-4.396

After computing the probability of occurrence of landslides within each sample unit using the above coefficients and the equation 5.20, they were assigned to the 100 *100 m sample units and converted into 3 m raster resolution by the re-sampling technique of Nearest Neighbor.

The out put values representing the probability of occurring landslide event varies from 0.00044 to 0.74693. The more these numbers are close to 1, the better they indicate the likelihood of finding the mapped landslides. The probability map was reclassified into five classes using Natural Breaks (Jenks) and crossed with the landslide map (Table 6.26). Figure 6.15*e* is the final out come with five major susceptibility classes, very low, low, medium, high and very high according to their hazard potentials defined using Natural Breaks.

Table 6.26: Calculated probabilities of landslide events, total area and the existing landslide area within each probability range.

Probability range	Susceptibility class	Number of total pixels	Number of LS pixels	% of total pixels (% of total area)	% of LS pixels (% of LS area)
0.0004 to 0.0383	Very low	17387001	29161	59.4671	11.8891
0.0383 to 0.0967	Low	7979854	82137	27.2927	33.4877
0.0967 to 0.1871	Medium	2886052	88849	9.8709	36.2242
0.1871 to 0.3416	High	783401	32563	2.6794	13.2761
0.3416 to 0.7469	Very high	201711	12565	0.6899	5.1228

According to the Table 6.26, the probability range of 0.00044-0.038348 that corresponds to the very low susceptibility class encloses 59.47% of the total land area with 11.89% of the existing landslides. Although an almost 40% of the study area is remained to represent the probabilities classified from low to very high susceptibility classes with 92% of all the landslides, only a 5.12% of the landslides are predicted by the very high susceptibility class. In addition, only 18.4% of the landslides are enclosed by both the very high and high susceptibility classes. Unlike in the other models, here majority of the landslides (almost 70%) are predicted by the probability ranges corresponding to the low and medium susceptibility classes together. Even though the distribution of the total area among probability ranges seems to be reasonably good, distribution of the amount of landslides within the higher probability values is inadequate for a model to be compared with the actual field conditions. This situation may have been arisen due to a few number of variables considered in the final analysis (Table 6.25) to fulfill the basic assumptions of logistic regression modeling. Although the grouping of factor classes into component variables seems to be as a good approach, total exclusion of some of the major factors such as geology, deviation angle, under-over dip scarp angles, soil type, soil thickness and some of the other factor classes could have been the reasons for a biased output.

6.4 Comparison of susceptibility models by success rate analysis

The Figure 6.16 shows the success rate curves prepared for all the five susceptibility models. For the comparison of different models, percentage of prediction scores (weights or probabilities) corresponding to 70% of the existing landslides was considered (Figure 6.16). Respective prediction score range, actual percentage of landslides and the percentage of total area covered by these prediction score ranges were calculated using the final weight/probability maps and their associated DBF tables. The summary information is provided in the Table 6.27.

Table 6.27: Prediction score (weight/probability) ranges and the percentage of total area which represent about 70% of the existing landslides.

Type of the model	Total prediction score range in the final model	% of scores related to 70% of LS	Prediction score range related to about 70% of LS	Actual % of LS	% of total area
Information Value (LS Index) method	-6.011 to +5.102	54-100%	-0.010 to +5.102	72.35%	23.50%
WOE-ArcGIS Spatial Analyst	-6.084 to +5.490	54-100%	+0.050 to +5.490	71.56%	22.21%
WOE-ArcSDM using 506 LS points	0.00 to 0.959	01-100%	0.000 to +0.959	Include all LS	Include all area
WOE-ArcSDM using 22137 LS points	0.00 to 0.998	02-100%	+0.010 to +0.998	73.64%	18.45%
Multivariate Logistic Regression model	0.0004 to 0.747	10-100%	+0.068 to +0.747	70.38%	21.96%

In the Information Value method, 72.35% of all the landslides are contained by 23.50% of the total map area with the highest prediction scores greater than minus (-) 0.01 (from 54 to 100%). Similarly, in the WOE-ArcGIS Spatial Analyst model, 71.56% of all the landslides are located within 22.21% of the total map area with the highest prediction scores greater than plus (+) 0.050 (from 54 to 100%). In both the models, 54% of the lowest prediction scores are remained with 30% of the landslides and almost 80% of the map area.

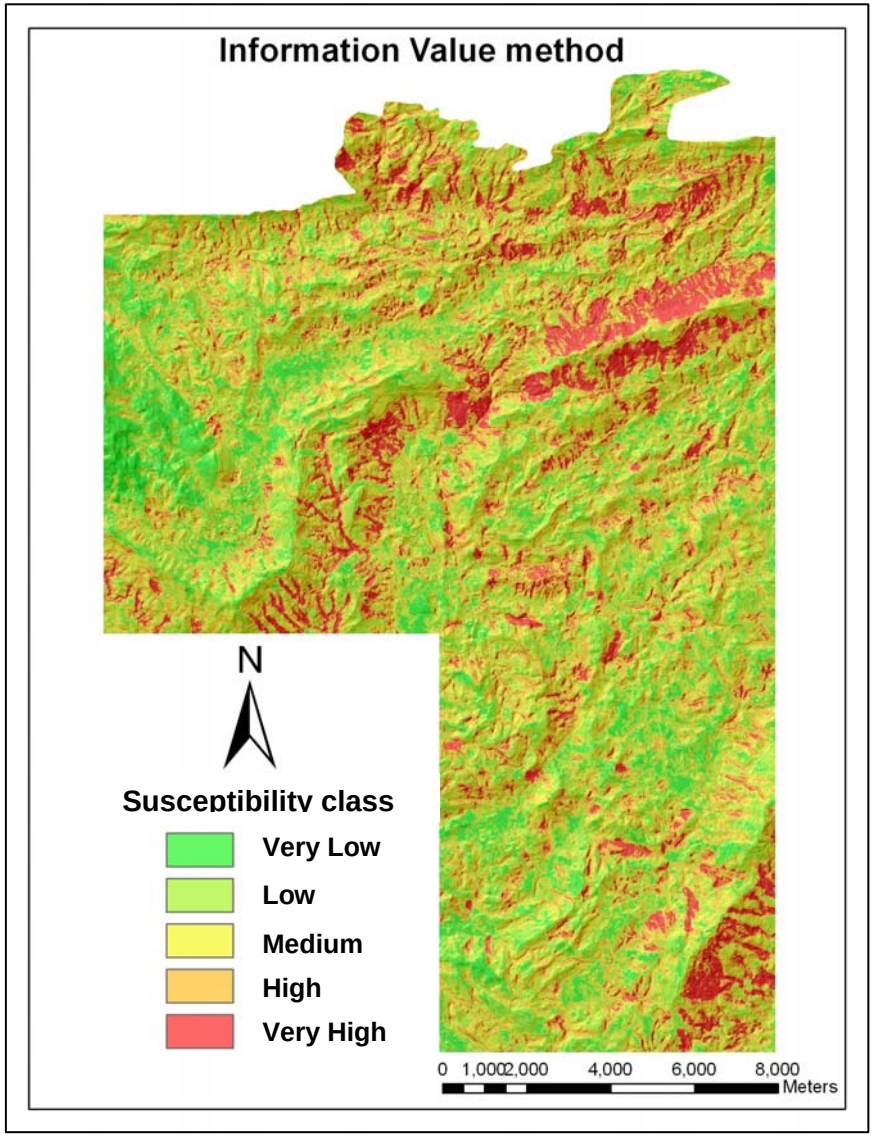

(a) Information Value method

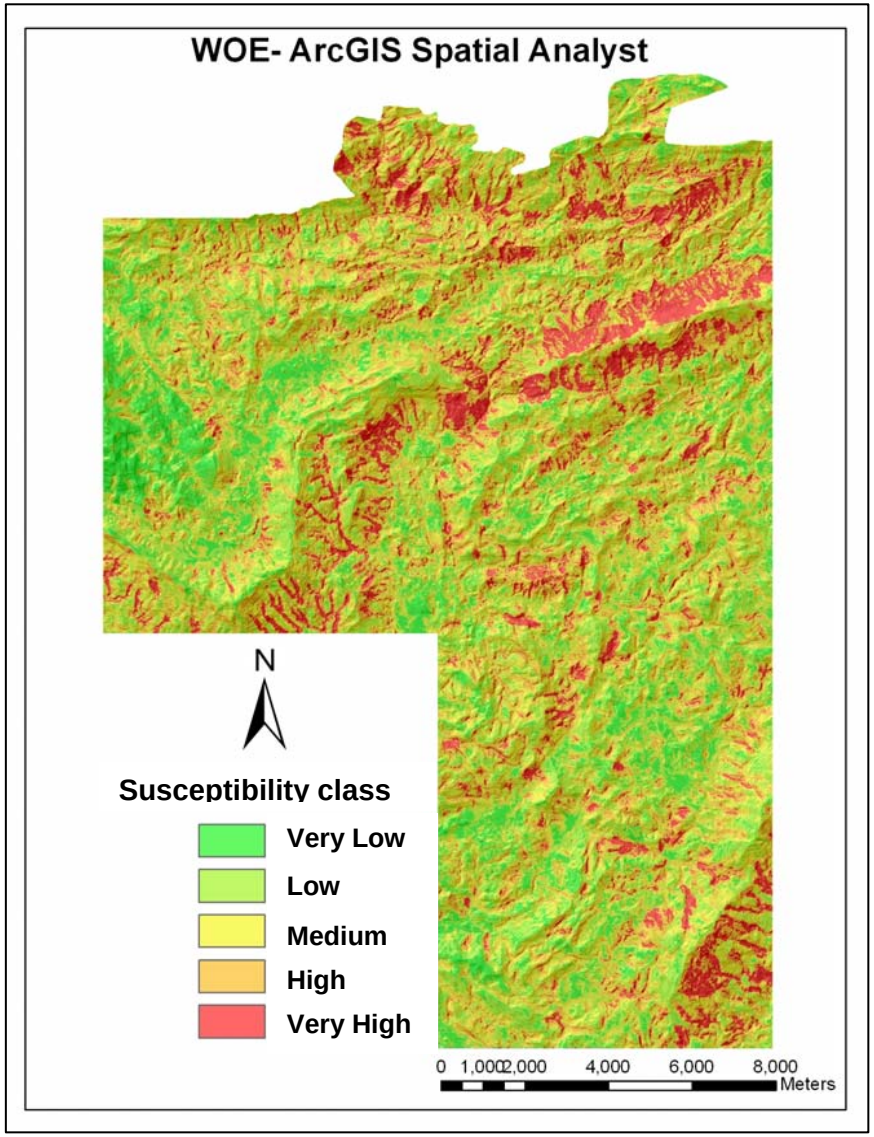

(b) Weights of Evidence (WOE) model - ArcGIS Spatial Analyst

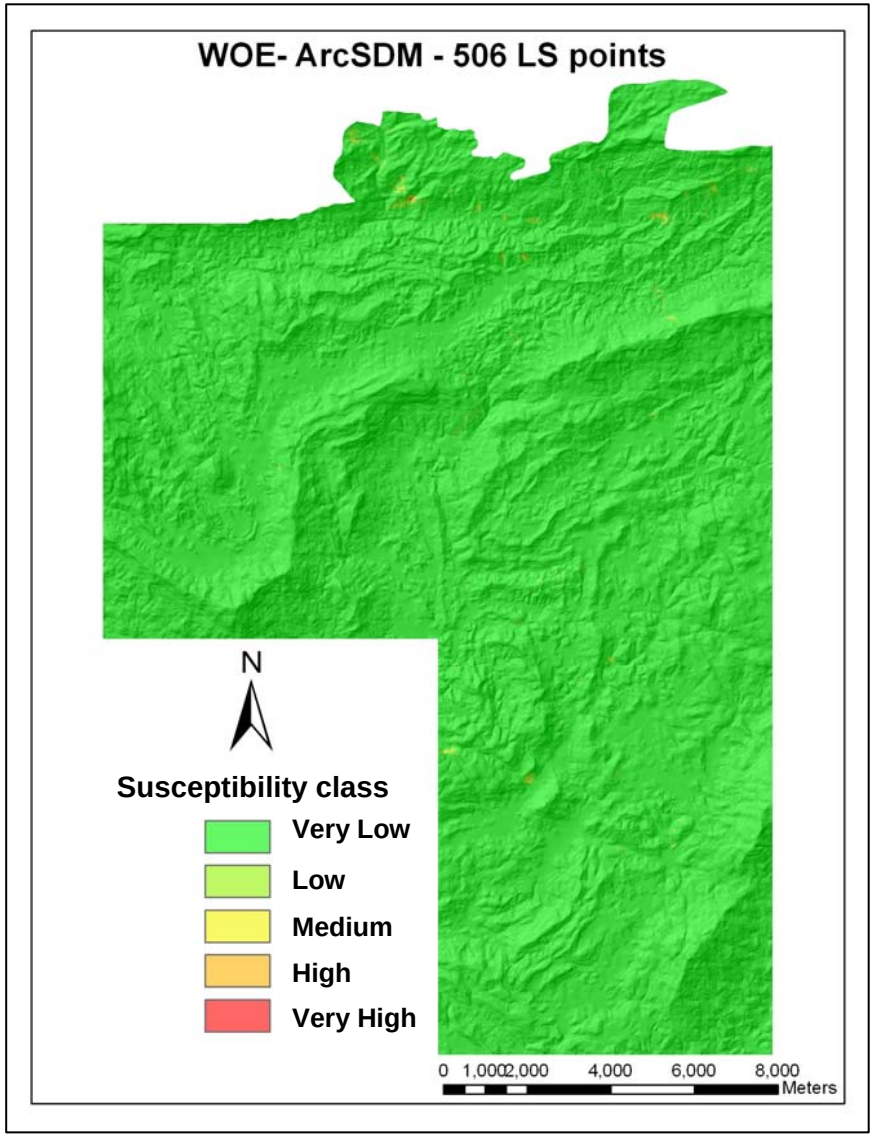

(c) WOE - ArcSDM with 506 Landslide points

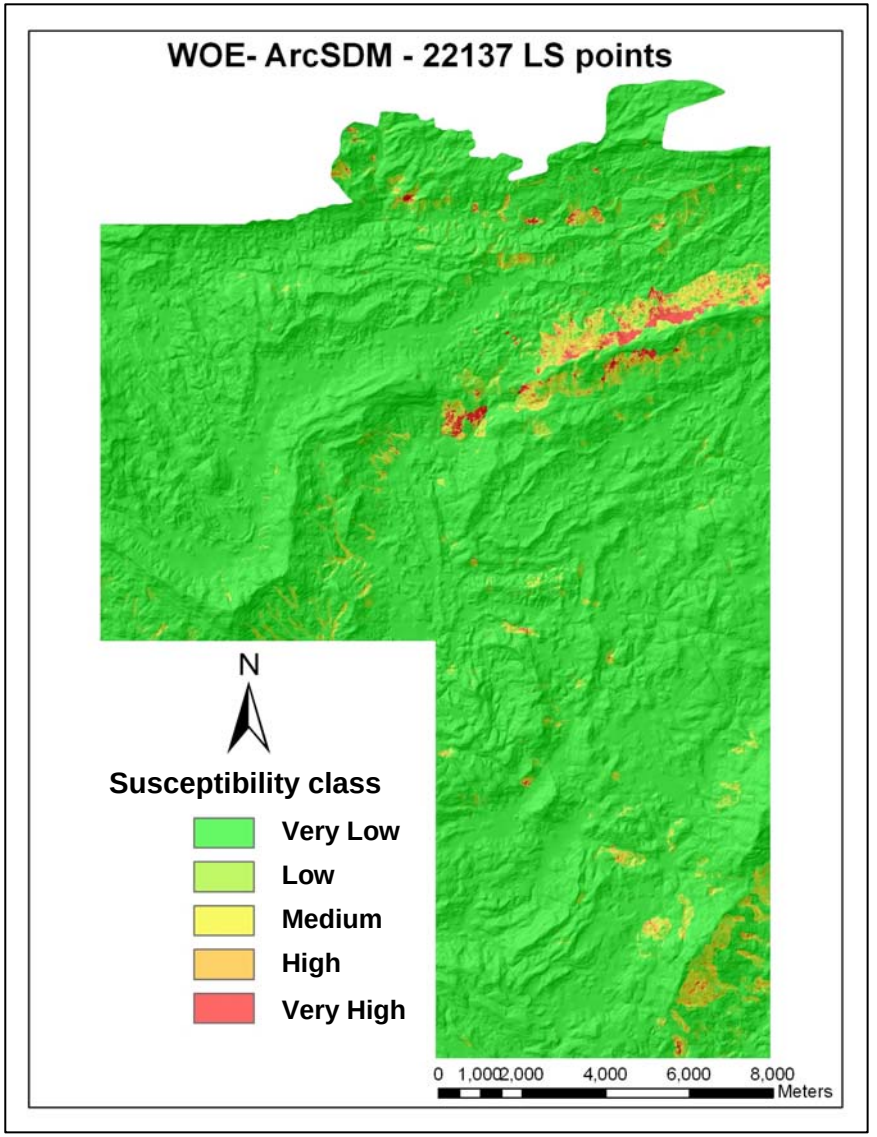

(d) WOE - ArcSDM with 22137 Landslide points

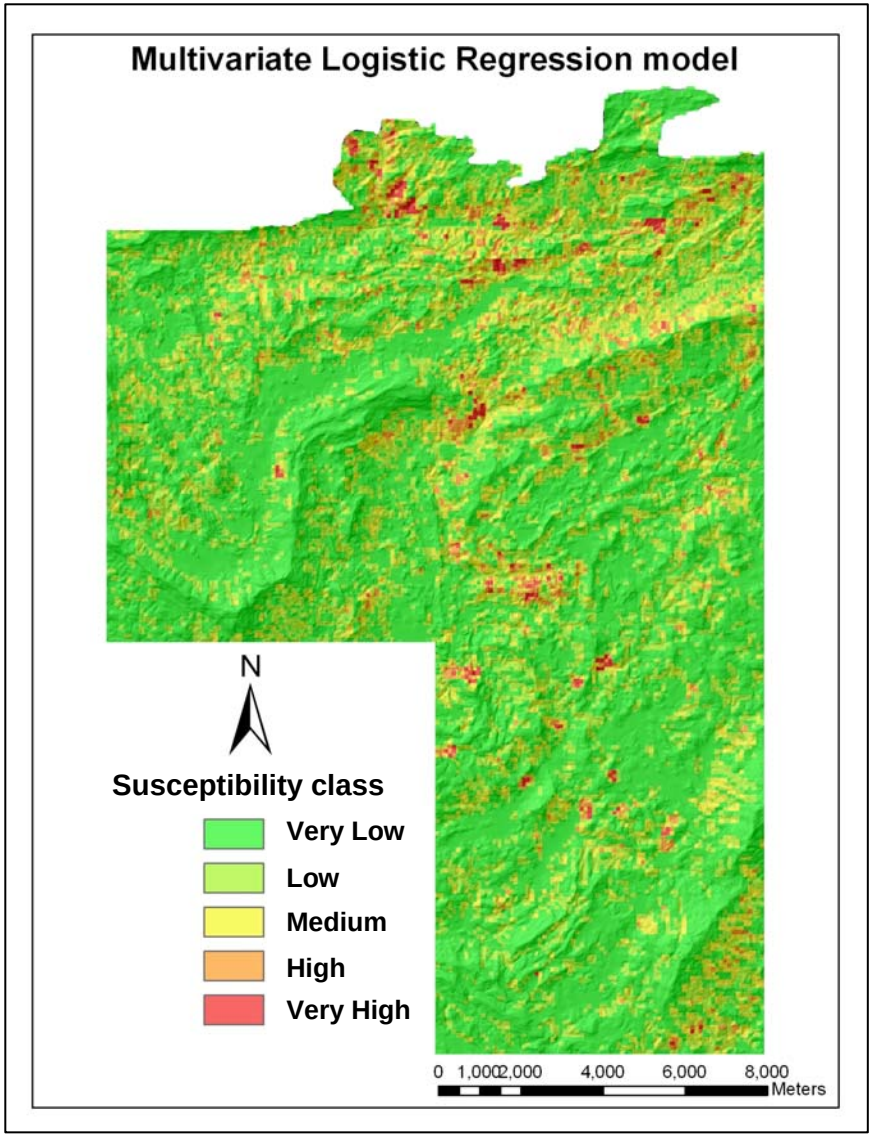

(e) Multivariate Logistic Regression model

Figure 6.15: Final weight/probability maps reclassified into five susceptibility classes based on Natural Breaks (Jenks).

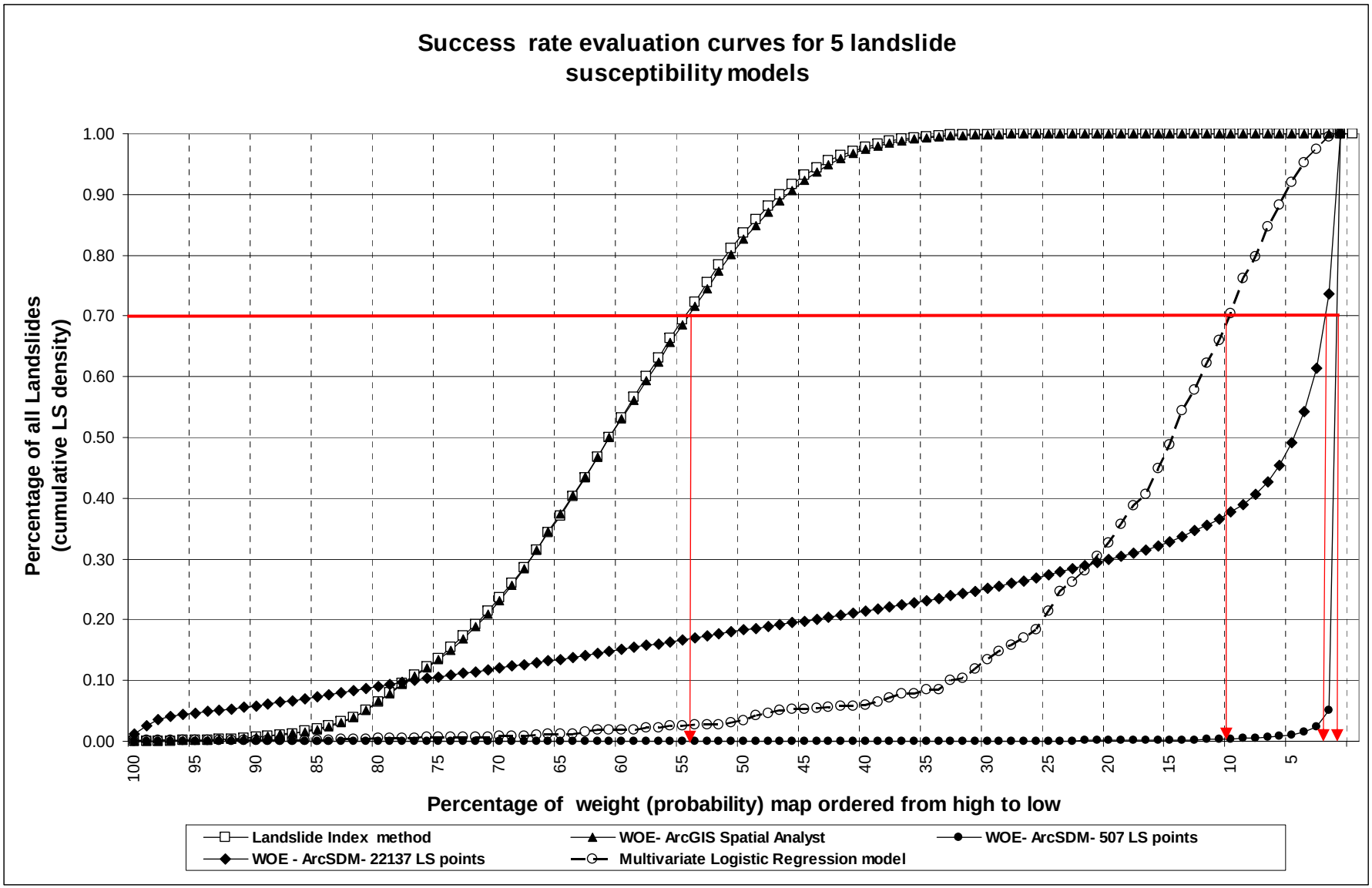

Figure 6.16: Success rate evaluation curves for the five landslide susceptibility models (showing percentages of prediction scores related to 70% of landslides).

The WOE–ArcSDM model using 506 LS points requires the entire range of probabilities (0.00 to 0.959) covering the whole map area to predict 70% of the existing landslides. The model here is extremely biased and hence can be rejected as an unsuccessful output. A 73.64% of the existing landslides are predicted by 18.45% of the total map area by the model of WOE-ArcSDM using 22137 LS points. Although the prediction here seems to be the best with the percentage of area covered, range of prediction scores extend from almost lowest (0.01) to the highest probabilities (from 2 to 100%). In the Multivariate Logistic Regression model, 70.38% of all the landslides are located in 21.96% of the total map area with the prediction scores greater than to 0.068 (10 to 100%). Even though, this can be considered as fairly a better model than to both of the WOE–ArcSDM models, only a 10% of the lowest prediction scores are remained with 30% of the landslides and almost 80% of the map area.

The classification based on Natural Breaks (Jenks) as well as the success rate analysis indisputably shows the models derived from the *Information Value method* and the *WOE-ArcGIS Spatial Analyst* are the best susceptibility models. Furthermore, unlike other 3 models where fully automated procedures have to be followed, these two models can be improved with the expertise of the field conditions. Given the fact that both the models offer almost similar result, the model prepared by the *Information Value method* was chosen for further modifications with expert knowledge.

6.5 Modified landslide susceptibility model with expert weighting

Although the above model based on *Information Value method* was prepared by summing up of equally weighted factor scores, in reality, this may not be the case, and various factors may have different degrees of influence for the occurrence of landslides. Thus, weighting of the factors according to their degree of influence can be very useful for the improvement of such models.

Since there is no direct approach to discover the relative importance of each factor, expert weighting with trial and error procedure was followed. A value of hundred was divided into the thirteen (13) factors in different ways according to expert judgment and a number of susceptibility maps were prepared. Among comparison of them with the landslide inventory map, the best weighting combination which is shown in the Table 6.28 was chosen.

Out of all the experimented combinations, the best representative output was given when the highest weight percentage of 27% is assigned to the slope angle factor. Even though some of the landuse classes like W2, JWb and JT1 provide ambiguous result according to the landslide densities, under the expert weighting, second highest percentage of 15% had to be assigned to obtain the best possible outcome in general. However, this may lead to deliver wrong predictions in some situations and hence field checking and the adaptation of site specific modifications where such problems exist is still needed. Even if the factors like aspect and watershed too have some kind of ambiguity, both contributes the least relative percentage of influence of 1% each and hence similar problem may not arise.

The normalized factor scores for each factor was multiplied by their respective percentage of influence (weight %) and then they were combined into a single map by summing up of all the values. The summation was done in the pixel basis and the total scores in the final map ranges from -67.6875 to + 37.1612.

The Figure 6.17 is the success rate evaluation curve for the model. Here, 70% of the existing landslide is predicted by the prediction scores greater than 2.56 (68 to 100%). Hence, this model demonstrates a 14%

improvement of the success rate with comparison to the equally weighted model (compare Figure 6.16, Figure 6.17 and Table 6.27).

The resultant total weight map was reclassified into three major susceptibility zones. Class boundaries were adjusted until satisfactory results were obtained by overlaying the susceptibility map with the landslide inventory map and calculating the landslide densities in each class. The class boundaries, class

Table 6.28: Percentage of weights for each factor according to an expert judgment.

Factor	Percentage of influence (weight %)
Lithology	2%
Landuse	15%
Landform	15%
Soil type	5%
Soil thickness (soil depth)	5%
Slope angle (gradient)	27%
Slope aspect	1%
Deviation angle	4%
Under/over dip - under/over scarp angle	4%
Watershed	1%
Distance to Springs	8%
Distance to Streams	8%
Distance to Joints	5%
Total percentage	**100%**

name, total area covered and its percentage and the total landslide within each class and its percentage for the final classification is shown in the Table 6.29.

Table 6.29: Total weight ranges, percentage of total area and the existing landslide area.

Total weight range	Susceptibility class	Number of total pixels	Number of LS pixels	% of total pixels (% of total area)	% of LS pixels (% of LS area)
-67.69 to -6.00	Low	14833614	14789	50.69	06.03
-6.00 to 3.50	Medium	10104313	70832	34.53	28.88
3.50 to 37.16	High	4325353	159654	14.78	65.09

The reclassified susceptibility map is shown as the final landslide susceptibility map of the study area (Figure 6.18). According to the classification, 50.69% of the study area is designated to be low susceptible with corresponding 6.03% of the total landslides. The zone related to high susceptibility class constitutes 14.78% of the total study area predicting 65.09% of the existing landslides. The rest of the area was classified as medium susceptibility that yields in 34.53% of the area with corresponding 28.88% of the total landslides.

According to the Figure 6.18, most of the high susceptible areas are concentrated to the north, central and northeast parts of the study area such as Bateyaya, Ensalwattha, Ullinduwawa, Panilkanda, Aninkanda,

Beralapanatara, Diyadawa, Kotapola. In addition to that, high susceptible areas can be seen at the southeast corner of the study area too. They are mostly topographically complex, hilly or mountainous areas. Most of the medium susceptible areas are concentrated surrounding the high susceptible zones and at the northwestern and eastern parts as well as along the southern slope of Morawakakanda area. The majority of the low susceptible areas can be observed at the western and the southern parts of the study area such as Pallegama, Ellegoda, Ehelapitigama, Rottumba, Thundolahena, Mawarala, Gombaddala and also Bengamuwa area.

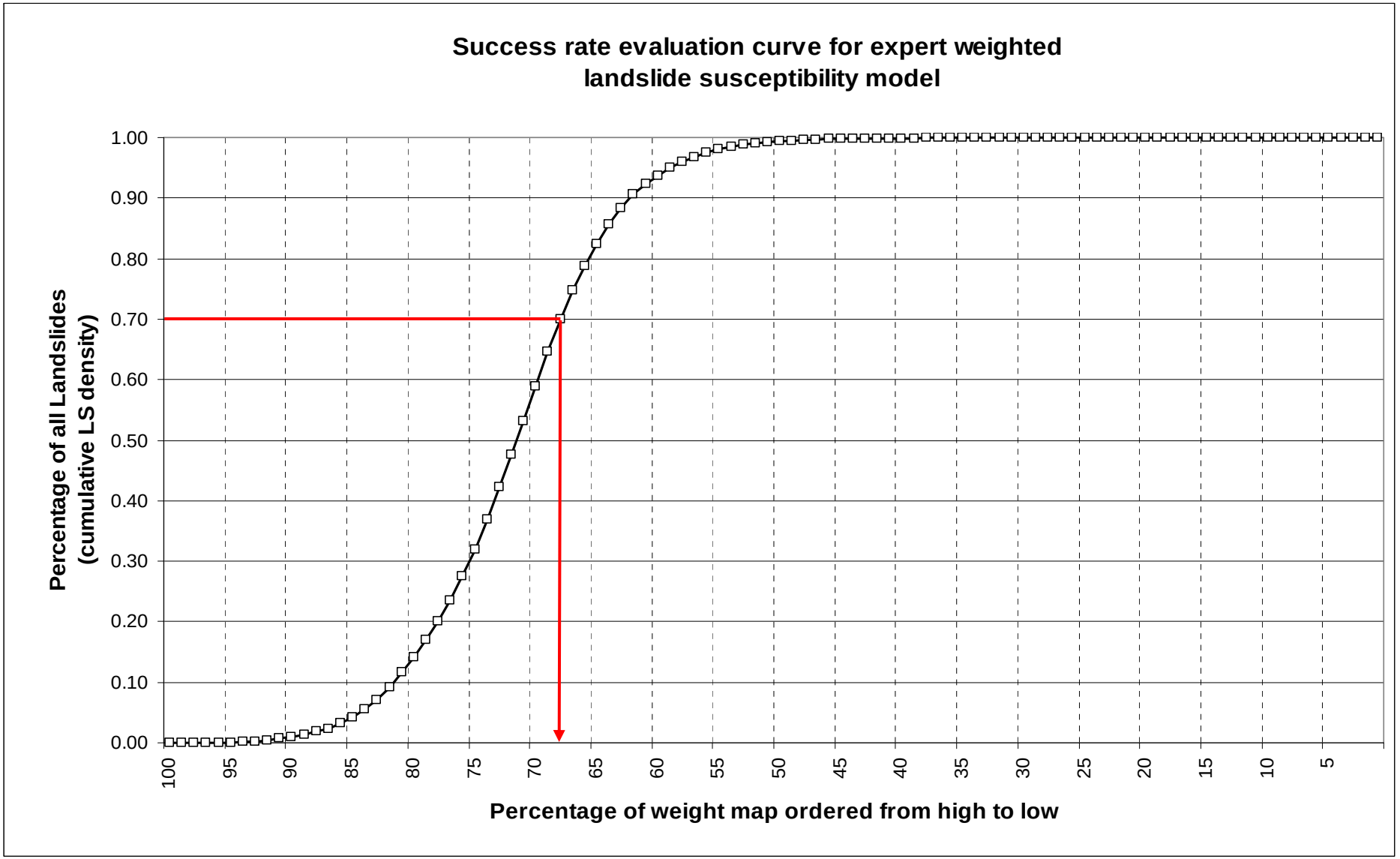

Figure 6.17: Success rate evaluation curve for the expert weighted landslide susceptibility model (based on the model of Information Value method).

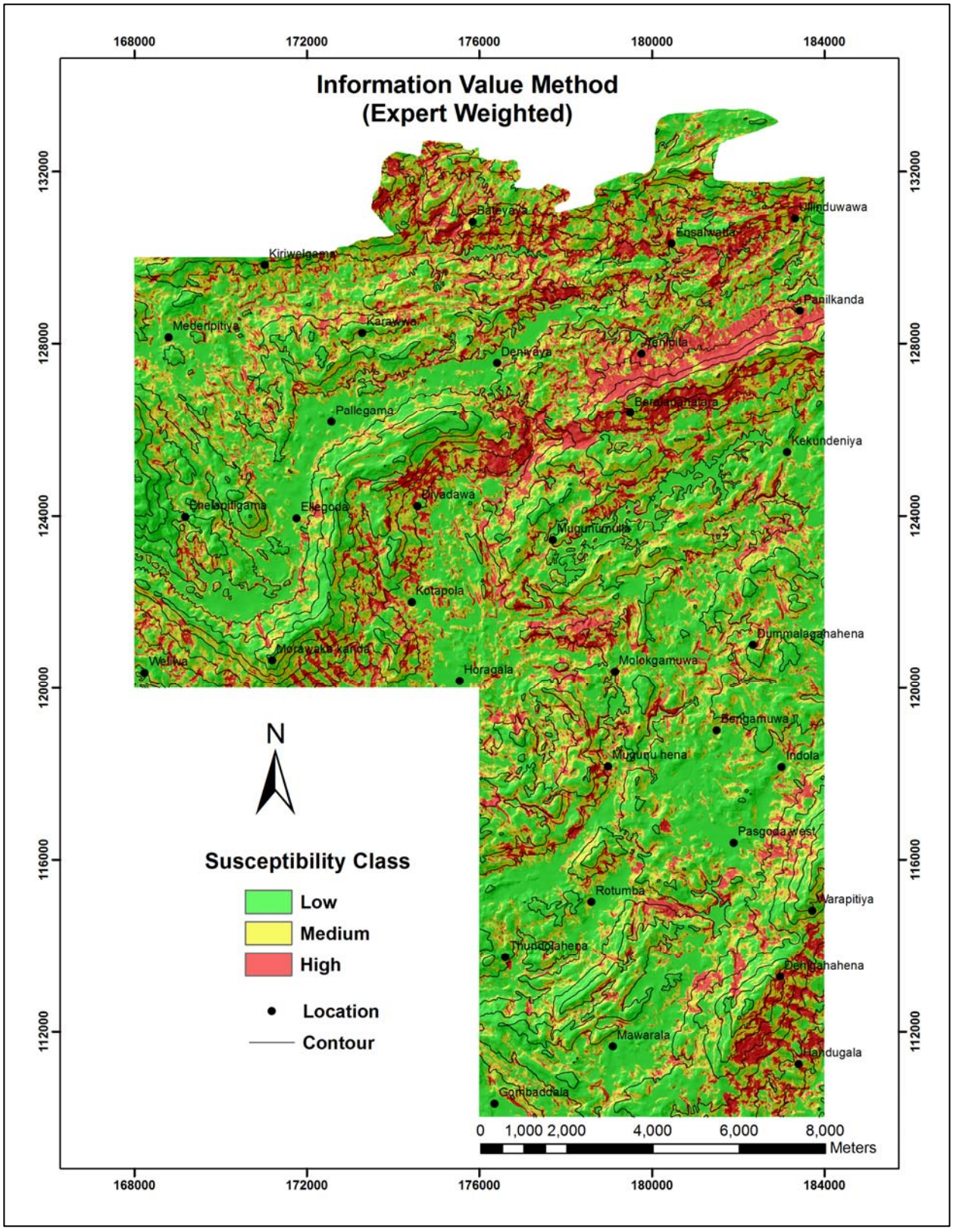

Figure 6.18: Expert weighted landslide susceptibility map classified into three classes (based on the model of Information Value method). Enlarged version of the map is attached at the end of the thesis.

6.6 A combined hydrological slope stability model - Dynamic modeling

Subsequently to the preparation of final, expert weighted landslide susceptibility map, two dynamic model scripts based on the theories described in the section 5.4.2 were employed within the PCRaster environment to assess the stability of slopes in terms of factor of safety (F_s); i.e., for $F_s > 1$, the slope is stable; as F_s approaches 1, it becomes unstable; and for $F_s \leq 1$, slope failure theoretically occurs. While one model script was based on one layer soil structure other was based on four strata of unsaturated layers. To avoid the complexity, the models were run only for a selected basin (Figure 6.19 and 6.20) within the study area. Data used in the models are illustrated in the Table 6.30 while the rainfall data for the month of May 2003 is shown in the Table 6.31.

Table 6.30: Summery of the data used in the dynamic modeling.

Type of data	Data used for testing the models	data used in the final model
Digital elevation model (DEM)	dem.map	dem.map
Local drain direction map	ldd.map	Idd.map
Daily rainfall for the month of May 2003 (cm/day) - Deniyaya Willi group station, Table 6.31.	raininp.tss	raininp.tss
Evaporation data (cm/day)	0.05 to 0.3	0.05
Saturated hydraulic conductivity (cm/day)	8 to 12	9.00
Soil depth map (in cm)	soildepth.map	soildepth.map
Maximum moisture content unsaturated layer	0.25 to 0.56	0.27
Minimum moisture content	0.01 to 0.04	0.04
Loss of groundwater to rock (cm/day)	1 to 3	2.00
Tangent value of the effective friction angle	tanphi.map*	0.46
Effective cohesion (kN/m^2)	cohesion.map*	3.00
Unit weight of soil (kN/m^3)	unitweght.map*	unitweight.map
Slope angle (percentage) – from DEM	slope.map	slope.map
Initial volumetric moisture content (cm^3/cm^3)	0.20 to 0.35	0.20
Initial water height (cm)	inwaterh.map	inwaterh.map
Pixel size	10 m	10 m

*IDW interpolated surfaces using soil sample data given in the Table 4.2 and 4.7.

The *Inwaterh.map* (initial water height map) was prepared by applying a constant rainfall of 0.32 cm per day for 1000 days with the evaporation of 0.1 cm per day and the loss of groundwater to rock of 0.2 cm per day. Assuming that the steady state condition is achieved at the end, average water height map delivered by the model for the last ten days was selected as the initial water height map.

Table 6.31: Rainfall data -Deniyaya Willi group station, May 2003.

Date	1	2	3	4	5	6	7	8	9	10	11	12	13	14
Rainfall (cm)	1.88	1.63	0.29	0.34	8.29	1.84	0.0	0.0	0.75	0.43	0.37	3.06	1.32	2.2

15	**16**	**17**	18	19	20	21	22	23	24	25	26	27	28	29	30	31
1.5	**16.3**	**73.0**	0.1	0.18	0.0	0.0	0.0	0.0	0.0	0.22	0.3	0.0	0.0	0.0	0.0	0.0

As a preliminary step, both the models were tested for different combinations of input values and the outputs were compared with the actual field conditions. The results delivered by the model with the four

layers system was always with great contrary to the actual field conditions whilst fairly better results could be obtained by the other model. Hence, one layer system was chosen as an appropriate model for the study area and simulations were continued with trial and error procedure. The final parameter combination which delivered acceptable results was show in the Table 6.30. For the final model, *tanphi.map* and *cohesion.map* were replaced by fixed values. When the *cohesion.map* is used in the model, safety factor remains always above 1.30 even at the peak rainfall values. Whereas, with the use of *tanphi.map*, fairly good results were delivered, however many of the unstable pixels at the peak rain fall were concentrated to the central part of the basin. The situation could have been arisen due to lack of representative soil parameter data within the study area. Number of soil data points used in the interpolation was limited (only 26 samples for the entire study area of 263 km^2) and at the same time the samples were collected from one to two meters depth from the surface even though the depths of slip surfaces are assumed to be equal to the depth of the soil (z) in the factor of safety equation. Hence the values derived from those soil samples might not have been much comparable with the actual values where slip surfaces may occur. In addition to that, the model shows a very sensitive behavior with the change of cohesion than to the friction angle.

Since the model was run for a period of one month (May 2003), thirty one (31) factors of safety (F_s) maps were delivered as an output. The minimum factor of safety value reported within the study area during the month is 0.84 while the maximum being 1.5. At the beginning of the simulation, the entire terrain remained at permanently stable condition ($F_s \geq 1.4$). According to the safety maps (Figure 6.19), it is very unlikely to see any change of safety level until 15th May 2003. On 16th May, with the starting of intense rain, slight indications of instability can be seen in some locations. With the peak rain fall on 17th May, model shows a clear indication of instabilities and the factor of safety decreases to the minimum of 0.84. Even though the rain was ceased, instabilities seem to be remained unchanged during the day of 18th May too. From 19th of May, factor of safety values began to increase again and the slopes started to regain the strength to resist itself for failure. Even though the slope stability condition improved after 19th May 2003, model shows some indications of instabilities even at the end of the month. Hence, in general it can be said, initially stable slopes became dramatically unstable during the storm, reaching the maximum on 17th and 18th of May and then slowly recovered to pre-storm conditions with time (Figure 6.19).

In nature, once the hydrostatic pressure is increased to a critical level, slope failures occur and the excess pore water pressure is released. However, as this state is not implemented in the model, it demonstrates high pressures inside the soil mass and thus low factor of safety values until the excess pressure is released according to the ground water flow of the system. That implies if the incident was not occurred on 17th May, it could have been taken place on the following day even after the rain was ceased which could have been more hazardous due to its unexpected nature. Therefore, such circumstances have to be taken into serious considerations when landslide predictions and early warnings are in concern.

For the verification of deterministically calculated factor of safety maps with the actual field conditions, landslide inventory map on 17th May 2003 was crossed with the factor of safety map of the same date. The outcome of the map crossing is given in the Table 6.32.

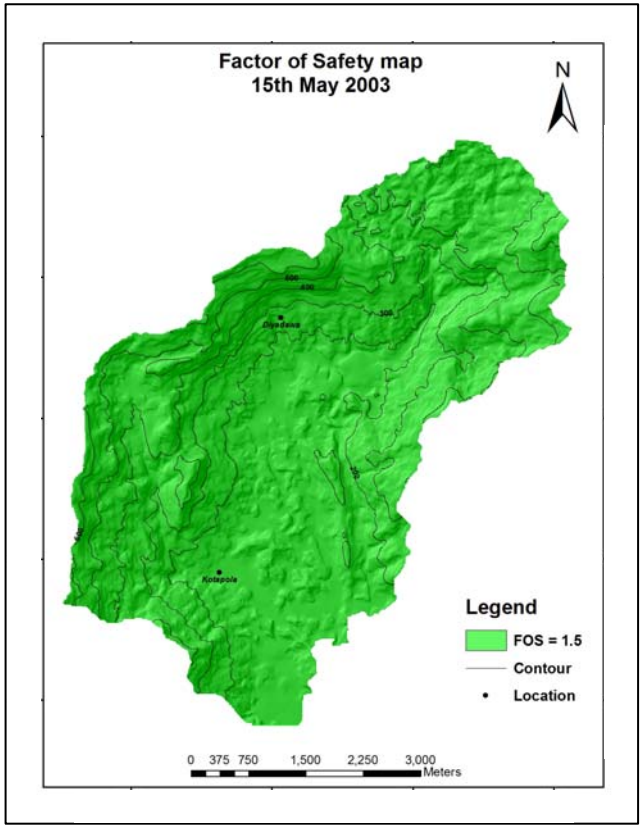
Factor of Safety map
15th May 2003
N
Legend
FOS = 1.5
Contour
Location
0 375 750 1,500 2,250 3,000
Meters

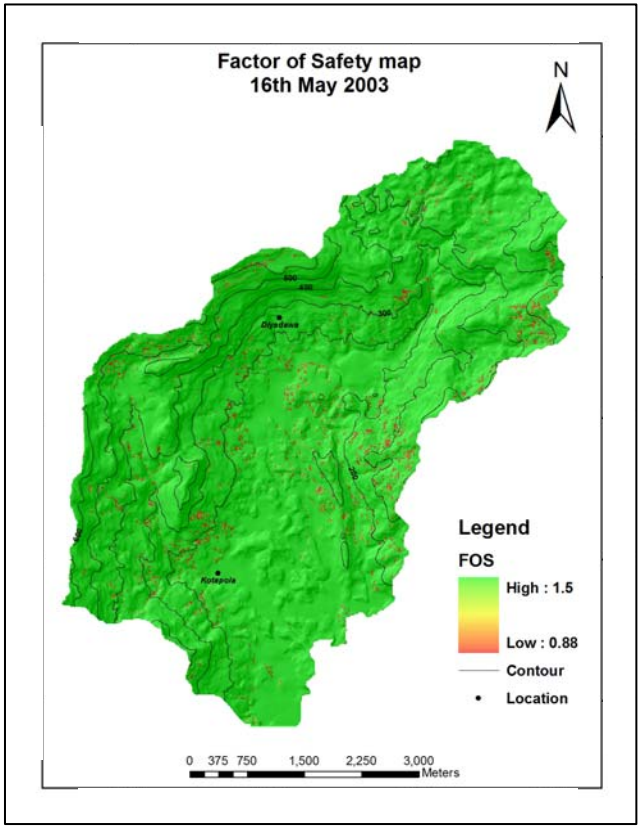
Factor of Safety map
16th May 2003
N
Legend
FOS
High : 1.5
Low : 0.88
Contour
Location
0 375 750 1,500 2,250 3,000
Meters

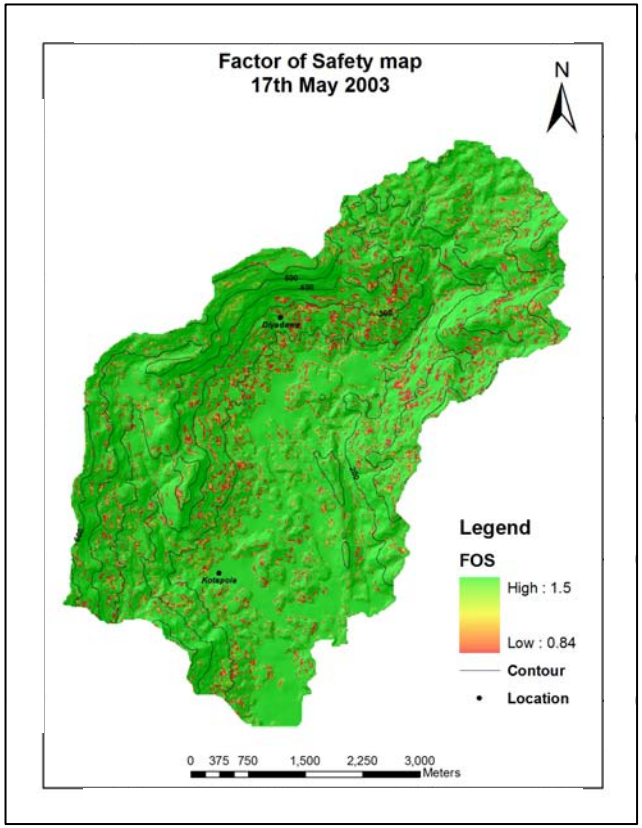
Factor of Safety map
17th May 2003
N
Legend
FOS
High : 1.5
Low : 0.84
Contour
Location
0 375 750 1,500 2,250 3,000
Meters

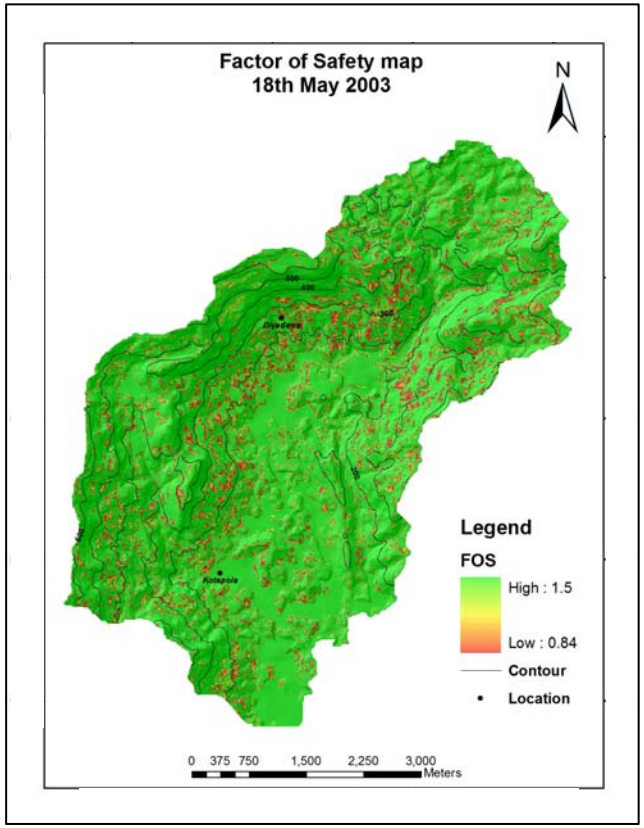
Factor of Safety map
18th May 2003
N
Legend
FOS
High : 1.5
Low : 0.84
Contour
Location
0 375 750 1,500 2,250 3,000
Meters

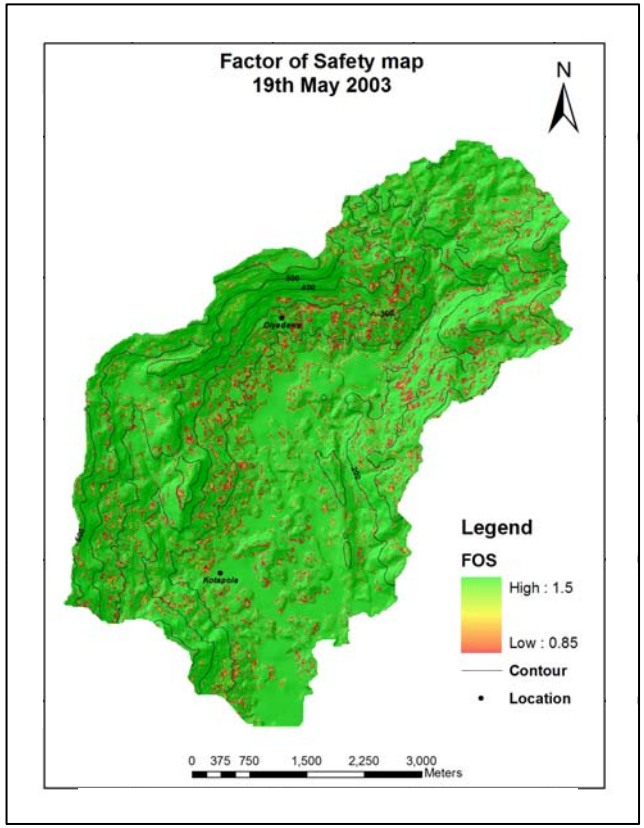
Factor of Safety map
19th May 2003
N
Legend
FOS
High : 1.5
Low : 0.85
Contour
Location
0 375 750 1,500 2,250 3,000
Meters

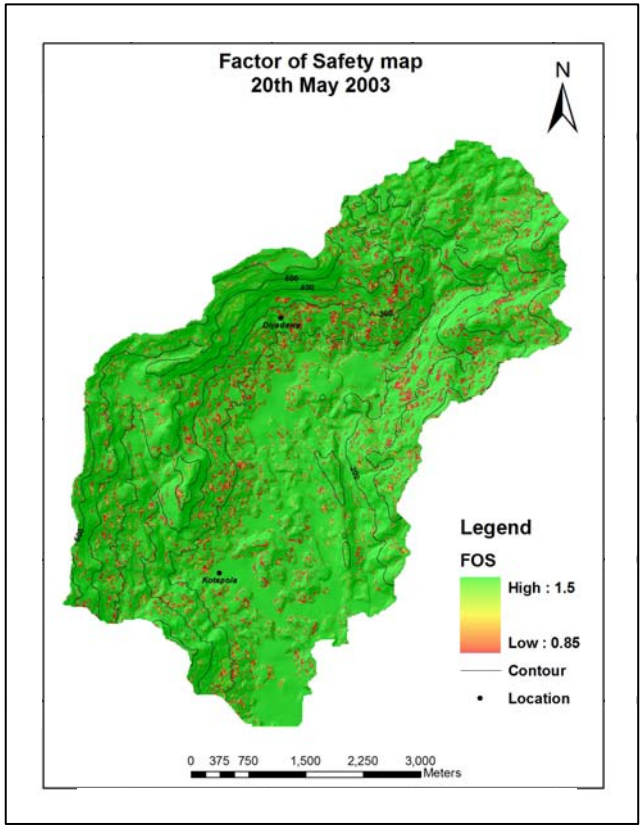
Factor of Safety map
20th May 2003
N
Legend
FOS
High : 1.5
Low : 0.85
Contour
Location
0 375 750 1,500 2,250 3,000
Meters

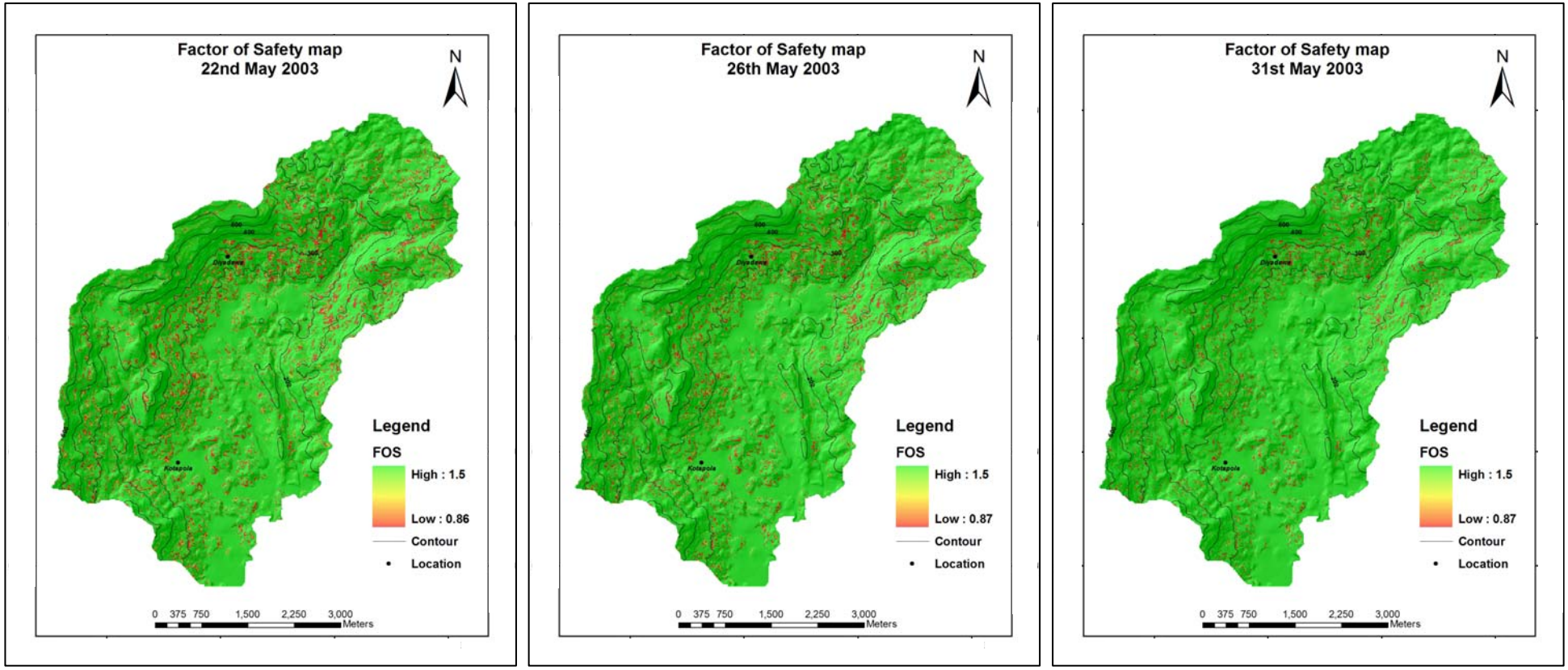

Figure 6.19: Factor of safety (F_s) maps delivered by the model for several days during the month of May 2003 (in the map legends, FOS is used to represent F_s).

Table 6.32: Factor of safety value ranges, number of calculated pixels and the number of actual landslide pixels within each F_s range, 17th May 2003.

F_s range	Number of pixels in F_s map	Percentage of pixels (%)	No. of actual LS pixels within each F_s range
0.84 to 1.00	5638	2.06	1071
1.00 to 1.50	268619	97.94	4019
Total	**274257**	**100.00**	**5090**

As shown in the Table 6.32, while there are 5090 actual landslide pixels in the landslide inventory map, the model has theoretically predicted 5638 pixels as unstable for the date of 17th May 2003. Hence, according to the number of pixels, very comparative result has been delivered by the model. However, if the spatial distribution of the calculated factor of safety values and the locations of the actual landslides are in concerned, out of 5090 landslide pixels, only a 1071 (21%) was accurately predicted by the model. That means majority of the existing landslides (79%) can be found in the areas where factor of safety is calculated as greater than one. Hence, considerable discrepancies exist between the predicted locations of instabilities and the actual failures. This can be partly due to the data accuracy, the simplicity of the model and the assumptions used in the algorithms for calculating water percolation, ground water flow and the factor of safety values. Nevertheless, even if the majority of the unstable pixels in the safety map do not overlap completely with the actual landslide areas, almost 62% of the unstable pixels are located within an area of 100 m buffer from the rupture zone of the existing landslides. Hence, this information can be very useful to identify the zones of instabilities with the help of susceptibility maps together with the expert knowledge about the terrain conditions for future planning and early warning activities.

In general, physically based models for shallow landslide analysis are used to incorporate the effect of rainfall infiltration on dynamic pore pressure response in soils. Many of the models combine digital terrain data with near surface through flow and infinite slope model. For simplicity, models assume that the slip surface of the landslide is running parallel to the topographic slope, slope parallel subsurface flow occurs, isotropic and homogeneous soil hydrological conditions and properties exist, and ignores the differences of soil behavior in the saturated and unsaturated zones, effect of vegetation root strength or continuous temporal changes in root cohesion and vegetation surcharge, storm characteristics such as mean and maximum hourly intensity and the temporal distribution of short term intensity and stochastic influence of actual rainfall patterns on pore water pressures.

As shown in the Table 6.30, many of the parameters used in the final model are single parameter values which might not be appropriate to represent spatially distributed nature of the parameters. Additionally, it is assumed that the rainfall within the study area is equal to the rainfall measured by the rain gauge located at the Deniyaya Willi group Estate even though this is not the case throughout the study area. Moreover, an accuracy of landslide prediction strongly depends on the initial water height map. Hence, such spatial uncertainties in input parameter values, initial water height map and the scale and accuracy of other distributed data might have been greatly influenced the precision of the model's predictions.

Furthermore, the most important physical properties of soils that affect slope stability are those that govern the rate of water movement into and through the hillslope, as well as water holding capacity. The rate of water entry into the soil is highly influenced by soil physical properties (e.g., porosity, hydraulic conductivity, pore size distribution, preferential flow networks), vegetation cover, cultural practices, and macro and micro topography. Additionally, the structure, density and orientation of fractures and

interstices in bed rock or other substrate that underlie the soil profile are important in determining whether subsurface water will drain from the soil or enter the soil from below. At the small scale, these intrinsic properties include the distribution of particle and pore sizes within the soil matrix: For bed rock, the matrix is generally considered impermeable. At micro scale, the rate of water movement in hillslope soil is best characterized by hydraulic conductivity (K), the subsurface flux of water per unit hydraulic gradient. The value of K varies none linearly with volumetric moisture content for a wide range of soil textures, from near zero for dry conditions to a maximum at saturation (K_{sat}). However, at the hillslope scale where slope stability concerns arise, large scale properties of the soil and regolith must be considered as well as these intrinsic properties.

From the large scale attributes that influence water intake and movement through the hillslope, the preferential flow network within the regolith is the most important and the most difficult to quantify. Subsurface water may also enter the soil or weathered regolith from fractures or cracks in the bed rock; however, most studies of pore water pressure changes during rain storms have failed to monitor pressures within the bed rock. Preferential flow network in regoliths are comprised of complicated combinations of vertical and slope oriented pathways and features. Tension cracks that exist in and around potential failure sites are the largest, primarily vertical, preferential flow paths. Soils high in clay content develop desiccation cracks that promote vertical transport of water. Fracture flow also occur in weathered, jointed, sheared, and foliated bed rock near the lithic contact of the soil. Preferential flow in these fractures may exchange into and out of the soil at the lithic contact, thus exerting positive pore pressure in areas of return flow. In addition to shallow flow paths, deeper water in bed rock fractures can ex-filtrate into the failure zone; the area where the fractures intersect the failure plane as well as the hydraulic head imposed by the fracture flow are important factors affecting landslide initiation. Inter- aggregate spaces within the soil fabric from yet another type of preferential flow paths, which can be oriented in various directions. Vegetation and fauna strongly contribute to preferential flow networks via live and decayed root channels, buried organic materials, zones of loose soil conditioned by insects or other fauna, earthworm passageways, and burrowing animals. These biological components of preferential flow networks all facilitate slope parallel movement of water and, in some cases, vertical transport. Large macro pores (pipes), typically oriented down slope, can be created by subsurface erosion. Pipes can develop in unstable soils when high hydraulic pressures occur just prior to failure.

Some studies have shown that dynamic response in the unsaturated zone contributes strongly to the timing and magnitude of pore pressure response in soils. Thus, while many studies focus on the role of dynamic pore pressures during rain storms on landslide initiation, there is a need to evaluate the effect of decreased soil suction above the wetting front on soil strength too. To characterize the permeability of soils in such wet, but not saturated conditions (saturated- unsaturated flow in soil), it is necessary to assess unsaturated K values or the hydraulic diffusivity. Accordingly, the accurate specifications of these unsaturated parameters may be important for slope stability, but poses difficulties related to availability of such spatially variable data.

Hence in addition to the accuracy of the input parameters, simplistic assumptions use to characterize hill slope hydrology for small areas may lead to discrepancies in spatially scaled hydrological behavior and grossly misrepresent the predictions of pore pressure development in hill slope soils distancing the model calculations from realistic prediction. Therefore, in many of the cases physically based models have not been precisely tested for conditions where actual landslides were triggered during specific rain event or even if tested, simulated landslides may have been occurred only near to the general locations of the

actual failures or it is mentioned that the precise locations of the actual landslides were not known. This is mainly due to the serious problems pose by extremely complicated, spatially and temporally variable hydraulic responses and other important processes which are not implemented in the simple models that assume isotropic, homogeneous or constant conditions. Therefore, such models have been so far accepted if the predictions agree even only reasonably or closely with the actual field conditions and expert knowledge have been utilized to improve the power of predictions.

6.7 Combined landslide hazard map (factor of safety map combined with final susceptibility map)

While susceptibility maps demonstrate ranks of landslide susceptibility according to critical combinations of favorable settings of static terrain parameters, factor of safety maps represent the dynamic changes of soil stability conditions according to the rainfall. Hence, if the rainfall is predicted by long term historical data (statistical way) or by the antecedent rainfall or known by real time meteorological data, factor of safety maps for different events can be prepared and also hydrological triggering thresholds for different areas can be established in a deterministic way. Subsequently, landslide susceptibility maps can be combined with such factor of safety maps and collective information can then be used for more appropriate hazard predictions.

For instance, by crossing the factor of safety map of 17th May 2003 with the final expert weighted landslide susceptibility map (Figure 6.18), a comparison between both the maps was made. Here, the number of unstable pixels, i.e., the pixels with $F_s \leq 1$ within each susceptibility zone was calculated and presented as the Table 6.33.

Table 6.33: Number of unstable pixels in the safety map of 17th May 2003 within each susceptibility zones of the final expert weighted landslide susceptibility map.

Susceptibility class	Total No. of pixels in each susceptibility class	No. of unstable pixels from F_s map
Low	117436	1725
Medium	99380	2648
High	57441	1265
Total	**274257**	**5638**

According to the data, out of 5638 unstable pixels calculated by the safety model, 1265 (22.44%) pixels are positioned within the high susceptibility zone. In addition to that, 3913 (69.40%) pixels are located within both the high and medium susceptibility classes.

Since the areas where F_s become less than 1 is theoretically considered as unstable, all such pixels either located within high, medium or low susceptibility classes can be regarded as potentially unstable areas and hence can be categorized as high hazards or very high hazard zones for a given rainfall event.

In this manner, susceptibility map for a particular area can be transformed to hazard map by combining it with factor of safety maps prepared for different rain fall scenarios (Figure 6.20), and hydrological triggering thresholds for different areas within each susceptibility zone can be established. Such combined information collectively with expertise about the terrain conditions can finally be utilized for better hazard predictions and early warnings in a particular area.

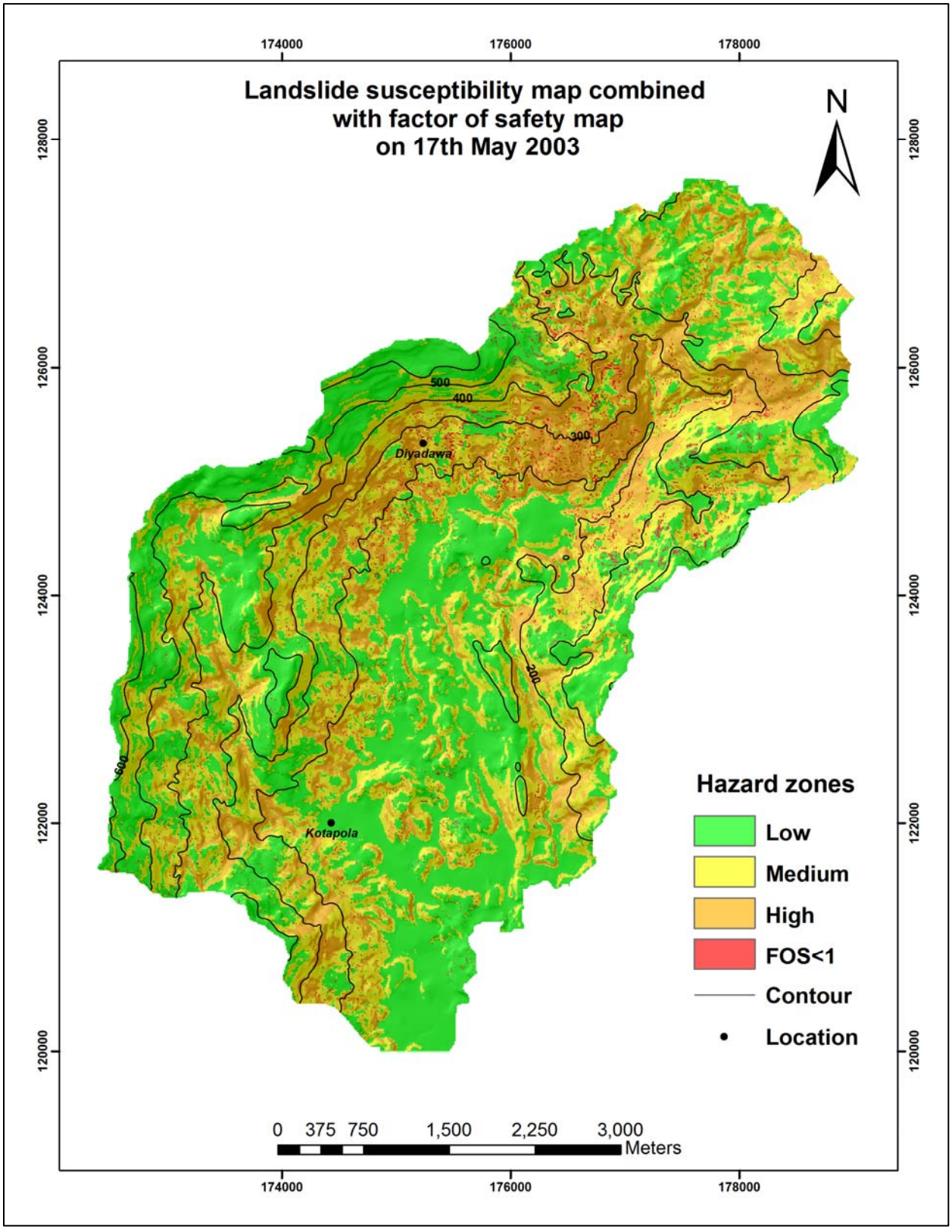

Figure 6.20: Final expert weighted landslide susceptibility map combined with factor of safety (F_s) map on 17th May 2003 (FOS=F_s). Enlarged version of the map is attached at the end of the thesis.

7 Conclusion and recommendation

Hazard zonation mapping is a major step forward in all kind of natural disaster management activities including landslides. Theoretically, the slope instability hazard zonation is defined as the mapping of areas with an equal probability of occurrence of landslides in a given area within a specific period of time. However, determination of the probability of occurrence of landslide is extremely difficult especially for large areas, due to lack of simple relation between the magnitudes of landslide events and return periods, and reliable historic records of landslide dates and triggering events. Thus, landslide hazard analysis is seldom executed in accordance with the definition given above. Therefore, most hazard maps do not provide more information than the susceptibility of certain areas to landsliding or relative indications of the degree of hazard, such as high, medium and low. Nevertheless, hazard predictions and early warnings against landslides are usually not meaningful unless given in relation to the exact location and timing of the anticipated event. Thus, susceptibility assessment to identify the critical locations and establishment of triggering thresholds to predict the timing of the events can be considered as a realistic approach in landslide hazard zonation.

The models to predict the locations of future landslides are fairly well developed and seem to be given acceptable results. However, when applying to natural processes like landslides; both the bivariate and multivariate statistical techniques in general have some drawbacks, their own limitations, and characteristic advantages and disadvantages. Thus, those methods may deliver unusually different results for the same data set; in fact they can be sometimes so different that an objective reader may confuse to understand whether they are from the same area.

Two of the five susceptibility maps prepared in the present study show almost similar result according to the predicted amount of landslides while others differ greatly. Also, even within those two comparable maps, 40% of spatial difference can be observed in the distribution. These outcomes reveal beyond doubt that the landslide susceptibility maps prepared using existing data for an area can be even very different when different analytical methods are used. Hence, assessments totally rely only on the sophisticated analytical methodologies can sometimes yield completely wrong result and provide ill-advised interpretations and conclusions. Therefore, selection of a best fit model for an area among comparison of many possible analytical approaches and integration of professional experience of the expert where necessary can be recommended as an appropriate way to come out with an acceptable model.

In general this may not lead to the conclusion, however that landslide susceptibility maps are totally unreliable. Two of the maps prepared using bivariate methodologies in this thesis shows a remarkable agreement and acceptable success with the exiting data. Thus, according to the present study, bivariate statistical methods that can provide satisfactory result with the use of capability of combination of both the professional geared direct mapping and the data driven analytical capabilities of a GIS can be recommended over multivariate methodologies for landslide susceptibility assessments. Additionally, even within the bivariate methodologies, fully automated procedures like WOE-ArcSDM have yielded controversial outputs. Hence, it can be concluded that the simplest analytical methodologies combined well with the professional expertise can yield the best fit model for an area rather than complex, highly objective and fully automated procedures.

To test the models success and the accuracy of the predictions, susceptibility maps were compared only with the landslide data which they were derived and, through an iterative process of analysis and

classification, an optimization of the models were established. Hence, maintaining of up to date landslide data base and, calibration, verification and validation of such models with multi-temporal landslide events is still essential and can be recommended for comprehensive understanding of the models ability to predict the future events.

WOE-ArcSDM method yielded fairly acceptable result when higher number of landslide points is used in the analysis. By comparing the *Model-1* and *Model-2*, increasing the number of training sites seems to be a better way to improve the model although it assumes a huge number of training sites is a violation of basic assumption of WOE. Hence testing of many models by changing the number of training sites and selection of optimal situation with the expert knowledge can be recommended as a better approach to come out with a realistic result if WOE methodology based on ArcSDM is to be followed for modeling purposes.

In multivariate methodology, 100 *100 m grid cells were used and probability of the occurrence of an event within each sample unit was calculated. When such large grid cells are used, they become less homogeneous and consequently it is more difficult to assign specific parameter class or the presence or absence of a landslide to a grid cell, when they affect only a small part of it. Such situations result errors in the evaluation of the relation between landslide and parameter class. If small grid cells are used, the matrices become extremely voluminous for the calculation. Hence, choice of comparatively small more homogeneous naturally occurring morphological units can be recommended as an acceptable compromise.

If huge number of variables is used in the Logistic Regression model, it would produce a long regression equation and may even create numerical problems. It may also work against some basic assumptions of logistic regression such as the absence of strong correlation among independent variables (multicollinearity). Because of such reasons, closely related variables were grouped together and reduced to a small number of significant components by Factor Analysis and Comparison of Means procedure. In this way, 304 factor classes were reduced to a 26 component variables. Here, in some cases a total factor such as soil thickness and watershed and in others, many of the factor classes (Table 6.23) which might be important for the occurrence of landslides were removed from the model. Hence, it is more advisable to use the professional experience of the expert or if possible a collective judgment of experts for the choice of variables as there is a possibility to integrate the subjective decisions at this stage even though the multivariate procedure is more objective after this point.

In the study, continuous data like slope, aspect and deviation angle layers were categorized according to subjective judgments. However, since the ease of analysis and the final result depend on the class ranges and number of categories, selection of suitable classes or grouping of closely related factor classes together using Factor Analysis or any other suitable method is recommended. This will be much helpful to minimize the complications by optimizing the number of categories and finally useful to develop an appropriate model. However, like in multivariate procedure, expulsion of variables from the bivariate models seems to be unrealistic and hence can not be recommended. Otherwise the models may finally depend only on very few variables and can yield unsuccessful results like in Logistic Regression model.

Rainfall is commonly known as one of the principal landslide triggers, and therefore the concept of hydrological triggering thresholds (section 5.1) can be utilized for the prediction of timing of rain induced landslides. Hydrological triggering thresholds can be established in a statistical or in a deterministic way.

Statistical triggering thresholds, combinations of antecedent and daily rainfall or rainfall intensity and duration that may initiate landslides proved to be useful for the development of landslide early warning systems. In many regions however statistical thresholds can not be established due to lack of rainfall data and landslide events and in such cases deterministic models have to be used. In order to apply deterministic models in a successful way, a detailed study of landslide triggering mechanisms and surface and subsurface conditions is required.

Under the present study, a combined hydrological slope stability model was utilized to calculate the variations of slope stability conditions within a catchments area according to a given rainfall scenario during a month. Deterministically calculated factor of safety map for the date of event was validated with the actual landslides occurred on the same day. The model predicts only a 21% of the actual landslide pixels accurately. However, although the majority of the unstable pixels in the safety map do not overlap completely with the actual landslide areas, almost 62% of the unstable pixels are located within an area of 100 m buffer from the rupture zone of the existing landslides showing evidence of instabilities within the regions of near proximity to those failures. This outcome provides very supportive evidence to identify the zones of instabilities with the combined application of other information such as susceptibility maps and expertise of the terrain conditions together to come out with more accurate predictions. Thus, even though the complexity associated with hydrological processes and the data uncertainties exist, the model can be accepted as a reasonably suitable approach to identify the dynamic slope stability conditions and hence to define hydrological triggering thresholds in catchments areas with the combination of other information. Once the hydrological triggering thresholds are established and critical zones are identified, detailed investigations and more sophisticated geotechnical methodologies must be followed additionally. Piezometers can be implemented and according to the actual pore water pressure measurements in real time, more precious predictions of slope instabilities and reliable warnings can be issued.

Due to the lack of recorded historical landslide events within the study area, the model was simulated only for a rainfall scenario during the month of May 2003 and the out put was validated with a single landslide event occurred on 17^{th} of the same month. However, without calibration, verification and validation of models with multi temporal landslide events, application of deterministic models to define hydrological triggering thresholds and to establish real time early warning system is worthless. Hence, it is an essential task to maintain an up to date landslide and rainfall data base for the improvement of the model through calibration, verification and validation with numerous events.

Recent modeling studies show that the number of landslides produced by different rain storms and the relative importance of rainstorms in triggering landslides depend on the combined influence of mean and maximum hourly intensity, duration, and total rainfall amount. In all rainstorms, most failures occur after some threshold of cumulative rainfall and maximum hourly rainfall intensity. Such findings are consistence with field observations from around the world. However, the influence of rainfall patterns on slope stability must be considered together with the hydrological characteristics and flow paths of the soil and weathered bedrock too.

Infiltration based one, two and three dimensions landslide models have been developed for many areas particularly for individual sites. Such models offer the advantage of a physics-based approach to assessing the dynamic changes in positive and negative (suction) pressure heads in the soil mantle during the infiltration process. Thus, they are valuable to predict the timing of the slope failures relative to rainfall inputs at individual sites with simple slope configurations. When such models are used in the catchments,

they necessarily require spatially and temporally distributed parameters since the model outputs must be spatially and temporally explicit to know the location and timing of the events. However, applying these theoretical models in topographically complex catchments or within a large area is extremely challenging due to the simplistic assumptions used in the models and their algorithms and given the difficulties of collecting the spatially and temporally representative input parameters. Hence in general it is more worthwhile to use physically based models for small areas where simple slope configurations and nearly homogeneous subsurface conditions exist and the types of landslides are known and relatively simple.

One possibility to overcome the problems associated with uncertainties of input data is to calculate the failure probabilities using probability-based modeling approach. Hydrological triggering thresholds where failure probability reaches a critical level can be determined on the forecast of calculated failure probabilities. However, in order to pursue the probabilistic approach, statistical description of the data is necessary.

Moreover, new concepts and comprehensive research for the implementation of sophisticated algorithms representing various failure mechanisms, effect of vegetation root strength or continuous temporal changes in root cohesion and vegetation surcharge, storm characteristics and complicated ground water flow processes within topographically complex, heterogeneous terrains and stochastic influence of actual rainfall patterns on pore water pressures is crucial for the development of dynamic modeling concepts in landslide processes.

All the complex analysis such as bivariate, multivariate or deterministic which involves huge amount of data and spatially and temporally variable numerous numbers of parameters are only possible due to the capabilities of computers and associated software utilized in the analysis. While computer memory and power is immensely vital to handle a huge data set, software like GIS that has sophisticated and versatile capabilities has proved to be an excellent tool for the analysis of parameters with high degree of spatial variability. However it must be noticed that such analysis outputs are only as good as the data bases from which they are derived. Hence, the scale and data accuracy is very important and the maximum benefit of GIS can be obtained at large scales. Thorough understanding of the data and its accuracy, terrain condition and, analytical methodologies and associated software including the selection of an appropriate grid resolution that can be suitable for the scale and the actual size of the features are vital. The automated procedures are extremely efficient and effective; in an iterative process the optimization of the hazard models can be achieved. Thus, GIS can be recommended as an ideal tool in landslide analysis and hazard zonation mapping.

Overall, the results of the research show that the direct application of analytical methodologies has serious limitations. They ask for a careful confrontation of the hazard prediction with the real world and an adaptation of flexible decision rules where differences are observed, this being mostly on experience driven criteria. While sophisticated analytical methodologies are very useful for the assessment of natural processes like landslides, complexity associated with such processes and uncertainties inherent to the data hold back the accurate predictions. If an appropriate expertise is not integrated, such models provide only theoretical descriptions of natural processes or may represent natural processes only by chance. Thus, professional experience of the expert is to be the most important factor in modeling natural processes like landslides. Therefore, as a concluding remark, it can be mentioned that the sophisticated analytical methodologies are useful only if the sound professional knowledge about the data, terrain conditions, landslide processes and the analytical methodologies are available.

While the research gave a thorough understanding about the limitations, characteristic advantages and disadvantages and associated drawbacks of scientific approaches to predict complex natural processes like landslides, the knowledge and the experience gained by this study will be much useful to come out with more pragmatic research out puts in future.

In general, landslide susceptibility maps are available for many regions. However most of them lacks any temporal implications or information about the intensity of triggering events and hence has very limited role in predicting the events accurately in real time. It is inappropriate to rely wholly on rainfall ignoring causative factors, or rely on susceptibility mapping, ignoring triggering event. Hence the approach of combined model can be used to develop real time early warning systems for shallow landslides based on rainfall data gathered from rainfall forecasting or telemetered network of recording rain gauges. While such systems are very useful and may save lives and property, such level of data collection, transmission and warning is not yet practical in most vulnerable regions of developing countries that need it the most.

References

Agterberg, F. P. (1989): Systematic approach to dealing with uncertainty of geosciences information in mineral exploration. In Proceedings of the 21st APCOM Symposium, Las Vegas, pp 165–178.

Agterberg, F. P., Bonham-Carter, G. F., Wright, D. F. (1990): Statistical pattern integration for mineral exploration. In Computer Application in Resources Estimation Prediction and Assessment for Metals and Petroleum (eds Gaal, D. F. and Merriam, D. F.), Pergamon Press, New York, pp 1–21.

Alfoldi, T. T. (1974): Landslide analysis and susceptibility mapping. Symposium on remote sensing and photo interpretation. Banff, Alberta, Proceedings of the International Society for Photogrammetry, Ontario, Canada, Vol. 1, pp 379–388.

Anderberg, M. R. (1973): Cluster analysis for applications. Academic, New York, pp 359.

Anderson, M. G., Kemp, M. J., Floyd, D. M. (1988): Applications of soil water finite difference models to slope problems. Proc. 5th Int. Symp. on Landslides, Vol. 1, pp 525-530, Lausanne, Switzerland.

Arias, A. (1970): A measure of earthquake intensity. In: Hansen RJ (ed) Seismic design for nuclear power plants. Massachusetts Institute of Technology Press, Cambridge, pp 438–483.

Asch, Th., W., J., van, Westen, C. J. van, Blijenberg, H., Terlien, M. T. J. (1992): Quantitative landslide hazard analysis in volcanic ashes of the Chinchina area, Colombia. Proceedings Primer Simposio Internacional sobre sensors remotosy sistemas de informacion geografica pare el studio de riesgos naturals, Bogota, Colombia, pp 433-443.

Ayala-Carcedo, F. J., Cubillo-Nielsen, S., Alvarez, A., Dominguez, M. J., Lain, L., Lain, R., Ortiz, G. (2003) Large scales rock fall reach susceptibility maps in La Cabrera Sierra (Madrid) performed with GIS and dynamic analysis at 1:5.000. In: Chacon J, Corominas J (eds) Special issue on Landslides and GIS. Nat Hazards 30(3):341–360.

Ayalew, L., Yamagishi, H., Ugawa, N. (2004): Landslide susceptibility mapping using GIS-based weighted linear combination, the case in Tsugawa area of Agano river, Niigata Prefecture, Japan. Landslide 1:73–81.

Ayalew, L., Yamagishi, H. (2005): The application of GIS-based logistic regression for landslide susceptibility mapping in the Kakuda-Yahiko Mountains, Central Japan. Geomorphology 65:15–31.

Baeza, C., Corominas, J. (1996): Assessment of shallow landslide susceptibility by means of statistical techniques. In: Kaare Senneset (ed) Proceedings of the VIth I.S.L., Trondheim, Norway, Vol. 1. A. A. Balkema, Rotterdam, pp 147–152.

Baeza, C., Corominas, J. (2001): Assessment of shallow landslide susceptibility by means of multivariate statistical techniques. Earth Surf Processes Landforms 26:1251–1263.

Bates, R. L., Jackson, J. A., eds. (1978): Glossary of Geology. American Geological Institute, Falls Church, Va., pp 788.

Baum, R. L., Savage, W. Z., Godt, J. W. (2002): TRIGRS-A Fortran program for transient rainfall infiltration and grid-based regional slope-stability analysis. Open-file report 02-424, pp 35 (2 appendices), U.S. geol. Surv.

Benda, L., Zhang, W. (1990): Accounting for the stochastic occurrences of landslides when predicting sediment yields. Proceedings of the Fiji Symposium, IAHS-AISH Publ. 192, pp 115-127.

Bernknopf, R. L., Champbell, R. H., Brookshire, D. S., Saphiro, C. D. (1988): A probabilistic approach landslide hazard mapping in Cincinnati, Ohio, with application of economic evaluation. Bulleting of the Association of Engineering Geologists, Vol. 25, No. 1, pp 39-56.

Beven, K. J., Kirkby, M. J. (1979): A physically based, variable contributing area model of basin hydrology. Hydrol Sci. Bull. 24:43–69.

Binaghi, E., Luzi, L., Madella, P., Pergalani, F., Rampini, A. (1998): Slope instability zonation: a comparison between certainty factor and fuzzy Dempster–Shafer approaches. Natural Hazards 17:77–97.

Bishop, A. W. (1995): The use of the slip circle in the stability analysis of slopes. Geotechnique, 5, pp 7-17.

Blank, R. P., Clevelend, G. B. (1968): Natural slope stability as related to geology, San Clemente Area, Orange and San Diego Countries, California. California Division of Mines and Geology, Special report 98, pp 19.

Bonham-Carter, G. F., Agterberg, F. P., Wright, D. F. (1988): Integration of geological datasets for gold exploration in Nova Scotia. Photogrammetric Engineering and Remote Sensing: Vol. 54, no. 11, pp 1585–1592.

Bonham-Carter, G. F., Agterberg, F. P. (1990): Application of a microcomputer based geographic information system to mineral potential mapping. In Microcomputer Based Applications in Geology (eds Hanley, T. and Merriam, D. F.), Pergamon Press, Oxford, Vol. 2.

Bonham-Carter, G.F. (1994): Geographic information systems for geoscientists. Modeling with GIS. Pergamon Press, Oxford and Elsevier Science Inc, New York, pp 398.

Bonham-Carter, G. F. and Agterberg, F. P. (1999): Arc-WofE: A GIS tool for statistical integration of mineral exploration datasets. In Proceeding of the International Statistical Institute, pp 497– 500.

Borga, M., Fontana, D. G., Cazorzi, F. (2002): Analysis of topographic and climatic control on rainfall-triggered shallow landsliding using a quasi-dynamic wetness index. J Hydrol. 268:56–71.

Borga, M., Fontana, D. G., Gregoretti, C., Marchi, L. (2002b): Assessment of shallow landsliding by using a physically based model of hill slope stability. Hydrol. Process., 16, pp 2833-2851.

Brabb, E. E., Pampeyan, E. H. (1972): Preliminary map of landslide deposits in San Mateo Country, California. US Geological Survey Miscellaneous Field Studies, Map MF-360, scale 1:62,500.

Brabb, E. E., Pampeyan, E. H., Bonilla, M. G. (1972): Landslide susceptibility in San Mateo County, California. US Geological Survey Miscellaneous Field Studies, Map MF-360, scale 1:62,500 (reprinted in 1978).

Brabb, E.E., Pampeyan, E.H., Bonilla, M.G. (1972): Landslide susceptibility in San Mateo County, California. US Geological Survey Miscellaneous Field Studies, Map MF-360, scale 1:62,500.

Brabb, E.E. (1984): Innovative approach to landslide hazard and risk mapping. Proc. 4th Intern. Symp. on Landslides , Vol. 1, pp 307-324, Toronto, Ontario, Canada.

Brass, A., Wadge, G., Reading, A. J. (1989): Designing a Geographic Information System for the prediction of landsliding potential in the West Indies. In Proc., Economic geology and geotechnics of active tectonic regions, University College, University of London, April, pp 13.

British Columbia Ministry of Forests (1995): Coastal Watershed Assessment Procedure Guidebook (CWAP), Forest Practices Code of British Columbia, pp 66, British Columbia Min. of For., Canada.

Bulletin of Engineering Geology and the Environment (2008): Official journal of the Association of Engineering Geology and the Environment, Volume 67.

Burrough, P. A. (1986): Principles of Geographical Information Systems and Land Resources Assessment. Clarendon Press, Oxford, England, pp 194.

Caine, N. (1980): Rainfall intensity-duration control of shallow landslides and debris flows. Geograf. Ann. 62A, pp 23-27.

Campbell, R.H. (1973): Isopleth map of landslide deposits. Point Duma Quadrangle, Los Angeles County, California: an experiment in generalizing and quantifying aerial distribution of landslides. US Geological Survey Misc. Field Investigation Map MF-535. USGS, California.

Cannon, S. H., Ellen S. D. (1985): Rainfall conditions for abundant debris avalanches, San Francisco Bay Region, California, Calif. Geol., 38, pp 267-272.

Canuti, P., Focardi, P., Garzonio, C. A. (1985): Correlation between rainfall and landslides. Bull. Int. Assoc. Eng. Geol., 32, pp 49-54.

Carrara, A., Merenda, L. (1976): Landslides inventory in northern Calabria, southern Italy. Geol. Soc. Am. Bull 87:1229–1246.

Carrara, A., Pugliese, E., Merenda, L. (1977): Computer based data bank and statistical analysis of slope instability phenomena. Z Geomorph NF 21(2):187–222.

Carrara, A., Catalano, E., Sorriso-Valvo, M., Really, C., Osso, I. (1978): Digital terrain analysis for land evaluation. Geologia Applicata e Idrogeologia 13:69–127.

Carrara, A. (1983): Multivariate methods for landslide hazard evaluation. Math Geol 15:403–426.

Carrara, A., Cardinali, M., Detti, R., Guzzetti, F., Pasqui, M., Reichenbach, P. (1991a): GIS techniques and statistical models in evaluation landslide hazard. Earth Surf Processes Landforms 16:427–445.

Carrara, A., Cardinali, M., Detti, R., Guzzeti, F., Pasqui, V., Reichenbach, P. (1991b): GIS techniques and statistical models in evaluating landslide hazard. Earth Surf Processes, Landforms 16:427–445. In: Carrara A, Guzzetti F (eds) Geographical information system in assessing natural hazards. Advances in Natural and Technological Hazards Research, vol 5. Kluwer, Dordrecht, pp 57–77.

Carrara, A., Cardinali, M., Guzzetti, F. (1992): Uncertainty in assessing landslide hazard and risk. ITC J 2:172–183.

Carrara, A., Cardinali, M., Guzzetti, F., Reichenbach, P. (1995): GIS technology in mapping landslide hazard. In: Carrara A, Guzzetti F (eds) Geographical information system in assessing natural hazards. Advances in Natural and Technological Hazards Research, vol 5. Kluwer, Dordrecht, pp 135-175.

Carrara, A., Crosta, G., Frattini, P. (2003): Geomorphological and historical data in assessing landslide hazard. Earth Surf Processes Landforms 28(10):1125–1142.

Carrasco, R.M., Pedraza, J., Martin-Duque, J.F., Mattera, M., Sanz, M.A., Bodoque, J.M. (2003): Hazard zoning connected to torrential floods in the Jerte valley (Spain) by using GIS techniques. In: Chacon J, Corominas J (eds) Special issue on Landslides and GIS. Nat Hazards 30(3):361–381.

Carter, W. N. (1991): Disaster Management. A disaster manager's hand book, Asian Development Bank, Manila, Philippines.

Chacon, J., Irigaray, C., Fernandez, T., El Hamdouni, R. (2006): Engineering geology maps: landslides and geographical information systems. Bulleting of Engineering Geology and the Environment, Vol. 65, Nr.04, Dec. 2006, pp 341-411.

Chung, C. F., Fabbri, A. G. (1993): The Representation of Geosciences information for data integration. Nonrenewable Resource Vol. 2, No. 3, pp 122–139.

Chung, C.F., Fabbri, A.G., van Westen, C.J. (1995): Multivariate regression analysis for landslide hazard zonation. In: Carrara A, Guzzetti F (eds) Geographical information systems in assessing natural hazards. Kluwer, Dordrecht, pp 135–17.

Chung, C. F., Fabbri, A. G. (1998): Three Bayesian prediction models for landslide hazard. In: Buscianti (ed) Proceedings of the International Association of Mathematical Geology, Ischia, Italy, pp 204–211.

Chung, C.F., Fabbri, A. G. (1999): Probabilistic prediction models for landslide hazard mapping. Photogrammetric Eng Remote Sen 65(12):1388–1399.

Clerici, A., Perego, S., Tellini, C., Vescovi, P. (2002): A procedure for landslide susceptibility zonation by the conditional analysis method. Geomorphology 48:349–364.

Close, U., McCormick, E. (1922): Where the mountains walked. National Geographic Magazine, pp 445-64.

Coe, J. A., Michael, J. A., Crovelli, R. A., Zavage, W. A. (2000): Preliminary map showing landslides densities, mean recurrence intervals, and exceedance probabilities as determined from historic records, Seattle, Washington. USGS Open- File report 00-303 on line edition, pp 12, 2 tables, 10 figures and 1 map. US Department of Interior, USA.

Connell, L. D., Jayatilaka, C. J., Nathan, R. (2001): Modeling flow and transport irrigation catchments, spatial application of subcatchment model. Water Resour Res 37(4):965–977.

Corominas, J., Copons, R., Vilaplana, J.M., Altimir, J., Amigo, J. (2003): Integrated landslide susceptibility analysis and hazard assessment in the principality of Andorra. In: Chacon J, Corominas J (eds) Special issue on Landslides and GIS. Natural Hazards 30(3):421–435.

Corominas, J., Moya, J., Masachs, I., Baeza, C., Hurlimann, M. (2004): Reconstructing recent activity of Pyrenean landslides by means of dendrogeomorphological techniques. In: Lacerda WA, Ehrlich M, Fontoura SAB, Sayao ASF (eds) Landslides: evaluation and stabilization. Balkema, Taylor & Francis Group, London, pp 363–371.

Craig, R. F. (1999): Soil mechanics. Sixth edition, E & FN Spon, London.

Cross, M. (1998): Landslide susceptibility mapping using the matrix assessment approach: a Derbyshire case study. In Maund JG, Eddlestonb M (eds) Geohazards in engineering geology. The Geological Society, London, Engineering Geology Special Publications 15, pp 247–261.

Cross, M. (2002): Landslide susceptibility maps using the matrix assessment approach: a Derbyshire case study. In Griffiths JS (ed) Mapping in Engineering Geology. The Geological Society London, Key Issues in Earth Sciences 1:267–282.

Crovelli, R. A. (2000): Probability models for estimation of number and costs of landslides. USGS Open-File Report 00-249, US Department of Interior, USGS, pp 18.

Cruden, D. M. (1991): A simple definition of a landslide. Bulletin of the International Association of Engineering Geology. No. 43, pp 27-29.

Cruden, D. M., Varnes, D. J. (1996): Landslide types and processes, in Landslides Investigation and Mitigation. Edited by A. K. Turner and R. L. Schuster, pp 36-75, Special Report 247, Transport research Board, National research Council, National Academic Press, Washington, DC.

Cuny, F. C. (1983): Disaster and Development. Oxford University press, USA.

Dahal, R.K., Hasegawa, S., Nonomura, A., Yamanaka, M., Dhakal, S., Paudyal, P. (2008): Predictive modeling of rainfall-induced landslide hazard in the Lesser Himalaya of Nepal based on weights-of-evidence. Geomorphology 102, pp 496–510.

Dai, F.C., Lee, C.F., Li, J., Xu, Z.W. (2000): Assessment of landslide susceptibility on the natural terrain of Lantau Island, Hong Kong. Environ Geol 40(3):381–391.

Dai, F.C., Lee, C.F. (2001): Frequency–volume relation and prediction of rainfall-induced landslides. Eng Geol 59(3/4):253– 266.

Dai, F.C., Lee, C.F. (2002a): Landslide characteristics and slope instability modeling using GIS, Lantau Island, Hong Kong. Geomorphology 42(3–4):213–228.

Dai, F.C., Lee, C.F. (2002b): Landslide on natural terrain—physical characteristics and susceptibility mapping in Hong Kong. Mt Res Dev 22(1):40–47.

Dai, F.C., Lee, C.F. (2003): A spatiotemporal probabilistic modeling of storm-induced shallow landsliding using aerial photographs and logistic regression. Earth Surf. Process. Landforms, 28, 527-545.

Das, B. M. (1985): Principles of Geotechnical Engineering. Third edition, PWS publishing company, Boston.

David, M., Cruden, D. M., Varnes, D. J. (1996): Landslide types and processes. In: Landslides investigation and Mitigation, special report, National Research Council, transportation research board, Washington, D. C. Edited by turner, A. K., Schuster,R. L. Chap. 3, pp 36-75 .

Davies, W. E. (1974a): Landslide susceptibility map of part of the Bridgeville 7-1/2 minutes quadrangle. Allegheny Country and vicinity, Pennsylvania. US Geological Survey Open-File Report 74-274, scale 1:24,000, pp 8.

Davies, W. E. (1974b): Landslide susceptibility map of part of the Canonsburg 7-1/2 minutes quadrangle. Allegheny Country and vicinity, Pennsylvania. US Geological Survey Open-File Report 74-276, scale 1:24,000, pp 8.

Davies, W. E. (1974c): Landslide susceptibility map of part of the Donora 7-1/2 minutes quadrangle. Allegheny Country and vicinity, Pennsylvania. US Geological Survey Open-File Report 74-277, scale 1:24,000, pp 8.

Davies, W. E. (1974d): Landslide susceptibility map of part of the Freeport 7-1/2 minutes quadrangle. Allegheny Country and vicinity, Pennsylvania. US Geological Survey Open-File Report 74-278, scale 1:24,000, pp 8.

Davies, W. E. (1974e): Landslide susceptibility map of part of the McKees-port 7-1/2 minutes quadrangle. Allegheny Country and vicinity, Pennsylvania. US Geological Survey Open-File Report 74-280, scale 1:24,000, pp 8.

Davies, W. E. (1974f): landslide susceptibility map of part of the Monongahela 7-1/2 minutes quadrangle. Allegheny Country and vicinity, Pennsylvania. US Geological Survey Open-File Report 74-281, scale 1:24,000, pp 8.

Davies, W. E. (1974g): Landslide susceptibility map of part of the New Kensington East 7-1/2 minutes quadrangle. Allegheny Country and vicinity, Pennsylvania. US Geological Survey Open-File Report 74-283, scale 1:24,000, pp 8.

Davies, W. E. (1974h): landslide susceptibility map of part of the New Kensington West 7-1/2 minutes quadrangle. Allegheny Country and vicinity, Pennsylvania. US Geological Survey Open-File Report 74-284, scale 1:24,000, pp 8.

Davies, W. E. (1974i): Landslide susceptibility map of part of the Braddock 7-1/2 minutes quadrangle. Allegheny Country and vicinity, Pennsylvania. US Geological Survey Open-File Report 74-273, scale 1:24,000, pp 8.

Davies, W. E. (1974j): landslide susceptibility map of part of the Curtisville 7-1/2 minutes quadrangle. Allegheny Country and vicinity, Pennsylvania. US Geological Survey Open-File Report 74-276, scale 1:24,000, pp 8.

DeGraff, J. V., Romesburg, H. C. (1980): Regional landslide- susceptibility assessment for wildland management: a matrix approach. In: Coates DR, Vitek JD (eds) Chap. 19, pp 401–414.

Derbyshire, E., Wang, J., Meng, X. (2000): A treacherous terrain: background to natural hazards in northern China with special reference to the history of landslide in Gansu Province. in Landslides in the Thick Loess Terrain of North-West China, edited by E. Derbyshire, X. Meng, and T. A. Dijkstra, pp 1-19, John Wiley & Sons.

Dhakal, A. S., Sidle, R. C. (2003): Long-term modeling of landslides for different forest management practices. Earth Surf. Process. Landforms 28, pp 853-868.

Dhakal, A. S., Sidle, R. C. (2004a): Distributed simulations of landslides for different rainfall conditions, Hydrol. Process., 18, pp 757-776.

Dhakal, A. S., Sidle, R. C. (2004b): Pore water pressure assessment in a forest watershed: simulations and distributed field measurements related to forest practices. Water Resour. Res., 40, W02405, doi: 1029/2003WR002017.

Dharmasena, U. K.N.P. (2004): Introduction of the factor of safety concept through deterministic approach for landslide hazards zonation mapping in the selected part of Rathnapura municipal council area. M. Sc. Thesis, Postgraduate institute of science, University of Peradeniya, Sri lanka.

Dias, E.C., Zuquette, L.V. (2004): Methodology adopted for probabilistic assessment of landslides in Ouro Preto, Brazil. In:Lacerda WA, Ehrlich M, Fontoura SAB, Sayao ASF (eds) Landslides: evaluation and stabilization. Balkema, Taylor & Francis Group, London, pp 287–292.

Dietrich, W. E., Montgomery, D. R. (1998): SHALSTAB: a digital terrain model for mapping shallow landslide potential. National Council of the Paper Industry for Air and Stream Improvement Technical Report, February 1998, pp 29.

Dietrich, W. E., Bullugi, D., Real de Asua, R. (2001): Validation of the shallow landslide model, SHALSTAB, for forest management. In Landuse and Watersheds, Human Influences on Hydrology and Geomorphology in Urban and Forest Areas, edited by M. S. Wigmosta and S. J. Burges, pp 195-227, Water Science and Application 2, Am. Geophys. Union, Washinton, DC.

Disaster Mitigation in Asia and the Pacific (1991). Collection of country reports, Asian Development Bank, Manila, Philippines.

Dobrovolny, E. (1971): Landslide susceptibility in and near anchorage as interpreted from topographic and geologic maps in the great Alaska earthquake of 1964-Geology volume. Publication 1603. U.S. Geological Survey Open_Field Report 86-329, National Research Council, committee on the Alaska earthquake, National Academy of Sciences, USA, pp 735-745.

Donati, L., Turrini, M.C. (2002): An objective method to rank the importance of the factors predisposing to landslides with the GIS methodology: application to an area of the Appenines (Valnerina; Perugia, Italy). Eng Geol 63:277–289.

Einstein, H. H. (1988): Special lecture: landslide risk assessment procedure. In: Proceedings of the Vth ISL Lausanne, vol 2, pp 1075–1090.

Ercanoglu, M., Gokceoglu, C., Van Asch, T. H. W. J. (2004): Landslide susceptibility Zoning North of Yenice (NW Turkey) by multivariate statistical techniques. Nat Hazards 32:1–23.

Fall, M., Azzam, R. (1998): Application de la ge´ologie de l'ingenieur et de SIG a` l'e´tude de la stabilite´ des versants coˆ tier, Dakar, Senegal. In: Moore D, Hungr O (eds) Proceedings of the 8th IAEG Congress, Vancouver. A.A. Balkema, Rotterdam, pp 1011–1018.

Fecker, E. (2002): Groundwater and Rock Mechanics. Lecture note 2002, International Masters Course-TrpoHy, Institute of Geology and Paleontology, University of Tübingen, Germany.

Fellenius, W. (1936): Calculation of the stability of earth dams. Transactions, 2nd Congress on Large Dams (Washington, DC), 4: 445-65.

Fernandes, N. F., Guimaraes, R. F., Gomes, R. A. T., Vieira, B. C., Montgomery, D. R., Greenberg, H. (2004): Topographic controls of landslides in Rio de Janeiro. Field evidence and modeling, Catena, 55, pp 163-181.

Field, A. (2005): Discovering statistics using SPSS. Second edition, Sage publications.

Frattini, P., Crosta, G. B., Fusi, N., Dal Negro, P. (2004): Shallow landslides in pyroclastic soils: a distributed modeling approach for hazard assessment. Eng Geol 73(3–4):277–295.

Fredlund, D. G., Krahn, J. (1977): Comparison of slope stability methods of analysis. Canadian Geotechnical Journal, Vol. 14, No. 3, pp 429-39.

Gray, D. H., Megahan, W. F. (1981): Forest vegetation removal and slope stability in the Idaho Batholith. Res. Pap. INT-271, pp 23, For. Serv., U. S. Dep. Of Agric., Ogden,Utah.

Gritzner, M.L., Marcus, W.A., Aspinall, R., Custer, S.G. (2001): Assessing landslide potential using GIS, soil wetness modeling and topographic attributes, Payette River, Idaho. Geomorphology 37(1–2):149–165.

Guillande, R, Gelunge, P., Bardintzeff, J.-M., Brousse, R., Chorowicz, J., Deffontaines, B., Parrott, J.-F. (1995): Automated mapping of the landslide hazard on the island of Tahiti based on digital sattelite data. Map. Sci. Remote Sens., 32(1), pp 59-70.

Guzzetti, F., Carrara, A., Cardinali, M., Reichenbach, P. (1999): Landslide hazard evaluation: a review of current techniques and their application in a multi-scale study, Central Italy. Geomorphology 31:181–216.

Guzzetti, F., Cardinali, M., Reinchenbach, P., Carrara, A. (2000): Comparing landslide maps: a case study in the Upper River Basin, Central Italy. Environ Manage 25(3):247–263.

Guzzetti, F., Reichenbach, P., Ghigi, S. (2004): Rockfall hazard and risk assessment along a transportation corridor in the Nera Valley, Central Italy. Environ Manage 34(2):191–208.

Hammond, C. J., Prellwitz, R. W., Miller, S. M. (1992): Landslide Hazard Assessment Using Monte Carlo Simulation. In Proc., Sixth International Symposium on Landslides (D. H. Bell, ed.), Christchurch, New Zealand, A. A. Balkema, Rotterdam, Netherlands, Vol. 2, pp 959-964.

Haneberg, W. C. (1991): Pore pressure diffusion and the hydrologic response of nearly-saturated, thin landslide deposits to rainfall. J. Geol., 99, 886-892.

Heckerman, D. (1986): Probabilistic interpretation of MYCIN's certainty factor. In: Kanal LN, Lemmer JF (eds) Uncertainty in artificial intelligence. Elsevier, New York, pp 298–311.

Hoek, E., Bray, J. W. (1981): Rock slope engineering. Third edition, Institute of Mining and Metallurgy.

Hungr, O., Evans, S. G., Bovis, M., Hutchinson, J. N. (2001): Review of the classification of landslides of the flow type. Environmental and Engineering Geoscience, VII, pp 221-238.

Hutchinson, J. N. (1973): The response of London clay cliffs to differing rates of toe erosion. Geologia Applicata e Idrogeologia, Vol. 8, pp 221-239.

Hutchinson, J. N., Gostelow, T. P. (1976): The development of an abandoned cliff in London clay at Hadleigh, Essex. Philosophical transactions of the Royal society of London, series A, Vol. 283, pp 557-604.

Hutchinson, J. N. (1988): General report: Morphological and geotechnical parameters of landslides in relation to geology and hydrogeology. In Proc., Fifth international symposium on landslides (C. Bonnard, ed.), A. A. Balkema, Rotterdam, Netherlands, Vol. 1, pp 3-35.

Iida, T. (2004): Theoretical research on the relationship between return period of rainfall and shallow landslides. Hydrol. Process., 18, 739-756.

Irigaray, C. (1990): Cartografia de riesgos geologicos asociados a movimientos de ladera en el sector de Colmenar (Ma´ laga). Unpublished Post-graduate Thesis. University of Granada, pp 390.

Irigaray, C. (1995): Movimientos de ladera: inventario, analisisy cartografia de susceptibilidad mediante un Sistema de Informacion Geografica: Aplicacio´n a las zonas de Colmenar(Ma´laga), Rute (Co´ rdoba) y Montefrı´o (Granada). Unpublished PhD Thesis. University of Granada, Spain.

Irigaray, C., Ferna´ndez , T., El Hamdouni, R., Chaco´n, J. (1999): Verification of landslide susceptibility mapping, a case study. Earth Surf Processes Landforms 24:537–544.

Irigaray, C., Ferna´ndez, T., El Hamdouni, R., Chaco´n, J. (2006): Evaluation and validation of landslide-susceptibility maps obtained by a GIS matrix method: examples from the Betic Cordillera (southern Spain). Natural Hazards, ISSN: 0921-030X (Paper) 1573-0840 (Online) DOI: 10.1007/s11069-006-9027-8.

Iiritano, G., Versace, P., Sirangelo, B. (1998): Real-time estimation of hazard for landslides triggered by rainfall. Environ. Geol., 35 (2-3), pp 175-183.

Isaaks, E. H., Srivastava, R. M. (1989): An introduction to applied geostatistics. Oxford University press.

Istanbulluoglu, E., Tarboton, D. G., Pack, R. T., Luce, C. H. (2004): Modeling of the interaction between forest vegetation, disturbances, and sediment yields. J. Geophys. Res., 109, F01009.

Iverson, R. M. (2000): Landslide triggering by rain infiltration. Water Resour. Res, 36(7), 1897-1910.

Janbu, N., Bjerrum, L., Kjaernsli, B. (1956): Soil mechanics applied to some engineering problems. (in Norwegian with English summary), Norwegian Geo-technical institute publication, 16 (Oslo: Norwegian Geotechnical Institute).

Jayathissa, G., Schröder, D. (2009): Integration of deviation and dip angle concepts using GIS in landslide hazard zonation in Sri Lanka. Geospatial crossroads at GI forum 2009, proceedings of the Geoinformatics forum, Salzburg, Austria, pp 76-85.

Jayathissa, G., Schröder, D., Fecker, E. (2009a): Geological structures in GIS based landslide hazard zonation. Second International Summer School and Conference for Applied Geo-informatics for Society and Environment (AGSE 2009), Stuttgart University of Applied Sciences, Germany, Vol. 103 (2009), pp 276-283.

Kawakami, H., Saito, Y. (1984): Landslide risk mapping by a quantification method. In: Proceedings of the IVth ISL Toronto, Canada, Vol. 2, pp 535–540.

Keefer, D. K., Wilson, R. C., Mark, R. K., Brabb, E. E., Brown, W. M., Ellen, S. D., Harp, E. L., Wieczorek, G. F., Alger, C. S., Zatkin, R. S. (1987): Real-time landslide warning during heavy rainfall. Science, 238, pp 921-925.

Keefer, D. K. (1984): Landslides caused by earthquakes. Geol. Soc. Am. Bull., 95, 406-421.

Kiersch, G. A. (1965): Vaiont reservoir disaster. Geotimes, 9: pp 9-12.

Kobashi, S., Suzuki, M. (1988): Hazard index for the Judgment of Slope Stability in the Rokko Mountain Region. In. Proc., Interpraevent 1988, Graz, Austria, Vol. 1, pp 223-233.

Krahn, J., Morgenstern, N. R. (1979): The ultimate frictional resistance of rock discontinuities. International Journal of Rock Mechanics and Mining Science, Vol. 16, No. 2, pp 127-133.

Krahn, J. (2004): Stability modeling with SLOPE/W. An engineering methodology, GEO-SLOPE/W International Ltd, Calgary, Alberta, Canada.

Kröner, A., Cooray, P. G., Vitanage, P. W. (1991): Lithotechtonic subdivision of the Precambrian basement in Sri Lanka. In : A. Kröner (Ed.) The Crystalline Crust of Sri Lanka, Part I, Summary of Research of the German-Sri Lankan Consortium. Geol. Surv. Dept. Sri Lanka, Prof. Paper 5, pp 5-21.

Lan, H.X., Zhou, C.H., Wang, L.J., Zhang, H.J., Li, R.H. (2004): Landslide hazard spatial analysis and prediction using GIS in the Xiaojiang watershed, Yunnan, China. Eng Geol: 20.

Landslide studies and services division, National Building Research Organization (1995): Landslide hazard mapping in Sri Lanka, User manual, landslide hazard mapping project, SRL 89/001.

Landslides-Investigation and mitigation (1996): Special report 247 edited by Turner, A. K., and Schuster, R. L., Transportation research board, national research council, Washington, D. C.

Larsen, M. C., Simon, A. (1993): A rainfall intensity-duration threshold for landslides in a humid-tropical environment, Puerto Rico. Geograf. Ann. 75A, pp 13-23.

Lee, S., Min, K. (2001): Statistical analysis of landslide susceptibility at Yongin, Korea. Environ. Geol., 40:1095–1113.

Lee, S., Chang, B., Choi, W., Shin, E. (2001): Regional susceptibility, possibility and risk analysis of landslide in Ulsan metropolitan city, Korea. In: Proceedings of the IGARSS 2001: scanning the present and resolving the future. IEEE, Australia, pp 1690–1692.

Lee, S., Chwae, U., Min, K. (2002): Landslide susceptibility mapping by correlation between topography and geological structures: the Janghung area, korea, Geomorphology, 46, pp 149-162.

Lee, S., Choi, J., Min, K. (2002a): Landslide susceptibility analysis and verification using the Bayesian probability model. Environ. Geol., 43: 120- 131.

Lee, S., Ryu, J-H., Lee, M-J., Won, J-S. (2003): Use of an artificial neural network for analysis of the susceptibility to landslides at Boun, Korea. Environ. Geol., 44: 820-833.

Lee, S. (2004): Application of likelihood ratio and logistic regression models to landslide susceptibility mapping using GIS. Environ. Manage, 34(2): 223–232.

Lee, S., Ryu, J.-H., Won, J.-S., Park, H.-J. (2004a): Determination and application of the weight for landslide susceptibility mapping using an artificial neural network. Eng. Geol., 71, pp 289-302.

Lessing, P., Kulander, B.R., Wilson, B.D., Dean, S.L., Woodring, S.M. (1976): West Virginia landslides and slide-prone areas. West Virginia Geol. Econ. Surv., Environ. Geol. Bull., 15:64.

Luzi, L., Pergalani, F. (1996a): Application of statistical and GIS techniques to slope instability zonation (1:50.000 Fabriano geological map sheet). Soil Dyn. Earthquake Eng., 15(2):83–94.

Luzi, L., Pergalani, F. (1996b): A methodology for slope vulnerability zonation using a probabilistic method. In: Chaco´n J, Irigaray C (eds) Proceedings of the Sexto Congreso Nacional y Conferencia Internacional sobre Riesgos Naturales, Ordenacio´ n del Territorio y Medio Ambiente, vol 1, S.E.G.A.O.T., Granada, Spain, pp 537–556.

Manual for zonation on areas susceptible to rain induced slope failure (1997): Asian technical committee on Geotechnology for natural hazards in ISSMFE, published by Japanese Geotechnical society.

Marzorati, S., Luzi, L., De Amicis, M. (2002): Rock falls induced by earthquakes: a statistical approach. Soil Dyn. Earthquake Eng., 22:565–577.

Mathavan, V., Prame, W. K. B. N., Cooray, P. G. (1999): Geology of the High Grade Proterozoic Terrains of Sri Lanka and the Assembly of Gondwana: an Updata on Recent Developments. International Association for Gondwana Research, Japan Vol. 2, No. 2, pp 237-250.

Mathew, J., Jha, V. K., Rawat, G. S. (2007): Weights of evidence modeling for landslide hazard zonation mapping in part of Bhagirathi valley, Uttarakhand. Current Science, Vol. 92, no. 5, pp 628-638.

MejIa-Navarro, M., Wohl, E.W., Oaks, S. D. (1994): Geological hazards, vulnerability, and risk assessment using GIS: model for Glenwood Springs, Colorado. Geomorphology 10:331–354.

Meneroud, J.P. (1978): Cartographie des risques dans les Alps-Maritimes (France). In: Proceedings of the IIIrd I.A.E.G. Congress, II, Chap. 46, pp 98–107.

Miller, D. J. (1995): Coupling GIS with physical models to assess deep-seated landslide hazards. Environ. Eng. Geosci., 1(3), pp 263–276.

Miller, D. J., Sias, J. (1998): Deciphering large landslides: linking hydrogeological, groundwater and slope stability models through GIS. Hydrol. Processes 12:923–941.

Montgomery, D. R., Dietrich, W. E. (1994): A physically based model for the topographic control on shallow landsliding. Water Resour. Res., 30(4), 1153-1171.

Montgomery, D. R., Sullivan, K., Greenberg, H. M. (1998): Regional test of a model for shallow landsliding, Hydrol. Process, 12, pp 943-955.

Moreiras, S. M. (2004): Landslide incidence zonation in the Rio Mendoza valley, Mendoza province, Argentina. Earth Surf Processes Landforms 29:255–266.

Moreiras, S. M. (2005): Landslide susceptibility zonation in the Rio Mendoza valley, Argentina. Geomorphology 66:345–357.

Morgenstern, N. R. (1985): Geotechnical aspects of environmental control. In Proc., 11th International conference on soil mechanics and foundation engineering, A.A. Balkema, Rotterdam, Netherlands, Vol. 1, pp 155-185.

Murphy, W., Vita_Finzi, C. (1991): Landslides and Seismicity: An application of remote sensing. In Proc., Eighth Thematic Conference on Geological Remote Sensing, Denver, Colo., Environmental research institute of Michigan, Ann Arbor, Vol. 2, pp 771-784.

Nash, D. (1987): A comparative review of limit equilibrium methods of slope stability analysis, in M. G. Anderson and K. J. Richards (eds), slope stability, John Wiley & Sons, pp 11-75.

Nemcok, A., Pasek, J., Rybar, J. (1972): Classification of landslides and other mass movements. Rock Mechanics, 4: pp 71-78.

Neuhauser, B., Terhorst, B. (2007): Landslide susceptibility assessment using "weights-of-evidence" applied to a study area at the Jurassic escarpment (SW—Germany), Geomorphology 86, pp 12–24.

Neulands, H., (1976): A prediction model of Landslip. Catena 5:215–30 engineering geology maps: landslides and GIS 405.

Newman, E. B., Paradis, A. R., Brabb, E. E. (1978): Feasibility and cost of using a computer to prepare landslide susceptibility maps of the San Francisco Bay region, California. US Geological Survey Bulletin 1443, USGS, USA, pp 23.

Nilsen, T. H., Wright, R. H. (1979): Relative slope stability and landuse planning in the San Francisco Bay region, California. US Geological Survey Professional Paper 944, US Department of Interior, Washington, pp 103.

Nilsen, T. H., Wright, R. H., Vlasic, T. C., Spangle, W. E. (1979a): Relative slope stability and land-use planning in the San Francisco Bay region, California. Prof. Pap. 944, pp 96, U. S. Geol. Surv.

Okimura , T., Kawatani, T. (1987): Mapping of the potential surface failure sites on granite mountain slopes. in V. Gardinar (ed), International Geomorphology, Part 1, john Wiley & Sons, pp 121-138.

Oregon Department of Forestry (2003): High landslide hazard locations, shallow, rapidly moving landslides and public safety: screening and practices. Forest practices Tech. Note No. 2, vers., 2.0., pp 12, Oregon Department of Forestry, Salem, OR.

Pack, R. T. (1997): New developments in terrain stability mapping in B. C., Proc. 11th Vancouver Geotech. Soc. Symp., May 30, 1997, Canada.

Pack, R. T., Tarboton, D. G., Goodwin, C. N. (1998): The SINMAP approach to terrain stability mapping. In: Moore D, Hungr O (eds) Proceedings of the 8th IAEG Congress, Vancouver. A.A. Balkema, Rotterdam, pp 1157–1165.

Pan, X., Nakamura, H., nozaki, T., Huang, X. (2008): A GIS based landslide hazard assessment by multivariate analysis. Journal of the Japan Landslide Society, Vol. 45, No. 3, pp 187-195.

Panet, M. (1969): Discussion of K. W. John's paper (ASCE Proc. Paper 5865, March 1968). Journal of the soil mechanics and foundation division, ASCE, Vol. 95, No. SM2, pp 685-686.

Parise, M., Jibson, R.W. (2000): A seismic landslide susceptibility rating of geologic units based on analysis of characteristics of landslides triggered by the 17 January, 1994 Northridge, California earthquake. Eng. Geol., 58:251–270.

Park, N. W., Chi, K. H. (2003): A probabilistic approach to predictive spatial data fusion for geological hazard assessment. In: Proceedings of the IGARSS2003: IEEE International Geosciences and Remote Sensing Symposium. Learning from earth's shapes and sizes, pp 2425–2427.

Plafker, G., Ericksen, G. E. (1978): Nevados Huascaran avalanches, Peru, in B. Voight (ed.), Rock slides and avalanches (Amstardam: Elsevier), pp 277-314.

Popescue, M. E., Trandafir, A., Fedrrico, A., Simeone, V. (1998): probabilistic risk assessment of landslide related geo-hazards. In: Geotechnical Hazards, edited by B. Mari, Z. Lisac, and A. Szavits-Nossan, pp. 863-870, Balkema, Rotterdam.

Porwal, A., Carranza, E. J. M., Hale, M. (2001): Extended weights of evidence of modeling for predictive mapping of base metal deposit potential in Aravalli Province, Western India. Explor. Min. Geol., 10, pp 273–287.

Pradhan, B., Lee, S., Manfred, F. (2010): Remote sensing and GIS–based landslide susceptibility analysis and its cross validation in three test areas using a frequency ratio model. Photogrammetrie - Fernerkundung – Geoinformation 1/2010, PFG 2010 / 1, 017-032, Stuttgart, Germany.

Radbruch, D. H. (1970): Map of relative amount of landslides in California. US Geological Survey open file report 70-1485, pp 36, map scale 1:500,000. US Geological Survey Open-File Report 85-585.

Radbruch, D. H., Crowther, K. C. (1973): Map showing areas of estimated relative susceptibility to landsliding in California. US Geological Survey Miscellaneous Geologic Investigations Map I-747, scale 1:1,000,000.

Radbruch, D. H. (1978): Gravitational creep of rock masses on slopes. In rockslides and avalanches (B. Voight, ed.), Vol. 1: Natural phenomena, Elsevier, Amsterdam, Netherlands, pp 607-657.

Regmi, N. R., Giardino, J. R., Vitek, J. D. (2009): Modeling susceptibility to landslides using the weight of evidence approach: Western Colorado, USA. Geomorphology (2009).

Ritchie, A. M. (1963): Evaluation of rock fall and its control. In Highway research record 17, HRB, National research council, Washington, D. C., pp 13-28.

Rollerson, T. P., Thomson, B., Millard, T. H. (1997): Identification of coastal British Columbia terrain susceptible to debris flows, in Debris Flow Hazards Mitigation: Mechanics, Prediction and Assessment, Am. Soc. Civ. Engr., San Francisco, CA.

Sammori, T., Tsuboyama, Y. (1990): Study on method of slope stability considering infiltration phenomenon. Shin Sabo J. (J. Jpn. Soc. Erosion Contr. Eng.) 43(4), 14-21 (in Japanese with English abstract).

Santacana, N., Baeza, C., Corominas, J., de Paz, A., Marturia,´ J. (2003): A GIS-based multivariate statistical analysis for shallow landslide susceptibility mapping in La Pobla de Lillet Area (Eastern Pyrenees, Spain). In: Chacon J, Corominas J (eds) Special issue on Landslides and GIS. Nat. Hazards 30(3):281–295.

Sassa, K. (1989): Geotechnical classification of landslides. Landslide News, 3: pp 21- 24.

Sawatzky, D. L., Raines, G. L., Bonham-Carter, G. F., looney, C. G. (2009): Spatial Data Modeller (SDM): ArcMAP 9.3 geoprocessing tools for spatial data modeling using weights of evidence, logistic regression, fuzzy logic and neural networks.

Schmid, R. H., MacCannel, J. (1955): Basic problems, techniques and theory of isopleth mapping. J. Am. Stat. Assoc., 50(269):220–239.

Schröder, D., Kettemann, R. (2007): Statistical landslide hazard analysis. Lecture note of GIS practice, Photogrammetry and Geoinformatics, University of Applied Sciences, Stuttgart, Germany.

Schuster, R. L. (1996): Socioeconomic significance of landslides: Landslides investigation and mitigation, Special Report 247, Transportation Research Board, National Research Council, Chapter 2, pp 12-35, National Academic Press, Washington, D. C.

Scott, G. R. (1972): Map showing landslides and areas susceptible to landslides in the Morrison Quadrangle, Jefferson Country, Colorado. US Geological Survey. Map I-790-B. USA.

Selby, M. J. (1993): Hillslope Materials and Processes. Second edition, Oxford University press, New York, United States.

Sharpe, C. F. S. (1938): Landslides and Related Phenomena (New Jersey: Pageant).

Shortliffe, E. H., Buchanan, G. G. (1975): A model of inexact reasoning in medicine. Math Biosci 23:351–379.

Shroder, J. F. (1971): Landslides of Utah. Bulletin 90. Utah Geological and Mineralogical survey, pp 50.

Sidle, R. C. (1984): Relative importance of factors influencing landsliding in coastal Alaska. Proc. 21st Ann. Eng. Geol. and Soils Eng. Symp., pp 331-325, Univ. of Idaho, Moscow.

Sidle, R. C. (1992): A theoretical model of the effects of timber harvesting on slope stability. Water Resour. Res., 28(7), pp 1897-1910.

Sidle, R. C., Wu, W. (1999): Simulating effects of timber harvesting on the temporal and spatial distribution of shallow landslides. Z. Geomorphol. N.F., 43, pp 185-201.

Sidle, R. C., Dhakal, A. S. (2003): Recent advances in the spatial and temporal modeling of shallow landslides. In Integrated Modeling of Biophysical, Social and Economic Systems for Resource Management Solution. Proc. Of MODSIM 2003, vol. 2, pp 602-607, Modeling and Simulation Society of Australia and New Zealand, Inc., Canberra, Australia.

Sidle, R. C., Ochiai, H. (2006): Landslides: Processes, Prediction, and Landuse. Americal Geophysical union, Washington, DC.

Simons, D. B., Li, R. M., Ward, T. J. (1978): Mapping of potential landslide areas in terms of slope stability. Fort Collins, Colorado. Civil Engineering Dept., Colorado State University, pp 75.

Singh, A. (1999): Basic soil mechanics and foundation. CBS publishers and distributors, New Delhi, India.

Skempton, A. W., De Lory, F. A. (1957): Stability of natural slopes in London Clay. Proceedings, 4th International Conference on Soil Mechanics and Foundation Engineering (London), 2: 378-81.

Skempton, A. W., Hutchinson, J. N. (1969): Stability of natural slopes and embankment foundations. In Proc., seventh international conference of soil mechanics and foundation engineering, Sociedad Mexicana de Mecana de Suelos, Mexico city, state of the art volume, pp 291-340.

Skempton, A. W. (1970): First–time slides in over consolidated clays. Geotechnique, Vol. 20, No. 3, pp 320-324.

Soeters, R., Westen, C. J. van. (1996): Slope instability recognition, analysis, and zonation- Landslides investigation and mitigation. Edited by A. K. Turner and R. L. Schuster, pp 129-177, special report 247, Transportation Research Board, National Research Council, National Academic Press, Washington, DC.

Spiegelhalter, D. J. (1986): A statistical view of uncertainty in expert systems. In: Gale, W. (Ed.), Artificial Intelligence and Statistics. Addison-Wesley, Reading, MA, pp 17–55.

Stevenson, P. C. (1977): An empirical method for the evaluation of relative landslide risk. Int. Ass. Eng. Geol. Bull., 16:69–72.

Süzen, M. L., Doyuran, V. (2004a): Data driven bivariate landslide susceptibility assessment using geographical information system: a method and application to Asarsuyu catchment, Turkey. Eng. Geol., 71: 303–321.

Süzen, M. L., Doyuran, V. (2004b): A comparison of the GIS based landslide susceptibility assessment methods: multivariate versus bivariate. Environ. Geol., 45:665–679.

Tarboton, D. (1997): A new method for the determination of flow directions and upslope areas in grid digital elevation models, Water Resour. Res., 33, 309-319.

Temesgen, B., Mohammed, M. U., Korme, T. (2001): Natural hazard assessment using GIS and remote sensing methods, with particular reference to the landslides in the Wondogenet Area, Ethiopia. Phys Chem Earth, Part C: Solar Terrest Planet Sci., 26/9:665–675.

Terlien, M. T. J., Asch, Th. W. J. van., Westen, C. J. van (1995): Deterministic modeling in GIS based landslide hazard assessment, in A. Carrara and F. Guzzetti (eds), Geographical Information systems in Assessing Natural hazards, kluwer Academic Publishers, pp 57-77.

Terlien, M. T. J. (1996): Modeling spatial and temporal variations in rainfall triggered landslides. Ph. D thesis, ITC Publ. Nr. 32, Enschede, The Netherlands, pp 254.

Terlien, M. T. J. (1997): Hydrological landslide triggering in ash-covered slopes of Manizales (Colombia). Geomorphology 20:165–175.

Terlien, M. T. J. (1997): The determination of statistical and deterministic hydrological landslide-triggering thresholds. Environmental geology 35 (2-3), pp 124-130.

Thapa, P. B., Esaki, T. (2007): GIS based quantitative landslide hazard prediction modeling in natural hillslope, Agra khola watershead, central Nepal. Bulleting of the Department of Geology, Tribhuvan University, Kathmandu, Nepal, vol. 10, pp 63-70.

Turner, A. K., Schuster, R. L. (1996): Landslides investigation and mitigation. Special Report 247, Transportation Research Board, National Research Council, National Academic Press, Washington, D. C.

Varnum, N. C., Tueller, P. T., Skau, C. M. (1991): A geographical information system to assess natural hazards in the east –central Sierra Navada, J. Imaging Technol., 17(2), pp 57-61.

Van Beek, L. P. H., Van Asch, T. H. W. J. (2004): Regional assessment of the effects of land-use change on landslide hazard by means of physically based modeling. Nat. Hazards 31:289–304.

Van Westen, C. J. (1993): Application of Geographic Information System to Landslide hazard Zonation. ITC publication No. 15. International Institute for Aerospace Survey and Earth Sciences (ITC), Enschede, Netherlands, pp 245.

Van Westen, C. J., Rengers, N. Terlien, M. T. J., Soeters, R. (1997): Prediction of the occurrence of slope instability phenomena through GIS-based hazard zonation. Geol. Rundsch (1997) 86: 404-414, Springer- Verlag 1997.

Van Westen, C. J., Seijmonsbergen, A. C., Mantovani, F. (1999): Comparing landslide hazard maps. Natural hazards 20: 137-158, Kluwer academic publishers, The Netherlands.

Van Westen, C. J. (2000): The modeling of landslide hazards using GIS. Surveys in Geophysics 21: 241-255. Kluwer Academic publishers, The Netherlands.

Van Westen, C. J. (2002): Use of weights of evidence modeling for landslide susceptibility mapping. International Institute for Geoinformation Science and Earth observation (ITC), Enschede, The Netherlands.

Van Westen, C. J., Rengers, N., Soeters, R. (2003): Use of geomorphological information in indirect landslide susceptibility assessment. In: Chacon J, Corominas J (eds) Special issue on Landslides and GIS. Nat. Hazards 30(3):399–419.

Van Westen, C. J, Van Asch, T. W. J., Soeters, R. (2005): Landslide hazard and risk zonation – why is it still so difficult? Bull. Eng. Geol. Env., (2006) 65: 167-184.

Varnes, D. J. (1958): Landslide types and processes. Highway Research Board, Special Report (Washington, DC), 29: pp 20-47.

Varnes, D. J. (1975): Slope movements in the Western United States. In Mass Wasting (Norwich: Geo Abstracts), pp 1-17.

Varnes, D. J. (1978): Slope movement types and processes. In Landslide Analysis and Control, edited by M. Clark, pp. 11-33, Special Report 176, Transportation Research Board, National Academy of Sciences, National Research Council Washington, DC.

Varnes, D. J. (1984): Landslide hazard zonation: a review of principles and practice, International Association of Engineering Geology, Commission on Landslides and Other Mass Movements on Slopes, UNESCO Natural Hazards Series no. 3, pp 61.

Vecchia, O. (1978): A simple terrain index for the stability of hillsides or scarps. In: Geddes J. D. (ed) Large ground movements and structures. Wiley, New York Toronto, pp 449-461.

Vees, E. (2001/2002): Fundamentals of Geotechnical Engineering. Lecture note WS 2001/2002, International Masters Course-TropHy/AEG, Institut für Geologie und Paläontologie, Universität Tübingen, Germany.

Wachal, D. J., Hudak, P. F. (2000): Mapping landslide susceptibility in Travis County, Texas, USA. Geol. Journal 51:245–253.

Wadge, G. (1988): The potential of GIS modeling of gravity flows and slope instabilities. Int. J. Geogr. Inf. Systems 2 (2): 143-152.

Ward, T. J., Li, R. M., Simons, D. B. (1981): Use of a mathematical model for estimating potential landslide sites in steep forested drainage basins, in Erosion and Sedimentation in the Pacific Rim Steeplands, IAHS publ. 132 pp 21-41.

Ward, T. J., Li, R. M., Simons, D. B. (1982): Mapping landslides in forested watersheds. Journal of the Geotechnical engineering Division 8, 319-324.

Whitman, R. V., Bailey, W. A. (1967): Use of computers for slope stability analysis. Proceedings, American Society of Civil Engineers, 93 (SM4): 475-98.

Wieczorek, G. F. (1984): Preparing a detailed landslide inventory map for hazard evaluation and reduction. Bulleting of the Association of Engineering Geologists, Vol. 21, No. 3, pp 337-342.

Wu, W. (1993): Distributed slope stability analysis in steep, forested basins. Ph. D. thesis, Utah State Univ., Logan, pp 148.

Wu, W., Sidle, R. C. (1995): A distributed slope stability model for steep forested hillslopes. Water Resour. Res. 31, pp 2097-2110.

Wu, W., Sidle, R. C. (1997): Application of a distributed shallow landslide analysis model (dSLAM) to managed forested catchments in coastal Oregon. IAHS Publ. 245, pp 213-221.

Xie, Q. M., Xia, Y. Y. (2004): Systems theory for risk evaluation of landslide hazard. Int. J Rock Mech. Min. Sci, vol. 41, no. 3, CD-ROM, Elsevier, Netherlands.

Xie, M., Esaki, T., Cai, M. (2004b): A time-space based approach for mapping rainfall-induced shallow landslide hazard. Environmental Geology (2004) 46:840–850.

Ying, K. L., Yan, T. Z. (1988): Statistical Prediction Model for Slope Instability of Metamorphosed Rocks. In Proc., Fifth International Symposium on Landslides, Lausanne (C. Bonnard, ed.), A. A. Balkema, Rotterdam, Netherlands, Vol. 2, pp 1269-1272.

Zhou, G., Esaki, T., Mitani, Y., Xie, M., Mori, J. (2003): Spatial probabilistic modeling of slope failure using an integrated GIS Monte Carlo simulation approach. Eng. Geol., 68(3– 4):373–386.

Web Reference:

PCRaster Version 2 Manual: http://pcraster.geo.uu.nl/documentation/pcrman/book1.htm.

http://www.nationalatlas.gov/articles/geology/a_landslide.html#one.

Annex- I

Table 6.16: Major factors and their classes, calculated class weights (scores) and contrast factors for Weights of Evidence, ArcGIS spatial analyst model.

Factor map	Factor class	Total class Weight ($W_{i\text{-Total}}$)	Contrast factor (C_w)
(1) Lithology	***Lithology type***		
	Ch	0.3741	0.5059
	Kh	-0.3903	-0.2585
	GtBtChGn	-0.3977	-0.2659
	HbBtGn	-0.6641	-0.5323
	QtFpGn	-1.0675	-0.9356
	MetaGabro	-2.0624	-1.9306
(2) Landuse	***Landuse map code***		
	W2	1.5423	1.5428
	JWb	1.3328	1.3333
	JT1	1.0685	1.0690
	W3	0.2031	0.2037
	S2	0.0327	0.0332
	HK	-0.0828	-0.0823
	JT2	-0.1652	-0.1647
	G1	-0.2668	-0.2662
	JR1	-0.2772	-0.2767
	S3	-0.4462	-0.4457
	S1	-0.5059	-0.5053
	S4	-0.7591	-0.7586
	HT	-0.8091	-0.8085
	W1	-1.1701	-1.1696
	JWp	-1.4928	-1.4923
	HP	-1.5758	-1.5753
	JR2	-3.7470	-3.7464
	G2	-4.5615	-4.5609
	HA	-5.1277	-5.1272
	JC	-5.6701	-5.6695
	G3	-5.7731	-5.7725
	HR	-6.0869	-6.0864
	HC	-6.2507	-6.2502
	W4	-6.3136	-6.3131
	Landform map code		
	X43	1.8312	1.8547
	D31	1.7191	1.7426
	E41	1.3461	1.3696
	X33	0.9989	1.0224
	E44	0.6963	0.7198
	E46	0.6366	0.6601
	E43	0.6229	0.6464
	E31	0.4175	0.4410
	E35	0.1756	0.1990
	E45	0.1377	0.1612
	D36	-0.0459	-0.0224
	E48	-0.0564	-0.0329
	E33	-0.3157	-0.2922
	D12	-0.3349	-0.3114

(3) Landform	E42	-0.4073	-0.3838
	E13	-0.4220	-0.3985
	X44	-0.4412	-0.4177
	E38	-0.5745	-0.5510
	F11	-0.7941	-0.7706
	E32	-0.8754	-0.8519
	E14	-0.9228	-0.8993
	E47	-1.0708	-1.0473
	E36	-1.1043	-1.0808
	D35	-1.2733	-1.2499
	E12	-1.3041	-1.2806
	E37	-1.3700	-1.3465
	D11	-1.5946	-1.5711
	X42	-1.6390	-1.6156
	E25	-1.8376	-1.8141
	X21	-1.9823	-1.9588
	D32	-2.4751	-2.4516
	X11	-2.7588	-2.7354
	E26	-3.3796	-3.3561
	D33	-3.7116	-3.6881
	X13	-3.8243	-3.8008
	E22	-3.8430	-3.8195
	E24	-4.4636	-4.4401
	X41	-4.7921	-4.7686
	E21	-4.9381	-4.9146
	E23	-5.1280	-5.1045
	D34	-6.4754	-6.4519
	D37	-6.8390	-6.8155
	E34	-6.9896	-6.9661
	E49	-7.3409	-7.3174
(4) Soil type	***Soil type***		
	Colluvium	2.5563	1.7116
	Colluvium/Residual	0.9909	0.1462
	Rock exposure	0.9746	0.1299
	Residual	-0.6350	-1.4797
	Soil thickness (m)		
	Coll>2+RS>3	3.8821	3.8609
	Coll=4-5	3.1691	3.1479
	Coll=1-2	2.5581	2.5369
	Coll>3	2.0069	1.9857
	RS=3	1.7355	1.7143
	Coll=3-4	1.5928	1.5716
	Coll>4	1.3250	1.3038
	RS=2-4	1.1355	1.1143
	Coll>2	0.8574	0.8362
	Coll=2-3	0.6052	0.5841
	RS=5-6	0.5313	0.5101
	Coll=1+ RS>2	0.4584	0.4372
	Coll=1-2+RS=1-2	0.4012	0.3800
	Coll>2+RS>2	0.2807	0.2595
	RS>3	0.1752	0.1540
	RE	0.1510	0.1298
	RS>4	0.0948	0.0736
	RS>5	-0.1312	-0.1524

(5) Soil thickness(m)	Coll=2	-0.2177	-0.2389
	RS=2-3	-0.2787	-0.2999
	RS=3-4	-0.5359	-0.5570
	RS=4-5	-0.6689	-0.6900
	RS>2	-0.9170	-0.9382
	RS<1	-1.0427	-1.0639
	Coll=1-2+RS>2	-1.2558	-1.2770
	RS=1-2	-1.3496	-1.3708
	RS<2	-1.4824	-1.5036
	Coll>2+RS=2	-1.5010	-1.5222
	RS=2	-1.8042	-1.8253
	RS=1	-2.9802	-3.0014
	RS>7	-3.1657	-3.1869
	RS=4	-3.5882	-3.6094
	RS<4	-3.6602	-3.6813
	Coll=1+RS=1	-3.7197	-3.7409
	Coll=1	-3.9221	-3.9433
	Coll=1+RS=1-2	-4.0611	-4.0823
	Coll=2+RS>1	-4.1325	-4.1537
	RS>6	-4.2160	-4.2372
	RS=1-3	-5.4287	-5.4499
	Coll=4	-5.8555	-5.8767
	Coll=1+RS>3	-6.3450	-6.3662
	RS>1	-6.5865	-6.6077
	Coll=3	-7.1341	-7.1553
***(6) Slope category* (degrees)**	***Slope angle category***		
	0-3	-3.5304	-3.5322
	3-6	-1.9232	-1.9250
	6-9	-0.8272	-0.8290
	9-12	-0.3464	-0.3482
	12-15	-0.1137	-0.1154
	15-18	0.0397	0.0379
	18-21	0.1905	0.1888
	21-24	0.3215	0.3197
	24-27	0.4268	0.4250
	27-30	0.5588	0.5570
	30-33	0.6616	0.6599
	33-36	0.7048	0.7030
	36-39	0.7591	0.7573
	39-42	0.8401	0.8383
	42-45	0.9311	0.9293
	45-48	0.9924	0.9906
	48-51	1.2051	1.2033
	51-54	1.3364	1.3346
	54-57	0.9644	0.9626
	57-60	1.1184	1.1166
	60-63	1.9786	1.9768
	63-66	2.4174	2.4156
	66-69	2.2633	2.2615
	69-73	-0.2809	-0.2827
	Aspect category		
	0-10	-0.2397	-0.2378
	10-20	-0.3129	-0.3110
	20-30	-0.3544	-0.3525

	30-40	-0.3518	-0.3499
	40-50	-0.3061	-0.3042
	50-60	-0.3541	-0.3521
	60-70	-0.2799	-0.2780
	70-80	-0.0035	-0.0016
	80-90	0.2488	0.2507
	90-100	0.3195	0.3214
	100-110	0.2215	0.2235
	110-120	0.3365	0.3384
	120-130	0.5655	0.5674
	130-140	0.5629	0.5648
	140-150	0.3648	0.3667
	150-160	0.0939	0.0958
	160-170	0.0716	0.0735
	170-180	-0.0831	-0.0812
	180-190	-0.2139	-0.2120
(7) Aspect category (degrees from North)	190-200	-0.2435	-0.2416
	200-210	-0.1957	-0.1938
	210-220	-0.1453	-0.1434
	220-230	-0.1759	-0.1740
	230-240	-0.1708	-0.1689
	240-250	-0.1111	-0.1092
	250-260	-0.3070	-0.3051
	260-270	-0.3185	-0.3166
	270-280	-0.4592	-0.4573
	280-290	-0.4067	-0.4048
	290-300	-0.4956	-0.4937
	300-310	-0.3044	-0.3025
	310-320	-0.1771	-0.1752
	320-330	0.1414	0.1433
	330-340	0.3482	0.3501
	340-350	0.4688	0.4707
	350-360	0.0554	0.0573
	Deviation angle category		
	0-10	0.2375	0.2391
	10-20	0.2959	0.2974
	20-30	0.2070	0.2086
	30-40	0.0880	0.0896
	40-50	-0.0610	-0.0594
	50-60	-0.2247	-0.2231
	60-70	-0.2681	-0.2665
	70-80	-0.3256	-0.3240
(8) Deviation angle category (degrees)	80-90	-0.3988	-0.3972
	90-100	-0.2649	-0.2634
	100-110	-0.0769	-0.0753
	110-120	0.0343	0.0358
	120-130	0.0944	0.0960
	130-140	0.0193	0.0208
	140-150	-0.0290	-0.0274
	150-160	0.0047	0.0063
	160-170	0.0482	0.0498
	170-180	0.1107	0.1123

	UD_80-90	-1.6720	-1.6690
	UD_70-80	-1.3178	-1.3148
	UD_60-70	-0.6903	-0.6873
	UD_50-60	-0.9824	-0.9794
	UD_40-50	-0.9518	-0.9488
	UD_30-40	-0.8543	-0.8513
	UD_20-30	-0.3375	-0.3344
	UD_10-20	-0.0715	-0.0685
	UD_00-10	0.0741	0.0771
	OD_00-10	0.2627	0.2657
	OD_10-20	0.4266	0.4296
	OD_20-30	0.4889	0.4920
	OD_30-40	0.6380	0.6410
	OD_40-50	0.4832	0.4862
	OD_50-60	-1.8939	-1.8909
	US_80-90	-2.0647	-2.0617
	US_70-80	-0.0760	-0.0730
(9) Over/under dip-scarp category (degrees)	US_60-70	-0.4735	-0.4705
	US_50-60	-0.9170	-0.9139
	US_40-50	-0.7515	-0.7484
	US_30-40	-0.5263	-0.5233
	US_20-30	-0.3625	-0.3595
	US_10-20	-0.3037	-0.3006
	US_00-10	-0.0463	-0.0432
	OS_00-10	0.2860	0.2890
	OS_10-20	0.5316	0.5346
	OS_20-30	0.6256	0.6286
	OS_30-40	0.6344	0.6374
	OS_40-50	0.5534	0.5565
	OS_50-60	0.5771	0.5802
	Watershed order		
	1st Order	0.2315	0.3842
	2nd Order	-0.6502	-0.4975
(10) Watershed	3rd Order	0.0527	0.2054
	4th Order	-0.2336	-0.0809
	5th Order	-1.0309	-0.8782
	6th Order	-3.7794	-3.6267
	Distance (m)		
	0-50	3.0582	2.4524
	50-100	2.0978	1.4920
	100-150	0.9450	0.3392
(11) Distance from spring	200-250	0.3618	-0.2441
	150-200	0.3821	-0.2238
	300-350	-0.0492	-0.6550
	>350	-0.0718	-0.6776
	Distance (m)		
	0-50	0.9341	1.1212
	50-100	-0.2484	-0.0613
	100-150	-0.9080	-0.7209
(12) Distance from stream	150-200	-1.3578	-1.1707
	200-250	-1.4231	-1.2360
	250-300	-1.3444	-1.1573
	>350	-1.3292	-1.1421
	Distance (m)		

(13) Distance from joint	0-50	1.5932	1.2096
	50-100	1.2114	0.8278
	100-150	1.2165	0.8329
	150-200	1.1276	0.7440
	200-250	0.7801	0.3965
	250-300	0.4843	0.1007
	>300	-0.4093	-0.7928

Annex- II

Landuse and landform map codes and their types

Landuse map code	Landuse type
JT1	Tea Estate (well managed (70-90% cover)
JT2	Tea Estate (poorly managed (20-70% cover)
JR	Rubber Estate (Seasonal leaf fall)
JC	Coconut Estate (well managed)
JQ	Estate Farms
JWB	Forest Plantations (Broadleaf varieties)
JWP	Forest Plantations (Pines gardens)
HP	Terraced Paddy
HK	Mixed, Agro-forestry/Home gardens
HA	Chena and other annual crops including tobacco
HM	Market Gardens (Potato, vegetable crops)
HT	Tea, Small Holder Management
HW	Village Woodlots
W1	Dense, Mixed, Evergreen Natural Forests
W2	Degraded Natural Forests (50-70% cover)
W3	Secondary Forest/Scrubland
W4	Gully and Stream Reservation Vegetation
G1	Natural Grasslands (Periodically Burnt)
G2	Open Country/Miscellaneous Uses
G3	Barren Lands, Escarpments/Erosional Remnants
S1	Urban Settlements/Built up areas
S2	Non Residential Lands/Non Agricultural Use
S3	Rural Settlements/Village/Hill Housing
S4	Estate Settlements and Housing
N1	Natural River Streams and Water Ways
N2	Natural Lakes and Ponds
N3	Artificial Lakes, Tanks and Reservoirs
G3/G2	Barren Lands, Escarpments/Erosional Remnants
Landform map code	**Landform type**
B11	Beaches
B12	Dunes
B13	Flat sandy deposits
B21	Marshes (Tree Vegetation, ex Mangrove)
B22	Coastal swamp
B23	Cultivated Coastal Swamp
C11	Undulating land (slope<8%)
C12	Rolling land (slope 8%-15%)
C13	Isolated monadnocks
C14	Undulating land (slope<8%) with monadonocks
C15	Rolling land (slope 8%-15%) with monadonocks
C16	Terraced Slopes
C21	Straight hill slope (inclined, flat and even surface)
C22	Complex slope (convex, concave, sigmoidal or more complicated)
C23	Corrugated slope (longitudinally straight)
D11	Undulating land

D12	Undifferentiated ridges (slopes cannot be denudated)
D21	Isolated hillocks
D22	Undulating land + hillocks
D23	Rolling land with hillocks and ridges
D24	Rolling hillocks an mini hills (dissected plateau)
D25	Foothill hillocks and Lanferes
D31	Straight slopes (no variation of slope)
D32	Complex slope (concave or convex, sigmoidal etc.)
D33	Corrugated slope (straight longitudinally, rolling later)
D34	Dissected slope, straight longitudinally, but dissected
D35	Corrugated land complex
D36	Dissected and complex
D37	Terraced Slopes
D38	Complex, corrugated and dissected
E11	Undulating plateau/peneplain
E12	Rolling area
E13	Rounded crests
E14	Flat to undulating crest
E21	Isolated hillocks (maximum relief amplitude 60 m)
E22	Undulating to rolling land + hillocks (plain mainly)
E23	Hillocks rolling pattern (plateau peniplain)
E24	Foothill hillocks
E25	Ridges with relief amplitude of 60 m
E26	Interhill rolling area
E31	Straight hill or ridge slope
E32	Complex hill slope
E33	Corrugated hill slope
E34	Dissected hill slope
E35	Complex and corrugated slope
E36	Complex and dissected slope
E37	Terraced slopes
E38	Complex corrugated and dissected
E41	Straight mountain slope
E42	Complex mountain slope
E43	Corrugated mountain slope
E44	Dissected mountain slope
E45	Complex and corrugated
E46	Complex and dissected
E47	Terraced slopes
E48	Complex, corrugated and dissected
E49	Rough broken and rocky slope complex slope
F11	Flat to undulating
F12	Undulating to Rolling
F21	Rounded Summits
F22	Flat to undulating summits
F31	Isolated hillocks
F32	Undulating to rolling land & hillocks
F33	Terraced slopes
F34	Rolling hillock area
F35	Ridges
F41	Straight
F42	Complex
F43	Terraced slopes
F44	Corrugated
F45	Dissected

F46	Complex and corrugated
F47	Complex and dissected
F48	Complex corrugated and dissected
F51	Straight
F52	Complex
F53	Terraced slopes
F54	Corrugated
F55	Dissected slopes with incised drainage
F56	Complex and corrugated
F57	Complex and dissected
F58	Complex corrugated and dissected
A10	River beds/stream beds
A11	Narrow river valleys and interhill flats
A12	Wide river valleys
A13	Levees and Flats
X11	Flat to undulating
X12	Rolling/hummocky
X13	Dissected/Terraced
X21	Talus/scree slopes (less than 60% slopes)
X22	Talus/scree slopes (more than 60% slopes)
X23	Slopes less than 25% scree and ground cover EO
X24	Slopes less than 25% scree and ground cover-EO
X31	Relatively recent landslide scars (soil exposed)
X32	Old landslide scars (Vegetation being rejuvenated)
X33	Fossil Landslide scars (Dissected and gullied surfaces)
X41	Rock out crops, erosional remnants
X42	Escarpments/Bluffs with near vertical slopes
X43	Dissected & gullied surfaces with non converging incised
X44	Badlands type rough broken and rocky lands, usually barren
X51	Water bodies
X52	Fault/fracture zones
X53	Sinkholes
X54	Waterfalls
X55	River/Stream capture zones
X6	Built up areas (50% of the surface built up)